A MECHANISTIC UNDERSTANDING OF LIGHT OLEFINS SELECTIVITY IN METHANOL-TO-HYDROCARBONS CONVERSION ON MFI

A DISSERTATION

SUBMITTED TO THE FACULTY OF THE GRADUATE SCHOOL

OF THE UNIVERSITY OF MINNESOTA

BY

Rachit Khare

IN PARTIAL FULFILLMENT OF THE REQUIREMENTS

FOR THE DEGREE OF

Doctor of Philosophy

Advised by Aditya Bhan

November 2016

“Be the change that you wish to see in this world”

Acknowledgements

First and foremost, I want to thank my adviser, Prof. Aditya Bhan, for being a constant source of guidance and inspiration to me. Five years ago, he accepted me into his research group and provided me with the opportunity to pursue my interests. In the last five years, he has put in a lot of effort to assist and guide me in each and every aspect of my research. His constant guidance and support have been the key factors in the fruitfulness of my research efforts.

I want to thank my fellow research group members, Joseph DeWilde, Cha Jung Chen, Minje Kang, Mark Sullivan, Udit Gupta, Andrew Hwang, Linh Bui, Anurag Kumar, Sukaran Arora, Mark Bachrach, Praveen Bollini, Brandon Foley, and Jake Miller, for their constant support and invaluable advice during numerous discussion sessions. Conversations with them about research during group meetings and in the office were always helpful. I am going to miss the weekly trips to Raising Canes. In particular, I want to thank Sukaran Arora for assisting me in the performing the experiments and collecting the data for the results presented in Chapter 7. I also want to thank Brandon Foley for assisting me in performing the experiments for the results presented in Appendix D.

I want to thank the former Bhan Research group members, Samia Ilias, Elizabeth Mallon, Ian Hill, Hsu Chiang, Mark Mazar, Srinivas Rangarajan, Wen Sheng Lee, Samuel Blass, and Jeremy Bedard, with whom I have had the chance of working and interacting with during my early years in the group. I want to especially thank Samia Ilias, for mentoring me in my first year and teaching me the necessary skills to perform experiments and analyze the data. We collaborated together in performing the experiments and analyzing the data for the results presented in Chapter 3.

I want to thank all my friends in Minneapolis and at the University of Minnesota for all the great moments I have had with them in the last five years. The numerous occasions spent with them will be some of the most cherished moments of my stay in Minneapolis. I want to especially thank Pooja Jambunathan and Sidd Chanpuriya for the wonderful time we spent together. I also want to thank all my friends from the University of Minnesota Badminton Club with whom I have had the chance to play badminton almost every day for the past 3 years.

I want to acknowledge the collaborators from The Dow Chemical Company, Dan Hickman, Dean Millar, Andre Malek, and Abe Schuitman, for their constant advice and support on my research work. I would especially like to thank Dean Millar for helping me in the synthesis of samples for the results reported in Chapter 4. I also want to thank Dr. Dongxia Liu and Dandan Xu for synthesizing several zeolite samples.

I would like to express my gratitude to Julie Prince and Teresa Bedahl for making my transition into the graduate school as an international student very smooth. I want to thank Daniel Williams for the numerous purchasing orders that I placed during the course of my stay and for efficiently processing them. I want to thank Bill from the CEMS machine shop for helping be build several reactor units.

Finally, I want to acknowledge National Science Foundation (CBET 1055846) and The Dow Chemical Company for their financial support. Parts of this work were carried out in the Characterization Facility, University of Minnesota, which receives partial support from NSF through the MRSEC program.

And last, but not the least, I want to thank my parents, Arpana Khare and Malay Khare, and my brother, Harshit Khare. I wouldn't be here where I am without them and their support.

Abstract

The methanol-to-hydrocarbons (MTH) conversion is the final processing step in converting alternative feedstock such as coal, natural gas, and biomass, to hydrocarbon fuels and important petrochemicals. Methanol and its dehydration product, dimethyl ether (DME), react on zeolites via the indirect hydrocarbon-pool mechanism to form a wide variety of hydrocarbons including light olefins, gasoline-range hydrocarbons, and aromatics. The hydrocarbon pool mechanism involves two reaction cycles simultaneously operating inside the zeolite pores: an olefins-based catalytic cycle and an aromatics-based catalytic cycle. In the olefins-based cycle, light olefins are methylated by methanol or DME to form higher olefins, which subsequently undergo β-scission to complete the catalytic cycle. In the aromatics-based cycle, methylbenzenes (MBs) are methylated to form more-substituted MBs, which then dealkylate and produce light olefins to complete the catalytic cycle. These two catalytic cycles are not independent of one another as C_6+ olefins undergo hydrogen transfer and cyclization to form MBs, which, on the other hand, dealkylate and produce light olefins.

The observed product distribution in MTH can be rationalized as an effect of the relative rates of propagation of the aromatics-based and the olefins-based catalytic cycles. Quantifying the relative propagation of these two catalytic cycles and understanding how these cycles contribute to the overall product distribution under varying reaction conditions, varying feed composition, and on different zeolite topologies or morphologies, is critical for developing structure-function relationships for MTH catalysts. In this dissertation, the effects of independently varying (i) the feed composition (by co-feeding hydrocarbons or oxygenates), (ii) the concentration of catalytically active sites (by varying the chemical composition of the zeolite), and (iii) the diffusion characteristics of the zeolite

(by changing crystallite size or silylating the external surface), on the relative extents of propagation of the aromatics- and the olefins-based catalytic cycles, and consequentially on the observed MTH product selectivity, is presented.

In the absence of kinetic rate constants of elementary steps, the ratio of the synthesis rates of ethene and the 2-methyl-2-butene + 2-methylbutane (referred to as ethene/2MBu) can be used as a descriptor to assess the relative extents of propagation of the two catalytic cycles. Co-feeding propene at 548 K on HZSM-5 enhanced the propagation of the olefins-based cycle and a concomitant 1.7-fold decrease in ethene/2MBu was observed. Co-feeding toluene at 548 K, on the other hand, enhanced the propagation of aromatics-based cycle and a 2.1-fold increase in ethene/2MBu was observed. The ethene/2MBu also increased from 1.2 to 2.1 as conversion increased from 5 – 62%; a concomitant increase in ethene and MBs selectivity was also observed. Ethene/2MBu varied systematically with feed composition and conversion, therefore showing that this ratio can be used to describe the relative propagation of the aromatics- and olefins-based catalytic cycles on HZSM-5.

Selectivity toward light olefins, for the reaction of DME at 623 K, increased monotonically from 22% on a zeolite with small (~1.5 nm) crystallites to 47% on a zeolite sample with large (~17 μm) crystallites, at 46 – 59% net DME conversion. Ethene selectivity, for the reaction of DME at 623 K, also increased monotonically from 5.7% on the HZSM-5 sample with low aluminum content (Si/Al = 1580) to 16% on the HZSM-5 sample with high aluminum content (Si/Al = 55), at 46 – 55% net DME conversion. Light olefins selectivity increases systematically with crystallite size or aluminum content in a zeolite because of increased interactions between MBs (which are precursors to ethene) and the catalytically active Brønsted acid sites. This enables these MBs to undergo

multiple methylation/dealkylation reactions before exiting the zeolite crystallite. A single-value descriptor – representing the average number of Brønsted acid sites that a MB molecule will encounter before it exits the zeolite crystallite – was used to describe the combined effects of aluminum content and crystallite size on ethene selectivity.

Co-feeding oxygenates (like acetaldehyde) increases the concentration of MBs inside the zeolite pores, which in turn increases the propagation of aromatics-based catalytic cycle and consequentially results in higher ethene selectivity. Ethene selectivity increased monotonically from 9.3% without co-feed to 15% in the presence of ~4% acetaldehyde co-feed. Ethene/2MBu also increased monotonically from 1.3 to 2.5 in the presence of ~4% acetaldehyde. In an isotopic experiment where $^{13}C_2$-acetaldehyde was co-reacted with unlabeled DME and methanol on HZSM-5, ethene present in the effluent was enriched with two ^{13}C labels and the net ^{13}C content in ethene (11 – 12%) was higher than the ^{13}C-content in MBs (5 – 6%). Ethene, therefore, besides being formed via aromatic-dealkylation reactions from MBs, was also being produced from $^{13}C_2$-acetaldehyde or its aldol-condensation products via a direct synthesis route.

Increasing the reaction temperature from 548 K to 723 K on HZSM-5 increased the propagation of the olefins-based cycle and a decrease in the ethene/2MBu from 2.1 to 0.4 was observed, suggesting that olefins-based catalytic cycle is favored at high temperatures. Under reaction conditions that resulted in complete DME/methanol conversion, the catalyst bed comprises of two stages: the first-stage performs MTH chemistry in the presence of DME and methanol; the second-stage begins after all DME or methanol is consumed. The aromatic methylation/dealkylation cycle is shut down in this stage of the catalyst bed. Olefin inter-conversion reactions, however, continue to propagate and produce light olefins via β-scission in the second-stage of the catalyst bed.

Table of Contents

List of Tables

List of Figures

List of Schemes

2,2-dmb:	2,2-Dimethylbutane
2MBu:	2-Methylbutane + 2-methul-2-butene
BET:	Brunauer-Emmett-Teller
BJH:	Barrett-Joyner-Halenda
DFT:	Density functional theory
DME:	Dimethyl ether
DTBP:	2,6-Di-*tert*-butylpyridine
ESCA:	Electron spectroscopy for chemical analysis
FID:	Flame ionization detector
FT-IR:	Fourier transform-infrared
GC:	Gas chromatograph
HexaMB:	Hexamethylbenzene
HTI:	Hydrogen transfer index
ICP-OES:	Inductively coupled plasma-optical emission spectroscopy
LHSV:	Liquid hourly space-velocity
MAS-NMR:	Magic angle spinning-nuclear magnetic resonance
MB:	Methylbenzene
MeOH:	Methanol
MFI:	Mordenite framework inverted
MS:	Mass spectrometer

MSD: Mass selective detector

MTG: Methanol-to-gasoline

MTH: Methanol-to-hydrocarbons

MTO: Methanol-to-olefins

MTP: Methanol-to-propene

PentaMB: Pentamethylbenzene

SEM: Scanning electron microscopy

TCD: Thermal conductivity detector

TEM: Transmission electron microscopy

TEOS: Tetraethyl orthosilicate

TetraMB: Tetramethylbenzenes

TOS: Time-on-stream

TPPO: Triphenylphosphine oxide

TriMB: Trimethylbenzene

WHSV: Weighted hourly space-velocity

XPS: X-ray photoelectron spectroscopy

XRD: X-ray diffraction

ZSM-5: Zeolite Socony Mobil – 5

CHAPTER ***ONE***

An Introduction to Methanol-to-Hydrocarbons Conversion

1.1 Motivation

Conversion of C_1-feedstock to liquid hydrocarbon fuels and petrochemicals is a promising approach towards replacing current petroleum-based feedstock with alternative feedstock such as coal, natural gas, and biomass. Methanol-to-hydrocarbons (MTH) conversion over zeolites represents one such technology with emerging commercial interest in the conversion of methanol to a wide variety of hydrocarbons, including light olefins,[1–3] gasoline-range hydrocarbons,[4–7] and aromatics.[8,9]. Several industrial processes have been developed and commercialized using this technology, such as the methanol-to-gasoline (MTG) process by Mobil,[10–12] the methanol-to-olefins (MTO) process by UOP and Norsk Hydro,[13] and the methanol-to-propene (MTP) process by Lurgi.[14]

1.2 The Mechanism of Methanol-to-Hydrocarbons Chemistry

Catalytic conversion of methanol or dimethyl ether (DME), its dehydration product, on acidic zeolite catalysts proceeds via the indirect hydrocarbon-pool mechanism, first proposed by Dahl and Kolboe.[15–19] In this mechanism, unsaturated hydrocarbons (olefins and aromatics) present inside the zeolite pores, together with the Brønsted acid sites, act as organic-inorganic hybrid co-catalysts for the production of hydrocarbons and result in the complex product distribution observed in the effluent.[15–22] The hydrocarbon pool mechanism comprises of two distinct catalytically active reaction cycles: an aromatics-based catalytic cycle and an olefins-based catalytic cycle.

In the olefins-based catalytic cycle, light olefins are methylated by methanol or DME to form higher olefins, which subsequently undergo *β*-scission to complete the reaction cycle. In the aromatics-based catalytic cycle, methylbenzenes (MBs) are methylated to form more-substituted MBs, which then dealkylate and produce light olefins to complete the catalytic cycle. These two catalytic cycles are not independent of one another as C_6+ olefins can undergo hydrogen transfer and cyclization to form MBs, which, on the other hand, can dealkylate and produce olefins. These two catalytic cycles are simultaneously active inside the zeolite pores and the product distribution in MTH can be viewed as a consequence of their relative rates of propagation.

1.3 Relative Propagation of Aromatics-Based and Olefins-Based Cycles

Quantifying the relative extents of propagation of the aromatics-based and the olefins-based catalytic cycles and understanding how these cycles contribute to the overall product distribution is critical for developing structure-function relationships for MTH catalysts. In Chapter 3, we report that the ratio of synthesis rates of ethene and the 2-methylbutane + 2-methyl-2-butene (referred to as ethene/2MBu) can be used to describe the relative propagation of aromatics- and olefins-based catalytic cycles. Ethene is primarily produced from the aromatics-based cycle while 2-methyl-2-butene and its hydrogen transfer product,2-methylbutane, are primarily produced in the olefins-based catalytic cycle. The co-reaction of ^{12}C-ethene or ^{12}C-isobutane with ^{13}C-DME on HZSM-5 at 623 K showed that the rate of DME conversion (1.6 – 1.8 mol C (mol Al s)$^{-1}$) was ~20 times faster than either ethene conversion rate (0.08 mol C (mol Al s)$^{-1}$) or isobutane conversion rate (0.09 mol C (mol Al s)$^{-1}$), suggesting that ethene can be considered a terminal product of the aromatics-based cycle while alkanes (like isobutane or 2-methylbutane) can be considered termination products of the olefins-based cycle.

At iso-conversion conditions at ~548, propene was co-reacted with DME to increase propagation of the olefins-based cycle and correspondingly a 1.7-fold decrease in the ethene/2MBu yield was observed. Similarly, co-reacting of toluene or *p*-xylene with DME increased the propagation of the aromatics-based cycle and a 2.1-fold increase in the ethene/2MBu yield was observed. Ethene/2MBu yield also increased from 1.2 to 2.1 as DME conversion increased from 5 to 62%, which was consistent with the observed concurrent increase in selectivity to ethene and MBs. Increasing reaction temperature from 548 K to 723 K increased the propagation of the olefins-based cycle and a concomitant decrease in the ethene/2MBu yield from 4.7 to 1.3 was noted. Ethene/2MBu yield varies systematically with feed composition, conversion, and reaction temperature, suggesting that this ratio can be used to describe the relative extents of propagation of the aromatics- and the olefins-based catalytic cycles on HZSM-5.

1.4 Effects of Zeolite Crystallite Size on Light Olefins Selectivity

Light olefins selectivity increases with zeolite crystallite size because intra-crystalline residence time of MBs increases as a consequence of increased transport restrictions, which enables these MBs to undergo multiple methylation/dealkylation reactions before exiting the zeolite crystallite. In Chapter 4, we show that light olefins selectivity, for the reaction of DME at ~623 K, increased monotonically from 22% on a zeolite with small (~1.5 nm) crystallites to 47% on a zeolite with large (~17 μm) crystallites at 46 – 59% net DME conversion. Transport restrictions were also introduced externally in a conventional MFI-type zeolite (with ~500 nm crystallites) by single- or multi-cycle silylation using TEOS. Light olefins selectivity, for the reaction of DME at ~623 K and at 46 – 59% net DME conversion, increased from 33% on the conventional zeolite sample to 49% on the sample that was silylated three times. Adsorption uptake measurements of

2,2-dimethylbutane were used to estimate the effective crystallite size of the silylated zeolite samples. The total light olefins selectivity and ethene/2MBu yield increased systematically with the effective crystallite size for all zeolite samples investigated, irrespective of their provenance, thereby suggesting that the mechanistic basis for the increase in light olefins selectivity with increasing crystallite size is the enhanced propagation of aromatics-based cycle relative to the olefins-based cycle.

1.5 Methanol-to-Hydrocarbons Conversion on Diffusion-Free MFI Zeolites

In Chapter 5, we report the intrinsic (i.e., in the absence of any diffusion limitations) propagation of the aromatics-based and the olefins-based catalytic cycles inside the pores of MFI-type zeolites (assessed using diffusion-free zeolite samples) and the contribution of these catalytic cycles towards ethene production at high – industrially relevant – reaction temperatures (>723 K) and <100% DME conversion conditions. Diffusion-free zeolites exhibited low ethene selectivity (<2.8%) for the catalytic reaction of DME to hydrocarbons at ~723 K. Co-feeding toluene or *p*-xylene with DME increased the number of chain carriers of the aromatics-based catalytic cycle, thereby enhancing its propagation, and resulted in a 2- to 3-fold increase in ethene selectivity. Co-feeding propene or 1-hexene, however, did not have any effect on the observed product distribution. A systematic investigation on diffusion-free MFI samples allowed us to infer that (i) MFI is a poor ethene synthesis catalyst in the absence of diffusion limitations, (ii) the number of chain carriers of the olefins-based catalytic cycle is saturated inside the pores of MFI at <100% DME conversion conditions, (iii) the aromatics-based catalytic cycle is intrinsically suppressed due to low concentration of MBs inside the zeolite pores, and (iv) the low ethene selectivity in diffusion-free MFI samples (<2.8%) can be enhanced 2- to 4-fold by co-feeding aromatics like toluene or *p*-xylene with DME.

1.6 Effects of Aluminum Content on Light Olefins Selectivity

Increasing aluminum content increases the concentration of Brønsted acid sites in the zeolite, which increases the average number of Brønsted acid sites that a MB molecule will encounter before it exits the zeolite crystallite. This enables these MBs to undergo multiple methylation/dealkylation reactions and produce light olefins in the process. In Chapter 6, we report that ethene selectivity, for the reaction of DME at ~623 K and iso-conversion conditions, increased monotonically from 5.7% on an HZSM-5 sample with low aluminum content (Si/Al = 1580) to 16% on an HZSM-5 sample with high aluminum content (Si/Al = 55). Ethene/2MBu yield also increased monotonically from 0.80 to 2.4 suggesting increased propagation of the aromatics-based cycle with increasing aluminum content. Adsorption uptake measurements of 2,2-dimethylbutane were used to estimate the average crystallite size of HZSM-5 samples. A single-value descriptor – which is a representative of the average number of Brønsted acid sites that a MB molecule will encounter before it exits the zeolite crystallite – is proposed to describe the combined effects of aluminum content and crystallite size on ethene selectivity in MTH conversion.

1.7 Effects of Oxygenate Co-Feed on MTH Product Distribution

Co-feeding acetaldehyde increases the concentration of MBs inside the zeolite pores, which in turn enhances the propagation of aromatics-based catalytic cycle and results in higher ethene selectivity. In Chapter 7, we report that co-feeding acetaldehyde (1 – 4%) with DME on HZSM-5 at ~673 K resulted in a monotonic increase in selectivity towards ethene (from 9.3 to 15%) and MBs (from 4.9 to 7.8%). The mechanistic basis for this increase is acetaldehyde undergoing multiple aldol-condensation reactions to form higher homologues that subsequently undergo ring-closure followed by dehydration to

form aromatics. In an isotopic experiment where $^{13}C_2$-acetaldehyde (~4%) was co-reacted with unlabeled DME on HZSM-5 at ~673 K, ethene present in the effluent was enriched with two ^{13}C labels and the net ^{13}C-content in ethene (11 – 12%) was higher than the ^{13}C-content in MBs (5 – 6%). Ethene, therefore, besides being formed via aromatic-dealkylation, is also being produced from $^{13}C_2$-acetaldehyde or its aldol-condensation products via a direct synthesis route.

1.8 Effects of Reaction Temperature and Space-Velocity on MTH Product Distribution

Reaction temperature and space-velocity vary the relative extents of propagation of the aromatics-based and the olefins-based catalytic cycles and consequentially have an effect on the observed product distribution. In Chapter 8, we report that selectivity to C_3+ olefins increases, while ethene and MBs selectivity decreases, with increasing reaction temperature (from 623 K to 723 K), suggesting that that at higher temperatures the olefins-based cycle is favored over the aromatics-based cycle, and vice versa. A concomitant decrease in ethene/2MBu yield was also observed with increasing reaction temperature. We also report the effects of varying space-velocity on the product distribution of DME conversion at ~723 K. DME space-velocity was varied between 0.3 and 17 mol C (mol Al-s)$^{-1}$. Complete conversion was achieved at space velocities ≤2.5 mol C (mol Al-s)$^{-1}$. Under reaction conditions that resulted complete DME conversion, the catalyst bed comprised of two stages: the first-stage of the catalyst bed performs MTH chemistry in the presence of a methylating agent; the second-stage begins after all DME and methanol is consumed and the aromatic cycle is shut down in this stage of the catalyst bed. Downstream olefin inter-conversion reactions, however, continue to propagate and produce ethene in the second-stage of the catalyst bed.

CHAPTER TWO

The Mechanism of Methanol-to-Hydrocarbons Catalysis

2.1 Introduction to Methanol-to-Hydrocarbons Conversion

Meeting the ever-increasing energy demand is a major technological challenge faced by the world in the twenty-first century.[23,24] As the global energy demand will increase and the supply of crude oil will dwindle, the need to develop alternative non-petroleum based energy sources such as coal, natural gas, and biomass, will become necessary to supply the world with liquid hydrocarbon fuels and chemicals.[25–29] The methanol-to-hydrocarbons (MTH) technology is the final processing step in converting these alternative feedstocks to current and future generation energy carriers as well as important organic chemicals and will therefore play an important role in meeting the requirements of the future. Any gasifiable carbon-rich feedstock can be reacted with steam and/or O_2 and transformed into synthesis gas ($CO + H_2$) that can be converted to methanol over mixed metal oxide catalysts (e.g. $Cu/ZnO/Al_2O_3$).[30] Methanol and its dehydration product, dimethyl ether (DME), can be subsequently converted on solid acid zeolites (HZSM-5, HSAPO-34, HBEA, etc.) to form hydrocarbons (Figure 2.1). There are two major

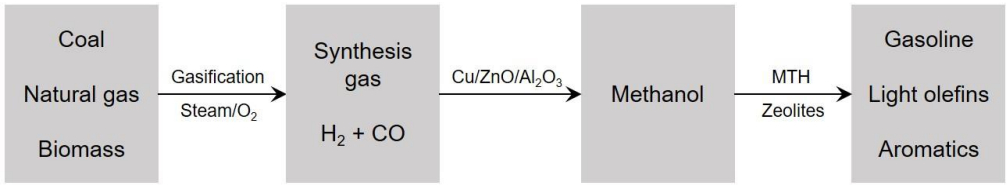

Figure 2.1: Conversion of alternative non-traditional carbon-based feedstocks to light olefins, aromatics, and gasoline-range hydrocarbons.

advantages of following this approach: (i) the final products do not depend on the source of carbon, and (ii) a high degree of flexibility is available in the choice of the final products.

The shape selective catalytic features of zeolites enable the formation of C-C bonds and at the same time the small sub-nanometer pore size restricts the length of formed carbon chains.[31–35] The MTH process therefore allows methanol to be converted to a wide variety of hydrocarbons products, including light olefins,[1–3] gasoline-range hydrocarbons,[4–7] and aromatics.[8,9] Gasoline is an important and efficient energy carrier while light olefins and aromatics play a significant role in chemical industry as raw materials and polymer precursors. The selectivity of MTH to any particular class of hydrocarbons varies with catalyst topology and morphology, feed composition, as well as reaction conditions like temperature and space-velocity.[1,32,36–39] Several industrial processes have been developed and commercialized using this technology, such as the methanol-to-gasoline (MTG) process by Mobil,[10–12] the methanol-to-olefins (MTO) process by UOP and Norsk Hydro,[13] and the methanol-to-propene (MTP) process by Lurgi.[14]

2.1.1 Zeolites as Solid Acid Shape-Selective Catalysts

Zeolites are crystalline microporous aluminosilicate materials. Currently, 231 different zeolite frameworks have been identified and classified by the International Zeolite Association.[40] The network of interconnected channels and cavities in the zeolites produces solids with very high surface area and pore volume that can adsorb large quantities of hydrocarbons making zeolites commonly used catalysts in the petrochemical

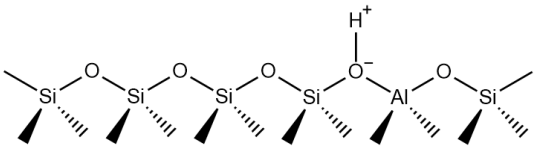

Figure 2.2: Catalytically active Brønsted acid sites in the aluminosilicate framework of zeolites.

industry. The aluminosilicate framework of zeolites consists of SiO_2 tetrahedrons with some degree of aluminum substitution. The framework becomes negatively charged when lattice Si^{4+} cations are replaced by lattice Al^{3+} cations. This excess negative charge in the framework is compensated by the presence of positively charged ions, commonly Na^+, NH_4^+ or H^+. The hydroxyl group that results when the counter-ion is a proton accounts for the catalytically active Brønsted acid sites in the zeolites (Figure 2.2).

ZSM-5 is the catalyst of choice in several commercial MTH processes like the MTP® process by Lurgi[14] and the MTG process by Mobil.[7] In fact, interest in MTH was triggered following the synthesis of ZSM-5 molecular sieves at Mobil Research Laboratories in the early 1970s.[4,7,41,42] ZSM-5 is a medium pore 10-membered ring zeolite with MFI type framework.[42,43] The structural framework of ZSM-5 consists of intersecting straight channels (with elliptical cross-section of diameter 0.51 nm × 0.55 nm) [42,43] and sinusoidal channels (with nearly circular cross-section of diameter 0.54 nm × 0.56 nm).[42,43] The channel intersections have a diameter of ~0.9 nm.[44,45] Figure 2.3a and Figure 2.3b show the cross-sections of straight channels and sinusoidal channels in ZSM-5 as viewed along [010] and [100], respectively.

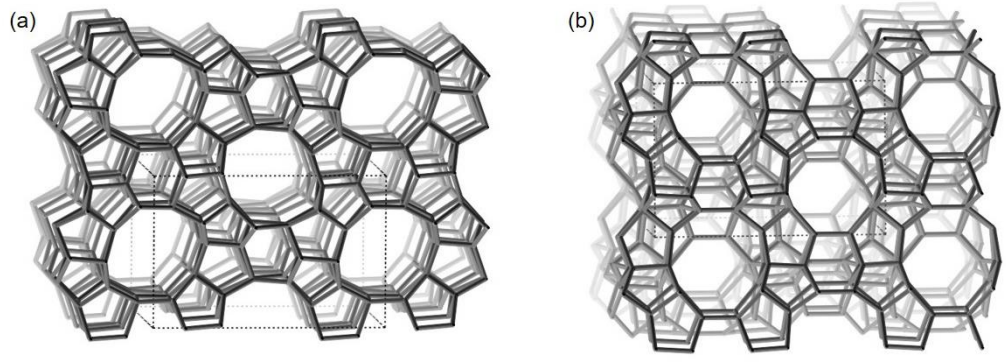

Figure 2.3: Cross-sections of (a) straight channels (0.51 nm × 0.55 nm) as viewed along [010] axis,[40] and (b) sinusoidal channels (0.54 nm × 0.56 nm) as viewed along [100] axis.[40]

2.2 The Hydrocarbon Pool Mechanism

Lesthaeghe et al.[46–48] performed density functional theory (DFT) calculations using ONIOM methods on pentatetrahedral zeolite clusters to extensively investigate several reaction pathways of C-C bond formation from methanol but could not find a direct reaction pathway of C-C coupling due to either unstable intermediates or formidably high activation energy barriers (<200 kJ mol^{-1}). Marcus et al.[49] pulsed a dimethyl ether isotopomer, CH_3OCD_3, over [H/D]-SAPO-34 (comprising of 50% H^+ sites and 50% D^+ sites) at 573 K thus allowing for the formation of Zeo-(O)-CH_3 and Zeo-(O)-CD_3 species on the surface, where Zeo-(O)- represents an active catalytic site. After giving the surface methoxy groups two hours to undergo H/D exchange, they pulsed the bed with a 1:1 mixture of H_2O and D_2O in order to sweep out the methyl groups as a mixture of DME isotopomers.[49] The isotopic analysis of DME isotopomers showed ~25% d_0-DME, ~50% d_3-DME, and ~25% d_6-DME, which confirmed that H/D exchange did not take place and that there was no C-H or C-D bond activation.[49] As C-H bond activation is necessary for direct C-C coupling reactions, these experimental findings support the hypothesis that direct C-C bond formation does not occur in zeolites during methanol conversion.

Song et al.[50] pulsed methanol containing <11 ppm total organic impurities over a highly purified catalyst bed and analyzed the effluent stream 2.4 s after the pulsing. The yield of hydrocarbons in the product stream was only 26 ppm for HSAPO-34 and 240 ppm for HZSM-5 after the first methanol pulse.[50] The hydrocarbon yields, however, significantly increased in case of the second and third methanol pulses when the catalyst bed contained hydrocarbons form the previous methanol pulse.[50] The hydrocarbon yields were also considerably higher when relatively impure methanol (containing ~36 ppm ethanol and ~100 ppm total impurities) was used in a similar experiment, highlighting the role of

the hydrocarbon impurities in methanol conversion.[50] These experimental evidences suggest that the rate at which methanol reacts with the trace impurities in the feed or in the catalyst bed is significantly faster than the rate at which direct C-C coupling proceeds. These experimental and theoretical findings provide strong evidence against direct C-C coupling and suggest that methanol conversion over zeolites proceeds via an indirect hydrocarbon-pool mechanism, first proposed by Dahl and Kolboe.[15–19] In this mechanism, unsaturated molecules trapped inside the zeolite pores act as co-catalytic species and constantly interact with the Brønsted acid sites in the zeolite framework leading to low energy pathways for the conversion of methanol to hydrocarbons.

2.2.1 Aromatics as Active Hydrocarbon Pool Species

Langner et al.[51] observed that $t_{1/2}$ (defined as time-on-stream, after which 50% conversion to hydrocarbons was achieved) decreased from 160 min with no co-feed to 9 min when small amounts of cyclohexanol (3.6×10^{-3} mol%) was co-reacted with methanol on HZSM-5. The strong influence of cyclohexanol on the kinetic induction period indicates the important role of cyclic compounds in MTH catalysis. Mole et al.[52,53] observed that conversion of methanol over HZSM-5 was enhanced by co-feeding toluene. Song et al.[22] reported that methanol conversion increased from 14% to 100% on HSAPO-34 when they compared the activity of a fresh catalyst to that of another catalyst that was pretreated with a methanol pulse to form MBs within zeolite pores. These experimental observations suggest that aromatics, in particular MBs, play an important role in MTH as active hydrocarbon pool species. Mikkelsen et al.[54] investigated the methylation of ^{12}C-toluene with ^{13}C-methanol on ZSM-5 and reported incorporation of ^{12}C atoms from toluene into ethene and propene. Their results provide further evidence that MBs are active species for light olefin production (Scheme 2.1).

2.2.2 Olefins as Active Hydrocarbon Pool Species

Ono and Mori[55] showed that co-processing ethene or *cis*-2-butene with methanol, reduces the induction period of methanol conversion by a factor of 2 and 4, respectively, compared to the reaction of methanol alone on HZSM-5 at 512 K. Chen and Reagan[56] studied the reaction rates for methanol conversion in an isothermal reaction system and concluded that the rate of olefin formation via an autocatalytic route is 50 times faster than the rate of initial formation of olefins, thus noting the autocatalytic effect of olefins in MTH reactions for the first time. Langner et al.[51] observed that co-feeding small amount of linear alcohols, which readily dehydrate to olefins under reaction conditions, resulted in a 2- to 4-fold decrease in the kinetic induction period. Dessau and LaPierre[57,58] studied the co-reaction of methanol with 1-hexene or 1-heptene over HZSM-5 and proposed an olefins-based catalytic cycle for methanol conversion. Light olefins may be methylated by methanol to form higher olefin homologues that can either crack to form light olefins, or undergo hydrogen transfer and cyclization to form aromatics and alkanes. These experimental findings suggest that olefins, like aromatics, also play an important role in MTH as active hydrocarbon-pool species (Scheme 2.1).

2.2.3 The Dual Cycle Hydrocarbon Pool Mechanism in MTH Catalysis

Isotopic switching experiments performed by Svelle, Bjørgen and coworkers,[20,59,60] in which ^{12}C-methanol was reacted over ZSM-5 at 623 K for 18 min followed by a rapid switch to ^{13}C-methanol under steady state conditions, showed that the fraction of ^{13}C-atoms incorporated in ethene after the switch closely matched the ^{13}C-content of MBs suggesting that ethene and MBs originate from the same catalytic cycle. In the same, set of experiments, a similar rate of ^{13}C-incorporation in C_3+ olefins implied that C_3+ olefins are a part of another catalytic cycle.[20,59,60] These experimental evidences delineated MTH

chemistry into two different catalytic cycles: an aromatics-based catalytic cycle and an olefins-based catalytic cycle. In the aromatics-based catalytic cycle, MBs dealkylate light olefins and form lower MB homologues, which are subsequently methylated to complete the catalytic cycle. In the olefins-based catalytic cycle, light olefins are methylated to form higher olefins that can crack to form light olefins, undergo isomerization, or undergo hydrogen transfer and cyclization reactions to produce aromatics and alkanes. The two catalytic cycles are not independent of each other as MBs can dealkylate to form propene or butene, and higher olefins can undergo cyclization and hydrogen transfer to form MBs. The observed MTH product distribution can therefore be viewed in terms of contribution from these reaction types: (i) olefin methylation, (ii) olefin cracking, (iii) hydrogen transfer, (iv) cyclization, (v) aromatic methylation, and (vi) aromatic dealkylation (Scheme 2.1).

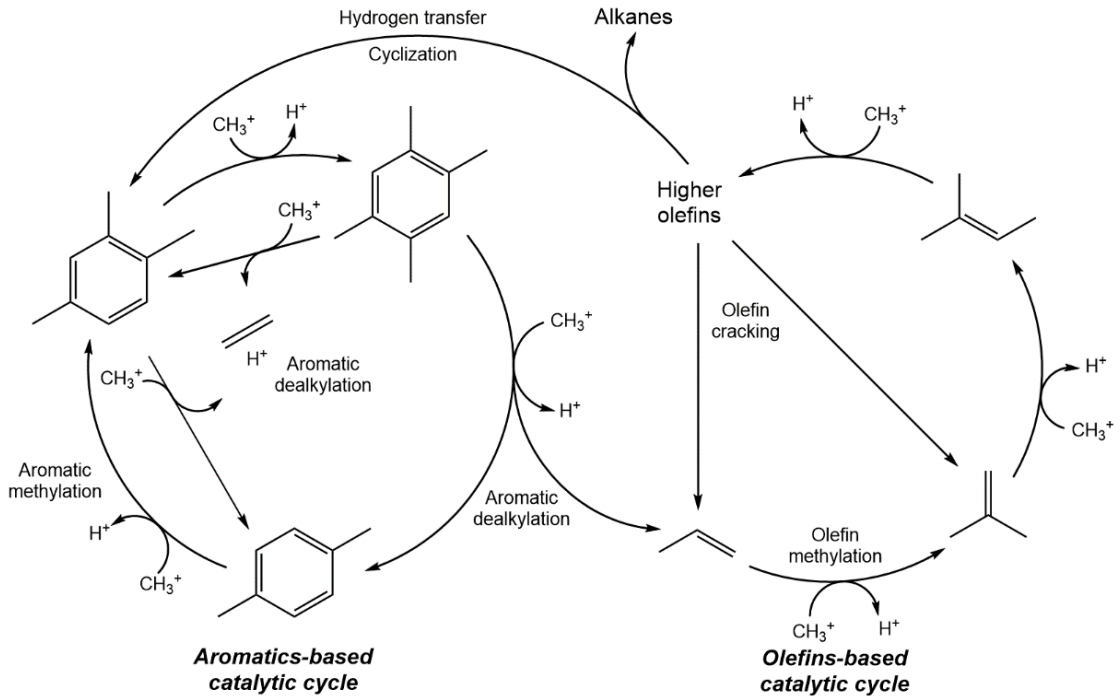

Scheme 2.1: A schematic of the aromatics-based and the olefins-based catalytic cycles in MTH conversion.

2.2.4 MTH Catalysis on Zeolites: A Carbocation-Based Chemistry

The first step in the MTH catalytic process is the equilibration between methanol, dimethyl ether, and water that results in a surface saturated by methoxy groups. The methanol molecule is physisorbed or chemisorbed on the surface, which eventually leads to the formation of surface methoxy groups and elimination of a water molecule (Scheme 2.2). The surface methoxy groups react with the hydrocarbons present in the gas phase to form adsorbed alkoxide species. The adsorbed alkoxides can either desorb to regenerate the acid site or undergo subsequent reactions. For example, *β*-scission results in the elimination of an alkene and formation of another surface alkoxide, which can eventually desorb as another alkene and regenerate the Brønsted acid site. A schematic of methylation of 2-hexene to form the corresponding surface alkoxide followed by *β*-scission to form 3-methyl-1-butene and ethene is presented in Scheme 2.3.

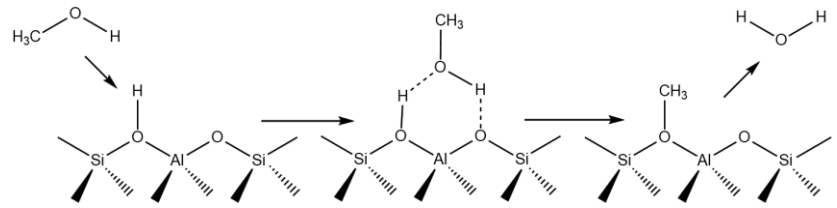

Scheme 2.2: Reaction of methanol and formation of surface methoxy groups on the Brønsted acid sites in the zeolites.

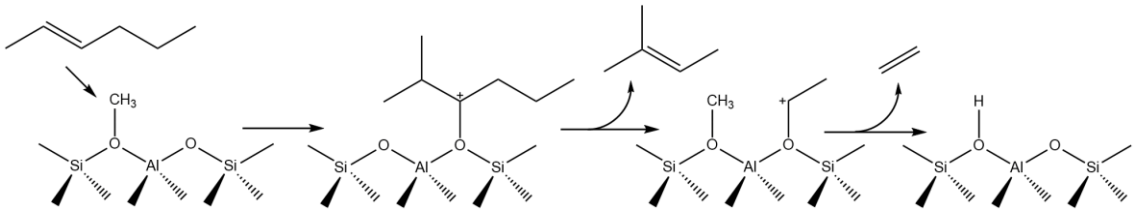

Scheme 2.3: Methylation of 2-hexene to form corresponding alkoxide followed by *β*-scission to form 3-methyl-1-butene and ethene.

2.2.5 Light Olefins Production from Aromatic Dealkylation Reactions

Isotopic experiments that involved co-reactions of ^{13}C-labeled MBs with methanol or DME on HZSM-5 and HBEA have shown that ethene and propene contain carbon atoms originating from the labeled MBs.[52,54,61,62] These observations suggest that ethene and propene are mechanistically linked to MBs. Experimental and theoretical studies have postulated that these light olefins are formed from MBs via (i) side-chain methylation mecahnism,[52,53,63–66] (ii) paring (ring-contraction) mechanism,[67,68] or (iii) ring-expansion mechanism.[69] These mechanisms are initiated by the methylation of an already methylated ring-carbon in the MB to form a gem-methylated species.[70]

In the side-chain methylation mechanism, which was first introduced by Mole et al.,[52,53] the formed methylbenzenium cation can deprotonate to form an exocyclic double bond. The exocyclic double bond can get methylated to form a carbocation with a side ethyl group, which can either eliminate an ethene molecule by intramolecular hydrogen shift or lose a proton to the zeolite framework. The so formed exocyclic double bond can undergo further methylation to form a carbocation with a side isopropyl group, which can eliminate a propene molecule or undergo deprotonation followed by further methylation eventually leading to the elimination of an isobutene molecule. The original MB can be regenerated by a series of methyl/proton shifts to complete the cycle.[71]

In the paring mechanism, on the other hand, the gem-methylated carbenium ion undergoes a ring-contraction step to form a bicyclic intermediate.[68] In the elimination of propene, an intramolecular hydrogen-shift leads to the formation of another bicyclic species that can split-off propene to form a methylcyclopentadienyl cation. Alternatively, in the elimination of isobutene, an intramolecular methyl shift results in the formation of a methylcyclopentadienyl cation with a *tert*-butyl group, which can split-off isobutene. The

regeneration of original MB from the methylcyclopentadienyl cation involves ring-expansion facilitated by protonation and deprotonation between the organic intermediate and the zeolite framework, and subsequent methylation steps.[68] The paring mechanism, however, does not explain the elimination of ethene from MBs.[69] Arstad et al.[69] suggested a mechanism that involves ring-expansion to a seven-membered carbon ring that can eventually lead to the elimination of ethene from MBs.

Ilias et al.[36] performed isotopic experiments on HZSM-5 where ^{12}C- or ^{13}C-labeled dimethyl ether was co-reacted with isotopically labeled toluene, *p*-xylene, or 4-ethyltoluene at 523 – 723 K. The ^{13}C-content in ethene and propene was predicted, based on the side-chain, paring (ring-contraction), or the ring-expansion mechanisms, from the isotopologue distribution of various MBs present in the reaction effluent. The predicted ^{13}C content of ethene and propene formed from 1,2,4-triMB and 1,2,4,5-tetraMB via the paring mechanism matched the experimentally observed ^{13}C content of ethene and propene, suggesting that 1,2,4-triMB and 1,2,4,5-tetraMB are the dominant precursors to ethene and propene in MTH conversion on HZSM-5.[36]

2.3 Tuning Light Olefins Selectivity in MTH Conversion

The observed hydrocarbon selectivity in MTH can be viewed as a consequence of the relative propagation of the aromatics- based and the olefins-based catalytic cycles.[36,72] Increased propagation of the olefins-based catalytic cycle increases the selectivity towards C_3+ olefins,[72–75] while increased propagation of the olefins-based catalytic cycle increases selectivity towards ethene and MBs. [72–75] The relative rates of propagation of these two catalytic cycles, and consequentially the observed MTH product distribution, can be systematically tuned by independently varying (i) feed composition (by co-feeding hydrocarbons or oxygenates), (ii) concentration of Brønsted acid sites (by varying the

aluminum content in the zeolite), and (iii) the diffusion characteristics of the zeolite (by varying the crystallite size or by silylation treatment).

2.3.1 Effects of Feed Composition on MTH Product Distribution

Ilias et al.[72,73] showed that co-feeding small amounts of propene (4 kPa) with DME (70 kPa) on HZSM-5 at 548 – 623 K increased the propagation of the olefins-based catalytic cycle and resulted in higher selectivity toward C_3+ aliphatic hydrocarbons. Experimental investigation by Sun et al.,[74,75] on the other hand, showed that co-feeding C_3 – C_6 olefins (10 – 40 C%) with methanol at higher temperature (~723 K) and complete DME conversion conditions did not selectively enhance the propagation of the olefins-based catalytic cycle, and no increase in C_3+ selectivity was observed. Sun et al. [74,75] suggested that the addition of olefins enhanced the aromatization of higher olefins, which increased the concentration of aromatics inside the zeolite pores, thereby enhancing the propagation of both the aromatics-based and the olefins-based catalytic cycles simultaneously. The relative propagation of the olefins-based catalytic cycle was therefore not affected by the C_3 – C_6 olefin co-feed. [74,75]

Ilias et al.[72,73] showed that co-feeding aromatics like toluene or *p*-xylene (4 kPa) with DME (70 kPa) on HZSM-5 at 548 – 723 K favored the aromatics-based catalytic cycle and resulted in higher selectivity toward ethene and MBs. Sun et al., [74,75] in an independent experimental study, also showed that cofeeding aromatics like benzene, toluene, or *p*-xylene with methanol on HZSM-5 at ~723 K enhanced the propagation of the aromatics-based methylation/dealkylation cycle and resulted in higher ethene selectivity. These experimental findings suggest that increased propagation of the olefins-based catalytic cycle results in higher selectivity toward C_3+ olefins. MBs and ethene, on the other hand,

are selectively formed under reaction conditions that favor the aromatics-based catalytic cycle over the olefins-based catalytic cycle.

Co-feeding oxygenates like aldehydes, ketones, furans, and alcohols, also affects the relative propagation of aromatics- and olefins-based cycles and consequentially the observed MTH product distribution. Aldehydes undergo multiple aldol-condensation on Brønsted acid sites to form higher homologues that can subsequently undergo ring-closure followed by dehydration to form MBs. Chang and Ko[76] investigated the vapor-phase reaction of acetaldehyde on zeolite HX at ~673 K and ~26% conversion, and observed ~8% selectivity toward 3-hydroxybutanal (the aldol-condensation product of acetaldehyde) and ~47% selectivity toward 2-butenal (the dehydration product of 3-hydroxybutanal). Chang and Silvestri[77] investigated the catalytic conversion of propanal on HZSM-5 at ~644 K and high conversion (>99.9%) and reported >80% selectivity toward aromatics in the reaction effluent. Hoang et al.,[78] in another experimental study, also reacted propanal on HZSM-5 at ~673 K and ~76% conversion and reported ~41% selectivity toward aromatics. Hutchings et al.[79] reacted propanal on zeolite β at ~643 K and ~31% conversion and reported ~60% selectivity to benzene, toluene, and xylenes.

2.3.2 Effects of Morphology and Chemical Composition on MTH Product Distribution

Sugimoto et al.[80] studied the effects of crystallite size on the catalytic properties of HZSM-5 and showed that ethene selectivity increases from 0.7% in HZSM-5 with <200 nm crystallites to 12.9% in ZSM-5 with larger crystallites (3 – 4 μm); propene selectivity increased from 1.5% to 9.6%. This increase in light olefin selectivity was attributed to the improved product shape selectivity of the catalyst, which favored smaller hydrocarbons that can easily diffuse out of the crystallite.[80] Rownaghi et al.[81,82] synthesized HZSM-5 nanocrystals (~120 nm) and compared their catalytic performance, for methanol

conversion at ~643 K, with a conventional HZSM-5 zeolite with larger crystallites (wide range) and observed that ethene selectivity in HZSM-5 nanocrystals (6.6%) was lower than that observed in the conventional HZSM-5 sample (9.6%).

Choi et al.[83] synthesized MFI-nanosheets that were only single unit cell thick (~2.5 nm) along the *b*-axis and reported five-time longer catalytic lifetimes and slower coke deposition rates (45 versus 170 mg g^{-1} after 5 days) compared to a conventional MFI zeolite, for methanol conversion at ~673 K. Bleken and coworkers[84] reported that MFI nanosheets exhibited lower C_2 selectivity, and correspondingly a higher C_3-to-C_2 ratio, than a conventional MFI zeolite for MTH conversion at ~623 K. More recently, Kim and Ryoo[85] investigated the effects of external Brønsted acid sites (which correspond to ~30% of all the Brønsted acid sites) in MFI-nanosheets and showed that external surface does not play any role in MTH chemistry. The external acid sites were poisoned by triphenylphosphine oxide (TPPO), which completely suppressed the catalytic cracking of tri-*iso*-propylbenzene, a reaction that can only occur on the external surface.[85] The MTH conversion at 523 – 653 K was, however, unaffected by TPPO-poisoning.[85]

Wei et al.[86] investigated the effects of aluminum content (SiO_2/Al_2O_3) in HZSM-5 on the product distribution for methanol conversion at ~773 K and reported that ethene selectivity increased from 14.6 mol% on HZSM-5 with SiO_2/Al_2O_3 = 133 to 25.4 mol% on HZSM-5 with SiO_2/Al_2O_3 = 58, while propene selectivity decreased from 43.2 mol% to 32.3 mol%. Wan et al.[87] also studied the effects of aluminum content (SiO_2/Al_2O_3) on methanol conversion to gasoline-range hydrocarbons at ~648 K and reported a monotonic increase in selectivity towards C_1 – C_4 hydrocarbons as SiO_2/Al_2O_3 in ZSM-5 decreased from 411 to 23. The authors also noted a concomitant monotonic increase in aromatics selectivity with decreasing SiO_2/Al_2O_3.[87]

2.3.3 Effects of Reaction Conditions on MTH Product Distribution

Chang and Silvestri[77] investigated the effects of space-velocity on methanol conversion to hydrocarbons on HZSM-5 and noted that C_2 – C_5 olefin selectivity decreased, while the selectivity toward paraffins, C_6+ olefins, and aromatics increased with decreasing space-velocity. Chang et al.[88] reported, in independent experimental studies, that C_2 – C_3 olefin selectivity decreased, while selectivity to paraffins and aromatics increased with a decrease in space-velocity after 100% DME/methanol conversion was achieved over HZSM-5 at ~773 K. Chang and Silvestri[77] also investigated the effects of reaction temperature (533 – 841 K) on MTH product distribution over HZSM-5 at a fixed space-velocity. The conversion increased with reaction temperature and reached completion between 613 and 648 K. At lower temperatures, C_2 – C_5 olefins were the predominant products; an increase in temperature was accompanied by an increase in the formation of aromatics suggesting that secondary reactions like hydrogen transfer and cyclization become prominent at higher temperatures. Ilias et al.[73] studied the effects of temperature (548 – 723 K) on MTH product selectivity at <100% DME conversion and showed that ethene selectivity as well as MBs selectivity decreased with an increase in the reaction temperature. Ilias et al.[73] proposed that the decrease in ethene selectivity with increasing reaction temperature is a result of a decrease in the extent of propagation of the aromatics-based cycle relative to the olefins-based cycle. The propagation of the aromatics-based cycle is suppressed at higher temperatures because of a decrease in the number of chain carriers of the aromatics-based catalytic cycle.[73] At 723 K, higher olefins prefer to crack or desorb rather than cyclize and undergo hydrogen transfer reactions, thereby decreasing the concentration of aromatics inside the zeolite pores, which suppresses the propagation of the aromatics-based catalytic cycle.[73]

CHAPTER ***THREE***

Relative Propagation of the Aromatics-Based and the Olefins-Based Catalytic Cycles

* Reported from S. Ilias, R. Khare, A. Malek, A. Bhan, *Journal of Catalysis* **303** (2013) 135–140.

3.1 Introduction

The observed product distribution in MTH can be rationalized as a consequence of the relative extents of propagation of the aromatics-based and the olefins-based catalytic cycles. Ilias et al.[72] showed that co-feeding small amounts of propene (4 kPa) with DME at ~548 K increased the propagation of olefins-based catalytic cycle relative to the aromatics-based catalytic cycle, which resulted in an increase in C_3+ olefin selectivity. Sun and coworkers[74,75] additionally noted that at higher temperature and complete methanol conversion (relevant conditions for industrial processes), addition of C_3 – C_6 olefins (10 – 40 C%) with methanol did not selectively suppress the aromatics-based catalytic cycle relative to the olefins-based catalytic cycle and C_3+ hydrocarbon selectivity remained unchanged. Both Ilias et al.[72] and Sun et al.[74,75] showed that co-feeding aromatics such as benzene, toluene, or *p*-xylene with methanol or DME at 548 – 723 K significantly enhanced the propagation of the aromatics-based cycle and suppressed the olefins-based cycle, resulting in higher selectivity to ethene and MBs.

Quantifying the relative extents of propagation of the aromatics-based and the olefins-based catalytic cycle and understanding how these cycles contribute to the overall product distribution under different reaction conditions is critical for developing structure-

function relationships for MTH catalysts. In the absence of experimental studies detailing kinetic parameters for the various elementary steps in MTH, we propose that the ratio of the synthesis rates of ethene and the sum of 2-methyl-2-butene and 2-methylbutane (referred to as ethene/2MBu) can be used as a descriptor to assess the relative extents of propagation of the aromatics-based and the olefins-based catalytic cycles. We show that this ratio varies systematically and predictably with olefin or aromatic co-feeds at iso-conversion conditions. Co-feeding propene with DME resulted in increased propagation of the olefins-based cycle relative to the aromatics-based cycle, whereas co-feeding toluene or *p*-xylene with DME resulted in increased propagation of the aromatics-based catalytic cycle. In this work, we show that the ethene/2MBu yield is a valid descriptor to assess the relative extents of propagation of the aromatics-based and the olefins-based catalytic cycles as a function of olefin or aromatic co-feeds, reaction temperature, and fractional DME conversion.

3.2 Materials and Methods

3.2.1 Catalyst Preparation and Pretreatment

A conventional ZSM-5 catalyst (referred to as HZSM-5) was obtained in its ammonium form Zeolyst International Inc. (CBV 8014, Si/Al ~43). An HZSM-5 sample with large (~17 μm) crystallites and Si/Al ~38 was synthesized according to the procedure described in Reference 89.The zeolite samples were converted to their protonated forms by treating in 1.67 cm^3 s^{-1} dry air (Minneapolis Oxygen, 20 – 21% O_2, <10 ppm H_2O) at 773 K for 4 h. The temperature was increased from ambient to 773 K in 12 h and was held at 773 K for 4 h before cooling down to the ambient temperature. The catalyst samples were then pressed into pellets, crushed, and sieved between 40- and 80-mesh sieves to obtain uniform particles with size between 180 and 425 μm. Quartz sand (Acros Organics)

was used as a diluent in the catalyst bed to prevent temperature rise due to the exothermic nature of MTH reactions. Prior to its use, the quartz sand was washed with 1 M nitric acid (Sigma-Aldrich), rinsed several times with deionized water, dried, and sieved between 40- and 80-mesh sieves.

3.2.2 Structural and Chemical Characterization

The Si/Al in the zeolite samples was determined by ICP-OES elemental analysis performed by Galbraith Laboratories, Inc. The analytical method used was GLI procedure ME-70. The concentration of Brønsted acid sites was determined by DME titration (performed previously by Chiang et al.)[90] using a tubular packed-bed quartz reactor (10 mm ID) under atmospheric pressure. A mixture of DME/Ar/He (0.17 cm^3 s^{-1}, Praxair, 24.9% DME, 25.1% Ar, and 50% He) was pulsed (with 90 s intervals) over the catalyst bed using He (0.67 cm^3 s^{-1}, Minneapolis Oxygen, 99.995% purity) as the carrier gas. The physisorbed DME and water formed were subsequently removed by treating in He (1.67 cm_3 s^{-1}) for 1.5 – 2.5 h.

Textural characteristics of the zeolite samples were determined by N_2 adsorption-desorption measurements (previously carried out by Liu et al.)[91] at the liquid N_2 boiling temperature (~77 K) on a Quantachrome Instruments Autosorb-1 analyzer. Prior to the measurements, the samples were evacuated overnight at 573 K under high vacuum conditions. The surface area and the pore-size distribution were calculated using the BET and BJH methods, respectively, and *t*-plot methods were used for estimating the micropore volume and external surface area. The powder XRD pattern of HZSM-5 was previously collected by Liu et al.[91] on a Bruker AXS D5005 diffractometer using Cu-Kα radiation (1.54056 Å). The scans were collected for 2θ values between 5° and 55° at a scan rate of 0.02° min^{-1}.

3.2.3 Catalytic Reactions of DME with/without Co-Feeds

A 316/316L stainless steel packed-bed reactor (1/4 in OD; 0.035 in wall thickness), equipped with a concentric thermal well (1/ 16 in OD, 0.014 in wall thickness), was used to carry out the catalytic reactions. The catalyst bed was supported between quartz wool (PerkinElmer) plugs and operated at isothermal conditions using a heating coil (ARi Industries Inc., AeroRod® heating assembly) regulated by a Watlow 96 series temperature controller. Temperature of the catalyst bed was measured using a K-type thermocouple (Omega Engineering) inserted into the concentric thermal well. Prior to every reaction, the catalysts were pretreated in situ in 1.67 cm^3 s^{-1} He (Minneapolis Oxygen, 99.995% purity) at 773 K for 4 h. The temperature was increased from ambient to 773 K in 8 h and was held at 823 K for 4 h before reducing it to the reaction temperature.

The reactions were performed using 4 – 100 mg of catalyst to achieve the desired chemical conversions (5 – 62%). The reactant stream constituted DME (Matheson Tri-Gas, 99.5% purity) and a mixture of CH_4 and Ar (Airgas, 10% CH_4, 90% Ar) that was used as an internal standard for the FID. A balance of He (Minneapolis oxygen, 99.995% purity) was used, if necessary, to keep the concentration of internal standard comparable to the concentration of the effluent products. In some cases, propene (Praxair, 50% propene, 50% Ar), toluene (Sigma-Aldrich, 99.9% purity), or *p*-xylene (Sigma-Aldrich, 99% purity) were co-fed with DME (70 kPa pressure) so that the co-feed partial pressure was ~4 kPa. Gas flow rates were maintained using Brooks Instrument 5850S/SLA5850 series mass flow controllers. Liquids were fed through a 1.0 mL SGE syringe using a Cole Palmer EW-74900-00 syringe pump. The total feed pressure was maintained at 115 – 130 kPa and all reactions were carried out at 548 K, 623 K, or 723 K. The temperature variation in the catalyst bed was less than 1 K during the reaction.

The reactor effluents were analyzed using an online Agilent 7890 series GC – 5975C series MS equipped with a 100% dimethylpolysiloxane Agilent J&W HP-1 column (50 m × 320 μm × 0.52 μm) connected to an FID and a (5%-phenyl)-methylpolysiloxane Agilent J&W HP-5ms column (25 m × 320 μm × 0.25 μm) connected to an MSD. The product distributions shown in Section 3.3 include C_8+ hydrocarbons that were not identified separately and are classified as "Others". The average hydrogen-to-carbon ratio in the hydrocarbon species present in the "Others" fraction was calculated from the hydrogen- and carbon-content of known hydrocarbon species in the converted feed and the reaction effluent, and is reported with the data in some cases.

3.2.4 Catalytic Reactions of ^{13}C-Labeled DME with Unlabeled Ethene or Isobutane

In the case of isotopic co-feed experiments, the reactant stream constituted $^{13}C_2$-DME (IsoTec, 99% purity, 99 atom% ^{13}C), $^{12}C_2$-ethene (Matheson Tri-Gas, chemical purity grade) or $^{12}C_4$-isobutane (Matheson Tri-Gas, chemical purity grade), and the CH_4/Ar internal standard (Airgas, 10% CH_4, 90% Ar). These reactions were run using ~10 mg HZSM-5 catalyst at 623 K. The isotopologue distributions were determined from the mass fragmentation patterns using the method outlined by Price and Iglesia.[92] The mass fragmentation patterns were corrected for the natural abundance of ^{13}C atoms (1.07%) following the method described by Moseley et al.[93]

3.3 Results and Discussion

3.3.1 Structural and Chemical Characterization

The structural and chemical characterization of the zeolite sample with ~17 μm crystallites is described in the Supplementary Information section of Reference 89. Table 3.1 shows the Si/Al, DME uptake per aluminum during DME titration measurements, and

the textural characteristics of HZSM-5. The DME uptake ratio per aluminum was found to be 0.49. Cheung et al.[94] showed that each Brønsted acid site in ZSM-5 can adsorb half DME molecule because DME reacts with surface hydroxyl groups to form persistent methyls. The concentration of Brønsted acid sites in HZSM-5 was nearly identical to that inferred from the framework aluminum-content. The XRD pattern of HZSM-5 using the Cu-Kα radiation (1.54056 Å) is presented in Figure 3.1. The XRD pattern confirms that the HZSM-5 catalyst used in this work was crystalline and had an MFI-type framework.

Table 3.1: Silicon-to-aluminum ratio, DME uptake per aluminum, and the textural characteristics of HZSM-5 (Si/Al ~43) catalyst investigated in this work.

Zeolite sample	Si/Al	DME/Al	Surface area /m^2 g^{-1}	Micropore volume /cm^3 g^{-1}
HZSM-5	43[a]	0.49[b]	406[c]	0.13[c]

[a] Estimated from ICP-OES elemental analysis, performed my Galbraith Laboratories, Inc.

[b] Estimated from DME titration, performed by Chiang et al.[90]

[c] Determined from N_2 adsorption-desorption measurements, performed by Liu et al.[91]

3.3.2 Reactivity of Ethene and Isobutane on HZSM-5 in MTH Chemistry

Svelle, Bjørgen, and coworkers[20,59,60] performed transient isotopic switching experiments in which ^{12}C-methanol was reacted on HZSM-5 at ~623 K for 18 min followed by a rapid switch to ^{13}C-methanol. Their results showed that the time-evolution of the incorporation of ^{13}C atoms in ethene was similar to that in MBs but was different from the time-evolution of ^{13}C-incorporation in C_3+ olefins implying that ethene is primarily a product of the aromatics-based cycle and not the olefins-based catalytic cycle. Additionally, kinetic measurements by Hill et al.[95–97] and Svelle et al.[98,99] have shown that the rate of ethene methylation is at least an order of magnitude slower than propene or butene methylation, therefore suggesting that ethene can be considered a terminal product of the aromatics-

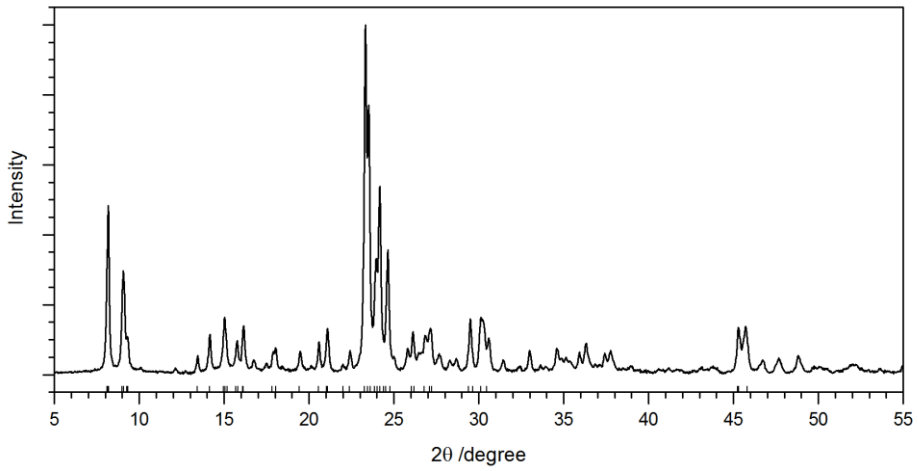

Figure 3.1: XRD pattern of the HZSM-5 (Si/Al ~43) catalyst investigated in this work using the Cu-Kα radiation (1.54056 Å). The markers represent the simulated XRD pattern of an MFI-type zeolite.

based catalytic cycle. To confirm that ethene can be considered as a termination product, ^{13}C-labeled DME (~70 kPa) was co-reacted with 7 – 8 kPa of ^{12}C-ethene. These results, summarized in Table 3.2, show that although some ethene was consumed when co-processed with DME, it reacted ~20 times slower than DME and, hence, it can be considered a termination product of the aromatics-based catalytic cycle.

The isotopic switching experiments by Svelle, Bjørgen, and coworkers[20,59,60] also showed that the time-evolution of ^{13}C incorporation in C_3+ olefins was similar therefore suggesting that olefins like isobutene and 2-methyl-2-butene are the products of the olefins-based catalytic cycle. Olefins subsequently form alkanes via hydrogen transfer reactions, and in general, alkanes are less reactive than either olefins or aromatics. Alkanes can therefore be considered as the termination products for the olefins-based catalytic cycle. To confirm that alkanes can be considered as terminal products, ^{13}C-labeled DME (~70 kPa) was co-reacted with 7 – 8 kPa of unlabeled isobutane and the results (summarized in Table 3.2) show that isobutane reacted ~20 times slower than

DME. Hence, alkanes (like isobutane and 2-methylbutane) can be considered as the termination products of the olefins-based catalytic cycle in MTH conversion.

Table 3.2: Feed flow rates, fractional conversion, and the conversion rates of DME and ethene or isobutane co-feeds, for the catalytic reaction of ~70 kPa $^{13}C_2$-DME with 7 – 8 kPa of $^{12}C_2$-ethene or $^{12}C_4$-isobutane at 623 K.

	DME	**Co-feed**
Catalytic reaction of $^{13}C_2$-DME and $^{12}C_2$-ethene		
Feed flow rate /mol C (mol Al-s)$^{-1}$	4.09	0.44
Net conversion /%	40	19
Conversion rate /mol C (mol Al-s)$^{-1}$	1.62	0.08
Catalytic reaction of $^{13}C_2$-DME and $^{12}C_4$-isobutane		
Feed rate /mol C (mol Al-s)$^{-1}$	4.09	0.78
Net conversion /%	35	11
Conversion rate /mol C (mol Al-s)$^{-1}$	1.78	0.09

The selectivity to both alkanes and olefins in MTH conversion is dependent on the extent of hydrogen transfer. Figure 3.2 shows the extent of hydrogen transfer, measured by the ratio of alkanes to alkenes, with a higher ratio indicating a greater extent of hydrogen transfer, occurring under different reaction conditions. It can be observed that the extent of hydrogen transfer in MTH is dependent on conversion, reaction temperature, as well as the identity of the co-feed. Individual alkane or olefin synthesis rates therefore cannot be used as a representative of the olefins-based cycle because the relative amount of olefins or alkanes is dependent on the extent of hydrogen transfer. To eliminate the effect of hydrogen transfer on the descriptor for the relative propagation of the aromatics- and olefins-based catalytic cycles, we use the sum of the synthesis rates of 2-methylbutane and its hydrogen transfer product, 2-methyl-2-butene (referred to as 2MBu).

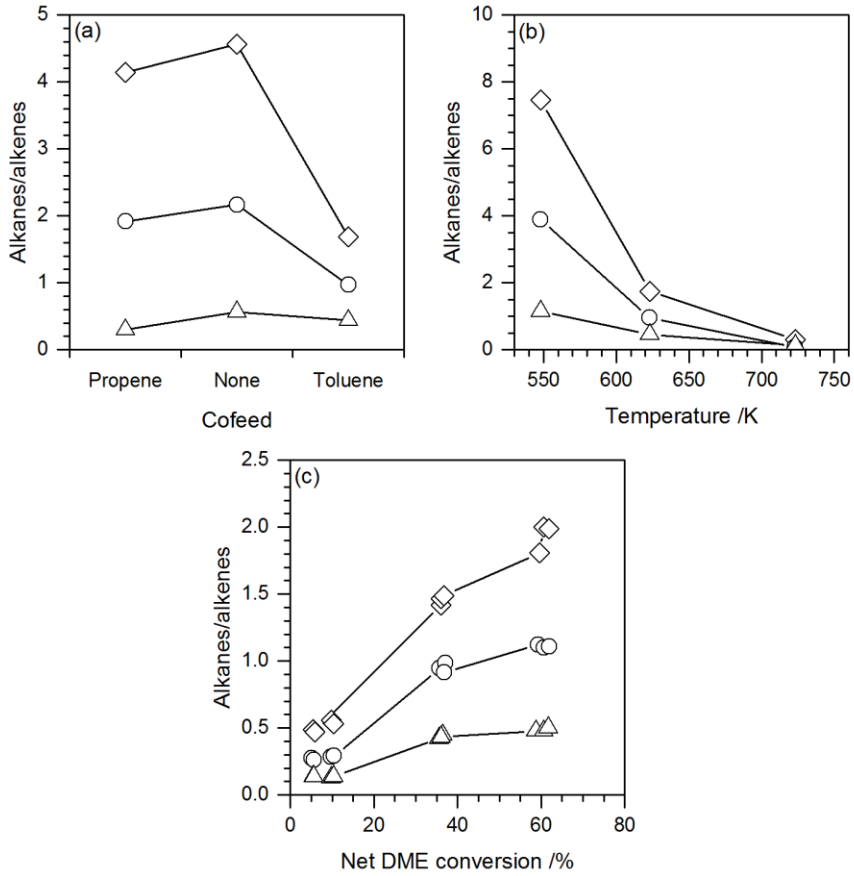

Figure 3.2: The ratio of alkanes to alkenes for C_4 (△), C_5 (○), and C_6 (◇) hydrocarbons on HZSM-5 (Si/AL ~43) catalyst for the catalytic reaction of ~70 kPa DME (a) with and without ~4 kPa of co-feed at ~548 K and 18 – 19% net DME conversion, (b) at 548 – 723 K and 59 – 61% net DME conversion, and (c) at ~623 K and 5 – 62% net DME conversion.

3.3.3 Effects of Olefin or Aromatic Co-Feeds on Ethene/2MBu Yield

Ilias et al.[72] reported that at iso-conversion conditions (18 – 19% net DME conversion) at ~548 K on HZSM-5, co-feeding ~4 kPa propene with ~70 kPa DME propagated the olefins-based cycle as evidenced by selectivity to C_4 – C_7 increasing 2.5-fold compared to when ~4 kPa toluene was co-reacted with DME. Co-feeding toluene increased the propagation of the aromatics-based cycle and a corresponding increase in ethene and MBs selectivity was observed. Figure 3.3 shows the effect of feed composition

on the product distribution and the ethene/2MBu yield at ~548 K and iso-conversion conditions (18 – 19% net DME conversion). For these experiments, propene and toluene co-feeds were completely ^{13}C-labeled and any $^{13}C_3$-propene or $^{13}C_7$-toluene in the reaction effluent was not included in the assessment of product selectivity. Additionally, the isotopologue distribution of propene and toluene in the reaction effluent was used to determine conversion of the $^{13}C_3$-propene and $^{13}C_7$-toluene co-feed, which were 52% and 40%, respectively.

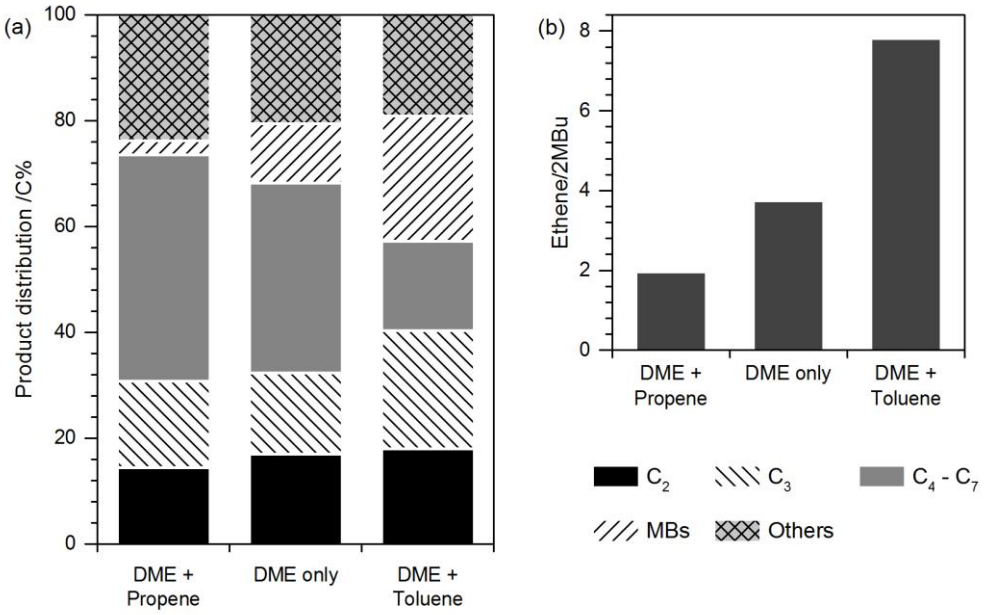

Figure 3.3: The effects of feed composition on (a) product distribution, and (b) ethene/2MBu yield, for the reaction of ~70 kPa DME (+ 4 kPa co-feed) at ~548 K and 18 – 19% DME conversion on HZSM-5 (Si/Al ~43) catalyst. The H/C in ‘‘Others’’ fraction was: 2.03 for DME + propene, 1.85 for DME, and 1.29 for DME + toluene.

The ethene/2MBu yield decreased by a factor of 1.9 when propene was co-reacted with DME compared to the reaction of DME alone as a result of increased propagation of the olefins-based catalytic cycle (Figure 3.3b). In contrast, ethene/2MBu yield increased

by a factor of 2.1 when toluene was co-processed with DME due to increased propagation of the aromatics-based catalytic cycle (Figure 3.3b). These results show systematic trends in the ethene/2MBu yield with aromatic or olefin co-feed and support our hypothesis that ethene/2MBu can be used as a descriptor of the relative propagation of the aromatics-based and the olefins-based catalytic cycles.

Figure 3.4 shows the effect of co-processing propene, toluene, or *p*-xylene with DME at ~623 K on product distribution and ethene/2MBu yield at iso-conversion conditions (34 – 37% net DME conversion). The effects of co-processing propene with DME on the ethene/2MBu yield compared to DME alone was relatively small (only a 26% decrease). We postulate that this small change in ethene/2MBu yield is a result of the large fraction of olefins already present when DME alone is reacted at 623 K, with olefin pressure

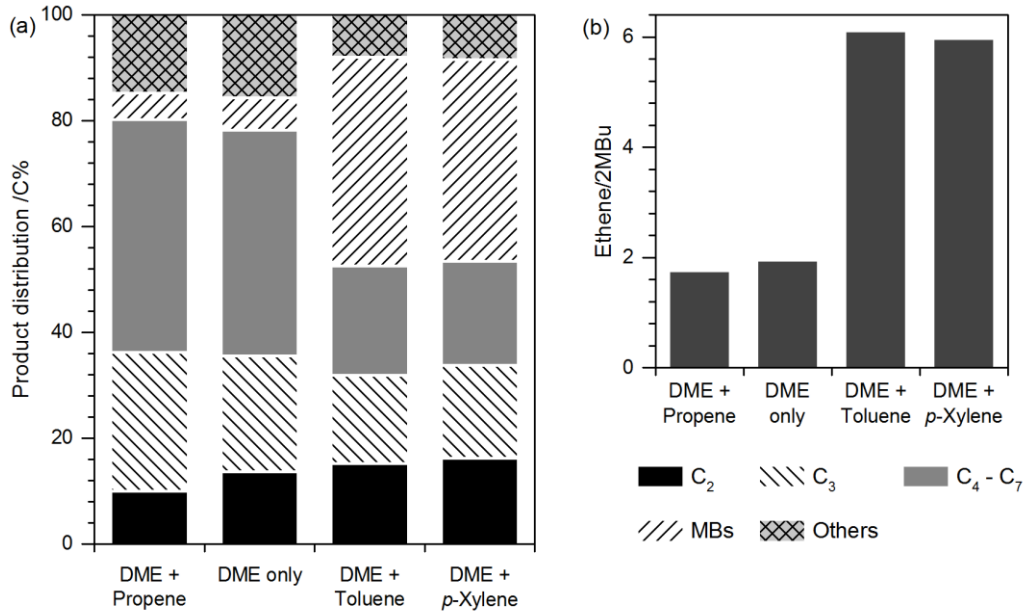

Figure 3.4: The effects of feed composition on (a) product distribution, and (b) ethene/2MBu yield, for the reaction of ~70 kPa DME (+ 4 kPa co-feed) at ~623 K and 34 – 37% DME conversion on HZSM-5 (Si/ Al ~43) catalyst. The H/C in "Others" fraction was: 1.85 for DME + propene, 1.89 for DME only, 1.65 for DME + toluene, and 1.57 for DME + *p*-xylene.

increasing by less than 50% with the addition of a propene co-feed. In contrast, the addition of ~4 kPa toluene increased the amount of aromatics in the system significantly, by ~580%. The co-reaction of DME with toluene increased the ethene/2MBu yield by a factor of 3.2 compared to the reaction of DME alone as a result of increased propagation of the aromatics-based catalytic cycle relative to the olefins-based catalytic cycle, which is similar to the observations at 548 K shown in Figure 3.3b.

Co-feeding *p*-xylene with DME had similar effects on both the product distribution (Figure 3.4a) and the ethene/2MBu yield (Figure 3.4b) as co-feeding toluene with DME, with ethene/2MBu yield increasing by a factor of 3.2 compared to the reaction of DME alone. The similarity in ethene/2MBu yield and product distribution for the co-reactions of *p*-xylene or toluene with DME shows that both aromatic co-feeds influence the propagation

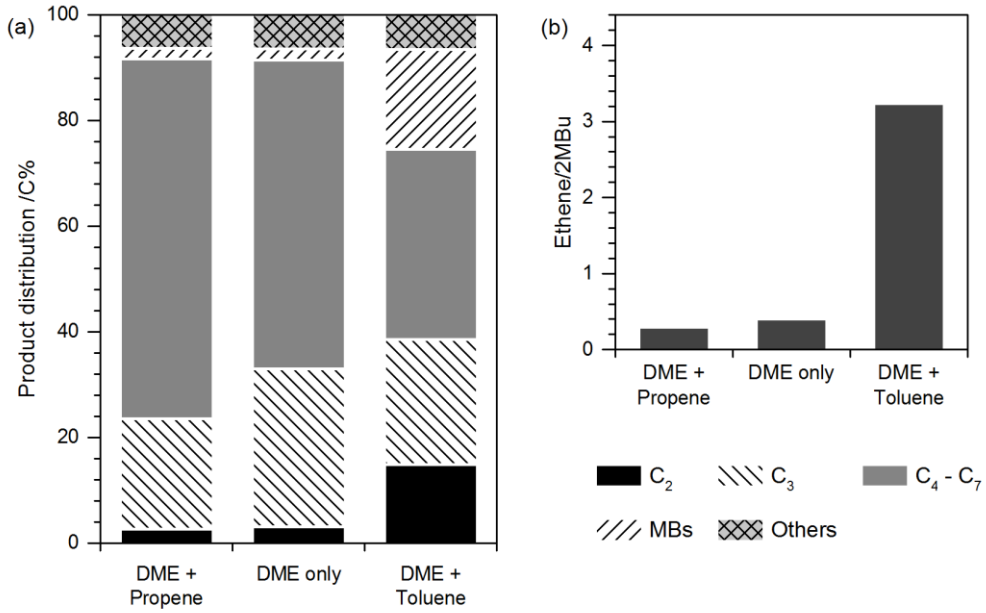

Figure 3.5: The effects of feed composition on (a) product distribution, and (b) ethene/2MBu yield, for the reaction of ~70 kPa DME (+ 4 kPa co-feed) at ~723 K and 60 – 73% DME conversion on HZSM-5 (Si/Al ~43) catalyst.

of the aromatics-based catalytic cycle in a similar manner i.e., increasing the overall partial pressure of aromatics in the system and increasing the propagation of the aromatics-based catalytic cycle. Similar trends in selectivity and ethene/2MBu yield for propene and toluene co-feeds with DME were also observed at 723 K (Figure 3.5a and Figure 3.5b).

3.3.4 Effects of DME Conversion on Ethene/2MBu Yield

The product distribution for the reaction of DME alone on HZSM-5 at ~623 K varied slightly for DME conversions between 5 – 62% (Figure 3.6a). Correspondingly, the ethene/2MBu yield varied slightly, between 1.2 and 2.1 (Figure 3.6b). This small increase in the ethene/2MBu yield at 623 K as DME conversion increases from 5% to 62% suggests that the relative rate of propagation for the aromatics-based cycle increased marginally compared to the propagation of the olefins-based cycle with an increase in DME

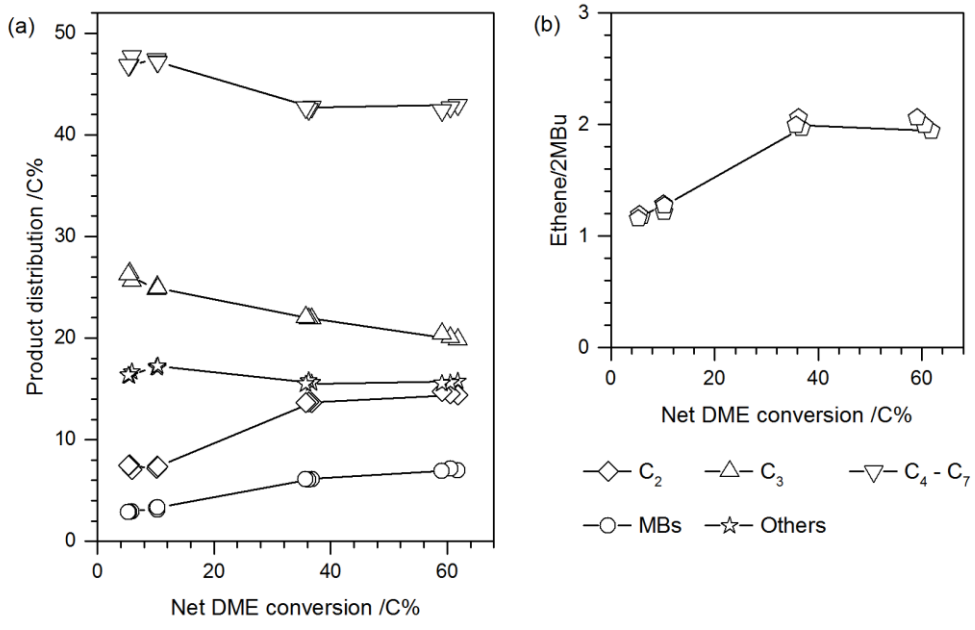

Figure 3.6: The effects of DME conversion on (a) product selectivity, and (b) ethene/2MBu yield, for the reaction of ~70 kPa DME at ~623 K on HZSM-5 (Si/Al ~43) catalyst. The H/C in "Others" fraction varied between 1.87 – 1.96.

conversion. The effects of DME conversion were also examined for the reaction of DME on the HZSM-5 sample with ~17 μm crystallites at ~623 K between 9 – 32% conversion (Figure 3.7). While the changes in product selectivity on the conventional HZSM-5 sample with conversion were small, product selectivity on the large crystal HZSM-5 sample was nearly invariant for the range of conversions studied. The ethene/2MBu yield was also relatively invariant with increasing DME conversion.

3.3.5 Effects of Reaction Temperature on Ethene/2MBu Yield

Figure 3.8a shows the selectivity of DME conversion on HZSM-5 catalyst at 548 K, 623 K, and 723 K, at iso-conversion conditions (59 – 61% DME conversion). Under these conditions, the selectivity to C_2 hydrocarbons (>99% of which is ethene), MBs, and "Others" systematically decreases with increasing reaction temperature. With increasing

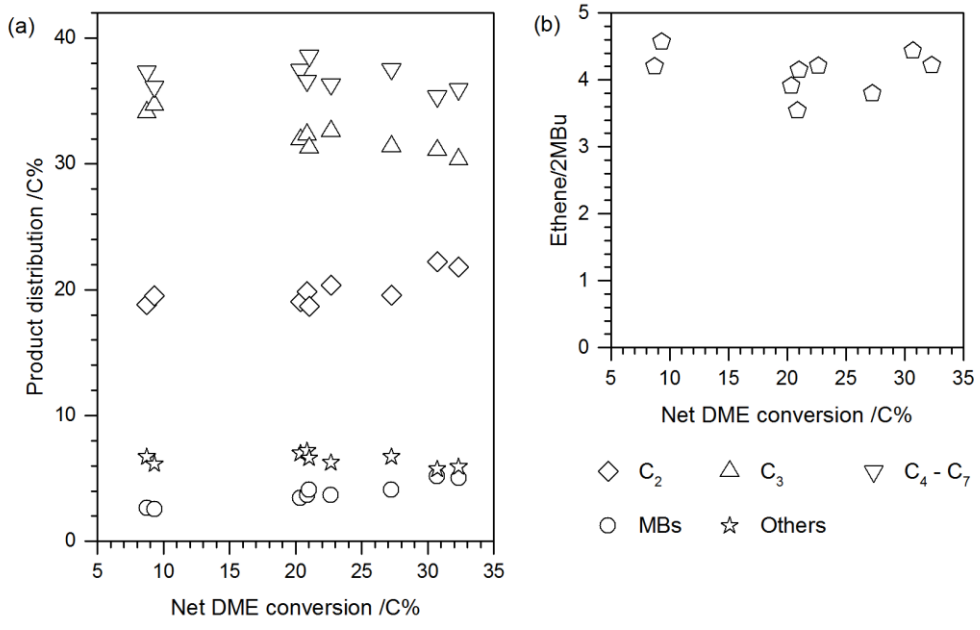

Figure 3.7: The effects of DME conversion on (a) product selectivity, and (b) ethene/2MBu yield, for the reaction of ~70 kPa DME at ~623 K on HZSM-5 (Si/Al ~38) catalyst with large (~17 μm) crystallites.

temperature, an increase in selectivity to C_3 – C_7 hydrocarbons is also observed. These trends in selectivity show that as the reaction temperature increases, the rate of propagation of the olefins-based cycle increases more than the rate of propagation of the aromatics-based cycle. The selectivity of MTH therefore systematically varies with reaction temperatures at iso-conversion conditions and a concomitant monotonic decrease in the ethene/2MBu yield is also observed, as shown in Figure 3.8b.

At 723 K, the selectivity to ethene and MBs was low compared to that at lower temperatures (Figure 3.8a). To further understand if ethene selectivity was lower at higher temperatures at least in part because of lower concentration of MBs, toluene was co-reacted with DME at 723 K. At ~73% DME conversion and ~74% net toluene conversion, ethene selectivity increased from 3% to 15% and correspondingly, the ethene/2MBu yield

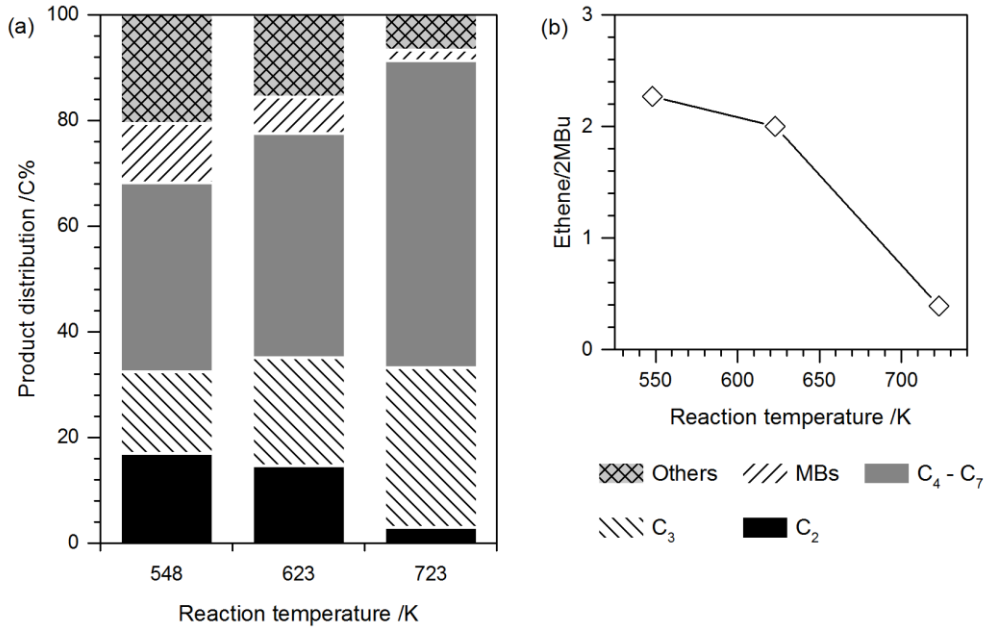

Figure 3.8: The effects of reaction temperature on (a) product distribution, and (b) ethene/2MBu yield, for the reaction of ~70 kPa DME on HZSM-5 (Si/Al ~43) catalyst. The H/C in ‘‘Others’’ fraction was: 1.85 at 548 K, 1.88 at 623 K, and 1.77 at 723 K.

increased from 0.4 to 3.2, compared to the reaction of DME alone at ~723 K and 60%. This increase in ethene selectivity shows that one reason that the selectivity of DME conversion to ethene was low at 723 K was due to the low concentration of MBs, and not necessarily because the rate of aromatic dealkylation was slower relative to olefin methylation and cracking rates. The selectivity to MBs was low for the reaction of DME alone at 723 K because MB formation, which requires olefins to undergo both cyclization and dehydrogenation reactions, occurs to a lesser extent at higher temperatures, therefore suggesting that at higher temperatures (723 K), olefins prefer other pathways, such as methylation and cracking.

3.4 Conclusions

The ratio of synthesis rates of ethene and 2-methyl-2-butene + 2-methylbutane (ethene/2MBu) was used to describe the relative extents of propagation of the aromatics-based and the olefins-based catalytic cycles in MTH catalysis, where a high ethene/2MBu yield indicates increased propagation of the aromatics-based catalytic cycle and a low ethene/2MBu yield indicates increased propagation of the olefins-based catalytic cycle. Isotopic experiments $^{12}C_2$-ethene or $^{12}C_4$-isobutane with $^{13}C_2$-DME on HZSM-5 at ~623 K showed that the rate of DME conversion (1.6 – 1.8 mol C (mol Al s)$^{-1}$) was ~20 times faster than either ethene conversion rate (0.08 mol C (mol Al s)$^{-1}$) or isobutane conversion rate (0.09 mol C (mol Al s)$^{-1}$).

At iso-conversion conditions at 548 – 723 K, propene and toluene were co-reacted with DME to increase the propagation of the olefins-based and the aromatics-based catalytic cycles, respectively. The ethene/2MBu yield correspondingly decreased with the addition of propene and increased with the addition of toluene. The ethene/2MBu yield also increased marginally (from 1.2 to 2.1) with increasing conversion of DME (from 5%

to 62%) at ~623 K on HZSM-5 catalyst, showing that the aromatics-based catalytic cycle propagates more relative to the olefins-based catalytic cycle at higher conversions. For the reaction of DME alone, a monotonic increase in selectivity towards C_3 – C_7 hydrocarbons and a monotonic decrease in selectivity to MBs and ethene with increasing reaction temperature from 548 K to 723 K was observed, showing that selectivity can be systematically tuned at iso-conversion conditions and that at higher temperatures the olefins-based catalytic cycle dominates over the aromatics-based catalytic cycle resulting in lower ethene/2MBu yield.

The ethene/2MBu yield varies systematically with varying feed composition, DME conversion, and reaction temperature, showing that the relative rates of propagation of the aromatics-based and the olefins-based catalytic cycles in MTH catalysis on HZSM-5 can be described by this ratio.

CHAPTER ***FOUR***

Effects of Zeolite Crystallite Size on Light Olefins Selectivity in Methanol-to-Hydrocarbons Conversion

* Reported from R. Khare, D. Millar, A. Bhan, *Journal of Catalysis* **321** (2015) 23–31

4.1 Introduction

Sugimoto et al.[80] studied the effects of crystallite size on the catalytic properties of HZSM-5 and reported that ethene selectivity increased from 0.7% on HZSM-5 with <200 nm crystallites to 12.9% on HZSM-5 with larger crystallites (3 – 4 μm); propene selectivity also increased from 1.5% to 9.6%. The authors attributed this increase in light olefins selectivity to improved product shape selectivity of the catalyst, which favored smaller hydrocarbons that can easily diffuse out of the crystallite.[80] Rownaghi et al.[81,82] synthesized HZSM-5 nanocrystals (~120 nm) and compared their catalytic performance to a conventional HZSM-5 sample with larger crystallites (wide-range) for methanol conversion at ~643 K and reported that ethene selectivity on HZSM-5 nanocrystals (6.6%) was lower than the ethene selectivity on the conventional HZSM-5 sample (9.6%).

Choi et al.[83] synthesized MFI nanosheets that were single unit cell thick (~2.5 nm) along the *b*-axis and reported a five-times longer catalytic lifetime and slower coke deposition rate (45 vs. 170 mg g^{-1} after 5 days) compared to a conventional MFI zeolite for MTH reaction at ~673 K. Bleken et al.[84] reported that MFI nanosheets exhibited lower C_2 selectivity, and correspondingly a higher C_3-to-C_2 ratio, than a conventional MFI zeolite for MTH reaction at ~623 K. Kim and Ryoo[85] investigated the effects of external Brønsted

acid sites, which correspond to ~30% of all Brønsted acid sites, in MFI nanosheets and showed that external surface does not play a role in MTH chemistry. The external acid sites were poisoned by triphenylphosphine oxide (TPPO), which completely suppressed the catalytic cracking of 1,3,5-tri-*iso*-propylbenzene, a reaction that can only occur on the external surface.[85] MTH conversion was, however, unaffected by the poisoning.[85]

In this work, we show that the increase in ethene and total light olefins selectivity in MTH with increasing crystallite size can be rationalized as an effect of increased propagation of the aromatics-based catalytic cycle. A monotonic trend in light olefins selectivity was observed with (i) increasing crystallite size of MFI, and (ii) increasing transport restrictions in the zeolite, which were introduced by silylation of the external surface by tetraethyl orthosilicate (TEOS). The increase in light olefins selectivity was accompanied by a concomitant increase in ethene/2MBu yield, a descriptor that reflects the relative propagation of the aromatics-based and the olefins-based catalytic cycles.[73] We postulate that transport restrictions within a zeolite increase with an increase in the crystallite size of MFI, which consequentially increases the intra-crystalline residence time of bulkier hydrocarbons such as MBs. This enables the entrained MB molecules to undergo multiple methylation/dealkylation reactions before exiting the zeolite whilst producing a light olefin (ethene or propene) molecule during each cycle.

Transport characteristics in the silylated zeolite samples were not directly measured, however, we have described the change in transport restrictions by studying the uptake characteristics of 2,2-dimethylbutane (2,2-dmb) at 298 K and 20 kPa 2,2-dmb pressure. The adsorption uptake curves of 2,2-dmb were used to estimate the effective crystallite size of the silylated zeolite samples relative to the parent zeolite. A monotonic trend in ethene and light olefins selectivity as well as ethene/2MBu yield, at identical

temperature and iso-conversion conditions (46 – 59% net DME conversion), was observed with an increase in the effective crystallite size for all the zeolite samples investigated in this work (including the silylated MFI samples) thereby establishing a mechanistic basis for the effects of crystallite size on total light olefins selectivity in MTH conversion on MFI-type zeolites.

4.2 Materials and Methods

4.2.1 Synthesis of Zeolite Samples with Varying Crystallite Sizes

Two commercial zeolite samples were acquired from Zeolyst International Inc. (CBV 8014, referred to as 500nm-MFI) and ZEOCHEM (ZEOcat PZ-2/100 H, referred to as 2μm-MFI), respectively. Three zeolite samples were synthesized according to the procedures described in Reference 89: a self-pillared pentasil MFI sample (referred to as 2nm-MFI), a 3DOm-i MFI sample (referred to as 40nm-MFI), and a conventional HZSM-5 sample with large ~17 μm crystallites (referred to as 17μm-MFI).

4.2.2 Synthesis of Silylated Zeolite Samples

External transport restrictions were introduced in the 500nm-MFI sample by silylating the external surface using TEOS. Chemical liquid deposition of silicon oxides like TEOS is an effective way to modify the external surface of zeolites having MFI-type topology.[100] MFI has a three-dimensional porous network consisting of straight-channels (0.51 nm × 0.55 nm) and sinusoidal-channels (0.54 nm × 0.56 nm).[42,43] The diameter of pore-openings in MFI (~0.55 nm)[42,43] is smaller than the kinetic diameter of TEOS (~0.96 nm).[100] This prevents TEOS from entering the zeolite pores. Silylation treatment with TEOS, therefore, deposits an inert layer of SiO_2 on the external surface and near the pore-mouth region, but does not affect the internal micropore structure of the zeolite. Single-

cycle silylation (for SiMFI-1x) as well as multi-cycle silylation (twice and thrice for SiMFI-2x and SiMFI-3x, respectively) treatments were performed following the procedure described by Zheng et al.,[100] to obtain three silylated zeolite samples with varying amounts of SiO2 deposited on the external surface.

4.2.2.1 Synthesis of SiMFI-1x Zeolite Sample

A 500 cm^3 flask with a stir bar was loaded with 175 cm^3 *n*-hexane (Sigma-Aldrich, chemical purity grade), followed by the addition of ~7 g of 500nm-MFI zeolite sample, and stirred vigorously. Using an auto-pipette, 1.05 cm^3 TEOS (Sigma-Aldrich, chemical purity grade) was added. A reflux condenser was attached and vented to a N_2 source/bubbler to keep a positive N_2 pressure. The system was heated to reflux, held for 1 h, and then allowed to cool to 323 K. Volatiles were removed under vacuum and dry solids were collected. Solids were then placed in a porcelain dish and heated to 393 K in an oven for 2 h. The dish was then transferred to a calcination furnace. The temperature of the furnace was increased from ambient to 773 K in 2 h, held at 773 K for 4 h, and slowly allowed to cool to the ambient temperature.

4.2.2.2 Synthesis of SiMFI-2x Zeolite Sample

In the same manner as described above, ~5 g of SiMFI-1x was suspended in 125 cm^3 hexane and 0.75 cm^3 TEOS was added. Following reflux and removal of volatiles, solids were dried and calcined using the same procedure.

4.2.2.3 Synthesis of SiMFI-3x Zeolite Sample

Using the same procedure, ~3 g of SiMFI-2x was suspended in 75 cm^3 hexane and 0.45 cm^3 TEOS was introduced. Following reflux and removal of volatiles, solids were collected, dried, and calcined.

Prior to the catalytic reactions, all zeolite samples were treated in 1.67 cm^3 s^{-1} of dry air (Minneapolis Oxygen, 20 – 21% O_2, <10 ppm H_2O) at 823 K for 4 h. The temperature was increased from ambient to 823 K in 8 h and was held at 823 K for 4 h before cooling to ambient temperature. The zeolite samples were then pressed into pellets, crushed, and sieved between 40- and 80-mesh sieves to obtain uniform particles with size between 180 and 425 μm. Quartz sand (Acros Organics) was used as a diluent in the catalyst bed to prevent temperature rise due to the exothermic nature of MTH reactions. Prior to its use, the quartz sand was washed with 1 M nitric acid (Sigma-Aldrich), rinsed with deionized water, dried, and sieved between 40- and 80-mesh sieves.

4.2.3 Structural and Chemical Characterization

Crystallite size of 500nm-MFI was determined by SEM analysis performed on a JEOL 6700 field emission gun scanning electron microscope using lower secondary electron image mode at 1.5 kV accelerating voltage and 8.3 mm working distance. The sample was coated with a layer of Pt before the analysis. Crystallite size of 2μm-MFI was determined by SEM performed on an FEI inspect scanning electron microscope using the Everhart-Thornley detector at 15 kV accelerating voltage and 12.4 mm working distance. The sample was coated with a layer of Au-Pd before the analysis.

The Si/Al the zeolite samples was determined by ICP-OES elemental analysis performed at Galbraith Laboratories, Inc. The analytical method used was GLI procedure ME-70. Total surface area, micropore surface area, and the external surface area were determined by N_2 adsorption-desorption measurements performed on a Micromeritics ASAP 2000 Surface Area analyzer at liquid N_2 boiling temperature (~77 K). Total surface area was determined using the BET method and the micropore and the external surface areas were determined by the *t*-plot methods.

The concentration of Brønsted acid sites in the silylated zeolite samples was determined by FT-IR spectroscopy of adsorbed pyridine using a high-temperature Specac IR transmission cell in conjunction with a Nicolet 6700 FT-IR spectrometer with MCT HighD detector. Zeolite samples (10 – 15 mg) were pressed into self-supporting 13 mm diameter wafers. Once loaded into the IR cell, samples were pretreated in 0.75 $cm^3\ s^{-1}$ He flow at 773 K for 1 h. Background spectra were recorded at 423 K. Multiple 5 mm^3 injections of liquid pyridine were added to the He flow through a heat-traced line that passed through the samples until the acid sites were saturated. Samples were then flushed with He for several minutes to remove any physisorbed pyridine. Spectra were again recorded at 423 K and now included the IR absorption features of the adsorbed pyridine. Baseline corrected spectra between 2000 – 1350 cm^{-1} and integrated peak intensities were obtained using OMNIC software. Due to a measurement error, no data was collected for SiMFI-2x sample at 623 K.

Following the procedure described by Emeis et al.[101] and Zheng et al.,[100] the concentration of Brønsted acid sites was determined using the peak near 1546 cm^{-1}. To allow quantitative comparison of the peak intensities, all IR spectra were normalized using the overtone lattice vibration band of the zeolites near 1850 cm^{-1}. The Brønsted acid site concentration (in mmol g^{-1}) was calculated using the expression:

$$C_{Brønsted} = 1.88\ (\text{integrated intensity at } 1546\ cm^{-1})\ R^2/W \qquad (4.1)$$

Where $C_{Brønsted}$ is the concentration of Brønsted acid sites (in mmol g^{-1}), R is the radius of catalyst wafer (in mm), and W is the weight of the catalyst wafer (in mg).

Adsorption uptake measurements of 2,2-dmb were performed on a Hiden IsoChema IGA series microbalance equipped with a stainless steel reactor and a vapor

dosing option. Zeolite samples (85 – 205 mg) were loaded into a quartz bucket and were counterbalanced in the unit. Once sealed in the reactor, samples were treated under high vacuum (6 – 10 mbar) at 423 K until no further mass loss was observed. The reactor furnace was then substituted with an ethylene glycol-water chiller unit for adsorption measurements at ~298 K. Adsorption uptake data were collected at ~20 kPa 2,2-dmb pressure. The pressure was ramped to 20 kPa at a rate of 0.031 kPa s^{-1} and was maintained at 20 kPa for the duration of the analysis. The weight change over time was recorded until the sample reached equilibrium or a maximum time of 24 h was reached.

4.2.4 Catalytic Reaction of DME to Hydrocarbons

Catalytic reactions of DME were carried out in a 316/316L stainless steel packed-bed reactor (1/4 in OD; 0.035 in wall thickness) equipped with a concentric thermal well (1/16 in OD, 0.014 in wall thickness). Isothermal conditions were maintained in the catalyst bed using a heating coil (ARi Industries Inc., AeroRod® heating assembly) regulated by a Watlow 96 series temperature controller. Temperature of the catalyst bed was measured using a K-type thermocouple (Omega Engineering) inserted into the concentric thermal well. Prior to every reaction, the catalyst samples were pretreated in situ in 1.67 cm^3 s^{-1} He (Minneapolis Oxygen, 99.995% purity). The temperature of the catalyst bed was increased from ambient to 823 K in 8 h and was held at 823 K for 4 h before reducing it to the reaction temperature.

The reactions were run using 13 – 40 mg catalyst to achieve the desired chemical conversions (46 – 59% net DME conversion). The catalyst bed was diluted with 100 – 200 mg of quartz sand. Methanol was considered as a reactant in the calculation of net conversion. The reactant stream constituted DME (Matheson Tri-Gas, 99.5% purity) and a mixture of CH_4 and Ar (Airgas, 10% CH_4, 90% Ar) that was used as an internal standard

for the FID. The total feed pressure was maintained at 115 – 130 kPa and all reactions were carried out at ~623 K. The temperature variation in the catalyst bed was less than 1 K during the reaction.

The reactor effluents were analyzed using an online Agilent 7890 series GC – 5975C series MS equipped with a 100% dimethylpolysiloxane Agilent J&W HP-1 column (50 m × 320 μm × 0.52 μm) connected to an FID and a (5%-phenyl)-methylpolysiloxane Agilent J&W HP-5ms column (25 m × 320 μm × 0.25 μm) connected to an MSD. The product distributions shown in Section 4.3 include C_8+ hydrocarbons that were not identified separately and are classified as “Others”. The average hydrogen-to-carbon ratio in the hydrocarbon species present in the “Others” fraction was calculated from the hydrogen- and carbon-content of known species in the converted feed and the reaction effluent, and is reported with the data in some cases.

4.3 Results and Discussion

4.3.1 Structural and Chemical Characterization

The structural and chemical characterization of 2nm-MFI, 40nm-MFI and 17μm-MFI zeolite samples is described in detail in the Supplementary Information section of Reference 89. The Si/Al in the zeolite samples investigated in this work, as determined from the ICP-OES elemental analysis, is reported in Table 4.1 and Table 4.2. The amount of the SiO_2 deposited on the external surface of the silylated zeolite samples was calculated from the experimentally observed Si/Al and the Si/Al in the parent material and is also reported in Table 4.2. It was assumed in the calculations that SiO_2 was the only silicon species present on the external surface and that no dealumination occurred during the silylation treatment.

Table 4.1: Silicon-to-aluminum ratio and crystallite size of zeolite samples investigated in this work.

Zeolite sample	Si/Al[a]	Crystallite size /nm
2nm-MFI	88	2[b]
40nm-MFI	72	40[b]
500nm-MFI	43	500[c]
2µm-MFI	60	1750[c]
17µm-MFI	38	17000[b]

[a] Estimated from ICP-OES elemental analysis, performed by Galbraith Laboratories, Inc.

[b] Estimated from the diffusion lengths reported by Zhang et al.[89]

[c] Estmated from SEM micrographs.

Table 4.2: Silicon-to-aluminum ratio, amount of SiO_2 deposited on the external surface by single-/multi-cycle silylation treatment, and the effective crystallite size, of the silylated zeolite samples investigated in this work.

Zeolite sample	Si/Al[a]	Amount of SiO_2 deposited /wt%	Effective crystallite size[d] /nm
500nm-MFI	42.6	0	500
Si-MFI-1x	45.8[b]	7[c]	1250
Si-MFI-2x	47.6[b]	12[c]	5200
Si-MFI-3x	49.5[b]	16[c]	17600

[a] Determined from ICP-OES elemental analysis, performed by Galbraith Laboratories, Inc.

[b] The effective Si/Al is the same as that in the parent zeolite (500nm-MFI). The experimentally observed Si/Al is however higher because of SiO_2 deposited on the external surface.

[c] Estimated after assuming that SiO_2 is the only silicon species present on the external surface and that no dealumination occurred during the silylation treatment.

[d] Estimated from 2,2-dmb adsorption uptake measurements.

The SEM micrograph of 500nm-MFI sample is presented in Figure 4.1a and shows that the crystallite size of 500nm-MFI varies between 200 and 1500 nm. Agglomeration of individual crystallites is visible and therefore it is difficult to estimate the accurate crystallite

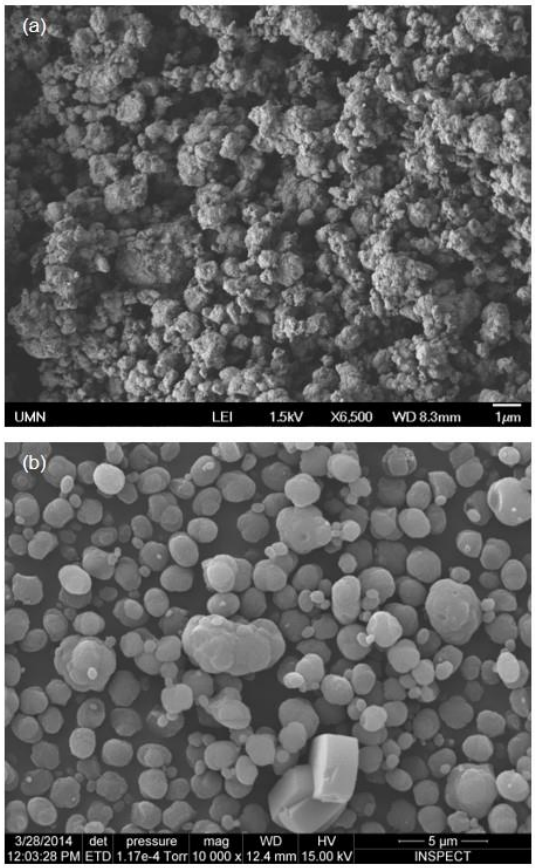

Figure 4.1: SEM micrographs of (a) 500nm-MFI, and (b) 2μm-MFI.

size of the zeolite sample. The crystallite size of 500nm-MFI, however, is between that of 40nm-MFI (~20 nm crystallites) and 2μm-MFI (~1.8 μm crystallites) and is considered to be ~500 nm in the calculation of effective crystallite size of the silylated zeolite samples. SEM micrograph of 2μm-MFI is also presented in Figure 4.1b. Crystallite size of 2μm-MFI was estimated to be 1744 ± 136 nm from the micrograph. The crystallite sizes of 2nm-MFI, 40nm-MFI, and 17μm-MFI were estimated from the diffusion lengths reported in Reference 89 and are reported in Table 4.1.

Total surface area, micropore surface area, and external surface area, of the silylated zeolite samples as well as that of the parent zeolite (500nm-MFI), as determined

from N_2 adsorption-desorption measurements at liquid N_2 boiling temperature (~77 K), are reported in Table 4.3. The micropore surface area of SiMFI-1x (318 $m^2 g^{-1}$), SiMFI-2x (312 $m^2 g^{-1}$), and SiMFI-3x (305 $m^2 g^{-1}$) were 91 – 95% of the micropore surface area of the parent zeolite (334 $m^2 g^{-1}$) suggesting that the internal micropore structure remained intact and was unaffected by the silylation treatment.

Table 4.3: Textural characteristics as determined from N_2 adsorption-desorption measurements at liquid N_2 boiling temperature (~77 K). The areas reported are corrected for mass increase due to SiO_2 deposition during the silylation treatment.

Zeolite sample	Total surface area[a] /$m^2 g^{-1}$	Micropore surface area[b] /$m_2 g^{-1}$	External surface area[b] $m^2 g^{-1}$
500nm-MFI	461	334	127
Si-MFI-1x	449	318	135
Si-MFI-2x	433	312	119
Si-MFI-3x	430	305	124

[a] Estimated by the BET method.

[b] Estimated by the *t*-plot methods.

4.3.1.1 Determination of Brønsted Acid Site Concentration by FT-IR Spectroscopy

The concentration of Brønsted acid sites in the silylated zeolite samples as well as the parent zeolite (500nm-MFI) was determined by FT-IR spectroscopy of adsorbed pyridine and is reported in Table 4.4. The results reported are compared to those reported by Zheng et al.[100] for HZS, HZS-4%, and HZS-3×4% zeolite samples, which correspond to the parent zeolite and silylated samples with 4 wt% and 12 wt% SiO_2 deposition, respectively. The concentration of Brønsted acid sites in 500nm-MFI (0.265 mmol g^{-1}) was lower than that calculated from the Si/Al after assuming one Brønsted acid site per aluminum (0.344 mmol g^{-1}). A reason for this may be that some aluminum sites are either

inaccessible to pyridine or are in the form of Lewis acid sites which have an adsorption band (1455 cm^{-1}) distinct from the adsorption band for Brønsted acid sites (1546 cm^{-1}). A monotonic decrease in the concentration of Brønsted acid sites is observed with an increase in the amount of SiO_2 deposited suggesting that silylation treatment passivated some of the Brønsted acid sites present near the pore-mouth region and on the external surface of the zeolite. Another reason for this decrease in Brønsted acid site concentration may be that some of the aluminum sites become inaccessible to pyridine due to increased transport restrictions within the zeolite due to silylation treatment.

Table 4.4: Concentration of Brønsted acid sites, as determined by FT-IR spectroscopy of adsorbed pyridine at 423 K, in the silylated zeolites and the parent zeolite (500nm-MFI). The results are compared to those reported by Zheng et al.[100]

Zeolite sample	**SiO_2 deposited /wt%**	**$C_{Brønsted}$ /mmol g^{-1}**
500nm-MFI	0	0.265, 0.344[a]
Si-MFI-1x	7	0.229
SI-MFI-3x	16	0.161
Results reported by Zheng et al.[100]		
HZS	0	0.213[b], 0.326[a]
HZS-4%	4	0.187
HZS-3×4%	12	0.154

[a] Estimated from aluminum content after assuming one Brønsted acid site per aluminum.

[b] Estimated by NH_3 adsorption measurements

4.3.1.2 Determination of Effective Diffusion Length by 2,2-Dimethylbutane Adsorption

Transport restrictions in the silylated zeolite samples were estimated by the adsorption uptake measurements of 2,2-dimethylbutane (2,2-dmb). The structural framework of MFI consists of intersecting straight-channels (0.51 nm × 0.55 nm) and

sinusoidal-channels (0.54 nm × 0.56 nm).[42,43] The channel intersections have a diameter of ~0.9 nm.[44,45] The critical kinetic diameter of 2,2-dmb is 0.63 nm,[102,103] which is close to the diameter of the pore-openings in MFI. Any change in transport restrictions within the zeolite will strongly affect the adsorption uptake of 2,2-dmb. A zeolite with higher transport restrictions will hinder the transport of 2,2-dmb inside the zeolite and will result in a slower uptake, and vice versa. The uptake rate of 2,2-dmb can, therefore, be used as a descriptor of transport limitations in the silylated zeolite samples.[104] There are two possible sites for the adsorption of hexane isomers on MFI: the straight-channels or the channel intersections, and 2,2-dmb preferentially adsorbs in the channel intersections of MFI.[103] A unit cell of MFI contains 4 channel intersections and therefore the theoretical adsorption capacity of 2,2-dmb in zeolites with MFI-type framework is calculated to be equal to 4 molecules per unit cell or ~60 mg g^{-1}.[104]

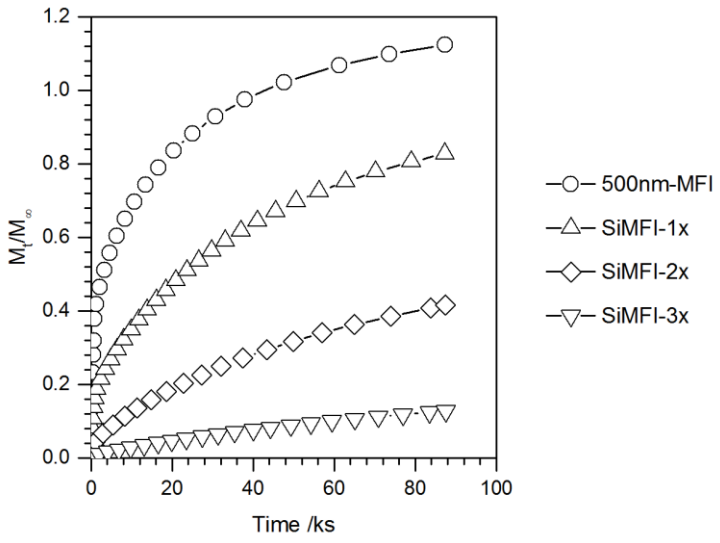

Figure 4.2: Adsorption uptake curves of 2,2-dmb on silylated zeolite samples at ~298 K and ~20 kPa 2,2-dmb pressure. The adsorbed amount was normalized to the theoretical adsorption capacity of 2,2-dmb in MFI. The results were corrected for the increase in weight of silylated samples due to SiO_2 deposition during silylation treatment.

Figure 4.2 shows the uptake curves of 2,2-dmb on the silylated zeolite samples at ~298 K and ~20 kPa 2,2-dmb pressure. The amount of 2,2-dmb adsorbed was normalized to the theoretical adsorption capacity of 2,2-dmb in MFI. The uptake rate of 2,2-dmb was also corrected for the increase in weight of silylated samples due to SiO_2 deposition on the external surface during silylation treatment. The uptake of 2,2-dmb was fastest in the parent zeolite (500nm-MFI), decreased monotonically, and was slowest in the sample that was silylated three times (SiMFI-3x), therefore suggesting that silylation treatment introduced external transport restrictions in the parent zeolite. The relative transport restrictions in the silylated zeolite samples, based on the uptake of 2,2-dmb, increases in the following order:

500nm-MFI < SiMFI-1x < SiMFI-2x < SiMFI-3x

The uptake of 2,2-dmb did not reach saturation capacity in 24 h in all cases. Also, the amount of 2,2-dmb adsorbed in 500nm-MFI was higher than the theoretical adsorption capacity suggesting that some 2,2-dmb was adsorbed on the external surface of the zeolite or in some of the straight channels.

4.3.1.3 Calculation of Effective Diffusion lengths in the Silylated Zeolite Samples

A simple Fickian diffusion model was used to describe the concentration profile of 2,2-dmb inside the zeolite crystallites. After assuming that all crystallites were spherical (with radius R equal to the diffusion length in the zeolite) and that other transport restrictions were absent, the equations governing the concentration profile of 2,2-dmb inside the zeolite crystallite was derived from Fick's second law. In the absence of concentration gradients in directions other than radial, the expression takes the form:[105]

$$\frac{\partial C(r,t)}{\partial t} = \frac{1}{r^2}\left\{\frac{\partial}{\partial r}\left(D_{eff} r^2 \frac{\partial C(r,t)}{\partial r}\right)\right\} \qquad (4.2)$$

Where C(r,t) is the concentration profile of 2,2-dmb inside the spherical particle, r is the radial coordinate, t is temporal coordinate, and D_{eff} is the effective Fickian diffusivity, which is assumed to be constant in all zeolites with MFI-type framework. The relevant boundary conditions are:

1. $C = C_\infty$ at $r = R$ and $t > 0$
2. C is finite at the center of the spherical particle
3. $C = 0$ at $t = 0$ and $0 \leq r \leq R$

Where C_∞ corresponds to the saturation loading of 2,2-dmb in MFI.

For isothermal conditions and in the absence of other transport restrictions, the mathematical solution to Equation 4.2 can be obtained by separation of variables, and the resulting expression for the concentration profile takes the form:[105,106]

$$\frac{C(r,t)}{C_\infty} = 1 - \frac{2R}{\pi r}\sum_{n=1}^{\infty}\left[\frac{(-1)^n}{n}\sin\left(\frac{n\pi r}{R}\right)\exp\left(-\frac{D_{eff}n^2\pi^2 t}{R^2}\right)\right] \qquad (4.3)$$

The uptake characteristics of 2,2-dmb by the zeolite can be obtained from Equation 4.3 by integrating C(r,t) between r = 0 and r = R,[105,106]

$$\frac{M_t}{M_\infty} = 1 - \frac{6}{\pi^2}\sum_{n=1}^{\infty}\left[\frac{1}{n^2}\exp\left(-\frac{D_{eff}n^2\pi^2 t}{R^2}\right)\right] \qquad (4.4)$$

Where M_t and M_∞ are the adsorbed amounts at time t and at saturation, respectively.

The overall uptake profile of 2,2-dmb is affected by the heat of adsorption and wide crystallite size distribution. The uptake profile at short times was therefore used to estimate the effective diffusion lengths as it is less susceptible to thermal effects and wide crystallite size distribution.[103,107] For short contact times, Ruthven and Kärger[106] describe the uptake of 2,2-dmb in spherical crystallites as:

$$\frac{M_t}{M_\infty} = \frac{6}{\sqrt{\pi}}\sqrt{\frac{D_{eff}t}{R^2}} \qquad (4.5)$$

The plot of M_t/M_∞ versus $\sqrt{t}$ is linear at short contact times, and D_{eff}/R^2 values can be estimated from the initial slope of the curve.

Figure 4.3 shows the plots of M_t/M_∞ versus $\sqrt{t}$ at short contact times for the adsorption uptake of 2,2-dmb on the silylated zeolite samples as well as the parent zeolite (500nm-MFI). The observed initial slopes are not perfectly linear because the pressure was not constant at short contact times. The pressure was increased at a rate of 0.031 kPa s^{-1} to a final value of 20 kPa. The amount of 2,2-dmb adsorbed (M_t/M_∞) was, therefore, lower than the expected value at short contact times due to lower pressure. The effective diffusivity of 2,2-dmb in 500nm-MFI was estimated to be 8.8×10^{-19} m^2 s^{-1} assuming ~500 nm crystallites. This value is similar to the values obtained previously by Cavalcante and

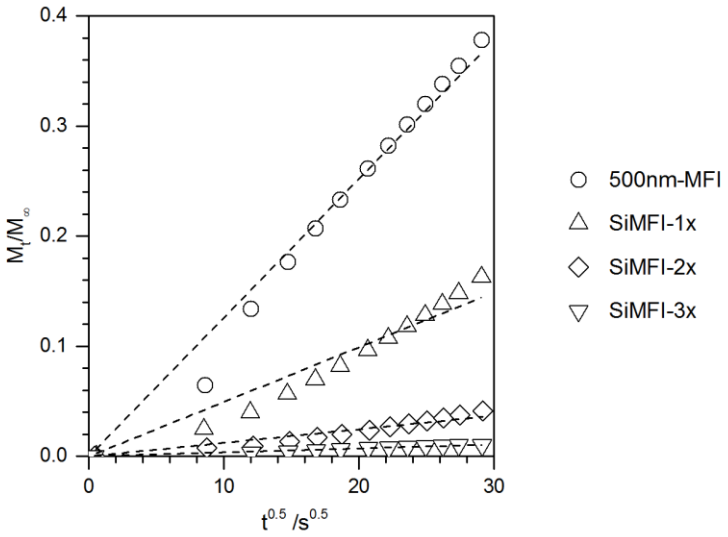

Figure 4.3: M_t/M_∞ versus $\sqrt{t}$ at short contact times for the adsorption of 2,2-dmb on silylated zeolite samples. The results were corrected for increase in the weight of silylated MFI samples due to SiO_2 deposition on the external surface during silylation treatment. The dotted lines represent the linear fits to the uptake curves.

Ruthven (1×10^{-19} at 296 K),[108] Xiao and Wei (4×10^{-19} at 298 K),[109] and Yu et al. (5×10^{-20} at 295 K).[103] Assuming that the diffusivity of 2,2-dmb in the silylated MFI samples was the same as that in the parent zeolite (500nm-MFI), the effective crystallite size of the silylated zeolite samples was estimated from the initial slope of M_t/M_∞ versus $\sqrt{t}$ plots. The effective crystallite sizes of silylated zeolite samples, as estimated from 2,2-dmb adsorption uptake measurements, are reported in Table 4.2, and show that the effective diffusion lengths increase in the order:

500nm-MFI < SiMFI-1x < SiMFI-2x < SiMFI-3x

4.3.2 Effects of Crystallite Size on Light Olefins Selectivity in MTH Conversion

DME (at 57 – 66 kPa pressure) was reacted on zeolite samples with crystallite sizes varying between 2 nm and 17 μm at ~623 K and 115 – 130 kPa total feed pressure.

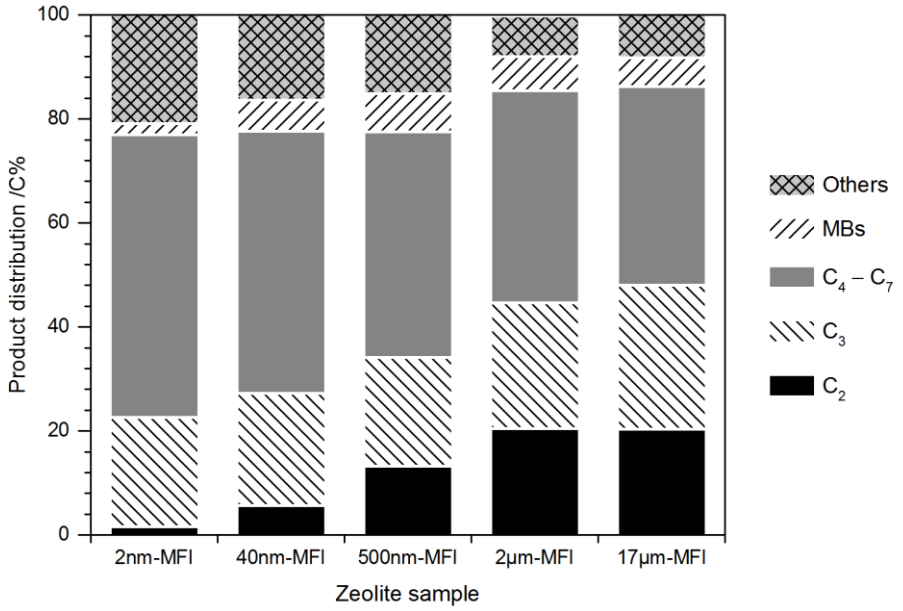

Figure 4.4: Product distribution for the catalytic reaction of DME on zeolite samples with varying crystallite sizes (2 nm – 17 μm) at ~623 K, 57 – 66 kPa DME partial pressure, 46 – 59 % net DME conversion, and ~20 min TOS.

DME space-velocity was varied between 0.6 – 4.3 mol C (mol Al-s)$^{-1}$ to achieve iso-conversion (46 – 59% net DME conversion). Reaction conditions and product distribution for these catalytic reactions are reported in Table 4.5 and Figure 4.4. It can be observed that C_2 selectivity increased monotonically with increasing crystallite size of MFI while the selectivity to C_4 – C_7 hydrocarbons and "Others" fraction decreased with increasing crystallite size of MFI. No particular trends were observed for C_3 and MBs selectivity with the zeolite crystallite size.

Ethene selectivity, propene selectivity, 2MBu selectivity, and ethene/2MBu yield for DME conversion on zeolite samples with varying crystallite sizes are reported in Table 4.6. It can be observed that ethene selectivity was very low on 2nm-MFI (1.5%). MBs, once formed, are likely to exit the small crystallites of 2nm-MFI without undergoing further dealkylation reactions. The near absence of the aromatic dealkylation reactions in the pores of 2nm-MFI resulted in low ethene selectivity (1.5%). It must be noted that MBs are still formed inside the pores of 2nm-MFI but the absence of dealkylation reactions that are essential for light olefin formation, leads us to conclude that ethene production from the aromatics-based cycle was suppressed.

It can also be observed that ethene selectivity was significantly lower (1.5% on 2nm-MFI) compared to propene selectivity (20% on 2nm-MFI) on zeolite samples with small crystallite size. This was because ethene is predominantly produced from the aromatics-based catalytic cycle and is less likely to react further as ethene methylation rate is an order of magnitude slower than propene methylation rate.[95,98,110] Abbot et al.[111,112] showed that ethene is nearly absent in the primary cracking products of linear alkenes at 623 – 678 K on HZSM-5 suggesting that it is not a significant product of the olefins-based cycle and, therefore, is predominantly formed from the aromatics-based

catalytic cycle. Propene, on the other hand, is a product of both the aromatics-based and the olefins-based catalytic cycles. Isotopic experiments by Svelle, Bjørgen, and coworkers[20,59,60] have shown that propene is a part of the olefins-based catalytic cycle; experimental and theoretical studies have shown that propene is also formed from the aromatics-based catalytic cycle via aromatic dealkylation.[36,54,64,66] The relatively high selectivity of propene (20% on 2nm-MFI) can be attributed to its production from the olefins-based catalytic cycle.

Table 4.5: Reaction conditions and product distribution for the catalytic reaction of DME on zeolite samples with varying crystallite sizes (2 nm – 17 μm) at ~623 K, 57 – 66 kPa DME partial pressure, 46 – 59 % net DME conversion, and ~20 min TOS.

Zeolite sample	**2nm-MFI**	**40nm-MFI**	**500nm-MFI**	**2μm-MFI**	**17μm-MFI**
DME space velocity /mol C (mol Al-s)$^{-1}$	1.8	2.2	3.2	2.5	0.6
DME partial pressure /kPa	66	64	62	61	57
Net DME conversion /C%	59	57	46	47	48
Product selectivity (in %, on a carbon basis):					
C_2	1.6	5.7	13.2	20.5	20.4
C_3	21.0	21.6	21.0	24.2	27.6
C_4	16.7	16.4	14.1	15.4	14.6
C_5	12.2	11.7	9.6	9.6	8.6
C_6	14.1	12.8	10.9	9.0	8.5
C_7	11.4	9.5	8.7	6.8	6.5
Methylbenzenes	2.1	5.9	7.4	6.5	5.6
Others[a]	21.0	16.4	15.1	7.8	8.2
H/C in Others[b]	1.8	1.8	1.8	1.8	1.8

[a] The “Others” fraction includes all C_8+ hydrocarbons except polyMBs.

[b] Hydrogen-to-carbon ratio in the “Others” fraction was calculated based on difference in carbon- and hydrogen-content of known species in the reaction effluent and converted feed.

Table 4.6: Selectivity towards ethene, propene, 2MBu, and ethene/2MBu yield, for the catalytic reaction of DME on zeolite samples with varying crystallite sizes (2 nm – 17 μm) at ~623 K, 57 – 66 kPa DME partial pressure, 46 – 59 % net DME conversion, and ~20 min TOS.

Zeolite sample	Ethene	Propene	2MBu[a]	Ethene/2MBu[b]
2nm-MFI	1.5	20.5	7.9	0.2
40nm-MFI	5.7	21.0	8.1	0.7
500nm-MFI	13.2	20.0	7.0	1.9
2μm-MFI	20.4	22.8	6.4	3.2
17μm-MFI	20.3	26.2	5.7	3.6

[a] 2-methylbutane + 2-methyl-2-butene.

[b] Ratio of the synthesis rates of ethene and the sum of 2-methylbutane and 2-methyl-2-butene.

It can be observed from Table 4.6 that ethene selectivity increased substantially from 1.5% to 20% while propene selectivity increased only marginally from 21% to 26% as the crystallite size of MFI increased from 2 nm to 17 μm. Consequentially, the total light olefin selectivity also increased from 22% on 2nm-MFI to 47% on 17μm-MFI. Enhanced transport restrictions in zeolite samples with larger crystallites result in (i) an increase in the intra-crystallite residence time of bulkier hydrocarbons like MBs, and/or (ii) an increase in the concentration of these bulky hydrocarbons inside the zeolite pores. An increase in the intra-crystallite residence time of MBs allows these MBs to interact with more Brønsted acid sites and undergo multiple methylation/dealkylation reactions before exiting the zeolite thereby increasing light olefin production. A higher concentration of MBs inside the zeolite pores, on the other hand, enhances the number of chain carriers of the aromatics-based catalytic cycle. Both these effects result in higher selectivity towards light olefins (ethene and propene) because of increased propagation of the aromatics-based catalytic cycle. Based on the data acquired in this study, we cannot distinguish between the two

effects and either, or both, of these effects could be responsible for the higher light olefins selectivity observed in zeolite samples with larger crystallites.

Another observation that can be made (from Figure 4.4) is that ethene selectivity increased substantially and monotonically while propene selectivity was nearly invariant and increased only marginally with increasing crystallite size of MFI. The 14-fold increase in ethene selectivity with increasing crystallite size is attributed to increased propagation of the aromatics-based catalytic cycle. An explanation for the near invariance in propene selectivity when comparing samples of different crystallite size is the higher reactivity of propene. An alternative explanation is that any increase in propene production due to the increased propagation of the aromatics-based catalytic cycle may be compensated by a decrease in propene production from the olefins-based catalytic cycle. Table 4.6 shows the effects of increasing crystallite size on 2MBu selectivity and ethene/2MBu yield for DME conversion at ~623 K. It can be observed that the selectivity towards 2MBu, which is a representative of the extent of propagation of olefins-based catalytic cycle, decreased with increasing crystallite size, suggesting that the olefins-based catalytic cycle was suppressed, at least to some extent, and resulted in a decrease in propene production from this catalytic cycle. Ethene/2MBu yield increased monotonically from 0.2 to 3.6 with increasing crystallite size thereby supporting our hypothesis that the aromatics-based catalytic cycle propagated to a greater extent relative to the olefins-based catalytic cycle in zeolite samples with large crystallites.

4.3.3 Effects of Crystallite Size on Methylbenzenes Production

Normalized FID chromatograms of the reaction effluent of DME conversion on zeolite samples with varying crystallite sizes (2 nm to 17 μm) at ~623 K and ~20 min time-on-stream are presented in Figure 4.5. It can be observed that the crystallite size of MFI

affected the relative concentration of MBs present in the reaction effluent. A noticeably higher concentration of hexaMB and pentaMB was observed in the reactor effluent of DME conversion on 2nm-MFI. The reactor effluent of DME conversion on 17μm-MFI, on the other hand, had a significantly higher concentration of xylenes. The distribution of MBs shifted towards MBs with less methyl substituents as the crystallite size of MFI was increased. Table 4.7 shows the average number of methyl substituents in MBs present in the reaction effluent. The average number of methyl substituents in MBs decreased monotonically from 3.6 to 2.0 with increasing zeolite crystallite size. It is likely that enhanced transport restrictions inside the zeolite samples with large crystallites prevented MBs with more methyl substituents from exiting the zeolite thereby decreasing their relative concentration in the reactor effluent.

4.3.4 Effects of Silylation Treatment on Light Olefins Selectivity in MTH

DME was reacted on silylated zeolite samples at ~623 K, 62 – 64 kPa DME pressure, and 115 – 118 kPa total feed pressure. DME space-velocity was varied between 2.4 – 3.6 mol C (mol Al-s)$^{-1}$ to achieve iso-conversion (46 – 59% net DME conversion). Reaction conditions and product distribution for these catalytic reactions are reported in Table 4.8 and Figure 4.6. We reported in Section 4.3.1.2 that the relative transport restrictions (and the effective diffusion length) in the silylated zeolite samples, based on the 2,2-dmb adsorption uptake measurements, increases in the order:

500nm-MFI < SiMFI-1x < SiMFI-2x < SiMFI-3x.

It can be observed from Figure 4.6 that C_2 and C_3 selectivity increased monotonically with increasing transport restrictions while the selectivity to C_4 – C_7 hydrocarbons and MBs decreased with increasing transport restrictions in the silylated zeolite samples.

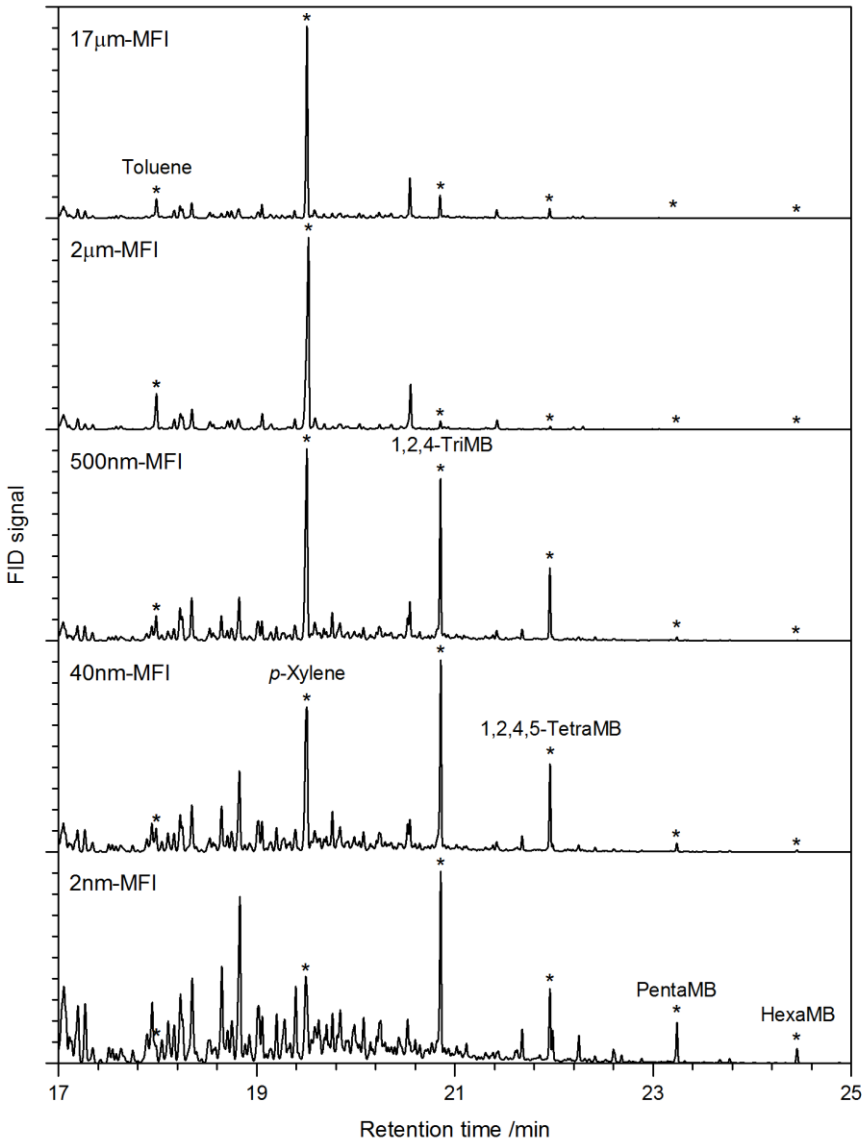

Figure 4.5: Normalized (to total MBs concentration) FID chromatograms of the reactor effluent of DME conversion on zeolite samples with varying crystallite sizes (2 nm – 17 μm) at ~20 min TOS.

Table 4.7: Average number of methyl substituents in the MBs present in the reaction effluent of DME conversion on zeolite samples with varying crystallite sizes (2 nm – 17 μm) at ~20 min TOS.

Zeolite sample	Average number of methyl substituents
2nm-MFI	3.6
40nm-MFI	2.7
500nm-MFI	2.4
2μm-MFI	1.9
17μm-MFI	2.0

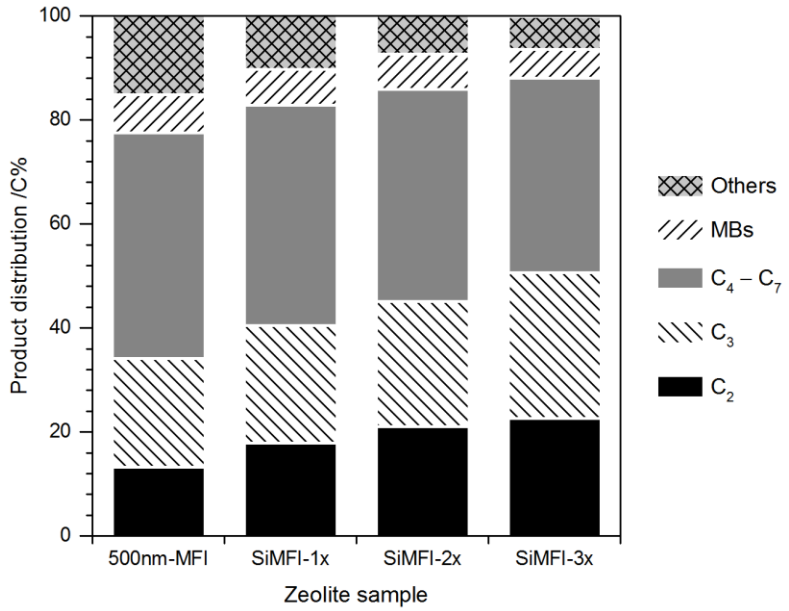

Figure 4.6: Product distribution for the catalytic reaction of DME to hydrocarbons on silylated zeolite samples at ~623 K, 62 – 64 kPa DME partial pressure, 46 – 59% net DME conversion, and ~20 min TOS.

The effects of external transport restrictions in the silylated zeolite samples on ethene selectivity, propene selectivity, 2MBu selectivity, and ethene/2MBu yield, are presented in Table 4.9. It can be observed that ethene selectivity increased monotonically

with increasing transport restrictions. Similar to the observations made for samples with varying crystallite sizes (from 2 nm to 17 μm) in Section 4.3.2, ethene/2MBu yield increased monotonically while 2MBu selectivity decreased monotonically with increasing transport restrictions suggesting that the propagation of the aromatics-based catalytic cycle was enhanced while that of the olefins-based catalytic cycle was suppressed in zeolite samples with more transport limitations, which consequentially resulted in higher ethene and total light olefins selectivity.

Table 4.8: Reaction conditions and product distribution for the catalytic reaction of DME on silylated zeolite samples at ~623 K, 62 – 64 kPa DME partial pressure, 46 – 58% net DME conversion, and ~20 min TOS.

Zeolite sample	**500nm-MFI**	**Si-MFI-1x**	**Si-MFI-2x**	**Si-MFI-3x**
DME space velocity /mol C (mol Al-s)$^{-1}$	3.2	3.6	3.3	2.4
DME partial pressure /kPa	62	62	64	62
Net DME conversion /C%	46	53	58	53
Product selectivity (in %, on a carbon basis):				
C_2	13.2	17.9	21.0	22.6
C_3	21.0	22.6	24.1	28.0
C_4	14.1	14.9	15.5	15.2
C_5	9.6	9.9	9.8	8.6
C_6	10.9	10.1	9.3	8.1
C_7	8.7	7.4	6.2	5.6
Methylbenzenes	7.4	6.9	6.8	5.5
Others[a]	15.1	10.3	7.3	6.3
H/C in Others[b]	1.8	1.8	1.8	1.8

[a] The “Others” fraction includes all C_8+ hydrocarbons except polyMBs.

[b] Hydrogen-to-carbon ratio in the “Others” fration was calculated based on differences in carbon- and hydrogen-content of known species in the reaction effluent and the converted feed.

Table 4.9: Selectivity towards ethene, propene, 2MBu, and ethene/2MBu yield, for the reaction of DME on silylated zeolite samples at ~623 K, 62 – 64 kPa DME partial pressure, 46 – 59 % net DME conversion, and ~20 min TOS.

Zeolite sample	Ethene	Propene	2MBu[a]	Ethene/2MBu[b]
500nm-MFI	13.2	20.0	7.0	1.9
SiMFI-1x	17.9	21.2	6.9	2.6
SiMFI-2x	20.9	22.4	6.5	3.2
SiMFI-3x	22.5	26.7	5.5	4.1

[a] 2-methylbutane + 2-methyl-2-butene.

[b] Ratio of the synthesis rates of ethene and the sum of 2-methylbuatne and 2-methyl-2-butene.

4.3.5 Effects of Effective Crystallite Size on Ethene and Total Light Olefins Selectivity

Figure 4.7 shows the changes in ethene selectivity and total light olefins selectivity, as well as ethene/2MBu yield, with increasing crystallite size of all zeolite samples investigated in this work including the silylated MFI samples for which the effective crystallite size was estimated from 2,2-dmb adsorption uptake measurements. It can be observed that ethene selectivity and total light olefins selectivity increased monotonically with increasing effective crystallite size of zeolites irrespective of whether the transport restrictions within the zeolites arise due to longer diffusion lengths or due to silylation of the external surface. Ethene/2MBu also increased monotonically from 0.2 to 4.1 as effective crystallite size increased from ~2 nm to ~18 μm. This monotonic increase in ethene/2MBu yield with increasing crystallite size suggests that the propagation of the aromatic-based catalytic cycle was increased relative to the olefins-based catalytic cycle in zeolite sample with larger crystallites. The enhanced propagation of the aromatics-based catalytic cycle is a consequence of MBs interacting with more Brønsted acid sites and undergoing multiple methylation/dealkylation reactions before exiting the zeolite,

whilst producing a light olefin during each catalytic cycle, thereby providing a mechanistic basis for the increase in ethene and total light olefins selectivity with increasing crystallite size of zeolites for MTH conversion.

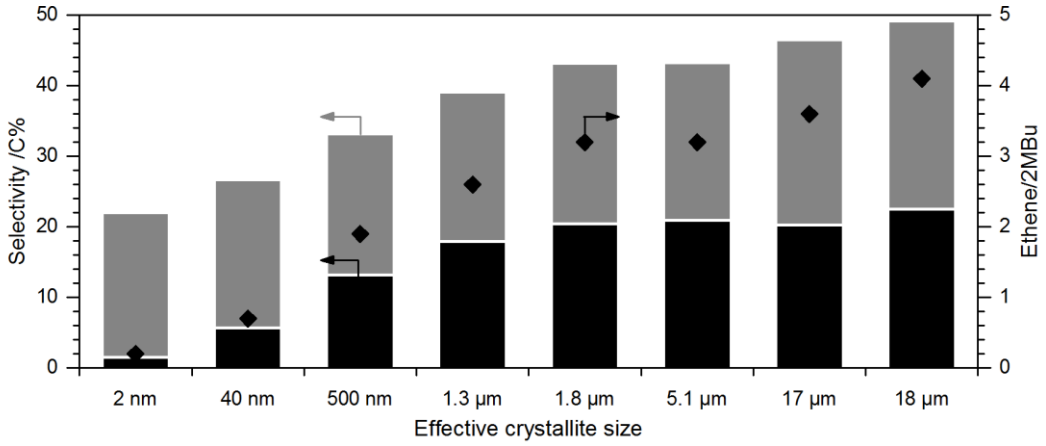

Figure 4.7: Ethene selectivity (■), propene selectivity (■), and ethene/2MBu yield (◆), as a function of effective crystallite size for all zeolite samples, including the silylated zeolite samples, investigated in this work, for the catalytic reation of DME at ~623 K and iso-conversion conditions (46 – 59% net DME conversion).

4.4 Conclusions

Five zeolite samples with MFI-type framework and crystallite size varying between 2 nm and 17 µm were investigated for DME conversion to hydrocarbons at ~623 K and 57 – 66 kPa DME pressure. Ethene selectivity, at 46 – 59 % net DME conversion, increased from 1.5% on a zeolite sample with small (~2nm) crystallites to 20% on a zeolite sample with large (~17 µm) crystallites, and total light olefins selectivity increased from 22% to 47%. External transport restrictions were introduced in a conventional zeolite sample with ~500 nm crystallites by silylation treatment using TEOS. Three silylated MFI samples (SiMFI-1x, SiMFI-2x, and SiMFI-3x) were synthesized by single- or multi-cycle silylation

treatments, and based on the adsorption uptake measurements of 2,2-dmb, transport restrictions (and the effective diffusion length) in the silylated zeolite samples increased in the following order:

500nm-MFI < SiMFI-1x < SiMFI-2x < SiMFI-3x

The silylated zeolite samples were investigated for DME conversion at ~623 K, 62 – 64 kPa DME pressure, and 46 – 58 % net DME conversion. Ethene selectivity increased from 13% to 23% and the total olefin selectivity increased from 33% to 49% with increasing transport restrictions.

Ethene and total olefins selectivity increased monotonically with the effective crystallite size for all zeolite samples used in this study, irrespective of their provenance. This increase is attributed to (i) an increase in the concentration of MBs inside the zeolite pores, and/or (ii) an increase in the intra-crystallite residence time of MBs. Both these effects enhance the propagation of the aromatics-based catalytic cycle, which enables the MBs present inside the zeolite pores to interact with multiple Brønsted acid sites and undergo multiple aromatic methylation/dealkylation reactions whilst producing a light olefin during each catalytic cycle. Enhanced propagation of the aromatics-based catalytic cycle relative to the olefins-based catalytic cycle was substantiated by a monotonic increase in ethene/2MBu yield with increasing effective crystallite size.

CHAPTER FIVE

Methanol-to-Hydrocarbons Conversion on Diffusion-Free Self-Pillared Pentasil MFI and 3DOm-i MFI Zeolites

* Reported from R. Khare and A. Bhan, *Journal of Catalysis* **329** (2015) 218–228

5.1 Introduction

In Chapter 4, we reported that the crystallite size of MFI affects the product distribution in MTH by altering the relative extents of propagation of the aromatics-based and the olefins-based catalytic cycles. We showed that ethene and total light olefins selectivity, for the catalytic conversion of DME on MFI-type zeolites at ~623 K and iso-conversion conditions (46 – 59% net DME conversion), increased monotonically with increasing effective crystallite size of zeolite (from ~2 nm to ~18 μm). This increase in ethene selectivity with increasing crystallite size was attributed to an increase in the intra-crystalline residence time of MBs, which enhances the propagation of the aromatics-based catalytic cycle relative to the olefins-based catalytic cycle. A concomitant monotonic increase in ethene/2MBu yield was also observed as the effective zeolite crystallite size was increased from ~2 nm to ~18 μm.

Sugimoto et al.[80] also showed that ethene selectivity increased from 0.7% on HZSM-5 with ~200 nm crystallites to 12.9% on HZSM-5 with 3 – 4 μm crystallites. Rownaghi et al.[81,82] investigated methanol conversion on HZSM-5 zeolites with varying crystallite sizes at ~643 K and observed that ethene selectivity increased from 6.6% on HZSM-5 nanocrystals (~120 nm crystallites) to 9.6% on a conventional ZSM-5 zeolite with

larger crystallites (wide-range). Bleken et al.[84] reported that MFI nanosheets, which were only single unit cell thick (~2.5 nm) along the *b*-axis, exhibited lower selectivity towards C_2 hydrocarbons than a conventional HZSM-5 catalyst at 623 K.

In this work, we report the intrinsic propagation of the aromatics-based and the olefins-based catalytic cycles inside the pores of MFI-type zeolites (assessed using diffusion-free MFI zeolites) and the contribution of these catalytic cycles towards ethene production at industrially relevant reaction temperatures (>723 K) and sub-complete DME conversion conditions. A systematic investigation on two diffusion-free zeolite samples, specifically, a self-pillared pentasil MFI zeolite (~1 nm diffusion length) and a 3DOm-i MFI zeolite (~20 nm diffusion length), allowed us to infer that (i) MFI is intrinsically a poor ethene synthesis catalyst at industrially relevant reaction temperatures and <100% conversion, (ii) the number of chain carriers of the olefins-based catalytic cycle is saturated inside the zeolite pores at <100% DME conversion, (iii) the aromatics-based catalytic cycle is suppressed due to low concentration of MBs inside the zeolite pores, and (iv) the low ethene selectivity in diffusion-free MFI zeolites (<2.8%) can be enhanced 2- to 4-fold by co-feeding aromatics like toluene or *p*-xylene with DME.

5.2 Materials and Methods

5.2.1 Catalyst Synthesis and Preparation

The self-pillared pentasil (SPP) MFI zeolite and the 3DOm-i MFI zeolite, were synthesized according to the procedures described in Reference 89. The zeolite samples were converted to their respective protonated forms by treating in 1.67 $cm^3\ s^{-1}$ dry air (Minneapolis Oxygen, 20 – 21% O_2, <10 ppm H_2O) at 823 K for 4 h. The temperature was increased from ambient to 823 K in 12 h and was held at 823 K for 4 h before reducing to

the ambient temperature. The samples were then pressed into pellets, crushed, and sieved between 40- and 80-mesh sieves to obtain aggregate particles with uniform size between 180 and 425 μm. Quartz sand (Acros Organics) was used for diluting the catalyst bed to prevent temperature rise due to exothermic nature of MTH reactions. Prior to its use, the quartz sand was washed with 1 M nitric acid (Sigma-Aldrich), then rinsed several times with deionized water, dried, and sieved between 40- and 80-mesh sieves.

5.2.2 Structural and Chemical Characterization

The Si/Al in the zeolite samples was determined from ICP-OES elemental analysis performed by Galbraith Laboratories, Inc. The analytical method used was GLI procedure ME-70. Zhang et al.[89] estimated the average diffusion length in the zeolite samples. The fraction of external Brønsted acid sites in the zeolite samples was also estimated by Zhang et al.[89] from the ratio of the number of Brønsted acid sites determined from 2,2-di-*tert*-butylpyridine (DTBP) titration and the number of Brønsted acid sites determined by DME titration.

5.2.3 Catalytic Conversion of DME to Hydrocarbons

Catalytic reactions of DME were carried out in a 316/316L stainless steel packed-bed reactor (1/4 in OD; 0.035 in wall thickness) equipped with a concentric thermal well (1/16 in OD, 0.014 in wall thickness). Isothermal conditions were maintained in the catalyst bed using a heating coil (ARi Industries Inc., AeroRod® heating assembly) regulated by a Watlow 96 series temperature controller. Temperature of the catalyst bed was measured using a K-type thermocouple (Omega Engineering) inserted into the concentric thermal well. The reactions were run using 7 – 40 mg catalyst to achieve the desired chemical conversions. Methanol was considered as a reactant in the calculations of net conversion. The catalyst bed was diluted with 100 – 150 mg of quartz sand to prevent exotherms. Prior

to every reaction, the catalyst bed was pretreated in situ in 1.67 cm^3 s^{-1} He (Minneapolis Oxygen, 99.995% purity) at 823 K for 4 h. The temperature was increased from ambient to 823 K in 8 h and was held at 823 K for 4 h before reducing to the reaction temperature.

The reactant stream consisted of DME (Matheson Tri-Gas, 99.5% purity) and a mixture of CH_4 and Ar (Airgas, 10% CH_4, 90% Ar) that was used as an internal standard for the FID. In some cases, He (Minneapolis Oxygen, 99.995% purity) was used in balance to keep the concentration of the internal standard comparable to that of the effluent products. Propene (Praxair, 50% propene, 50% argon), 1-hexene (Sigma-Aldrich, 99% purity), toluene (Sigma-Aldrich, 99.5% purity), *p*-xylene (Sigma-Aldrich, 99% purity), 1,2,4-triMB (Sigma-Aldrich, 99% purity), or DTBP (Sigma-Aldrich, 97% purity) were co-fed with DME in some cases. Gas flow rates were maintained using Brooks Instrument 5850S/SLA5850 series mass flow controllers and the liquids were fed through a 1.0 mL or a 2.5 mL SGE syringe using a Cole Palmer EW-74900-00 syringe pump. The total feed pressure was maintained at ~120 kPa and the reactions were carried out at 723 K. The temperature variation in the catalyst bed was less than 1 K during the reaction.

The reactor effluents were analyzed using an online Agilent 7890 series GC – 5975C series MS equipped with a 100% dimethylpolysiloxane Agilent J&W HP-1 column (50 m × 320 μm × 0.52 μm) connected to an FID and a (5%-phenyl)-methylpolysiloxane Agilent J&W HP-5ms column (25 m × 320 μm × 0.25 μm) connected to an MSD. The product distributions shown in Section 5.3 include C_8+ hydrocarbons that were not identified separately and are classified as “Others”. The average hydrogen-to-carbon ratio in the hydrocarbon species present in the “Others” fraction was calculated from the hydrogen- and carbon-content of known species in the converted feed and the reaction effluent, and is reported with the data in some cases.

5.3 Results and Discussion

5.3.1 Structural and Chemical Characterization

The detailed structural and chemical characterization of SPP MFI and 3DOm-i MFI zeolite samples is described in the Supplementary Information section of Reference 89 The diffusion length, fraction of external Brønsted acid sites, and silicon-to-aluminum ratio, in SPP MFI and 3DOm-i MFI zeolite samples are reported in Table 5.1.

Table 5.1: Diffusion length, fraction of external Brønsted acid sites, and silicon-to-aluminum ratio, in the zeolite samples investigated in this work.

Zeolite samples	Diffusion length /nm	Fraction of external Brønsted acid sites	Si/Al
SPP MFI	1[c]	0.29[a]	84[b]
3DOm-i MFI	20[c]	0.14[a]	72[b]

[a] Ratio of the number of Brønsted acid sites as determined from DTBP titration and the number of Brønsted acid sites as determined by DME titration; performed by Zhang et al.[89]

[b] Estimated from ICP-OES elemental analysis, performed by Galbraith Laboratories, Inc.

5.3.2 Catalytic Reactions of DME on SPP MFI and 3DOm-i MFI

DME conversion was investigated at ~723 K as higher temperatures are more relevant to ZSM-5 based industrial processes. Table 5.2 shows the reaction conditions and product distribution for the reaction of DME on SPP MFI and 3DOm-i MFI at 623 K and 723 K. It can be observed that the selectivity towards C_2, MBs, and “Others” fraction decreased while C_3 and C_4 – C_7 hydrocarbons selectivity increased with an increase in the reaction temperature. These results suggest that the aromatics-based catalytic cycle is suppressed at higher reaction temperatures. A possible reason for this decrease in the propagation of the aromatics-based catalytic cycle is a decrease in the concentration of chain carriers of the aromatics-based catalytic cycle with increasing reaction temperature.

At higher temperatures, we infer that higher olefins prefer to crack or desorb instead of cyclizing and undergoing hydrogen-transfer reactions to form MBs. This decrease in the concentration of MBs inside the zeolite pores decreases the probability that MBs will undergo a dealkylation event to produce ethene and complete the catalytic cycle. These observations suggest that the propagation of the aromatics-based catalytic cycle is intrinsically suppressed relative to the propagation of the olefins-based catalytic cycle in the pores of MFI, especially at industrially relevant reaction temperatures (>723 K), due to lower concentration of MBs in the zeolite pores.

Table 5.2: Reaction conditions and product distribution for the catalytic reaction of DME on SPP MFI and 3DOm-i MFI at 623 K and 723 K, ~120 kPa total feed pressure, and ~20 min TOS.

Zeolite sample	**SPP MFI**		**3DOm-i MFI**	
Reaction temperature /K	623	723	623	723
Carbon space-velocity /mol C (mol Al-s)$^{-1}$	1.8	9.7	2.2	11
DME partial pressure /kPa	66	63	64	62
Net DME conversion /%	59	47	57	57
Product distribution (in %, on a carbon basis)				
C_2 (Ethene)	1.6 (1.5)	1.1 (1.1)	5.7 (5.7)	2.8 (2.8)
C_3 (Propene)	21.0 (20.5)	26.6 (26.2)	21.6 (21.0)	28.7 (28.0)
C_4 – C_7	54.4	60.4	50.4	57.7
Methylbenzenes	2.1	1.5	5.9	2.8
Others[a]	21.0	10.4	16.4	8.0
Ethene/2MBu[b]	0.19	0.15	0.70	0.36
H/C in "Others"[c]	1.76	1.81	1.78	1.71

[a] The "Others" fraction includes C_8+ hydrocarbons except polyMBs.

[b] Ratio of the synthesis rates of ethene and the sum of 2-methylbutane and 2-methyl-2-butene.

[c] Hydrogen-to-carbon ratio in the "Others" fraction was calculated based on the difference in carbon- and hydrogen-content of known hydrocarbon species in the reaction effluent and the converted feed.

5.3.3 Effects of External Brønsted Acid Sites on DME Conversion

The crystallite size of SPP MFI is very small (~1.5 nm), which results in ~29% of the total Brønsted acid sites being present on the external surface of the catalyst.[89] In comparison, a conventional MFI zeolite from Zeolyst International, Inc. (CBV 8014) with ~500 nm crystallites has <3% Brønsted acid sites on the external surface.[89] The large fraction of external Brønsted acid sites in SPP MFI can have an effect on the selectivity of DME conversion. The catalytic conversion of DME was therefore carried out in the presence of DTBP to passivate the external Brønsted acid sites and study their effect on MTH product distribution. The large kinetic diameter of DTBP (~1.05 nm)[100] prevents it from entering the pores of MFI and therefore, DTBP only interacts with acid sites present on the external surface and near the pore-mouth region of MFI. The Brønsted acid sites present within the zeolite pores are largely unaffected by DTBP titration.

5.3.3.1 Effects of Co-Feeding 2,6-Di-*tert*-butylpyridine on Catalyst Deactivation

Figure 5.1 shows the deactivation behavior of SPP MFI for DME conversion at ~723 K in the presence of DTBP co-feed. DME space-velocity was 8.0 – 8.8 mol C (mol Al-s)$^{-1}$ and DTBP pressure in the feed was varied from 0.03 to 0.85 kPa. The catalyst deactivated rapidly in the presence of DTBP co-feed, especially at higher DTBP pressures. A possible explanation for this fast deactivation is the adsorption of DTBP on Brønsted acid sites near the pore-mouth region. It is likely that this prevented bulkier molecules like MBs and other coke precursors from exiting the zeolite thereby resulting in faster catalyst deactivation at higher DTBP pressures in the feed. All subsequent catalytic reactions of DME (with DTBP co-feed) were therefore carried out at the lowest DTBP pressure (~0.03 kPa) and the reaction effluents were analyzed only at short times-on-stream (~5 min).

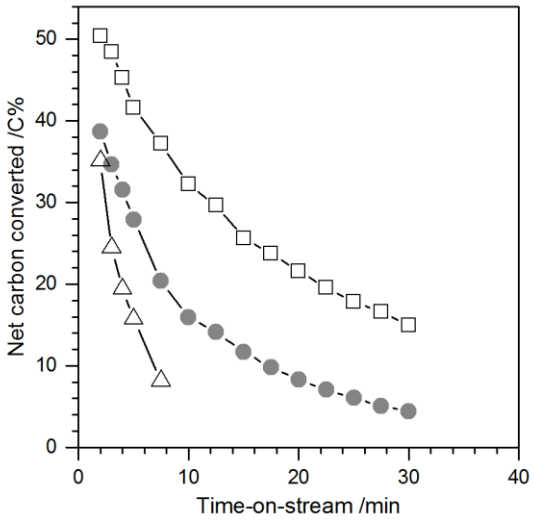

Figure 5.1: Change in net carbon converted versus TOS, for the catalytic reaction of DME on SPP MFI at ~723 K, 58 – 60 kPa DME pressure, and 115 – 125 kPa total feed pressure. DME space-velocity was 8.0 – 8.8 mol C (mol Al-s)$^{-1}$ and DTBP pressure was 0.03 kPa (□), 0.08 kPa (●), or 0.85 kPa (△).

Two factors must be taken into considerations when reporting the selectivity data at short times-on-stream: (i) the reported data could be affected by coke deposition, even at short times-on-stream as the catalyst deactivated rapidly, and (ii) the reported product selectivity could be in the induction period, and therefore not represent stable catalytic behavior. Figure 5.2 shows the change in product distribution with net DME conversion for the reaction of DME on SPP MFI at ~723 K in the presence of ~0.03 kPa DTBP. DME conversion, in this case, varied due to deactivation of the catalyst bed. Figure 5.2 also shows the change in product selectivity with net DME conversion for the reaction of DME alone (without DTBP) on SPP MFI at ~723 K. In this case, DME conversion was varied by changing the space-velocity between 7.8 and 17 mol C (mol Al-s)$^{-1}$. It must be noted that the latter data constitutes of individual experiments and the product selectivity reported is outside the induction period (at >20 min time-on-stream) and is not affected by catalyst deactivation or coke deposition.

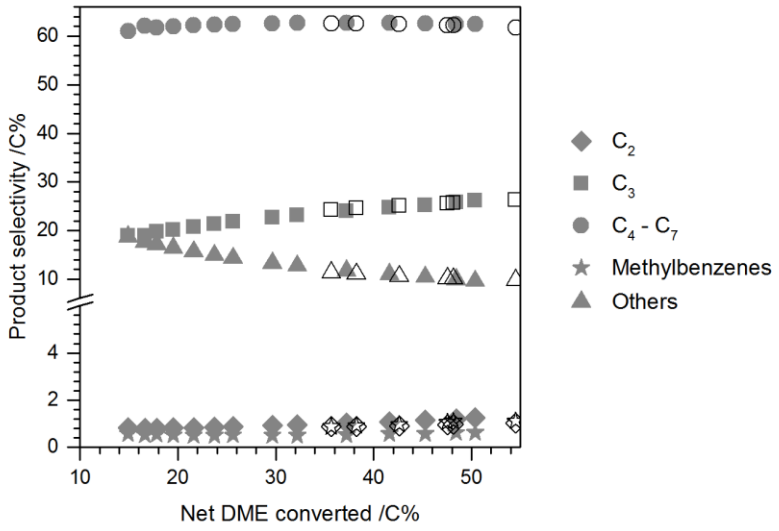

Figure 5.2: Changes in product distribution with net DME conversion for the catalytic reaction of DME on SPP MFI at ~723 K, ~58 kPa DME pressure, and ~125 kPa total feed pressure. DME space-velocity was ~8.0 mol C (mol Al-s)$^{-1}$ and DTBP pressure was ~0.03 kPa. These data are represented by filled symbols. Change in product selectivity with net DME conversion for the reaction of DME alone (without DTBP co-feed) on SPP MFI is also shown (represented by open symbols). DME conversion, in this case, was varied by changing the DME space-velocity between 7.8 and 17 mol C (mol Al-s)$^{-1}$.

It can be observed that the two data-sets overlap suggesting that the product selectivity reported for the DTBP co-feed experiments are outside the induction period. These results also suggest that the only effect of coke deposition is a decrease in the number of active sites, which resulted in rapid deactivation of the catalyst bed, and the product selectivity reported for DTBP co-feed experiments was not affected by the coke deposition. Bleken et al.,[84] in an independent experimental study, also investigated the effects of catalyst deactivation on MTH conversion on HZSM-5 at 623 K and showed that the product selectivity in MTH is largely independent of coke content.

5.3.3.2 Effects of Co-Feeding 2,6-Di-*tert*-butylpyridine on MTH Product Distribution

Reaction conditions and product distribution, for the reaction of DME on SPP MFI at ~723 K, in the presence of ~0.03 kPa DTBP co-feed, are reported in Table 5.3. Reaction

conditions and product distribution for the reaction of DME alone (without DTBP co-feed) on SPP MFI at 723 K and iso-conversion conditions (42 – 43% conversion) are also reported in Table 5.3. Figure 5.3 shows the effects of co-feeding DTBP, and therefore the effects of passivating external Brønsted acid sites, on the product selectivity. The observed product distribution (except for marginal changes in MBs and ethene selectivity,) was largely unaffected by the passivation of external Brønsted acid sites and therefore we conclude that external acid sites do not play a significant role in determining the MTH selectivity. Kim and Ryoo[85] also investigated the effects of external surface in MFI nanosheets (with ~30% external Brønsted acid sites) on MTH conversion and showed that when the external sites were poisoned by TPPO, the catalytic cracking of 1,3,5-tri-*iso*-propylbenzene, a reaction that occurs only on the external surface, was completely suppressed. Methanol conversion was, however, unaffected by TPPO-poisoning.

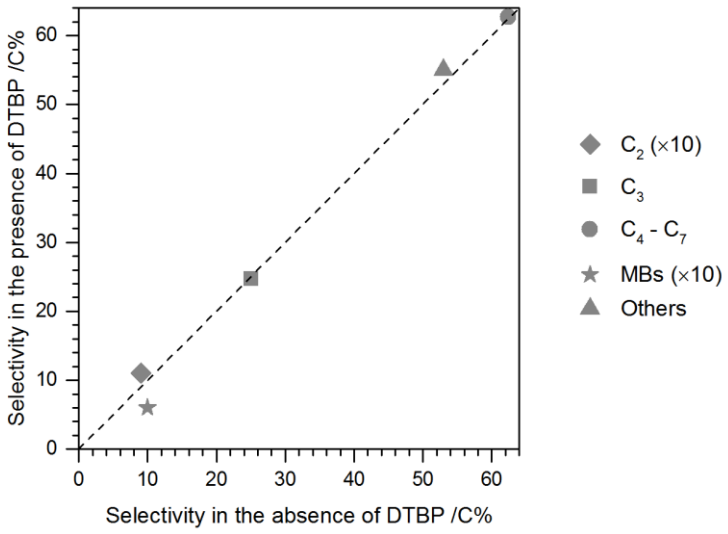

Figure 5.3: Effects of co-feeding DTBP, and therefore the effects of passivating external Brønsted acid sites, on product selectivity of DME conversion on SPP MFI at ~723 K and 42 – 43% net DME conversion. The data in the absence of DTBP is reported at ~20 min TOS while the data in the presence of DTBP is reported at ~5 min TOS.

Table 5.3: Reaction conditions and product distribution for the catalytic reaction of DME with/without DTBP on SPP MFI at ~723 K and 115 – 125 kPa total feed pressure. The data in the absence of DTBP is at ~20 min TOS while the data in the presence of DTBP is at ~5 min TOS. Reaction conditions and product distribution for the catalytic reaction of DME on 3DOm-i MFI at ~723 K, ~120 kPa total feed pressure, and ~20 min TOS is also reported.

Reactant feed	**DME**	**DME + DTBP**	**DME**
Zeolite sample	SPP MFI	SPP MFI	3DOm-i MFI
DME space-velocity /mol C (mol Al-s)$^{-1}$	11	8.0	11
DME partial pressure /kPa	60	58	64
DTBP pressure /kPa	-	~0.03	-
Net DME conversion /%	43	42	57
Product selectivity (in %, on a carbon basis)			
C_2 (Ethene)	0.9 (0.9)	1.1 (1.1)	2.8 (2.8)
C_3 (Propene)	25.1 (24.5)	24.7 (24.4)	28.7 (28.0)
C_4 – C_7	62.4	62.7	57.7
Methylbenzenes	1.0	0.6	2.8
Others[a]	10.6	11.0	8.0
Ethene/2MBu[b]	0.15	0.16	0.36
H/C in "Others"[c]	1.83	1.80	1.71

[a] The "Others" fraction includes C_8+ hydrocarbons except polyMBs.

[b] Ratio of the synthesis rates of ethene and the sum of 2-methylbutane and 2-methyl-2-butene.

[c] Hydrogen-to-carbon ratio in the "Others" fraction was calculated based on the difference in carbon and hydrogen content of known hydrocarbon species in the reaction effluent and the converted feed.

It can be observed from Figure 5.3 that MBs selectivity decreased marginally from 1.0% without DTBP to 0.6% with DTBP, and ethene selectivity increased marginally from 0.9% in the absence of DTBP to 1.1% in the presence of DTBP. A possible explanation for this observation is the adsorption of DTBP on Brønsted acid sites close to the pore-mouth region, which prevented bulkier molecules like MBs from exiting the zeolite crystallite and, as a result, increased their intra-crystallite residence time. Adsorption of

DTBP on acid sites close to pore-mouth region, therefore, increased the effective diffusion length in the zeolite and resulted in enhanced propagation of the aromatics-based catalytic cycle resulting in higher ethene selectivity.

5.3.3.3 Effects of Co-Feeding 2,6-Di-*tert*-butylpyridine on Effective Diffusion Length

The reaction conditions and product selectivity for the catalytic reaction of DME on 3DOm-i MFI at ~723 K, ~120 kPa total feed pressure, and ~20 min time-on-stream are reported in Table 5.3. The diffusion length in 3DOm-i MFI (~20 nm) is longer than the diffusion length in SPP MFI (~1 nm) and as a result, ethene selectivity on 3DOm-i MFI (2.8%) was higher than the ethene selectivity on SPP MFI (0.9%). Ethene/2MBu yield on 3DOm-i MFI (0.36) was also significantly higher than ethene/2MBu yield on SPP MFI (0.15) indicating a significant enhancement in the propagation of the aromatics-based catalytic cycle with increasing diffusion length. In comparison to 3DOm-i MFI, both ethene selectivity (from 0.9 to 1.1) and ethene/2MBu yield (from 0.15 to 0.16) increased only marginally as a result of DTBP adsorption on the external surface of SPP MFI. These results suggest that the increase in the effective diffusion length in SPP MFI, due to adsorption of DTBP on acid sites close to the pore-mouth region, is insignificant and can be neglected while making conclusions regarding the effects of passivating external Brønsted acid sites in SPP MFI on the product selectivity of DME conversion.

5.3.4 Effects of Co-Feeding Olefins with DME

Table 5.4 shows the reaction conditions and product distribution, and Figure 5.4 shows ethene selectivity, 2MBu selectivity, and ethene/2MBu yield, for the catalytic conversion of DME in the presence 1-hexene or propene co-feed on SPP MFI at ~723 K. It can be observed that co-feeding small amounts (2 – 4 kPa) of propene or 1-hexene with DME (~61 kPa) had no effect on the overall product distribution. This observation suggests

that the number of chain-carriers of the olefins-based catalytic cycle is saturated inside the pores of MFI and co-feeding propene or 1-hexene did not significantly enhance their concentration inside the zeolite pores. The propagation of the olefins-based catalytic cycle was therefore not enhanced by co-feeding olefins under the investigated reaction conditions. This hypothesis is also substantiated by the fact that ethene/2MBu yield remained unaffected by the presence of propene or 1-hexene co-feed (Figure 5.4). It is however important to note that even under the conditions where the number of chain-carriers of the olefins-based catalytic cycle was saturated inside the pores of MFI, ethene selectivity was low (~1%). The implication of this observation is that even if all ethene were being produced from the olefins-based cycle, the production of ethene via olefin *β*-scission reactions on diffusion-free MFI samples at <100% conversion, thereby representing the intrinsic mechanistic behavior of MTH conversion on MFI, is insignificant under the investigated reaction conditions.

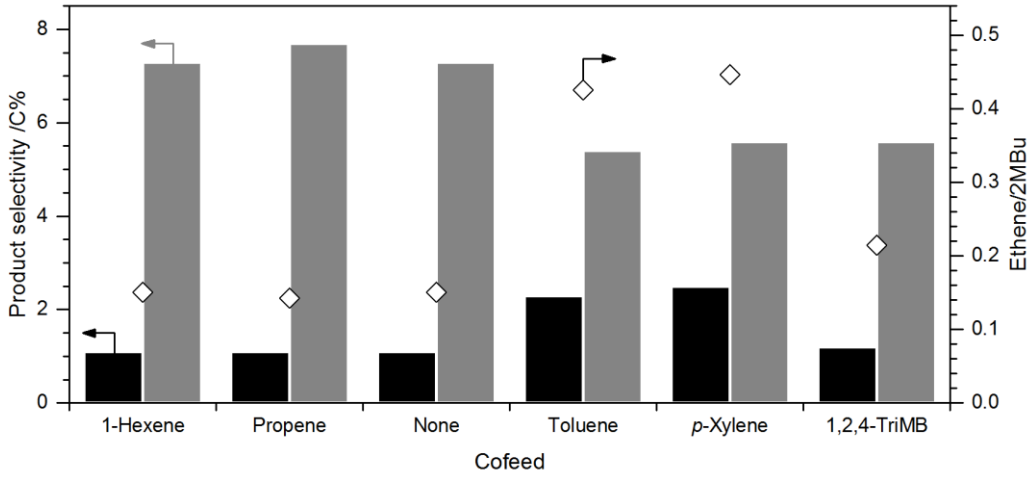

Figure 5.4: Ethene selectivity (■), 2MBu selectivity (■), and ethene/2MBu yield (◇), for the catalytic reactions of DME with olefin/aromatic co-feeds on SPP MFI at ~723 K, ~120 kPa total feed pressure, 47 – 64% net carbon conversion, and ~20 min TOS.

Table 5.4: Reaction conditions and product distribution, for the reaction of DME with olefin/aromatic co-feeds on SPP MFI at ~723 K, ~120 kPa total feed pressure, and ~20 min TOS.

Co-feed	**1-Hexene**	**Propene**	**None**	**Toluene**	***p*-Xylene**	**1,2,4-triMB**
Space-velocity /mol C (mol Al-s)$^{-1}$	9.4	10	9.7	10	8.7	9.4
DME partial pressure /kPa	61	61	63	62	60	61
Co-feed partial pressure /kPa	2	4	-	2	2	2
Net carbon conversion /%	64	52	47	51	55	49
Feed composition (in %, on a carbon basis)						
DME	91	92	100	90	89	87
Co-feed	9	8	-	10	11	13
Product distribution (in %, on a carbon basis)						
C_2	1.1	1.1	1.1	2.3	2.5	1.3
C_3	26.9[a]	28.3	26.6	20.1	20.7	20.4
C_4 – C_7	61.8	60.9[a]	60.4	47.9	48.5	48.3
Methylbenzenes[a]	1.2	0.6	1.5	21.4[a]	19.4[a]	21.7[a]
Others[b]	9.1	9.4	10.4	8.4	8.8	8.4
Ethene/2MBu[c]	0.14	0.14	0.15	0.42	0.45	0.22
H/C in "Others"[d]	1.80	1.74	1.81	1.74	1.72	1.85

[a] Reported selectivity includes the unreacted co-feed.

[b] The "Others" fraction includes C_8+ hydrocarbons except polyMBs.

[c] Ratio of the synthesis rates of ethene and the sum 2-methylbutane and 2-methyl-2-butene.

[d] Hydrogen-to-carbon ratio in the "Others" fraction was calculated based on the difference in carbon and hydrogen content of known hydrocarbon species in the reaction effluent and the converted feed.

5.3.5 Effects of Co-Feeding Aromatics with DME

Table 5.4 shows the reaction conditions and product distribution, and Figure 5.4 shows ethene selectivity, 2MBu selectivity, and ethene/2MBu yield, for the reaction of DME with toluene or *p*-xylene on SPP MFI at ~723 K. It can be observed that ethene selectivity increased at least 2-fold when either toluene or *p*-xylene was co-reacted with

DME. The concentration of MBs in the reaction effluent also increased from 1.6% without any co-feed to 21% and 19% (including the unreacted co-feed) in the presence of toluene or *p*-xylene, respectively. The kinetic diameter of toluene and *p*-xylene (~0.59 nm)[106,113] is comparable to the diameter of pore-openings in MFI (~0.55 nm)[42,43] and these molecules can enter the pores of MFI. Co-feeding toluene or *p*-xylene therefore likely increased the concentration of MBs inside the zeolite pores. Higher concentration of MBs inside the zeolite pores increased the probability of these MBs to undergo a dealkylation event before exiting the zeolite crystallite thereby increasing the propagation of the aromatics-based catalytic cycle. Figure 5.4 shows that ethene/2MBu yield increased from 0.15 with no co-feed to 0.42 and 0.45 when either toluene or *p*-xylene were co-fed with DME, respectively, confirming that the propagation of the aromatics-based catalytic cycle was enhanced relative to the olefins-based catalytic cycle in the presence of aromatic co-feeds. These results suggest that the propagation of the aromatics-based catalytic cycle and its contribution towards ethene production is minimal (in the absence of co-feed) on diffusion-free MFI samples at ~723 K and <100% conversion because the number of chain carriers of aromatics-based cycle inside the zeolite pores is low. Increasing the number of chain carriers of the aromatics-based catalytic cycle significantly enhanced the propagation of the aromatics-based catalytic cycle and resulted in higher ethene selectivity.

5.3.6 Effects of Co-Feeding 1,2,4-Trimethylbenzene with DME

DME was also reacted with 1,2,4-triMB on SPP MFI at ~723 K. Reaction conditions, feed composition, and product distribution, as well as ethene selectivity, 2MBu selectivity, and ethene/2MBu yield, for this reaction are reported in Table 5.4 and Figure 5.4, respectively. Unlike toluene or *p*-xylene, co-feeding 1,2,4-triMB with DME did not increase ethene selectivity under similar reaction conditions. A possible reason for this

may be associated with the kinetic diameters of these molecules. The kinetic diameter of 1,2,4-triMB (~0.68 nm)[106,113] is larger than the kinetic diameters of toluene or *p*-xylene (~0.59 nm)[106,113] and significantly larger than the diameter of the pore-openings in SPP MFI (~0.55 nm).[42,43] It is likely that the bulkier nature of 1,2,4-triMB prevented it from entering the pores of MFI. Co-feeding 1,2,4-triMB with DME, therefore, did not increase the concentration of MBs inside the zeolite pores and as a result, propagation of the aromatics-based catalytic cycle was not enhanced. This is also reflected in the ethene/2MBu yield, which increased only marginally from 0.15 to 0.22 (Figure 5.4) when 1,2,4-triMB was co-fed with DME (in comparison to a ~3-fold increase in the case of toluene or *p*-xylene co-feed).

5.3.7 Effects of External Brønsted Acid Sites on MB Methylation

Table 5.5 shows the normalized molar flow rates of MBs in the reaction effluent, for the catalytic reaction of DME with 1,2,4-triB co-feed, on SPP MFI at ~723 K. Normalized MB flow rates for the reaction of DME alone (without any co-feed) on SPP MFI at ~723 K are also reported for comparison. It can be noted that even though 1,2,4-triMB did not enter the pores of MFI, methylation of 1,2,4-triMB still occurred as the concentration of more substituted MBs (i.e., tetraMBs, pentaMB, or hexaMB) in the effluent stream increased significantly in comparison to the experiment in which no 1,2,4-triMB was co-fed. We postulate, based on these observations, that methylation of MBs to higher MB homologues can occur on the external Brønsted acid sites, however, aromatic dealkylation reactions, which are precursors to ethene and other light olefins, require the confinement of the zeolite micropores; this is substantiated by the fact that no increase in ethene selectivity or ethene/2MBu yield was observed when 1,2,4-triMB was co-reacted with DME on SPP MFI.

Table 5.5: Normalized molar flow rates of MBs in the feed and the effluent, for the reaction of DME with toluene, *p*-xylene, or 1,2,4-triMB, in the presence/absence of ~0.03 kPa DTBP on SPP MFI at ~723 K, ~120 kPa total feed pressure, 53 – 62% net DME conversion, and ~5 min TOS.

	Without DTBP				**With DTBP**			
Co-feed	**None**	**Toluene**	***p*-Xylene**	**TriMB**	**None**	**Toluene**	***p*-Xylene**	**TriMB**
Normalized molar flow rates of MBs in the feed[a] /mmol (mol Al-s)$^{-1}$								
	-	158 ±12	137 ±5	179 ±33	-	104 ±7	111 ±25	99 ±11
Normalized molar flow rates of MBs in the effluent /mmol (mol Al-s)$^{-1}$								
Toluene	n/a[c]	23[b]	n/a[c]	n/a[c]	n/a[c]	17[b]	n/a[c]	n/a[c]
Xylenes	5.0	47	46[b]	7.2	n/a[c]	41	44[b]	4.4
TriMBs	2.3	33	42	102[b]	1.3	26	38	58[b]
TetraMBs	1.2	13	15	22	<1	6.0	8.0	6.3
PentaMB	<1	3.7	3.7	3.7	<1	<1	<1	<1
HexaMB	<1	1.4	1.2	1.1	n/a[c]	n/a[c]	n/a[c]	n/a[c]
Total	9.2	121	109	136	1.9	90	90	69

[a] Molar flow rates of the co-feed. The molar flow rates of other MBs were negligible.

[b] Reported molar flow rates include the unreacted co-feed.

[c] Molar flow rates were negligible and were therefore not calculated. Peak area in the GC chromatogram was small and indiscernible from the nearby peaks.

To confirm that MB methylation can occur on the external surface of MFI, DME was reacted with toluene, *p*-xylene, or 1,2,4-triMB, in the presence of ~0.03 kPa DTBP. Table 5.6 shows the reaction conditions and product distribution for the reaction of DME with toluene, *p*-xylene, or 1,2,4-triMB, in the presence of DTBP on SPP MFI at ~723 K. Table 5.6 also shows, for comparison, the reaction conditions and product distribution for the reaction of DME with aromatic co-feeds in the absence of DTBP. Figure 5.5 shows the effects of passivating external Brønsted acid sites on the product selectivity, for the reaction of DME with MB co-feeds on SPP MFI at ~723 K. It can be observed from Table 5.6 and Figure 5.5 that co-feeding small amounts of DTBP (~0.03 kPa), and therefore

passivating the external Brønsted acid sites, did not have any effect on the overall product distribution of DME conversion.

Table 5.6: Reaction conditions and product distribution for the reaction of DME with toluene, *p*-xylene, or 1,2,4-triMB, with/without of DTBP on SPP MFI at ~723 K, ~120 kPa total feed pressure, 53 – 62% net DME conversion, and ~5 min TOS. DTBP partial pressure was ~0.03 kPa.

	Without DTBP			**With DTBP**		
Aromatic co-feed	**Toluene**	***p*-Xylene**	**1,2,4-triMB**	**Toluene**	***p*-Xylene**	**1,2,4-triMB**
Space-velocity /mol C (mol Al-s)$^{-1}$	9.1	7.7	8.2	5.9	6.3	6.3
DME pressure /kPa	62	60	61	60	61	62
Co-feed pressure /kPa	2.0	1.9	2.0	1.9	1.8	1.9
Net DME conversion /%	55	62	59	53	59	58
Feed composition (in %, on a carbon basis)						
DME	90	89	87	90	89	88
Co-feed	10	11	13	10	11	12
Product distribution (in %, on a carbon basis)						
C_2 (Ethene)	2.2 (2.2)	2.6 (2.6)	1.5 (1.4)	3.4 (3.4)	3.7 (3.7)	1.4 (1.4)
C_3 (Propene)	21.2 (20.9)	22.3 (21.9)	21.3 (20.9)	21.1 (20.7)	22.0 (21.5)	22.7 (22.2)
C_4 – C_7	49.7	50.2	48.6	48.1	48.6	52.4
Methylbenzenes[a]	18.3	16.2	20.0	18.4	16.9	14.6
Others[b]	8.5	8.7	8.6	8.9	8.7	8.9
Ethene/2MBu[c]	0.39	0.43	0.25	0.61	0.65	0.23

[a] Reported selectivity includes the unreacted co-feed.

[b] The "Others" fraction includes C_8+ hydrocarbons except polyMBs.

[c] Ratio of the synthesis rates of ethene and the sum of 2-methylbutane and 2-methyl-2-butene.

The only exception is ethene selectivity, which, in the case of toluene co-feed, increased from 2.2% without DTBP to 3.4% with DTBP, and in the case of *p*-xylene co-feed, increased from 2.6% in the absence of DTBP to 3.7% in the presence of DTBP. The

increase in ethene selectivity for the case of 1,2,4-triMB co-feed was, however, only marginal as it increased from 1.3% without DTBP to 1.4% with DTBP. A possible reason for this increase in ethene selectivity is the increase in diffusion length in SPP MFI. Adsorption of DTBP on acid sites near the pore-mouth prevented bulkier molecules from exiting the zeolite thereby increasing their intra-crystallite residence time. This enhanced the propagation of the aromatics-based catalytic cycle and results in higher ethene selectivity. We however showed that the effects of this increase in diffusion length in the presence of DTBP are insignificant and can be neglected.

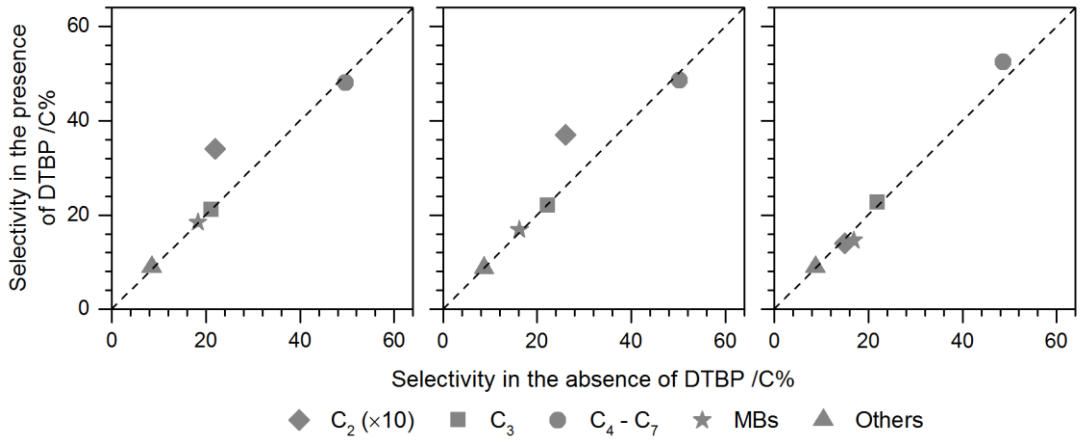

Figure 5.5: Effects of co-feeding DTBP on product selectivity towards C_2, C_3, C_4 – C_7, MBs, and "Others" fraction, for the reaction of DME with (a) toluene, (b) *p*-xylene, or (c) 1,2,4-triMB, on SPP MFI at ~723 K, 53 – 62% net DME conversion, and 5 – 8 min time-on-stream.

It must also be noted from Table 5.6 and Figure 5.5 that the increase in ethene selectivity (in the presence of DTBP) was much higher in the case of toluene or *p*-xylene co-feed in comparison to the case when 1,2,4-triMB was co-reacted with DME. A possible explanation for this observation resides in the kinetic diameter of these MBs. The kinetic diameter of 1,2,4-triMB (0.68 nm)[106,113] is larger than the kinetic diameters of toluene or *p*-

xylene (~0.59 nm)[106,113] and significantly larger than the diameter of the pore-openings in SPP MFI (~0.55 nm).[42,43] As a result, toluene or *p*-xylene can enter the pores of MFI while 1,2,4-triMB cannot enter the pores due to its bulkier nature. Co-feeding toluene or *p*-xylene therefore increased their concentration (and the concentration of their methylation homologues) inside the zeolite pores, while co-feeding 1,2,4-triMB does not increase its concentration inside the pores. The increase in ethene selectivity due to increase in the diffusion length in SPP MFI is magnified in the case of toluene or *p*-xylene co-feed because of higher concentration of MBs inside the zeolite pores.

Table 5.7 shows the distribution of MBs for the reaction of DME on SPP MFI at ~723 K, in the presence of aromatic co-feeds with/without DTBP. It can be observed that the selectivity towards more substituted MBs was lowered in the presence of DTBP. This implies that MB methylation was suppressed after the passivation of external Brønsted acid sites, suggesting that methylation of MBs to more substituted MB homologues occurred, at least to some extent, on the external surface of SPP MFI. Table 5.5 shows the molar flow rates of MBs in the feed and the effluent, for the reaction of DME on SPP MFI at 723 K with aromatic co-feeds in the presence/absence of DTBP.

Figure 5.6 shows the fraction of toluene, *p*-xylene, or 1,2,4-triMB, that underwent methylation in the presence/absence of DTBP. The fraction of MBs (with *j* methyls on the aromatic ring) that underwent methylation was estimated according to the formula:

$$\text{Fraction of MB methylated, } f_j = \frac{\sum_{i=j+1}^{i=6} C_i}{\sum_{i=j}^{i=6} C_i} \qquad (5.1)$$

Where C_i was the concentration of MBs, with *i* methyls on the aromatic ring, in the reaction effluent. Calculations were not performed for MBs with 4 or more methyls because of their low concentration in the effluent stream.

Table 5.7: Distribution of MBs on a carbon basis for the reaction of DME with toluene, *p*-xylene, or 1,2,4-triMB, on SPP MFI at ~723 K, 53 – 62% net DME conversion, and ~5 min TOS, in the presence/absence of ~0.03 kPa DTBP.

Co-feed	**Toluene**	***p*-Xylene**	**1,2,4-triMB**
(a) In the absence of DTBP (in the presence of external Brønsted acid sites)			
Toluene	16[a]	n/a[b]	n/a[b]
Xylenes	37	39[a]	4.6
TriMBs	29	39	74[a]
TetraMBs	13	16	17
PentaMB	4.0	4.3	3.3
HexaMB	1.6	1.6	1.0
(b) In the presence of DTBP (in the absence of external Brønsted acid sites)			
Toluene	16[a]	n/a[b]	n/a[b]
Xylenes	44	45[a]	5.6
TriMBs	32	44	83[a]
TetraMBs	8.0	10	10
PentaMB	<1	<1	<1
HexaMB	n/a[b]	n/a[b]	n/a[b]

[a] The reported selectivity includes the unreacted co-feed.

[b] The concentration was negligible and the selectivity was therefore not calculated. Peak area in the GC chromatogram was very small and the peak was indiscernible from the nearby peaks.

No significant change in toluene methylation was observed in the presence of DTBP co-feed. Methylation of *p*-xylene or 1,2,4-triMB was however suppressed in the presence of DTBP co-feed. In addition, methylation of 1,2,4-triMB was suppressed to a greater extent than *p*-xylene. These observations confirm our hypothesis that the methylation of MBs to more substituted MBs, which cannot enter the pores of MFI, occurs to a large extent on the external surface and is suppressed by the passivation of external Brønsted acid sites.

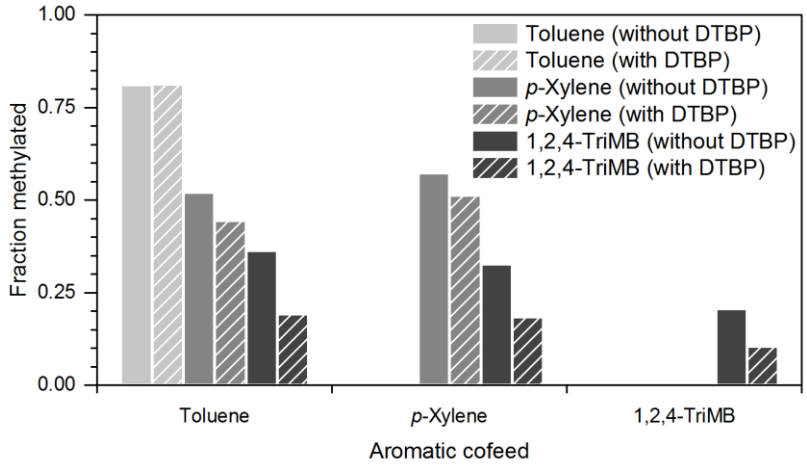

Figure 5.6: Fraction of toluene, *p*-xylene, or 1,2,4-triMB, that underwent methylation to higher MB homologues in the presence/absence of ~0.03 kPa DTBP, for the reaction of DME with aromatic co-feeds on SPP MFI at ~723 K.

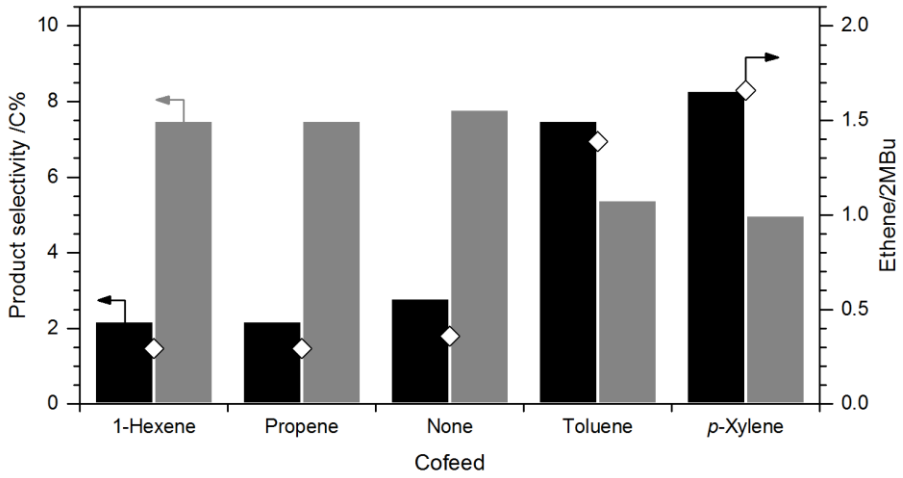

Figure 5.7: Ethene selectivity (■), 2MBu selectivity (■), and Ethene/2MBu (◇), for the reaction of DME with olefin/aromatic co-feed on 3DOm-i MFI at 723 K, 120 kPa total feed pressure, 45 – 57% net carbon conversion, and 20 min time-on-stream.

Table 5.8: Reaction conditions and product distribution, for the reaction of DME with olefin/aromatic co-feeds on 3DOm-i MFI at ~723 K, ~120 kPa total feed pressure, and ~20 min TOS.

Co-feed	**1-Hexene**	**Propene**	**None**	**Toluene**	**p-Xylene**
Carbon space-velocity /mol C (mol Al-s)$^{-1}$	12	13	11	13	13
DME partial pressure /kPa	61	60	62	62	61
Co-feed partial pressure /kPa	2	4	-	2	2
Net carbon conversion /%	52	55	57	46	45
Feed composition (in %, on a carbon basis)					
DME	91	91	100	91	89
Co-feed	9	9	-	9	11
Product selectivity (in %, on a carbon basis)					
C_2	2.2	2.3	2.8	7.5	8.3
C_3	27.4	31.5[a]	28.7	22.9	21.9
C_4 – C_7	60.7[a]	56.8	57.7	44.1	41.3
Methylbenzenes	2.1	2.1	2.8	18.9[a]	21.6[a]
Others[b]	7.7	7.3	8.0	6.6	6.9
Ethene/2MBu[c]	0.29	0.30	0.36	1.39	1.64
H/C in "Others"[d]	1.73	1.69	1.71	1.60	1.69

[a] Reported selectivity includes the unreacted co-feed.

[b] The "Others" fraction includes C_8+ hydrocarbons except polyMBs.

[c] Ratio of the synthesis rates of ethene and 2-methylbutane + 2-methyl-2-butene.

[d] Hydrogen-to-carbon ratio in the "Others" fraction was calculated based on the difference in carbon and hydrogen content of known hydrocarbon species in the reaction effluent and the converted feed

5.3.8 Effects of Co-Feeding Methylbenzenes/Olefins with DME on 3DOm-i MFI

Table 5.8 shows the reaction conditions and product distribution, and Figure 5.7 shows ethene selectivity, 2MBu selectivity, and ethene/2MBu yield, for the reaction of DME in the presence/absence of co-feeds on 3DOm-i MFI at ~723 K. Similar to the

observations on SPP MFI, co-feeding propene or 1-hexene with DME had no effect on ethene selectivity and ethene/2MBu, suggesting that the concentration of olefins inside the pores of 3DOm-i MFI was saturated and the olefins-based catalytic cycle was not enhanced in the presence of an olefin co-feed. Co-feeding toluene or p-xylene with DME, on the other hand, resulted in a 3-fold increase in ethene selectivity as well as a 4-fold increase in ethene/2MBu yield, suggesting that the relative extent of propagation of the aromatics-based catalytic cycle was enhanced by the presence of MB co-feed.

5.4 Conclusions

SPP MFI (~1 nm diffusion length) and 3DOm-i MFI (~20 nm diffusion length) exhibit low ethene selectivity (1.1% and 2.8%, respectively), for DME conversion to hydrocarbons at ~723 K suggesting that MFI-type zeolites, in the absence of any diffusion limitations, are poor ethene synthesis catalysts. Low ethene selectivity on MFI under these reaction conditions is attributed to the near absence of the aromatics-based catalytic cycle inside the zeolite pores. Co-feeding olefins with DME on SPP MFI and 3DOm-i MFI at 723 K did not affect the overall product selectivity, suggesting that the concentration of olefins is saturated inside the pores MFI samples and co-feeding olefins did not significantly enhance the propagation of the olefins-based catalytic cycle. The selectivity towards ethene was low (<2.8%) even under the conditions where the olefins-based hydrocarbon pool was saturated implying that the contribution of olefins-based catalytic cycle towards ethene production is minimal at 723 K and <100% conversion.

Co-feeding toluene or *p*-xylene with DME at ~723 K, on the other hand, enhanced the concentration of MBs inside the zeolite pores and a corresponding increase in ethene selectivity was observed suggesting that the low contribution of the aromatics-based catalytic cycle towards ethene production on SPP MFI is because the number of chain

carriers of the aromatics-based catalytic cycle, typically MBs, inside the zeolite pores is low. The presence of a large fraction of external Brønsted acid sites in SPP MFI (~29%) did not affect the overall product selectivity of MTH conversion at ~723 K. The methylation of MBs to higher MBs, which can occur on the external surface, is suppressed by passivation of the external acid sites. Aromatic dealkylation reactions, which are precursors to ethene formation, however occur only within the confinement of zeolite micropores and were therefore not affected by the passivation of external Brønsted acid sites by DTBP co-feed.

CHAPTER ***SIX***

Effects of Aluminum-Content on Light Olefins Selectivity in Methanol-to-Hydrocarbons Conversion

6.1 Introduction

In Chapter 4, we reported that ethene selectivity increases monotonically with increasing zeolite crystallite size. The mechanistic basis for this increase in ethene selectivity is the enhanced propagation of the aromatics-based catalytic cycle relative to the olefins-based catalytic cycle.[114] An increase in the diffusion length inside the zeolite results in an increase in the (i) concentration of MBs inside the zeolite pores, and/or (ii) intra-crystallite residence time of MBs.[114] Both these effects enhance the propagation of the aromatics-based catalytic cycle relative to the olefins-based catalytic cycle and consequentially result in higher selectivity towards ethene.[114]

In this chapter, we report the effects of aluminum content (or silicon-to-aluminum ratio) in HZSM-5 on ethene selectivity for DME conversion to hydrocarbons at ~623 K with the underlying postulate that increasing aluminum content, and therefore the concentration of Brønsted acid sites, will have a similar effect on ethene selectivity as increasing the zeolite crystallite size. An increase in the concentration of Brønsted acid sites will increase the probability that MBs, which are precursors to ethene, will interact with multiple Brønsted acid sites before exiting the zeolite crystallite. This increase in the number of interactions will enable these MB molecules to undergo multiple methylation/dealkylation reaction cycles before exiting the zeolite and produce light olefins, especially ethene, via aromatic dealkylation reactions in the process.

Wei et al.[86] investigated the effects of SiO_2/Al_2O_3 in HZSM-5 on the product distribution for methanol conversion at ~773 K and reported that ethene selectivity increased from 14.6 mol% on HZSM-5 with SiO_2/Al_2O_3 = 133 to 25.4 mol% on HZSM-5 with SiO_2/Al_2O_3 = 58, while propene selectivity decreased from 43.2 mol% to 32.3 mol%. Wan et al.[87] also studied the effects of SiO_2/Al_2O_3 on MTG conversion at ~648 K and reported a monotonic increase in selectivity towards C_1 – C_4 hydrocarbons as SiO_2/Al_2O_3 in ZSM-5 decreased from 411 to 23. The authors also noted a concomitant monotonic increase in aromatics selectivity with decreasing SiO_2/Al_2O_3.[87]

In this work, we also show that the crystallite size and the aluminum-content in HZSM-5 have similar effects on ethene selectivity for MTH conversion and we propose a unified descriptor (referred to as N_{H+}) that can be used to describes the combined effects of crystallite size and aluminum content on ethene selectivity in MTH. N_{H+} represents the average number of interactions between a MB molecule and a Brønsted acid site before the MB molecule exits the zeolite crystallite. A higher value of this descriptor implies a higher probability that a MB molecule will undergo multiple methylation/dealkylation reactions before exiting the zeolite crystallite and consequentially produce more ethene in the process, thereby resulting in higher ethene selectivity.

6.2 Materials and Methods

6.2.1 Catalyst Synthesis and Preparation

Five HZSM-5 samples with similar crystallite size (150 – 240 nm) but Si/Al varying between 55 and 1580 were synthesized via hydrothermal synthesis protocols according to a previously reported procedure.[115,116] These samples are referred to as HZSM-5-X, where X corresponds to Si/Al in the synthesis gel. In a typical synthesis of a ZSM-5 sample

(described for the HZSM-5-55), 0.54 g of $Al_2(SO_4)_3 \cdot 16H_2O$ (Sigma-Aldrich) was added to 10 cm^3 tetrapropylammonium hydroxide (15 wt%) aqueous solution (Sigma-Aldrich) under stirring, followed by the addition of 6 cm^3 of tetraethyl orthosilicate (Sigma-Aldrich). The mixture was stirred for 6 h and then transferred into an autoclave for crystallization at 453 K for 12 h. The products were recovered by centrifugation, washed several times with deionized water, and dried in air. The obtained powder was treated in dry air at 823 K for 6 h to remove the organic structure-directing agent. HZSM-5 samples with different Si/Al were synthesized by varying the amount of $Al_2(SO_4)_3 \cdot 16H_2O$ in the synthetic precursor with other conditions unchanged.

The catalyst powder (~8 g) was mixed with a 1 M NH_4NO_3 (Sigma-Aldrich) solution (~100 cm^3) and stirred using a magnetic stirrer at 353 K for 5 h. The powder was then filtered using a Buchner funnel and a 1-micron filter paper and subsequently washed till the pH was ~7. The filtered powder was dried in an oven at 393 K for 1 h. Finally, the ZSM-5 samples were treated in dry air (1.67 $cm^3\ s^{-1}$, Minneapolis Oxygen, 20-21% O_2, <10 ppm H_2O) at 823 K for 4 h. The temperature was increased from ambient to 823 K in 8 h and was held at 823 K for 4 h before slowly cooling down to the ambient temperature. This entire procedure was repeated three times to completely convert the ZSM-5 samples to their protonated forms. The HZSM-5 samples were then pressed into pellets, crushed, and sieved between 40- and 80- mesh sieves to obtain uniform particles with size between 180 and 425 µm. Quartz sand (Acros Organics) was used as a diluent in the catalyst bed to prevent temperature rise due to the exothermic nature of MTH conversion. Prior to its use, the quartz sand was washed with 1 M nitric acid (Sigma-Aldrich), rinsed several times with deionized water, dried, and sieved between 40- and 80-mesh sieves to obtain uniformly sized particles.

6.2.2 Structural and Chemical Characterization

XRD patterns were recorded on a Bruker D8 Advance diffractometer using Cu-Kα radiation (1.54056 Å). The scans were performed for 2θ ranging between 5° and 35° at a scan rate of 0.02°/min. TEM analysis were performed on an FEI-Tecnai T12 microscope operated at 120 KV. The silicon-to-aluminum ratio in the zeolite samples was determined by ICP-OES elemental analysis performed on a Thermo Fischer iCap 7000 instrument. The samples were digested in HF prior to the elemental analysis and Yttrium was used as an internal standard.

Ar adsorption-desorption isotherms were measured on a Micromeritics 3 Flex surface characterization Analyzer at the boiling temperature of liquid Ar (~87 K). Prior to the adsorption-desorption measurements, the samples were outgassed at 673 K for 8 h under high vacuum. Total surface area was calculated by BET method at absorption pressure $P/P_0 < 0.95$. Surface area of the micropores was estimated by the DFT method. Total pore volume was measured at the absorption pressure $P/P_0 = 0.95$, and the micropore volume (<1.5 nm) was estimated using the DFT method.

Adsorption uptake of 2,2-dimethylbutane (2,2-dmb) was used to estimate the effective Fickian diffusivity of 2,2-dmb in ZSM-5 zeolites at 298 K and the average crystallite size of the synthesized HZSM-5 samples. The adsorption uptake measurements were performed on a Micromeritics ASAP 2020 surface area and porosity analyzer equipped with a vapor option and the rate of adsorption software. The vapor source was filled with 2,2-dmb (Sigma-Aldrich, chemical purity grade) and was maintained at ~303 K. Prior to the uptake measurements, the catalyst samples (~25 mg) were outgassed at 723 K for 4 h under high vacuum conditions. The adsorption data were collected for 30 min at ~298 K and 13 – 15 kPa 2,2-dmb pressure.

6.2.3 Catalytic Conversion of DME to Hydrocarbons

Catalytic reactions of DME were carried out in a 316/316L stainless steel packed-bed reactor (1/4 in OD; 0.035 in wall thickness) equipped with a concentric thermal well (1/16 in OD, 0.014 in wall thickness). Isothermal conditions were maintained in the catalyst bed using a heating coil (ARi Industries Inc., AeroRod® heating assembly) regulated by a Watlow 96 series temperature controller. A K-type thermocouple (Omega Engineering, 0.020 in probe diameter), inserted into the concentric thermal well, was used for measuring the temperature of the catalyst bed during the reaction. Reactions were run using 13 – 45 mg catalyst diluted with ~100 mg quartz sand. Prior to every reaction, the catalyst was pretreated in situ in dry air (1.67 $cm^3\ s^{-1}$, Minneapolis Oxygen, 20-21% O_2, <10 ppm H_2O) at 823 K for 4 h. The temperature of the catalyst bed was increased from ambient to 823 K in 8 h and was held at 823 K for 4 h before the sample was cooled to the reaction temperature. Following the pretreatment, the catalyst was flushed with He (1.67 $cm^3\ s^{-1}$, Minneapolis Oxygen, 99.995% purity) for 1 h.

The reactant stream constituted DME (Matheson Tri-Gas, 99.5% purity) and a mixture of CH_4 and Ar (Airgas, 10% CH_4, 90% Ar) that was used as an internal standard. Gas flow rates were maintained using Brooks Instrument 5850S/SLA5850 series mass flow controllers. The space velocity was varied between 0.3 – 2.5 mol C (mol Al-s)$^{-1}$ to achieve the desired carbon conversions (46 – 54%). Methanol was considered as a reactant in the calculation of net carbon conversion. The total feed pressure was maintained at 105 – 120 kPa and all the reactions were carried out at 623 K. The temperature variation in the bed was less than 1 K during the reaction.

The reactor effluents were analyzed using an online Agilent 7890A series GC – 5975C series MS equipped with a 100% dimethylpolysiloxane Agilent J&W HP-1 column

(50 m × 320 µm × 0.52 µm) connected to an FID and an MSD, and an Agilent J&W GS-GasPro column (60 m × 320 µm) connected to a TCD. The product distributions shown in Section 6.3 include C_8+ hydrocarbons that were not identified separately and are classified as “Others”. The average hydrogen-to-carbon ratio of the hydrocarbon species present in the “Others” fraction was calculated from the hydrogen- and carbon-content of known hydrocarbon species in the converted feed and the reaction effluent and is reported with the data in some cases.

6.3 Results and Discussion

6.3.1 Structural and Chemical Characterization

The silicon-to-aluminum ratio in the synthesized HZSM-5 samples, as determined from ICP-OES elemental analysis, are reported in Table 6.1. The Ar adsorption-desorption isotherms of the synthesized ZSM-5 samples collected at the liquid argon boiling temperature (~87 K) are shown in Figure 6.1, and the estimated total surface area, micropore surface area, total pore volume, and micropore volume, are summarized in Table 6.1. The reported textural characteristics show that the synthesized materials have similar total surface area (412 – 443 $m^2\ g^{-1}$), micropore surface area (379 – 415 $m^2\ g^{-1}$), total pore volume (0.172 – 0.199 $cm^3\ g^{-1}$), and micropore volume (0.125 – 0.140 $cm^3\ g^{-1}$).

The XRD patterns of the synthesized HZSM-5 samples are presented in Figure 6.2. The measured XRD patterns suggest that the synthesized ZSM-5 samples are crystalline and have an MFI-type zeolite framework. The TEM images of the synthesized zeolite samples are presented in Figure 6.3 and show that the ZSM-5 samples investigated in this work have identical crystallite size and identical particle size distributions despite the varying aluminum-content.

Table 6.1: Silicon-to-aluminum ratio and textural characteristics of the synthesized HZSM-5 samples.

Zeolite samples	Si/Al[a]	Total surface area /m^2 g^{-1}	Micropore area /m^2 g^{-1}	Total volume /cm^3 g^{-1}	Micropore volume /cm^3 g^{-1}
HZSM-5-55	55	412	379	0.199	0.132
HZSM-5-115	115	443	415	0.196	0.140
HZSM-5-651	651	427	401	0.172	0.126
HZSM-5-1119	1119	419	395	0.173	0.129
HZSM-5-1580	1580	410	388	0.168	0.125

[a] Estimated from ICP-OES elemental analysis.

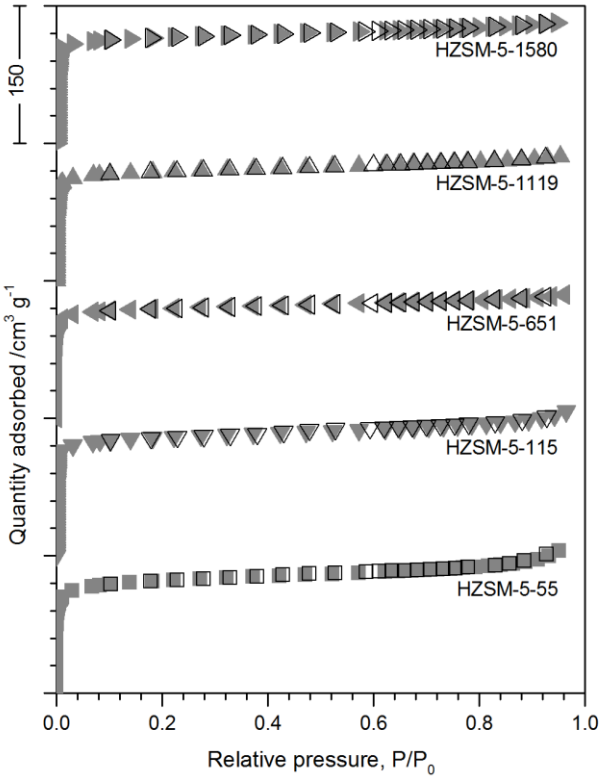

Figure 6.1: Ar adsorption (filled symbols) – desorption (open symbols) isotherms of HZSM-5-55 (■), HZSM-5-115 (▼), HZSM-5-651 (◄), HZSM-5-1119 (►), and HZSM-5-1580 (◆) at the liquid Ar boiling temperature (~87 K).

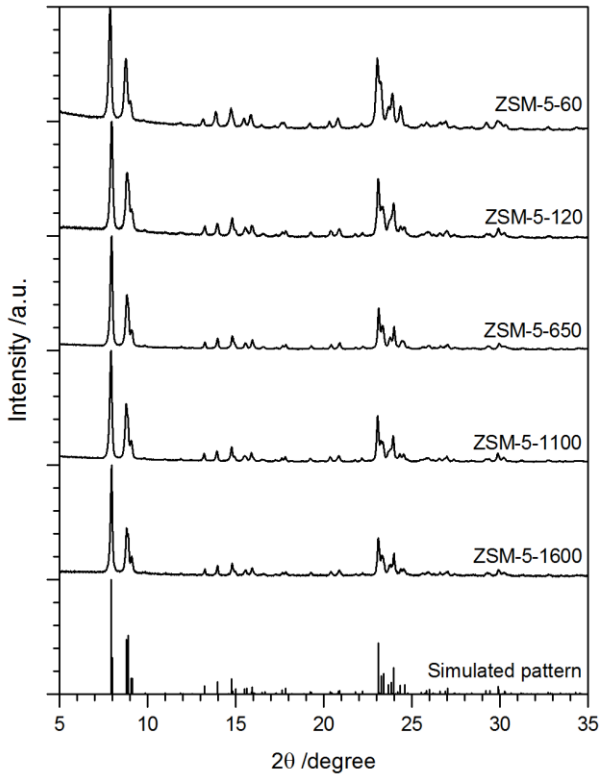

Figure 6.2: XRD patterns of the synthesized zeolite samples.

6.3.2 Adsorption Uptake Measurements of 2,2-Dimethylbutane

The average crystallite size of HZSM-5 samples was estimated from the adsorption uptake measurements of 2,2-dmb at ~298 K and 13 – 15 kPa 2,2-dmb pressure. The framework ZSM-5 consists of intersecting straight-channels (0.51 nm × 0.55 nm) and sinusoidal-channels (0.54 nm × 0.56 nm).[42,43] The kinetic diameter of 2,2-dmb is ~0.63 nm,[102,103] which is close to the diameter of the pore-openings in MFI. The adsorption uptake rate of 2,2-dmb can therefore be used to estimate the diffusion length (and therefore the crystallite size) in zeolites.[104,114] The theoretical adsorption capacity of 2,2-dmb (which preferentially adsorbs in the channel intersections) in ZSM-5 is 4 molecules per unit cell. [104]

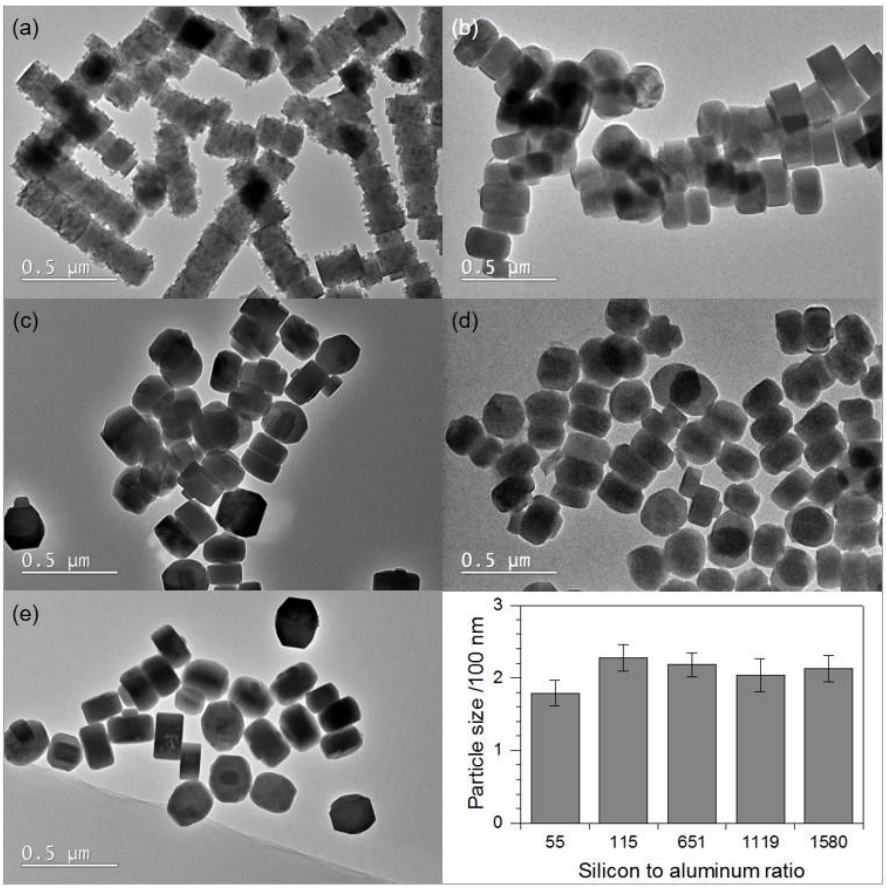

Figure 6.3: TEM images and particle size distribution of (a) HZSM-5-55, (b) HZSM-5-115, (c) HZSM-5-651, (d) HZSM-5-1119, and (e) ZSM-5-1580.

The adsorption uptake curves of 2,2-dmb, at ~298 K and 13 – 15 kPa 2,2-dmb pressure, on HZSM-5 samples investigated in this work are presented in Figure 6.4. The amount of 2,2-dmb adsorbed was normalized to the theoretical adsorption capacity of 2,2-dmb in ZSM-5. Assuming spherical crystallites (with diameter, 2R, equal to the crystallite size of the zeolite), a simple Fickian diffusion model can be used to describe the uptake of 2,2-dmb in HZSM-5. For isothermal conditions and in the absence of other transport restrictions, the concentration profile of 2,2-dmb inside the spherical zeolite crystallites is given by:[105,106]

$$\frac{C(r,t)}{C_\infty} = 1 - \frac{2R}{\pi r}\sum_{n=1}^{\infty}\left[\frac{(-1)^n}{n}\sin\left(\frac{n\pi r}{R}\right)\exp\left(-\frac{D_{eff}n^2\pi^2 t}{R^2}\right)\right] \qquad (6.1)$$

Where C(r,t) is the concentration of 2,2-dmb inside the spherical particle, r is the radial co-ordinate, t is the temporal coordinate, D_{eff} is the effective Fickian diffusivity of 2,2-dmb in ZSM-5 at 298 K, and C_∞ is the saturation capacity of 2,2-dmb in ZSM-5.

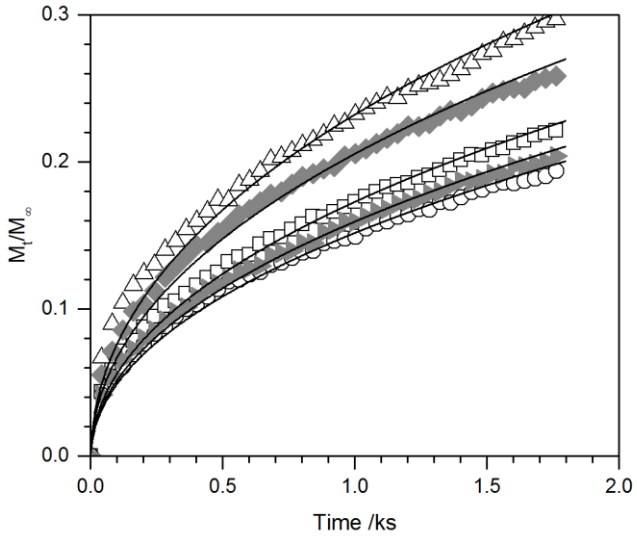

Figure 6.4: Adsorption uptake curves of 2,2-dmb on HZSM-5-55 (□), HZSM-5-115 (△), HZSM-5-651 (◆), HZSM-5-1119 (○), and HZSM-5-1580 (▶), at 298 K and 13 – 15 kPa 2,2-dmb pressure. The adsorbed amount was normalized to the theoretical adsorption capacity of 2,2-dmb in ZSM-5. The lines represent the fits to Equation 6.2.

The amount of 2,2-dmb adsorbed can be obtained from Equation 6.1 by integrating C(r,t) between r = 0 and r = R,[105,106]

$$\frac{M_t}{M_\infty} = 1 - \frac{6}{\pi^2}\sum_{n=1}^{\infty}\left[\frac{1}{n^2}\exp\left(-\frac{D_{eff}n^2\pi^2 t}{R^2}\right)\right] \qquad (6.2)$$

Where M_t and M_∞ are the adsorbed amount at time t and at saturation, respectively.

Assuming that the effective diffusivity is same for all ZSM-5 samples, Equation 6.2 was fitted to the experimental data and six parameters including D_{eff} and the average crystallite size of all ZSM-5 samples were estimated and are reported in Table 2. The Fickian diffusivity of 2,2-dmb was calculated to be 3×10^{-20} m^2 s^{-1} on ZSM-5 at 298 K. This value is similar to the values reported previously by Khare et al. (9×10^{-19} m^2 s^{-1} at 293 K),[114] Cavalcante and Ruthven (1×10^{-19} at 296 K),[108] Xiao and Wei (4×10^{-19} at 298 K),[109] and Yu et al. (5×10^{-20} at 295 K).[103] Adsorption uptake of 2,2-dmb, together with TEM, confirms that the average crystallite sizes of HZSM-5 samples investigated in this work are similar (150 – 240 nm).

Table 6.2: Effective diffusivity of 2,2-dmb and the crystallite size of ZSM-5 samples investigated in this work, as estimated from 2,2-dmb adsorption uptake measurements at ~298 K and 13 – 15 kPa 2,2-dmb pressure.

Parameters	**Estimated values**
D_{eff}	3×10^{-20} m^2 s^{-1}
Crystallite size of HZSM-5-55	210 nm
Crystallite size of HZSM-5-115	150 nm
Crystallite size of HZSM-5-651	180 nm
Crystallite size of HZSM-5-1119	240 nm
Crystallite size of HZSM-5-1580	230 nm

6.3.3 Effects of Aluminum-Content on Ethene selectivity in MTH Conversion

DME (at 49 – 57 kPa pressure) was reacted on HZSM-5 samples at 623 K and 103 – 106 kPa total feed pressure. DME space velocity was varied between 0.3 – 2.5 mol C (mol Al-s)$^{-1}$ to achieve iso-conversion (46 – 54%) of DME. Methanol was considered as a reactant in the calculation of net conversion. Figure 6.5 shows ethene selectivity,

propene selectivity, and ethene/2MBu yield, as a function of silicon-to-aluminum ratio in the ZSM-5 samples. It can be observed that ethene selectivity increased monotonically from 5.7% to 16% and total light olefins selectivity also increased monotonically from 23% to 38% as Si/Al decreased from 1580 to 55.

Ethene/2MBu, a descriptor of the relative extents of propagation of the aromatics-based and the olefins-based catalytic cycles, also increased monotonically from 0.80 to 2.4 with decreasing Si/Al suggesting that preferential propagation of the aromatics-based catalytic cycle occurs in HZSM-5 samples with lower Si/Al or higher aluminum content. These results support our postulate that a decrease in silicon-to-aluminum ratio or an increase in aluminum content results in enhanced propagation of the aromatics-based catalytic cycle relative to the olefins-based catalytic cycle and consequentially results in an increase in ethene selectivity.

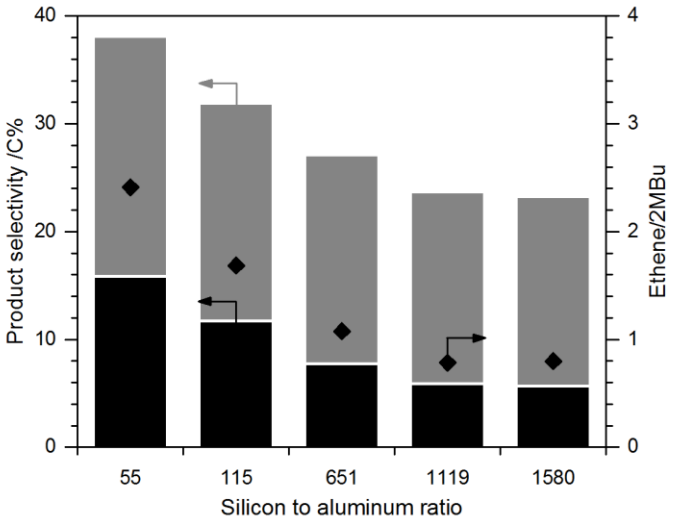

Figure 6.5: Ethene selectivity (■), propene selectivity (■), and ethene/2MBu yield (◆), for the catalytic reaction of DME on HZSM-5 samples with similar crystallite size (150 – 240 nm) and Si/Al varying between 55 and 1580 at ~623 K, 49 – 57 kPa DME pressure, and 46 – 54% net DME/Methanol conversion.

Table 6.3: Silicon-to-aluminum ratio, crystallite size, and N_{H+} for HZSM-5 samples investigated in this chapter, and for the zeolite samples investigated in Chapter 4.

Zeolite samples	Si/Al[a]	Crystallite size[b] /nm	Unified descriptor, N_{H+}
HZSM-5-55	55	210	3.8
HZSM-5-115	115	150	1.3
HZSM-5-651	651	180	0.27
HZSM-5-1119	1119	240	0.22
HZSM-5-1580	1580	230	0.15
2nm-MFI[c]	88	2	0.023
40nm-MFI[c]	72	40	0.56
500nm-MFI[c]	43	500	11.7
2µm-MFI[c]	60	1750	29.2
17µm-MFI[c]	38	17000	447
SiMFI-1x[c]	42	1250	29.8
SiMFI-2x[c]	42	5200	124
SiMFI-3x[c]	42	17600	419

[a] Estimated from ICP-OES elemental analysis.

[b] Estimated from 2,2-dmb adsorption uptake measurements or TEM.

[c] Zeolite samples investigated in Chapter 4.

6.3.4 A Single-Value Descriptor of Ethene Selectivity in MTH Conversion

In Chapter 4, we reported that ethene selectivity increases monotonically with increasing crystallite size of MFI-type zeolites.[114] The results presented in Section 6.3.3 show that ethene selectivity also increases monotonically with increasing aluminum content or decreasing silicon-to-aluminum ratio. The underlying mechanistic basis for this increase in ethene selectivity with crystallite size or aluminum content is the enhanced propagation of the aromatics-based catalytic cycle due to an increase in the number

interactions between MBs and Brønsted acid sites before these MB molecules exit the zeolite crystallite. Increasing aluminum content, or decreasing Si/Al, enhances the number of interactions by increasing the concentration of active sites. Increasing the crystallite size, on the other hand, increases the number of interactions by increasing the residence time of molecules within the zeolite crystallite. These two effects can be combined into a single-value descriptor (referred to as N_{H+}) of ethene selectivity. N_{H+} represents the average number of interactions between a MB molecule and a Brønsted acid site before the MB molecule exits the zeolite crystallite.

The average number of interactions between a MB molecule and an active site before it exits the zeolite crystallite will increase with increasing crystallite size and decrease with increasing Si/Al in the zeolite. N_{H+}, therefore, can be considered to be proportional to the ratio of the crystallite size of the ZSM-5 zeolite and its silicon-to-aluminum ratio.

$$N_{H+} = \frac{\text{Crystallite size}}{\text{Silicon-to-aluminum ratio}} \tag{6.3}$$

Table 6.3 shows the silicon-to-aluminum ratio (as estimated from ICP-OES elemental analysis), average crystallite size (as estimated from 2,2-dmb adsorption uptake measurements or TEM analysis), and the value of unified descriptor, N_{H+} (ratio of crystallite size and silicon-to-aluminum ratio) of HZSM-5 samples investigated in this chapter and the zeolite samples investigated in Chapter 4. Figure 6.6 shows ethene selectivity and 2MBu selectivity as a function of N_{H+} for the catalytic reaction of DME on HZSM-5 samples at ~623 K, 49 – 66 kPa DME pressure, and 46 – 59% net DME conversion. It can be observed that ethene selectivity increases with an increase in the value of N_{H+} therefore supporting our hypothesis.

The extent of propagation of the olefins-based catalytic cycle – represented by 2MBu selectivity – however, does not increase with increasing N_{H+}. In general, olefins have a smaller kinetic diameter compared to MBs, for example, the kinetic diameter of 2,2-dmb is 6.3 Å [102,103] and the kinetic diameter of 1,2,4-triMB is 7.6 Å.[117] The intra-crystalline residence time of MBs is therefore longer than that for the olefins. Also, any increase in the propagation of the olefins-based catalytic cycle increases the probability that C_6+ olefins will undergo cyclization and hydrogen-transfer to form MBs. The propagation of the aromatics-based catalytic cycle is therefore affected to a greater extent with increasing value of N_{H+}. It must be noted that lighter olefins methylate or oligomerize to form higher olefins, which in turn undergo *β*-scission to form lighter olefins. These olefin-interconversion reactions render the selectivity of the olefins invariant with the propagation of the olefins-based catalytic cycle.[118] An Increase in crystallite size or a decrease in

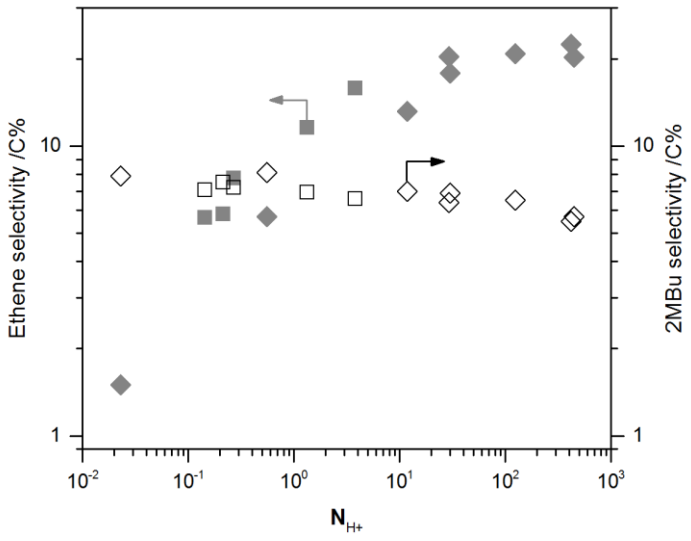

Figure 6.6: Ethene selectivity (filled symbols) and 2MBu selectivity (open symbols) as a function of N_{H+} for the catalytic conversion of DME on HZSM-5 samples investigated in this work (squares) and the zeolite samples investigated in Chapter 4 (diamonds) at ~623 K, 49 – 66 kPa DME pressure, and 46 – 59% net DME/Methanol conversion.

silicon-to-aluminum ratio i.e., an increase in the value of N_{H+}, results in enhanced propagation of both the catalytic cycles, however, the MTH product distribution is affected to a greater extent by the enhanced propagation of the aromatics-based catalytic cycle in comparison to enhanced propagation of the olefins-based catalytic cycle and therefore ethene selectivity increases with an increase in the value of N_{H+}.

6.4 Conclusions

Ethene selectivity, in the catalytic conversion of DME (at ~623 K and 46 – 54% net conversion) on five HZSM-5 samples with similar crystallite size (150 – 240 nm) and Si/Al varying between 55 and 1580, increased from 5.7% on the HZSM-5 sample with Si/Al = 1580 to 16% on the HZSM-5 sample with Si/Al = 55. The mechanistic basis for this increase in ethene selectivity with decreasing Si/Al or increasing aluminum content is an increase in the number of interactions between Brønsted acid sites and MBs before these molecules exit the zeolite crystallite. Ethene/2MBu also increased monotonically from 0.80 on HZSM-5 sample with Si/Al = 1580 to 2.4 on HZSM-5 sample with Si/Al = 55. A single-value descriptor, N_{H+}, which is a representative of the average number of Brønsted acid sites that a MB molecule will encounter before it exits the zeolite crystallite, can be used to describe the combined effects of crystallite size of ZSM-5 and its Si/Al on ethene selectivity in MTH conversion.

CHAPTER ***SEVEN***

Effects of Oxygenate Co-feed on MTH Product Distribution and its Mechanistic Interpretation

* Reported from R. Khare, S. Arora, A. Bhan, *ACS Catalysis* **6** (2016) 2314-2331

7.1 Introduction

Aldehydes undergo aldol-condensation on Brønsted acid sites to form higher homologues that can subsequently undergo ring-closure followed by dehydration to form aromatics (e.g., benzene, 1,3,5-triMB).[78,119] Chang and Ko[76] investigated the vapor-phase reaction of acetaldehyde on zeolite HX at 673 K and ~26% conversion, and observed ~8% selectivity towards 3-hydroxybutanal, the aldol-condensation product of acetaldehyde, and ~47% selectivity towards 2-butenal, the dehydration product of 3-hydroxybutanal. Chang and Silvestri[77] investigated the catalytic conversion of propionaldehyde on HZSM-5 at 644 K and high conversion (>99.9%) and reported >80% selectivity towards aromatics in the reaction effluent. Hoang et al.,[78] in another experimental study, also reacted propionaldehyde on HZSM-5 at 673 K and ~76% conversion and reported ~41% selectivity towards aromatics. Hutchings et al.[79] reacted propionaldehyde on zeolite *β* at 643 K and ~31% conversion and reported ~60% selectivity towards aromatics.

Aldol-condensation of aldehydes results in the formation of aromatics and therefore, selectively increases the concentration of aromatics inside the zeolite pores. A higher concentration of aromatics will enhance the propagation of the aromatics-based catalytic cycle and consequentially result in higher selectivity towards light olefins,

especially ethene, in MTH conversion. Co-feeding aldehydes with DME and MeOH, therefore, presents a simple approach to increase ethene selectivity in MTH conversion on MFI-type zeolites. Lee[120] reported that co-feeding formaldehyde or acetaldehyde with methanol on HZSM-5 at 573 – 648 K and ~50% methanol conversion increased the selectivity towards ethene from 27.7 mol% without co-feed to 31.1 mol% and 30.2 mol% in the presence of formaldehyde and acetaldehyde, respectively. Total light olefin (C_2 – C_4) selectivity also increased from 53.6 mol% without co-feed to 63.1 mol% in the presence of formaldehyde and 58.7 mol% in the presence of acetaldehyde.[120]

In this work, we report a mechanistic investigation of the effects of co-feeding acetaldehyde (1 – 4%, on a carbon basis) with DME and MeOH on two MFI-type zeolites, a conventional MFI zeolite and a self-pillared pentasil MFI zeolite, at 673 K and ~110 kPa total feed pressure. Acetaldehyde, when co-reacted with DME/MeOH under these reaction conditions, follows three separate reaction pathways: (i) an aldol-condensation pathway that results in the formation of aromatics, (ii) an aldehyde-decarbonylation pathway that involves the removal of carbonyl oxygen as CO and results in the formation of unsaturated aliphatics, which can subsequently oligomerize, cyclize, and undergo hydrogen-transfer to form aromatics, and (iii) a bimolecular hydrogen-transfer pathway that involves hydrogen-transfer to acetaldehyde or its aldol-condensation products (e.g., crotonaldehyde) to form the corresponding alcohols (e.g., ethanol, 2-buten-1-ol), which can then dehydrate on Brønsted acid sites to form ethene or polyenes. The bimolecular hydrogen-transfer pathway directly enhances ethene production. The aldol-condensation and the aldehyde-decarbonylation pathways, on the other hand, increase the production of aromatics inside the zeolite pores, which enhances the propagation of the aromatics-based catalytic cycle and consequentially results in higher ethene production.

7.2 Materials and Methods

7.2.1 Catalyst Preparation and Pretreatment

The conventional MFI sample was obtained from Zeolyst International Inc. (CBV 8014, SiO_2/Al_2O_3 ~80, diffusion length ~250 nm, referred to as Conv MFI). Detailed chemical and structural characterization of the Conv MFI sample is described in the supplementary material section of Reference [73]. A self-pillared pentasil zeolite sample (SiO_2/Al_2O_3 ~150, diffusion length ~1.5 nm, referred to as SPP MFI) was synthesized according to the procedure described in Reference [89]. Detailed structural and chemical characterization of the SPP MFI sample is described in the supplementary information section of Reference [89].

The zeolite samples were converted to their protonated forms by treating in dry air (1.67 $cm^3\ s^{-1}$, Minneapolis Oxygen, 20 – 21% O_2, <10 ppm H_2O) at 823 K for 4 h. The temperature was increased from ambient to 823 K in 8 h and was held at 823 K for 4 h before reducing it to the ambient temperature. The zeolite samples were then pressed into pellets, crushed, and sieved between 40- and 80-mesh sieves to obtain uniform particles with size between 180 and 425 μm. Quartz sand (Acros Organics) was used as a diluent in the catalyst bed to prevent temperature rise due to the exothermic nature of MTH conversion. Prior to its use, the quartz sand was washed with 1 M nitric acid (Sigma-Aldrich), rinsed several times with deionized water, dried, and sieved between 40- and 80-mesh sieves to obtain uniform particles with size between 180 and 425 μm.

7.2.2 Catalytic Reactions on a Packed-Bed Reactor

A 316/316L stainless steel packed-bed reactor (1/4 in OD; 0.035 in wall thickness), equipped with a concentric thermal well (1/16 in OD, 0.014 in wall thickness), was used to

carry out the catalytic reactions. Isothermal conditions were maintained in the catalyst bed using a heating coil (ARi Industries Inc., AeroRod® heating assembly) regulated by a Watlow 96 series temperature controller. A K-type thermocouple (Omega Engineering, 0.020 in probe diameter), inserted into the concentric thermal well, was used for measuring the temperature of the catalyst bed during the reaction. The reactions were run using 10 – 23 mg catalyst to achieve the desired chemical conversion and the catalyst bed was diluted with 100 mg of quartz sand. Prior to every reaction, the catalyst bed was pretreated in situ in dry air (1.67 cm^3 s^{-1}, Minneapolis Oxygen, 20 – 21% O_2, <10 ppm H_2O) at 823 K for 4 h. The temperature was increased from ambient to 823 K in 8 h and was held at 823 K for 4 h. Following the pretreatment, the catalyst was flushed with He (1.67 cm^3 s^{-1}, Minneapolis Oxygen, 99.995% purity) for 1 h.

7.2.2.1 Catalytic Reactions of DME and Methanol in the Presence of Acetaldehyde

The reactant stream constituted DME (Matheson Tri-Gas, 99.8% purity) and a mixture of CH_4 and Ar (Airgas, 10% CH_4, 90% Ar) which was used as an internal standard for the FID. Gas flow rates were maintained using Brooks Instrument 5850S/SLA5850 series mass flow controllers. The boiling point of acetaldehyde is 294 K,[121] and therefore, it cannot be fed as a pure liquid using a liquid syringe pump at ambient temperatures. Accordingly, a preconstituted mixture of acetaldehyde (Acros Organics, 99.5% purity) and MeOH (Fisher Scientific, HPLC grade, 99.9% purity) was fed through a 2.5 mL Hamilton syringe using a Cole Parmer EW-74900-00 syringe pump. The flow rates were adjusted such that the ratio of DME and MeOH in the feed was 9:1, on a carbon basis. In the case of isotopic co-feed experiments, a pre-constituted mixture of $^{13}C_2$-acetaldehyde (Sigma Aldrich, 99% purity, 99 atom% ^{13}C) and ^{12}C-MeOH (Fisher Scientific, HPLC grade, 99.9% purity) was used as the liquid-feed.

7.2.2.2 Catalytic Reactions of DME and Methanol without Acetaldehyde

The catalytic reactions of DME and MeOH (DME:MeOH ~9:1, on a carbon basis) without acetaldehyde co-feed were used as the reference to assess the effects of co-feeding acetaldehyde with DME and MeOH on MTH conversion. The reactant gas stream constituted DME (Matheson Tri-Gas, 99.8% purity) and the CH_4-Ar mixture. MeOH (Fisher Scientific, HPLC grade, 99.9% purity) was fed as a pure liquid through a 2.5 mL Hamilton syringe using the Cole Parmer EW-74900-00 syringe pump. The flow rates were adjusted to obtain the desired carbon space velocity while maintaining a 9:1 (on a carbon basis) ratio of DME and MeOH in the feed.

7.2.2.3 Catalytic Reactions of Acetaldehyde Only without DME or Methanol

A preconstituted mixture of acetaldehyde (Acros Organics, 99.5% purity) and deionized water was fed through a 2.5 mL Hamilton syringe using a Cole Parmer EW-74900-00 syringe pump. A mixture of He (Minneapolis Oxygen, 99.995% purity) and CH_4-Ar was used as the carrier gas.

The reactor effluents were analyzed using an online Agilent 7890A series GC (gas chromatograph) – Agilent 5975C series MS (mass spectrometer) equipped with a 100% dimethylpolysiloxane Agilent J&W HP-1 column (50 m × 320 μm × 0.52 μm) connected to an FID, and a (5%-phenyl)-methylpolysiloxane Agilent J&W HP-5ms column (30 m × 320 μm × 0.25 μm) connected to a MSD. A TCD was used to quantify CO present in the effluent. The product distributions shown in Section 7.3 include C_8+ hydrocarbons that were not identified separately and are classified as “Others”. The average hydrogen-to-carbon ratio of the hydrocarbon species present in the “Others” fraction was calculated from the hydrogen- and carbon-content of known hydrocarbon species in the converted feed and the reaction effluent, and is reported with the data in some cases.

The isotopologue distribution of selected hydrocarbon species was determined from mass fragmentation patterns using the method described by Price and Iglesia.[92] The mass fragmentation patterns were corrected for the natural abundance of ^{13}C atoms following the method described by Moseley.[93]

7.3 Results and Discussion

7.3.1 Catalytic Conversion of DME and Methanol

Table 7.1 shows the product distribution and the reaction conditions for the catalytic conversion of DME and MeOH (DME:MeOH ~9:1, on a carbon basis) without acetaldehyde co-feed on Conv MFI and SPP MFI at 673 K. Ethene selectivity was lower on SPP MFI (1.4 C%) compared to Conv MFI (9.4 C%) at 673 K and 47 – 48% net conversion. Ethene/2MBu, was also lower on SPP MFI (0.18) compared to Conv MFI (1.2) under similar reaction conditions, suggesting that the aromatics-based catalytic cycle propagated to a greater extent on Conv MFI. In Chapter 4, we showed that light olefins selectivity and specifically ethene selectivity increases monotonically with increasing crystallite size of MFI because the concentration as well as the intra-crystalline residence time of bulkier molecules like MBs increases with increasing crystallite size, which enables these MBs to undergo multiple methylation/dealkylation reaction cycles before exiting the zeolite crystallite, thereby resulting in higher ethene selectivity.[114,118]

7.3.2 Effects of Co-Feeding Acetaldehyde on MTH Conversion

The mechanistic consequences of co-reacting acetaldehyde with DME and MeOH were investigated by systematically co-feeding 1 – 4 C% acetaldehyde with a mixture of DME and MeOH on Conv MFI and SPP MFI at 673 – 675 K, 107 – 109 kPa total feed pressure, 50 – 56 kPa DME pressure, 11 – 12 kPa methanol pressure, and 0 – 2.5 kPa

acetaldehyde pressure. The total carbon space velocity was 10.6 – 11.7 mol C (mol Al-s)$^{-1}$ on Conv MFI and 2.7 – 2.8 mol C (mol Al-s)$^{-1}$ on SPP MFI. The catalytic reaction of DME and MeOH without acetaldehyde co-feed on Conv MFI and SPP MFI, carried out under similar reaction conditions, was used as a reference.

Table 7.1: Reaction conditions and product distribution for the catalytic reactions of DME and MeOH (DME:MeOH ~9:1, on a carbon basis) on Conv MFI and SPP MFI zeolite samples, at 673 K and 30 min TOS.

Zeolite sample	**Conv MFI**	**SPP MFI**
Total feed pressure /kPa	110	107
DME partial pressure /kPa	55	53
Methanol partial pressure /kPa	12	12
Total carbon space velocity /mol C (mol Al-s)$^{-1}$	11	2.7
Net carbon converted /%	47	48
Product distribution (in %, on a carbon basis)		
C_2 (Ethene)	9.4 (9.3)	1.4 (1.4)
C_3 (Propene)	25.2 (24.3)	23.3 (22.8)
C_4-C_7 olefins	31.5	40.1
C_4-C_7 alkanes	17.9	15.6
Methylbenzenes	4.9	2.6
Others[a]	11.2	17.0
H/C in "Others"[b]	1.75	1.81
Ethene/2MBu[c]	1.2	0.18
Hydrogen transfer index (HTI)[d]	0.22	0.20

[a] The "Others" fraction includes C_8+ hydrocarbons except polymethylbenzenes.

[b] The hydrogen-to-carbon ratio in "Others" fraction was calculated based on the difference in total carbon- and hydrogen-content of known hydrocarbon species in the reaction effluent and the converted feed.

[c] Ratio of the synthesis rates of ethene and sum of 2-methyl-2-butene and 2-methylbutane.

[d] The hydrogen-transfer index was defined as the ratio of C_2 – C_6 alkanes and total C_2 – C_6 aliphatics.

7.3.2.1 Effects of Co-Feeding Acetaldehyde on Catalyst Deactivation

Figure 7.1 shows the effects of co-feeding acetaldehyde on catalyst activity for the reaction of DME and MeOH with 1 – 4 C% acetaldehyde co-feed on Conv MFI and SPP MFI at 673 K. Figure 7.2 compares the deactivation profiles – represented by the relative decrease in net carbon converted versus TOS – of Conv MFI and SPP MFI for MTH conversion in the presence of 1 – 4 C% acetaldehyde co-feed. Finally, the rates of deactivation of Conv MFI and SPP MFI in the presence of 1 – 4 C% acetaldehyde were also estimated from their respective deactivation profiles and are presented in Figure 7.3.

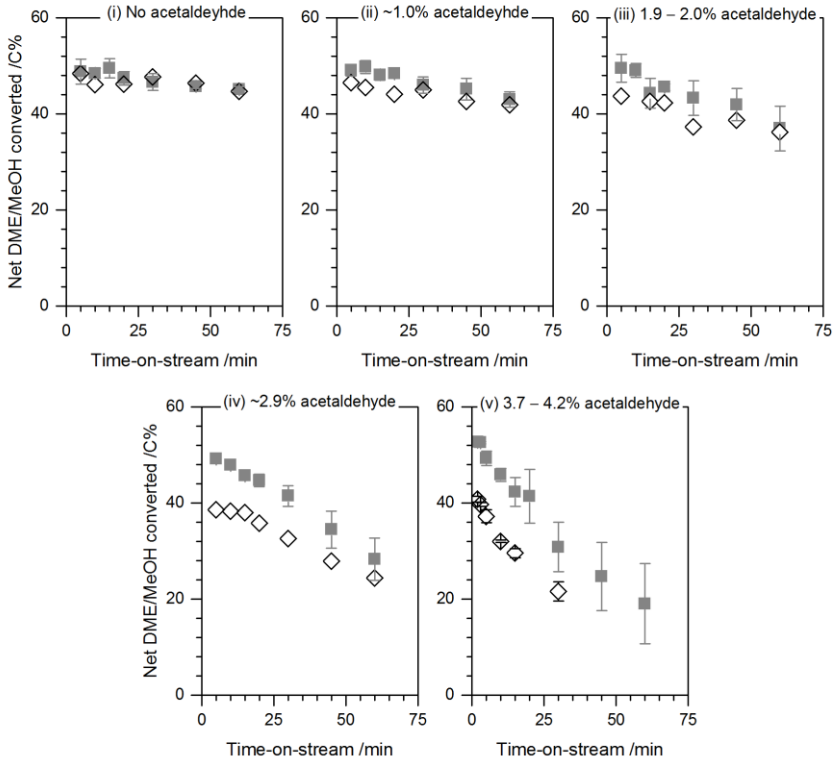

Figure 7.1: Net carbon converted versus time-on-stream for the catalytic reactions of acetaldehyde (1 – 4%, on a carbon basis) with DME and MeOH (DME:MeOH ~9:1, on carbon basis) on (i) Conv MFI (◇) and (ii) SPP MFI (■), at 672 – 675 K, 107 – 114 kPa total feed pressure, 50 – 57 kPa DME pressure, 11 – 13 kPa methanol pressure, and 0 – 2.5 kPa acetaldehyde pressure. Total carbon space velocity was 10.6 – 11.7 mol C (mol Al-s)$^{-1}$ on Conv MFI and 2.7 – 2.8 mol C (mol Al-s)$^{-1}$ on SPP MFI. Feed composition (on a carbon basis) was 86 – 90% DME, 9 – 10% methanol, and (i) no acetaldehyde, (ii) ~1.0% acetaldehyde, (iii) 1.9 – 2.0% acetaldehyde, (iv) ~2.9% acetaldehyde, (v) 3.7 – 4.2% acetaldehyde.

The deactivation rate was defined as the fraction of active sites deactivated per second and was considered to be invariant with conversion. It is evident that both catalysts deactivated faster in the presence of acetaldehyde, especially at high acetaldehyde concentrations. The deactivation rate increased monotonically, almost by an order of magnitude, from 2.3×10^{-5} s^{-1} without acetaldehyde to 1.7×10^{-4} s^{-1} when ~4 C% acetaldehyde was co-fed Conv MFI, and from 2.0×10^{-5} s^{-1} without acetaldehyde to 2.6×10^{-4} s^{-1} in the presence of ~4 C% acetaldehyde co-feed on SPP MFI.

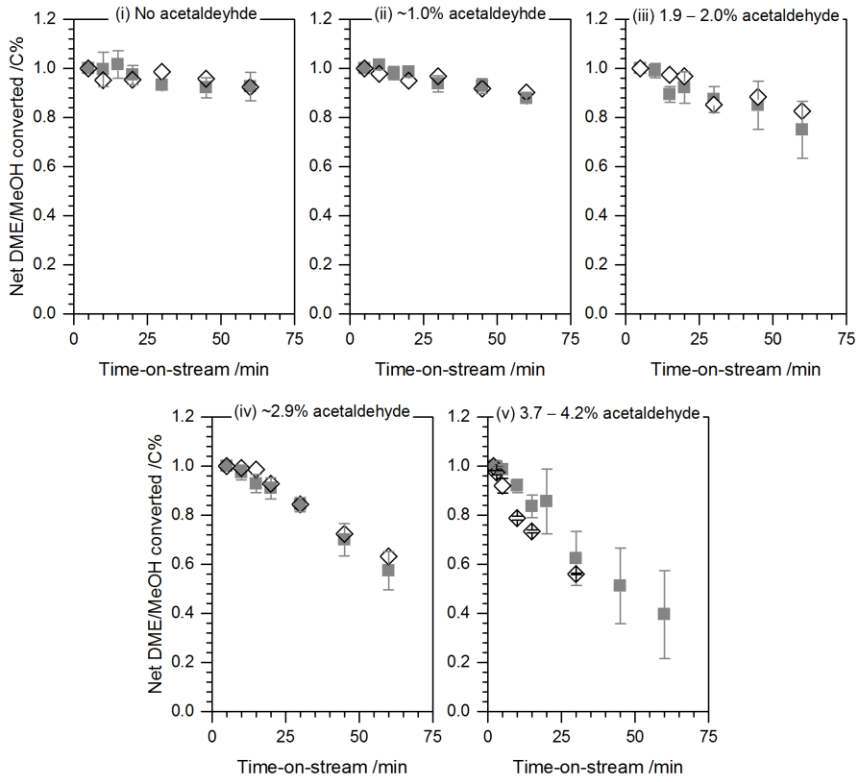

Figure 7.2: Deactivation profiles –relative change in net carbon converted versus TOS – for the catalytic reactions of acetaldehyde (1 – 4%, on a carbon basis) with DME and MeOH (DME:MeOH ~9:1, on carbon basis) on (i) Conv MFI (◇) and (ii) SPP MFI (■), at 672 – 675 K, 107 – 114 kPa total feed pressure, 50 – 57 kPa DME pressure, 11 – 13 kPa methanol pressure, and 0 – 2.5 kPa acetaldehyde pressure. Total carbon space velocity was 10.6 – 11.7 mol C (mol Al-s)$^{-1}$ on Conv MFI and 2.7 – 2.8 mol C (mol Al-s)$^{-1}$ on SPP MFI. Feed composition (on a carbon basis) was 86 – 90% DME, 9 – 10% MeOH, and (i) no acetaldehyde, (ii) ~1.0% acetaldehyde, (iii) 1.9 – 2.0% acetaldehyde, (iv) ~2.9% acetaldehyde, (v) 3.7 – 4.2% acetaldehyde.

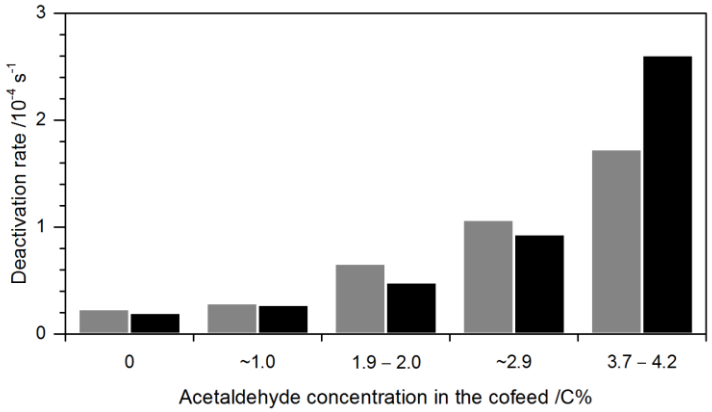

Figure 7.3: The deactivation rate – defined as the fraction of active sites getting deactivated per second – for the catalytic reactions of acetaldehyde (1 – 4%, on a carbon basis) with DME and MeOH (DME:MeOH ~9:1, on a carbon basis) on (i) Conv MFI (■) and (ii) SPP MFI (■), at 672 – 675 K, 107 – 114 kPa total feed pressure, 50 – 57 kPa DME pressure, 11 – 13 kPa methanol pressure, and 0 – 2.5 kPa acetaldehyde pressure. Total carbon space velocity was 10.6 – 11.7 mol C (mol Al-s)$^{-1}$ on Conv MFI and 2.7 – 2.8 mol C (mol Al-s)$^{-1}$ on SPP MFI.

The catalysts deactivated faster in the presence of acetaldehyde due to aldol-condensation reactions of acetaldehyde (Scheme 7.1) on Brønsted acid sites, which resulted in the formation of higher homologues that subsequently undergo ring-closure to form aromatics.[119] These aromatics are precursors to polycyclic species, like methyl-substituted naphthalenes and anthracenes, which have a larger kinetic diameter (0.77 nm for 1,5-dimethylnaphthalene)[122,123] than the diameter of the pore-openings in MFI (~0.55 nm).[42,43] These polycyclic species get trapped inside the zeolite pores and block the active sites causing catalyst deactivation. The formation of aromatics via the aldol-condensation pathway and the subsequent formation of polycyclic species is enhanced at higher acetaldehyde concentrations and therefore results in faster catalyst deactivation as observed in Figure 7.3.

Ramasamy et al.[124] investigated catalyst deactivation in the presence of acetaldehyde by reacting a mixture of 7.5 wt% acetaldehyde in ethanol on HZSM-5 at 633

K and 2 MPa total feed pressure and reported that the catalyst deactivated faster in the presence of acetaldehyde. The authors also noted rapid formation of higher molecular weight polycyclic species like naphthalenes and anthracenes from the analysis of the spent catalyst.[124] Gayubo et al.[125] investigated the reaction of pure acetaldehyde on HZSM-5 at 673 K and also observed rapid catalyst deactivation. They reported 4.2 – 4.7 wt% coke-content in the spent catalyst after 4 h of reaction at 673 K.[125]

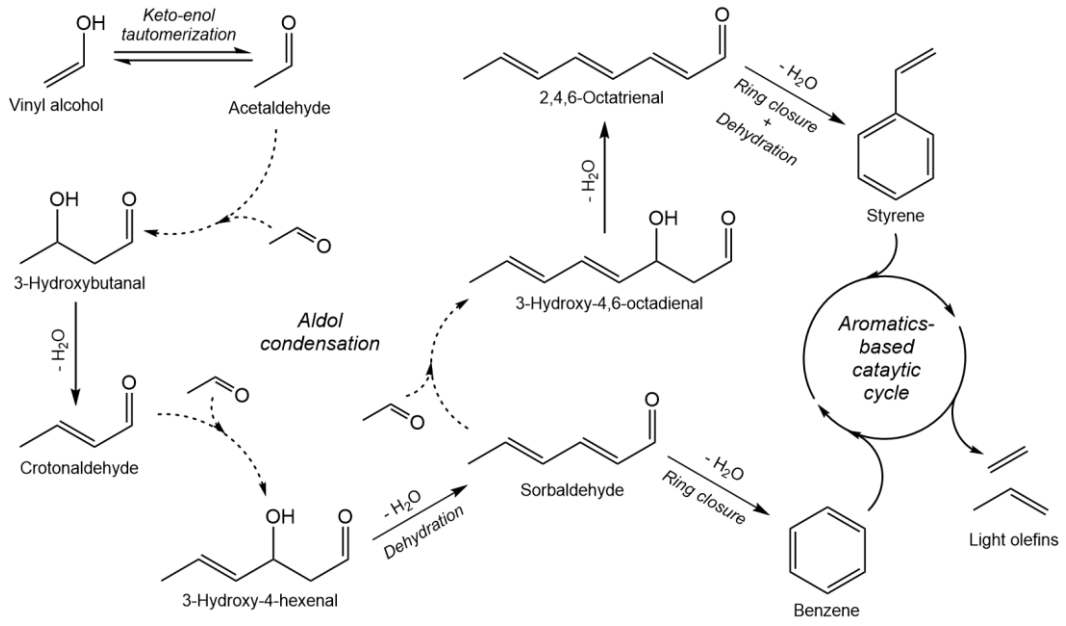

Scheme 7.1: A schematic of the aldol-condensation pathway of acetaldehyde conversion on MFI, which results in the formation of aromatics via aldol-condensation, ring-closure, and dehydration reactions. These aromatics subsequently propagate the aromatics-based methylation/dealkylation cycle and produce light olefins.

7.3.3 Effects of Co-Feeding Acetaldehyde on MTH Product Distribution

Figure 7.4 shows the effects of co-feeding acetaldehyde on the selectivity towards ethene, propene, $C_4 – C_7$ olefins, $C_4 – C_7$ alkanes, and MBs, for the catalytic reaction of acetaldehyde (1 – 4 C%) with DME and MeOH (DME:MeOH ~9:1, on a carbon basis) on Conv MFI and SPP MFI at 673 K. The selectivity towards ethene and MBs increased

monotonically with increasing acetaldehyde concentration in the feed. The selectivity towards C_4 – C_7 alkanes, on the other hand, decreased monotonically with increasing acetaldehyde concentration. A marginal decrease in propene and C_4 – C_7 olefins selectivity was also observed.

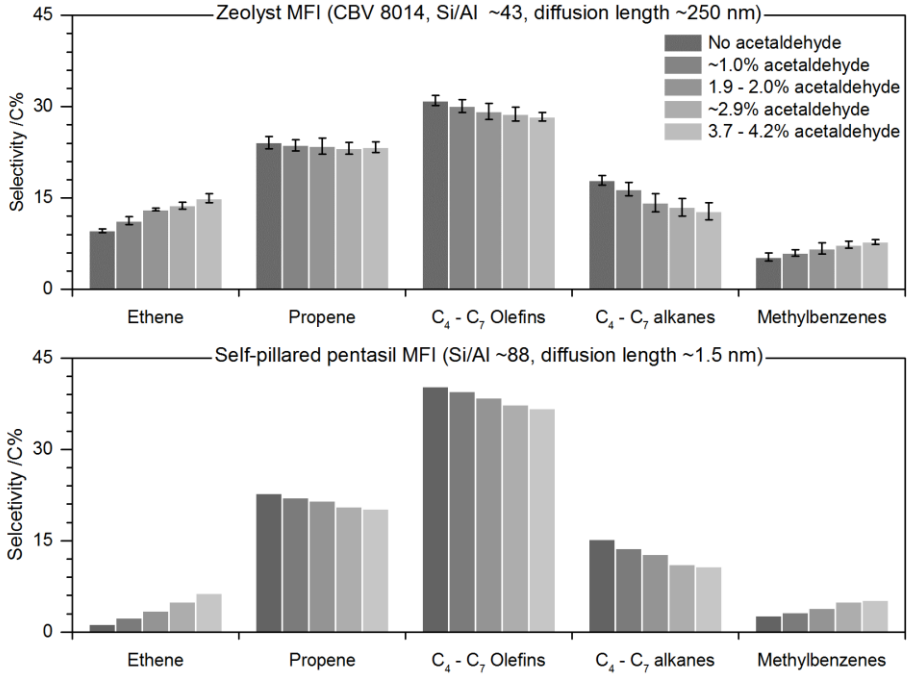

Figure 7.4: Effects of co-feeding acetaldehyde (1 – 4%, on a carbon basis) with DME and MeOH (DME:MeOH ~9:1, on a carbon basis) on the selectivity towards ethene, propene, C_4 – C_7 olefins, C_4 – C_7 alkanes, and MBs, for the catalytic reactions on (i) Conv MFI and (ii) SPP MFI, at 672 – 675 K, 107 – 114 kPa total feed pressure, 50 – 57 kPa DME pressure, 11 – 13 kPa MeOH pressure, 0 – 2.5 kPa acetaldehyde pressure, and 15 – 60 min time-on-stream. Net carbon converted was 37 – 48%. Total carbon space velocity was 10.6 – 11.7 mol C (mol Al-s)$^{-1}$ on Conv MFI and 2.7 – 2.8 mol C (mol Al-s)$^{-1}$ on SPP MFI.

7.3.3.1 Effects of Co-Feeding Acetaldehyde on Methylbenzenes Selectivity

MBs selectivity increased monotonically from 5.3 C% without acetaldehyde to 7.8 C% in the presence of ~4 C% acetaldehyde on Conv MFI, and from 2.7 C% to 5.3 C% on SPP MFI. As discussed above, acetaldehyde undergoes multiple aldol-condensation reactions (Scheme 7.1) on Brønsted acid sites to form higher homologues (e.g.,

sorbaldehyde), which can subsequently undergo ring-closure followed by dehydration to form aromatics (e.g., benzene). The aldol-condensation products of acetaldehyde (e.g., sorbaldehyde) can also undergo bimolecular hydrogen-transfer to form unsaturated aliphatics (e.g., 1,3,5-hexatriene), which can eventually oligomerize, cyclize, and undergo further hydrogen-transfer to form aromatics (Scheme 7.2). Both these reaction pathways result in the formation of aromatics, and therefore explain the observed increase in MB selectivity in the presence of acetaldehyde.

7.3.3.2 Effects of Co-Feeding Acetaldehyde on Ethene selectivity and Ethene/2MBu

Figure 7.5 shows the effects of co-feeding acetaldehyde on ethene/2MBu yield and HTI (ratio of the synthesis rates of C_2 – C_6 alkanes and total C_2 – C_6 aliphatics), for the catalytic reaction of acetaldehyde (1 – 4 C%) with DME and MeOH (DME:MeOH ~9:1, on a carbon basis) on Conv MFI and SPP MFI at 673 K An increase in the concentration of MBs inside the zeolite pores enhances the propagation of the aromatics-based catalytic cycle; this was corroborated by a corresponding increase in ethene/2MBu yield, which increased systematically from 1.3 without acetaldehyde co-feed to 2.5 in the presence of ~ 4 C% acetaldehyde on Conv MFI, and from 0.18 without acetaldehyde to 1.1 in the presence of ~ 4 C% acetaldehyde on SPP MFI (Figure 7.5). Aromatics, especially MBs, are the precursors to ethene and therefore, an increase in the propagation of the aromatics-based methylation/dealkylation cycle will enhance the production of ethene. Additionally, acetaldehyde and its aldol-condensation products can undergo bimolecular hydrogen-transfer to form the corresponding alcohols, which can dehydrate/crack on Brønsted acid sites to form ethene (Scheme 7.3). Ethene selectivity, as a result, increased monotonically from 9.6 C% without acetaldehyde to 15 C% in the presence of ~4 C% acetaldehyde on Conv MFI, and from 1.3 C% to 6.4 C% on SPP MFI (Figure 7.5).

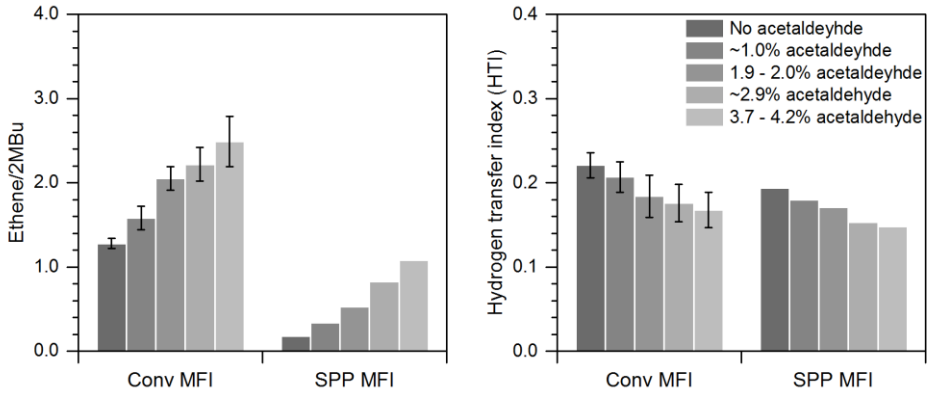

Figure 7.5: Effects of co-feeding acetaldehyde (1 – 4%, on a carbon basis) with DME and MeOH (DME:MeOH ~9:1, on a carbon basis) on ethene/2MBu and HTI, for the catalytic reactions on (i) Conv MFI and (ii) SPP MFI, at 672 – 675 K, 107 – 114 kPa total feed pressure, 50 – 57 kPa DME pressure, 11 – 13 kPa MeOH pressure, 0 – 2.5 kPa acetaldehyde pressure, and 15 – 60 min time-on-stream. Net carbon converted was 37 – 48%. Total carbon space velocity was 10.6 – 11.7 mol C (mol Al-s)$^{-1}$ on Conv MFI and 2.7 – 2.8 mol C (mol Al-s)$^{-1}$ on SPP MFI.

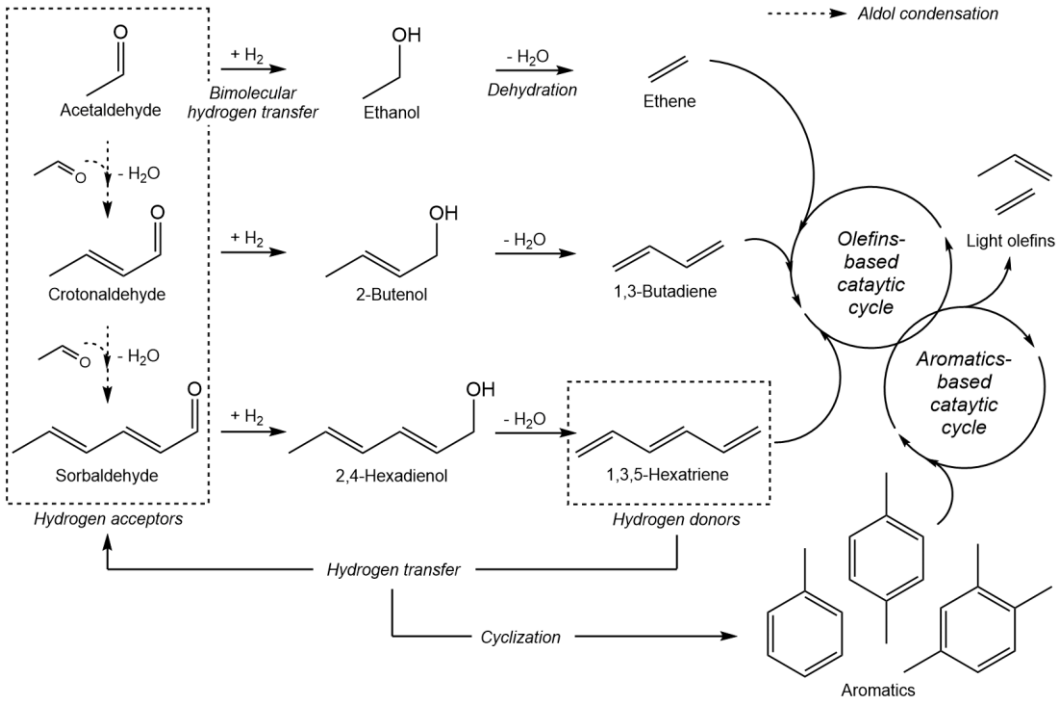

Scheme 7.2: A schematic of the bimolecular hydrogen-transfer pathway of acetaldehyde conversion on MFI. Aldehydes undergo hydrogen-transfer to form the corresponding alcohols, which dehydrate on Brønsted acid sites to form olefins or polyenes.

7.3.3.3 Effects of Co-Feeding Acetaldehyde on Propene Selectivity

It must be noted propene, like ethene, is also a product of the aromatics-based catalytic cycle. Propene selectivity however, unlike ethene selectivity, decreased marginally from 24 C% without acetaldehyde to 23 C% in the presence of ~ 4 C% acetaldehyde in the feed on Conv MFI, and from 23 C% to 20 C% on SPP MFI (Figure 7.4). Unlike ethene which is predominantly formed via aromatic-dealkylation under the reaction conditions investigated in this work, propene is a product of both aromatic-dealkylation and olefin-cracking. It is likely that an increase in the concentration of the chain-carriers of the aromatics-based catalytic cycle i.e., MBs, reduces the relative concentration of the chain-carriers of the olefins-based catalytic cycle i.e., olefins, and therefore suppresses the propagation of the olefins-based catalytic cycle. Any increase in propene formation due to enhanced propagation of the aromatics-based catalytic cycle is likely compensated by a corresponding decrease in propene formation from the olefins-based catalytic cycle. Furthermore, the rate of propene methylation is at least an order of magnitude higher than the rate of ethene methylation on MFI.[95,96] Excess propene formed due to enhanced propagation of the aromatics-based catalytic cycle may be getting converted to higher olefins via secondary reactions.

7.3.3.4 Effects of Co-Feeding Acetaldehyde on $C_4 – C_7$ Olefins Selectivity

$C_4 – C_7$ olefins selectivity decreased monotonically from 31 C% in the absence of acetaldehyde co-feed to 28 C% in the presence of ~4 C% acetaldehyde co-feed on Conv MFI, and from 40 C% to 37 C% on SPP MFI (Figure 7.4). This decrease in $C_4 – C_7$ olefins selectivity in the presence of acetaldehyde can be explained by the bimolecular hydrogen transfer pathway (Scheme 7.3). Aldehydes are hydrogen acceptors and can undergo hydrogen transfer to form the corresponding alcohols. The presence of these additional

hydrogen acceptors in the zeolite pores increases the driving force of olefins to donate hydrogen and form dienes or trienes, thereby increasing the concentration of polyenes inside the zeolite pores. These polyenes can subsequently undergo secondary reactions like cyclization and hydrogen transfer to form aromatics. The driving force for the formation from of aromatics from olefins is therefore enhanced due to the presence of additional hydrogen acceptors i.e., aldehydes, inside the zeolite pores thereby resulting in a decrease in $C_4 – C_7$ olefins selectivity and a corresponding increase in MBs selectivity in the presence of acetaldehyde.

7.3.3.5 Effects of Co-Feeding Acetaldehyde on $C_4 – C_7$ Alkanes Selectivity and HTI

Alkanes (C_nH_{2n+2}), in MTH conversion, are formed as a result of hydrogen transfer to monounsaturated olefins (C_nH_{2n}). Hydrogen transfer to aldehydes, on the other hand, results in the formation of polyenes (instead of alkanes). The presence of these additional hydrogen acceptors i.e., aldehydes, inside the zeolite pores reduces the probability of an olefin to accept hydrogen and form the corresponding alkane. $C_4 – C_7$ alkanes selectivity, therefore, decreased monotonically from 18 C% with no acetaldehyde co-feed to 13 C% in the presence of ~4 C% acetaldehyde co-feed on Conv MFI, and from 15 C% to 11 C% on SPP MFI (Figure 7.4). The hydrogen transfer index (HTI), which was defined as the ratio of the synthesis rates of $C_2 – C_6$ alkanes and total $C_2 – C_6$ aliphatic hydrocarbons and can be considered a measure of the extent of hydrogen transfer to olefins, also decreased monotonically from 0.22 to 0.17 on Conv MFI, and from 0.19 to 0.15 on SPP MFI, in the presence of ~4 C% acetaldehyde in the feed (Figure 7.5). These experimental observations support our postulate that hydrogen transfer to olefins to form the corresponding alkanes is suppressed in the presence of acetaldehyde and its homologues inside the zeolite pores.

7.3.4 Catalytic Reactions of $^{13}C_2$-Acetaldehyde with ^{12}C-Labeled DME and Methanol

Isotopically labeled acetaldehyde (~4 C%) was co-reacted with a mixture of ^{12}C-labeled DME and MeOH (DME:MeOH ~ 9:1, on a carbon basis) to further investigate the mechanistic pathways initiated by co-feeding acetaldehyde with DME-MeOH mixtures in

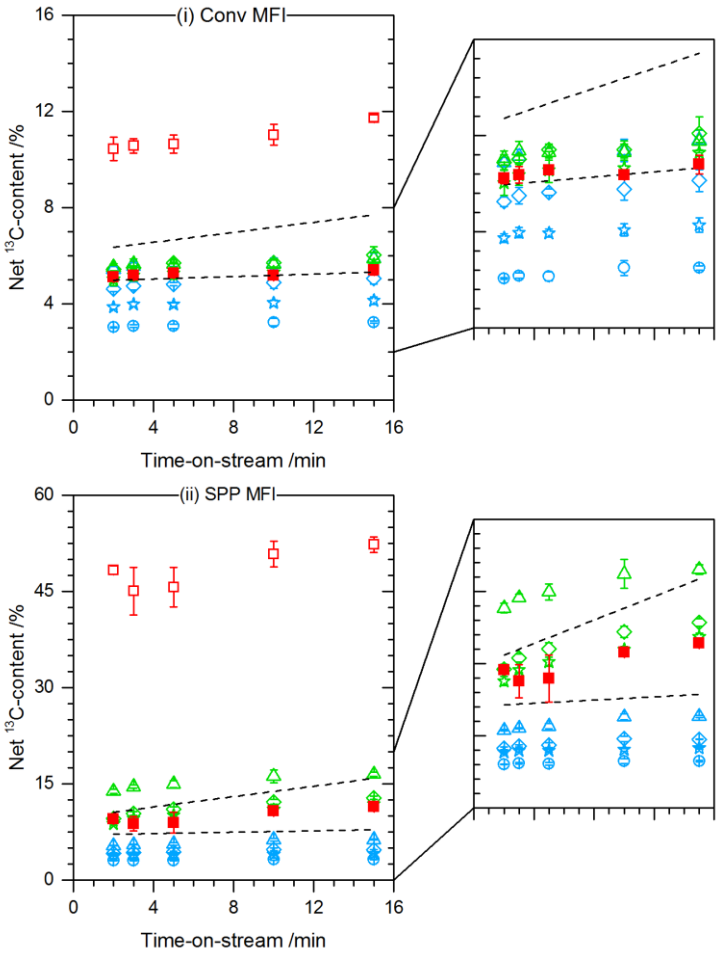

Figure 7.6: Net ^{13}C-content in ethene (□), $^{13}C_{bin}$-ethene (■), propene (△), *trans*-2-butene (◇), 2-methyl-2-butene (☆), 2-methyl-2-hexene (○), *p*-xylene (△), 1,2,4-triMB (◇), and 1,2,4,5-tetraMB (☆), versus TOS for the catalytic reactions of 3.7 – 4.2 C% acetaldehyde with DME and MeOH (DME:MeOH ~9:1, on a carbon basis) on (i) Conv MFI and (ii) SPP MFI, at 673 – 675 K, 107 – 109 kPa total feed pressure, 50 – 56 kPa DME pressure, 11 – 12 kPa methanol pressure, and 2.2 – 2.5 kPa acetaldehyde pressure. Total carbon space velocity was 10.8 – 11.6 mol C (mol Al-s)$^{-1}$ on Conv MFI and 2.7 – 2.8 mol C (mol Al-s)$^{-1}$ on SPP MFI. The dotted black lines represent the upper and lower bounds of ^{13}C-content in the converted carbon, which was estimated based on unconverted reactants present in the effluent.

MTH conversion. Figure 7.6 shows the net ^{13}C-content as a function of TOS in ethene and in representative hydrocarbon species of the aromatics-based catalytic cycle viz., *p*-xylene, 1,2,4-triMB, and 1,2,4,5-tetraMB, and of the olefins-based catalytic cycle viz., propene, *trans*-2-butene, 2-methyl-2-butene, and 2-methyl-2-pentene, for the reaction of ~4 C% acetaldehyde with DME/MeOH on Conv MFI and SPP MFI at 673 K. The dotted black lines represent the upper and lower bounds of ^{13}C-content in the converted carbon, estimated based on unconverted reactants present in the effluent.

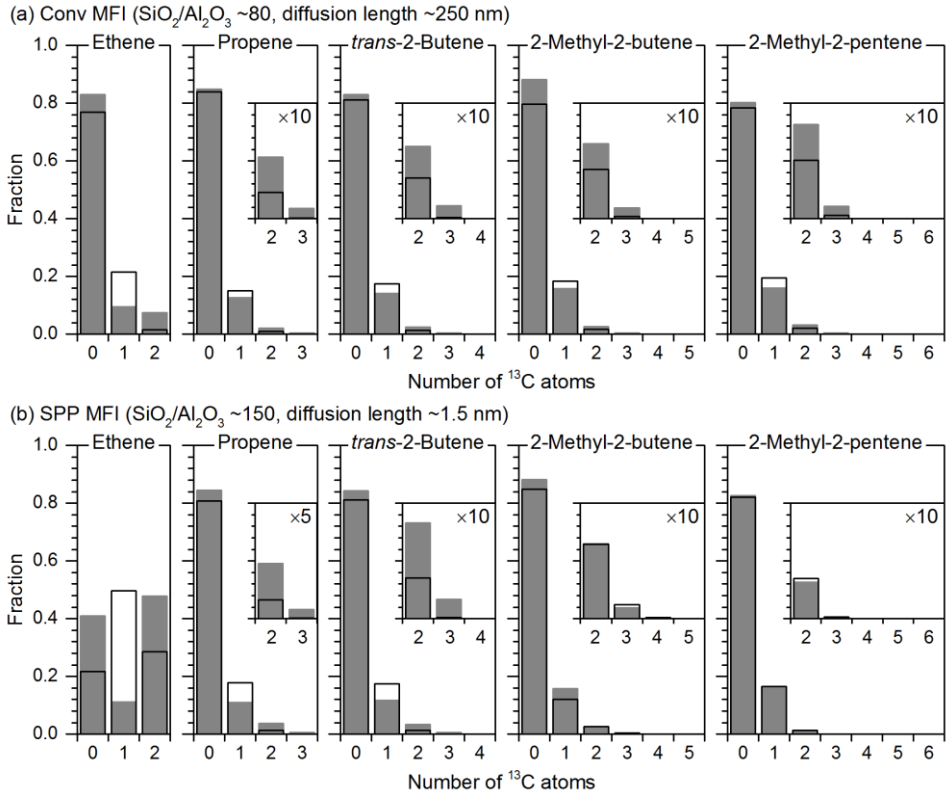

Figure 7.7: Experimentally observed isotopologue distributions (■) of ethene, propene, *trans*-2-butene, 2-methyl-2-butene, and 2-methyl-2-pentene for the catalytic reaction of 3.7 – 4.2 C% acetaldehyde with DME and MeOH (DME:MeOH ~9:1, on a carbon basis) on (a) Conv MFI and (b) SPP MFI, at 673 – 675 K, 107 – 109 kPa total feed pressure, 50 – 56 kPa DME pressure, 11 – 12 kPa MeOH pressure, 2.2 – 2.5 kPa acetaldehyde pressure, and 15 min TOS. Total carbon space velocity was 10.8 – 11.6 mol C (mol Al-s)$^{-1}$ on Conv MFI and 2.7 – 2.8 mol C (mol Al-s)$^{-1}$ on SPP MFI. The binomial distribution of the isotopologues (□) is also shown, for comparison.

It can be observed from Figure 7.6 that the ^{13}C-content in olefins and aromatics was similar to the ^{13}C-content in the converted carbon, suggesting that the isotopically labeled carbon atoms from acetaldehyde were blended, at least to some extent, into the pool of hydrocarbons formed by unlabeled DME and MeOH. There are, however, certain observable trends in the isotopic content of specific hydrocarbon species. The ^{13}C-content in aromatics was always higher than the ^{13}C-content in olefins implying that cyclization of olefins was not the only source of aromatics and that other pathways for aromatics formation that involve ^{13}C atoms from acetaldehyde are active inside the zeolite pores. One such pathway is the aldol-condensation pathway (Scheme 7.2), described later.

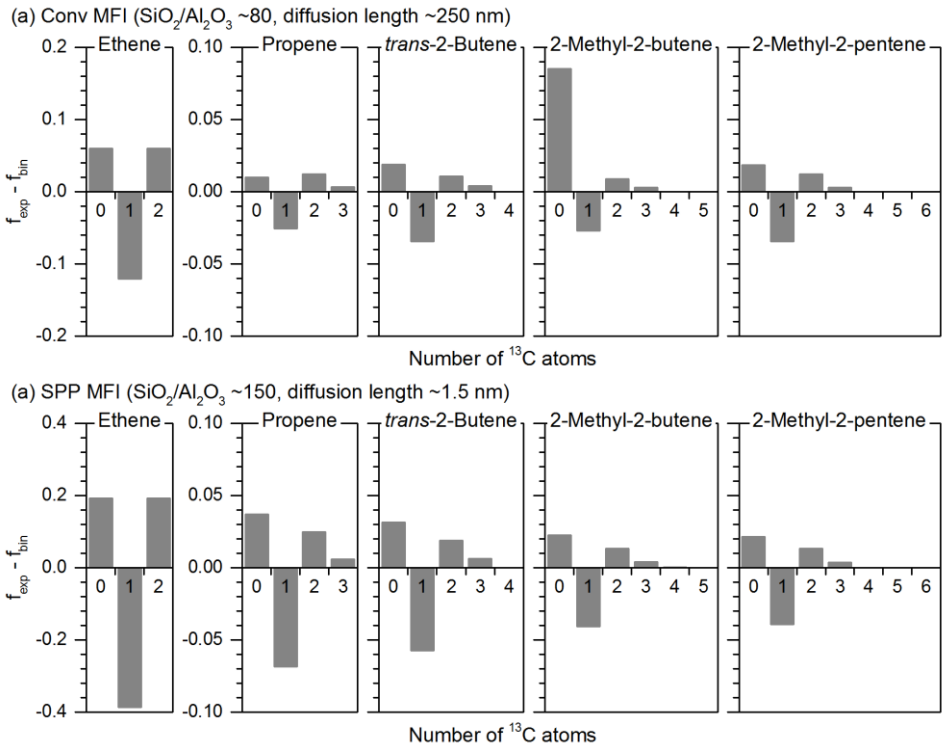

Figure 7.8: Difference between the experimentally observed distribution (f_{exp}) and the binomial distribution (f_{bin}) of the isotopologues of ethene, propene, *trans*-2-butene, 2-methyl-2-butene, and 2-methyl-2-pentene for the catalytic reactions of 3.7 – 4.2 C% acetaldehyde with DME and MeOH (DME:MeOH ~9:1, on a carbon basis) on (a) Conv MFI and (b) SPP MFI, at 673 – 675 K, 107 – 109 kPa total feed pressure, 50 – 56 kPa DME pressure, 11 – 12 kPa methanol pressure, 2.2 – 2.5 kPa acetaldehyde pressure, and 15 min TOS. Total carbon space velocity was 10.8 – 11.6 mol C (mol Al-s)$^{-1}$ on Conv MFI and 2.7 – 2.8 mol C (mol Al-s)$^{-1}$ on SPP MFI.

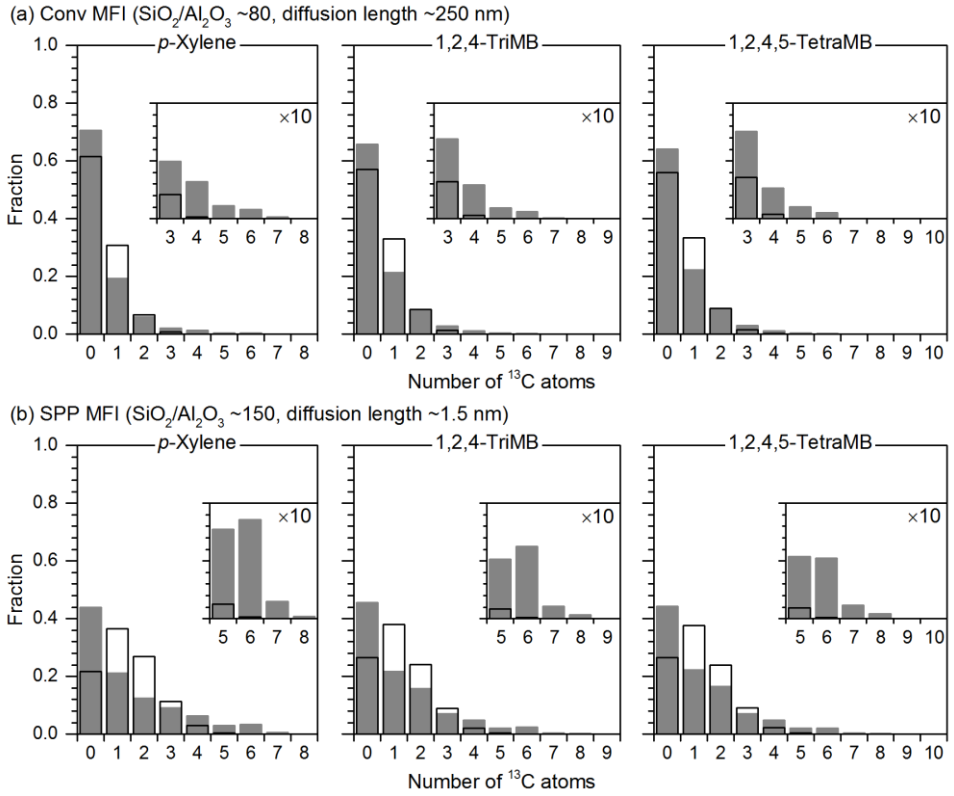

Figure 7.9: Experimentally observed isotopologue distributions (■) of *p*-xylene, 1,2,4-triMB, and 1,2,4,5-tetraMB, for the catalytic reaction of 3.7 – 4.2 C% acetaldehyde with DME and MeOH (DME:MeOH ~9:1, on a carbon basis) on (a) Conv MFI and (b) SPP MFI, at 673 – 675 K, 107 – 109 kPa total feed pressure, 50 – 56 kPa DME pressure, 11 – 12 kPa methanol pressure, 2.2 – 2.5 kPa acetaldehyde pressure, and 15 min TOS. Total carbon space velocity was 10.8 – 11.6 mol C (mol Al-s)$^{-1}$ on Conv MFI and 2.7 – 2.8 mol C (mol Al-s)$^{-1}$ on SPP MFI. The binomial distribution of the isotopologues (□) is also shown, for comparison.

Figure 7.7 shows the isotopologue distribution of ethene, propene, *trans*-2-butene, 2-methyl-2-butene, and 2-methyl-2-pentene, for the catalytic reaction of ~4 C% $^{13}C_2$-acetaldehyde with unlabeled DME and MeOH (DME:MeOH ~9:1, on a carbon basis) on Conv MFI and SPP MFI zeolite samples at 673 K. The binomial distribution of the isotopologues, which corresponds to a random incorporation of ^{13}C atoms, was calculated and is also reported in Figure 7.7, for comparison. The experimentally observed isotopologue distribution of olefins was skewed from the binomial distribution. Figure 7.8

shows the difference between the experimentally observed distribution (f_{exp}) and the binomial distribution (f_{bin}) of the isotopologues of olefins. The fraction of olefins with zero ^{13}C labels was higher than that predicted by the binomial distribution suggesting that a fraction of olefins is being formed directly from unlabeled DME and MeOH, without the involvement of $^{13}C_2$-acetaldehyde. The fraction of olefins with multiple (two or more) ^{13}C labels was also higher than that predicted by the binomial distribution implying that a fraction of olefins is being formed from a hydrocarbon pool that is rich in ^{13}C atoms originating from $^{13}C_2$-acetaldehyde.

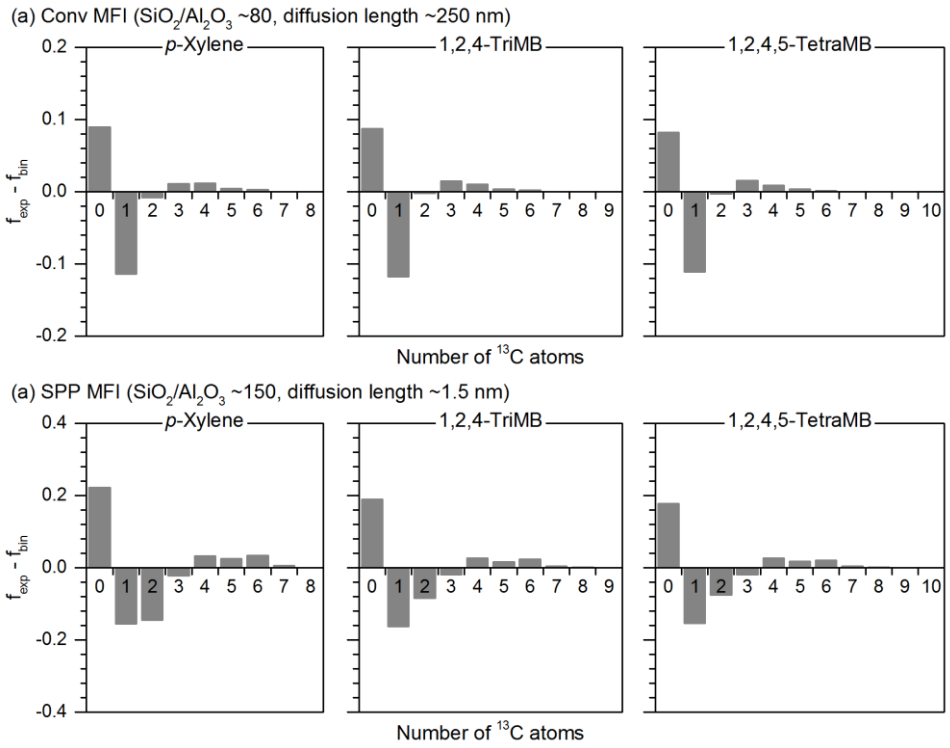

Figure 7.10: Difference between the experimentally observed distribution (f_{exp}) and the binomial distribution (f_{bin}) of the isotopologues of *p*-xylene, 1,2,4-trimethylbenzene, and 1,2,4,5-tetramethylbenzene, for the catalytic reactions of 3.7 – 4.2 C% acetaldehyde with DME and MeOH (DME:MeOH ~9:1, on a carbon basis) on (a) Conv MFI and (b) SPP MFI, at 673 – 675 K, 107 – 109 kPa total feed pressure, 50 – 56 kPa DME pressure, 11 – 12 kPa methanol pressure, 2.2 – 2.5 kPa acetaldehyde pressure, and 15 min TOS. Total carbon space velocity was 10.8 – 11.6 mol C (mol Al-s)$^{-1}$ on Conv MFI and 2.7 – 2.8 mol C (mol Al-s)$^{-1}$ on SPP MFI.

Acetaldehyde and its homologues can form unsaturated aliphatics via: (i) the bimolecular hydrogen-transfer pathway (Scheme 7.2) that involves hydrogen-transfer to aldehydes, and (ii) the aldehyde-decarbonylation pathway (Scheme 7.3) that involves the removal of carbonyl oxygen as CO. These unsaturated aliphatics, once formed, can undergo further methylation, oligomerization, or cracking reactions to form ^{13}C-enriched olefins, as observed in the reaction effluent. Another trend that is evident from Figure 7.6 is that the net ^{13}C-content in olefins decreases with increasing carbon chain-length, in the order: propene > *trans*-2-butene > 2-methyl-2-butene > 2-methyl-2-hexene; this trend is consistent with the methylation of olefins by ^{12}C-labeled DME or MeOH, which results in the formation of higher homologues with progressively lower net ^{13}C-content. Similar to olefins, the net ^{13}C-content in MBs also decreased with increasing carbon chain-length, in the order: *p*-xylene > *1,2,4-triMB* > 1,2,4,5-tetraMB.

Figure 7.9 shows the isotopologue distribution of *p*-xylene, 1,2,4-triMB, and 1,2,4,5-tetraMB, at 15 min time-on-stream, for the catalytic reaction of ~4 C% $^{13}C_2$-acetaldehyde with unlabeled DME and MeOH (DME:MeOH ~9:1, on a carbon basis) on Conv MFI and SPP MFI at 673 K. A binomial distribution of the isotopologues of *p*-xylene, 1,2,4-triMB, and 1,2,4,5-tetraMB is also reported in Figure 7.9. Similar to olefins, the experimentally observed isotopologue distribution of aromatics in all cases was skewed from the binomial distribution. Figure 7.10 shows the difference between the experimentally observed distribution (f_{exp}) and the binomial distribution (f_{bin}) of the isotopologues of *p*-xylene, 1,2,4-triMB, and 1,2,4,5-tetraMB. The fraction of isotopologues with zero ^{13}C labels was higher than that predicted by the binomial distribution, suggesting that some aromatics are being formed directly from unlabeled DME and methanol, without the involvement of $^{13}C_2$-acetaldehyde.

The fraction of isotopologues with multiple (3 or more on Conv MFI and 4 or more on SPP MFI) ^{13}C labels was also higher than that predicted by the binomial distribution (Figure 7.10). This implies that some aromatics are being formed from a hydrocarbon-pool that is rich in ^{13}C atoms from $^{13}C_2$-acetaldehyde. Possible reaction pathways for the formation of such ^{13}C-enriched aromatics are: (i) the aldol-condensation pathway (Scheme 7.1) that directly converts acetaldehyde to aromatics like benzene, which are subsequently methylated to form polyMBs, and (ii) the bimolecular hydrogen-transfer pathway (Scheme 7.2) or the aldehyde-decarbonylation pathway (Scheme 7.3), which convert acetaldehyde into unsaturated aliphatics that can subsequently form aromatics via hydrogen-transfer and cyclization reactions; both these reaction pathways result in the formation of aromatics with multiple ^{13}C labels from acetaldehyde, and therefore justify the skewed isotopologue distribution of aromatics in the reaction effluent. It is also worth noting that on SPP MFI, the fraction of isotopologues with six ^{13}C labels was especially higher than that expected from the binomial distribution (Figure 7.10). This observation further supports the reaction pathway that involves aldol-condensation of three $^{13}C_2$-acetaldehyde molecules to form $^{13}C_6$-benzene, which is subsequently methylated by unlabeled DME or MeOH to form MB isotopologues with six ^{13}C labels. A similar observation was however, not evident on the Conv MFI sample. It is likely that the shorter diffusion length in SPP MFI (diffusion length ~1.5 nm) compared to Conv MFI (diffusion length ~250 nm) suppressed the aromatic methylation/dealkylation reactions and prevented the scrambling of ^{13}C labels.

The net ^{13}C-content in ethene was always significantly higher than the ^{13}C-content in olefins, aromatics, as well as the ^{13}C-content in the converted carbon (Figure 7.6). The experimentally observed isotopologue distribution of ethene was also significantly different from the binomial distribution (Figure 7.7 and Figure 7.8). There was substantially more

$^{13}C_2$-ethene and $^{13}C_0$-ethene than that expected from a random incorporation of ^{13}C atoms. The enrichment of ethene with zero ^{13}C labels, similar to aromatics and olefins, is possibly due to direct ethene formation from unlabeled DME and methanol via the aromatics- or the olefins- based catalytic cycles. A high fraction of $^{13}C_2$-ethene, on the other hand, suggests that a fraction of ethene is being formed from a pool of hydrocarbons that is completely ^{13}C-labeled, or are at least significantly richer in ^{13}C labels compared to the rest of the hydrocarbon-pool. We surmise that this isotopic enrichment of ethene occurs because acetaldehyde or its aldol-condensation products undergo bimolecular hydrogen-transfer to form the corresponding alcohols, which then readily dehydrate/crack on Brønsted acid sites to form ethene (Scheme 7.2). Ethene formed via this reaction pathway will be completely ^{13}C-labeled, thereby resulting in the observed enrichment of ethene with two ^{13}C labels.

Based on our observations in the isotopic experiments discussed above, there are two distinct routes for the formation of ethene in MTH conversion in the presence of acetaldehyde: (i) ethene formation from aromatics via aromatic-dealkylation or from olefins via olefin-cracking, and (ii) direct ethene synthesis from acetaldehyde via a bimolecular hydrogen-transfer pathway. The former pathway will likely result in ethene with a random distribution of ^{13}C labels, while the latter pathway will result in ethene that is completely ^{13}C-labeled. The fraction of ethene formed via these two pathways was calculated by deconvoluting the experimentally observed isotopologue distribution and is reported in Table 7.2. Ethene formed via the first reaction pathway is denoted as $^{13}C_{bin}$-ethene while the ethene formed via the bimolecular hydrogen-transfer pathway is denoted as $^{13}C_2$-ethene. The net ^{13}C-content in $^{13}C_{bin}$-ethene was also estimated from the experimentally observed isotopologue distribution and is reported in Table 7.2 and in Figure 7.6. The ^{13}C-

content in $^{13}C_{bin}$-ethene was similar, as expected, to the ^{13}C-content in hydrocarbon species that are likely the precursors to $^{13}C_{bin}$-ethene i.e., olefins and aromatics, thereby supporting the postulate that $^{13}C_{bin}$-ethene is being formed via the olefins-based or the aromatics- based catalytic cycles as a result of olefin-cracking or aromatic-dealkylation reactions, respectively. Figure 7.11 shows the total ethene selectivity for the catalytic reaction of ~4 C% acetaldehyde with DME and MeOH on Conv MFI and SPP MFI at 673 K. The corresponding contributions from $^{13}C_{bin}$-ethene and $^{13}C_2$-ethene are also shown. Ethene selectivity in the catalytic reaction of DME and methanol without acetaldehyde co-feed on Conv MFI and SPP MFI at 673 K is also reported, for comparison. It is evident that both $^{13}C_{bin}$-ethene and $^{13}C_2$-ethene contributed significantly towards the excess ethene produced in the presence of acetaldehyde in the feed.

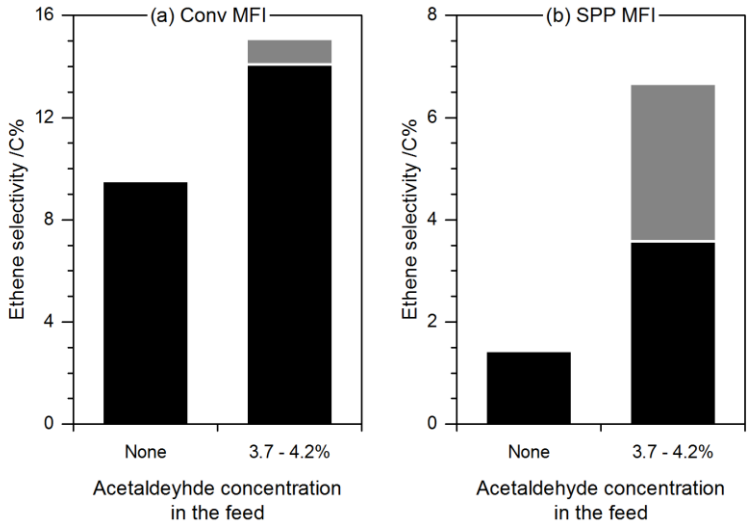

Figure 7.11: Selectivity towards $^{13}C_{bin}$-ethene (■) and $^{13}C_2$-ethene (■) for the reaction of 3.7 – 4.2 C% acetaldehyde with DME and MeOH (DME:MeOH ~9:1, on a carbon basis) on (a) Conv MFI and (b) SPP MFI, at 673 – 675 K, 107 – 109 kPa total feed pressure, 50 – 56 kPa DME pressure, 11 – 12 kPa methanol pressure, and 2.2 – 2.5 kPa acetaldehyde pressure. Total carbon space velocity was 10.8 – 11.6 mol C (mol Al-s)$^{-1}$ on Conv MFI and 2.7 – 2.8 mol C (mol Al-s)$^{-1}$ on SPP MFI. Ethene selectivity for the reaction of DME and MeOH without acetaldehyde co-feed under similar reaction conditions is also shown, for comparison.

Table 7.2: Total ethene selectivity, fraction of $^{13}C_{bin}$-ethene and its ^{13}C-content, as well as the fraction of $^{13}C_2$-ethene, for the catalytic reaction of 3.7 – 4.2 C% acetaldehyde with a mixture of DME and MeOH (DME:MeOH ~9:1, on a carbon basis) on (i) Conv MFI and (ii) SPP MFI, at 673 – 675 K, 107 – 109 kPa total feed pressure, 50 – 56 kPa DME pressure, 11 – 12 kPa methanol pressure, and 2.2 – 2.5 kPa acetaldehyde pressure. Total carbon space velocity was 10.6 – 11.7 mol C (mol Al-s)$^{-1}$ on Conv MFI and 2.7 – 2.8 mol C (mol Al-s)$^{-1}$ on SPP MFI.

Time-on-stream /min	**2**	**3**	**5**	**10**	**15**
(i) Conv MFI (SiO_2/Al_2O_3 ~80, diffusion length ~250 nm)					
Ethene selectivity /C%	14.0	14.2	14.8	14.9	15.4
Fraction of $^{13}C_{bin}$-ethene	0.94	0.94	0.94	0.94	0.93
^{13}C-content in $^{13}C_{bin}$-ethene	0.05	0.05	0.05	0.05	0.05
Fraction of $^{13}C_2$-ethene	0.06	0.06	0.06	0.06	0.07
(ii) SPP MFI (SiO_2/Al_2O_3 ~150, diffusion length ~1.5 nm)					
Ethene selectivity /C%	6.3	6.1	6.4	6.7	6.9
Fraction of $^{13}C_{bin}$-ethene	0.57	0.60	0.60	0.55	0.54
^{13}C-content in $^{13}C_{bin}$-ethene	0.10	0.09	0.09	0.11	0.11
Fraction of $^{13}C_2$-ethene	0.43	0.40	0.40	0.45	0.46

7.3.5 Catalytic Reactions of Acetaldehyde Alone without DME or Methanol

The product distribution of the catalytic conversion of acetaldehyde only (without DME or MeOH) on Conv MFI and SPP MFI at 673 K, 108 – 109 kPa total feed pressure, and 1.9 kPa acetaldehyde partial pressure, is reported in Figure 7.12. The total carbon space velocity was 0.46 mol C (mol Al-s)$^{-1}$ on Conv MFI and 0.12 mol C (mol Al-s)$^{-1}$ on SPP MFI. The reaction conditions were similar to the reaction conditions in the acetaldehyde co-feed experiment in which ~4 C% acetaldehyde was co-reacted with DME and MeOH. Acetaldehyde partial pressure was 2.2 – 2.5 kPa and the total carbon space velocity was 0.40 – 0.49 mol C (mol Al-s)$^{-1}$ on Conv MFI and 0.10 – 0.12 mol C (mol Al-s)$^{-1}$ on SPP MFI in the ~4 C% acetaldehyde co-feed experiments.

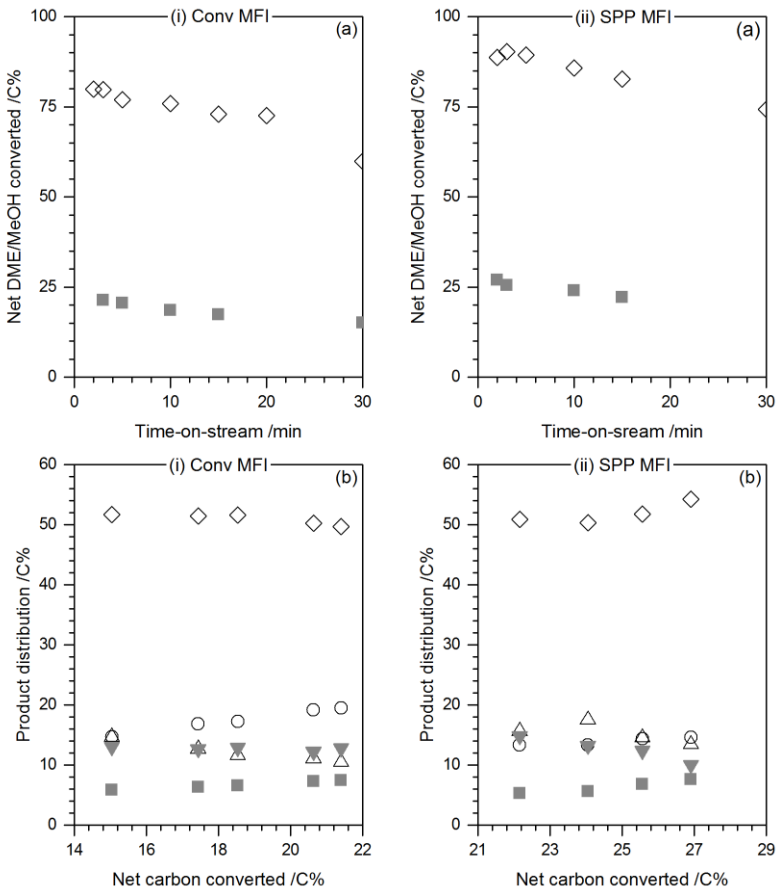

Figure 7.12: (a) Net DME/MeOH converted (■) versus TOS, and (b) selectivity towards ethene (■), propene (◇), C_4 – C_8 aliphatics (△), MBs (○), and C_9+ hydrocarbons (▼), versus net carbon converted, for the catalytic reaction of acetaldehyde on (i) Conv MFI and (ii) SPP MFI, at 673 K, 108 – 109 kPa total feed pressure, and ~1.9 kPa acetaldehyde pressure. Total carbon space velocity was 0.46 mol C (mol Al-s)$^{-1}$ on Conv MFI and 0.12 mol C (mol Al-s)$^{-1}$ on SPP MFI. Acetaldehyde conversion in the presence of DME and MeOH (◇), calculated based on unconverted acetaldehyde present in the effluent, for the catalytic reactions of 3.7 – 4.2 C% acetaldehyde in the presence of DME and MeOH (DME:MeOH ~9:1, on a carbon basis) on Conv MFI and SPP MFI under similar reaction conditions is also shown, for comparison.

Marginal catalyst deactivation was observed on both the catalyst samples as acetaldehyde conversion decreased from 21% to 15% in 30 min on Conv MFI and from 27% to 22% in 15 min on SPP MFI (Figure 7.12a). Acetaldehyde conversion, in the presence of DME and methanol, estimated based on unconverted reactants present in the reaction effluent, during the ~4 C% acetaldehyde co-feed experiments on Conv MFI and

SPP MFI is also shown in Figure 7.12a, for comparison. Acetaldehyde conversion was significantly higher in the presence of DME and methanol; decreasing from 80% to 60% in 30 min on Conv MFI and from 90% to 83% in 15 min on SPP MFI. This implies that (i) additional pathways for acetaldehyde conversion exist in the presence of a methylating agent, and/or (ii) reaction pathways of acetaldehyde conversion that exist in the absence of DME and methanol are enhanced under MTH conditions.

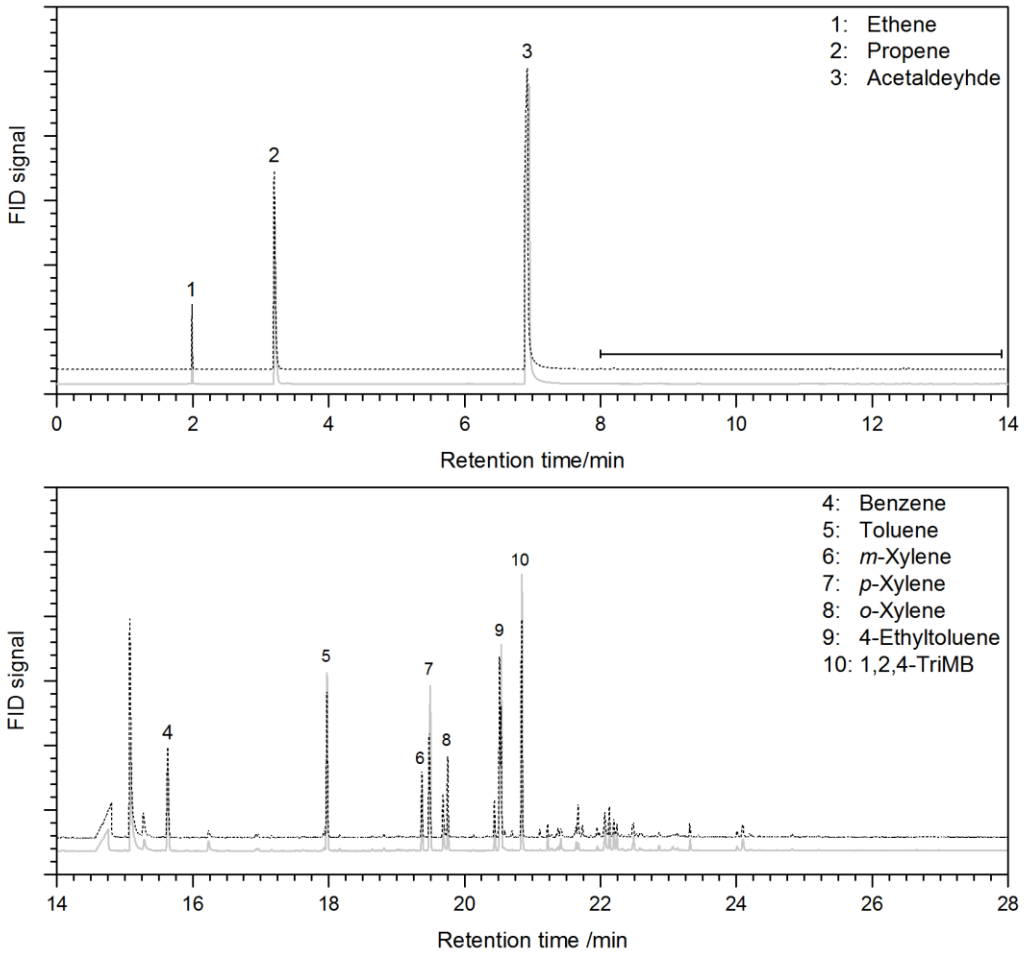

Figure 7.13: FID chromatograms of reactor effluents at 10 min TOS showing the product distribution of acetaldehyde conversion on Conv MFI (solid-gray) and SPP MFI (dotted-black), at 673 K, 108 – 109 kPa total feed pressure, and ~1.9 kPa acetaldehyde pressure. Total carbon space velocity was 0.46 mol C (mol Al-s)$^{-1}$ on Conv MFI and 0.12 mol C (mol Al-s)$^{-1}$ on SPP MFI.

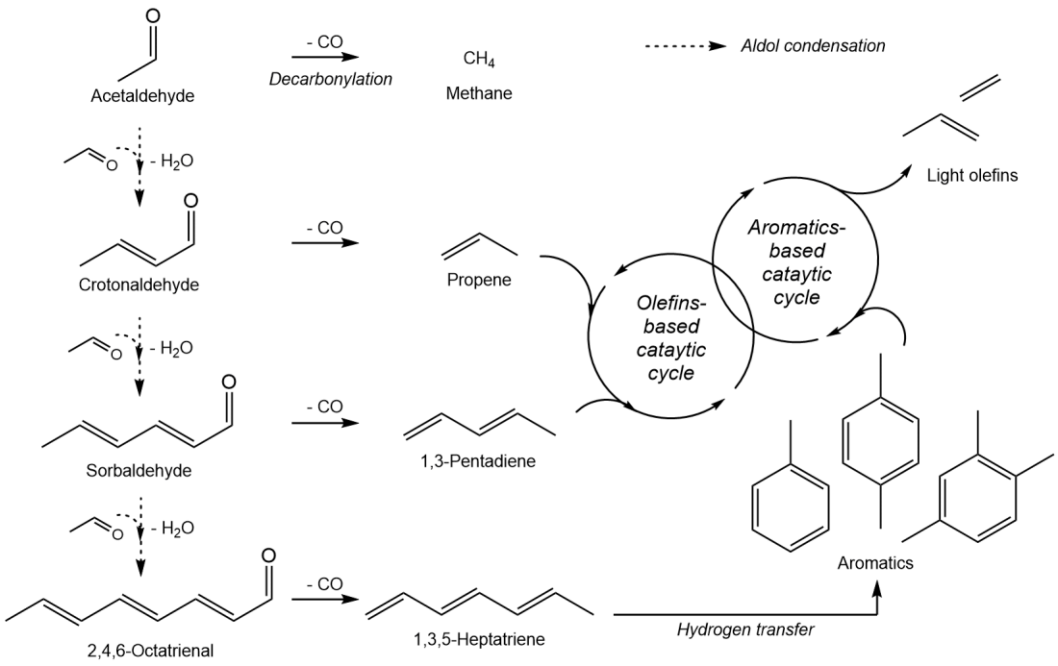

Scheme 7.3: A schematic of the aldehyde-decarbonylation pathway of acetaldehyde conversion on MFI to produce the corresponding unsaturated aliphatics, which subsequently undergo oligomerization, hydrogen-transfer, and cyclization reactions to form aromatics. These aromatics propagate the aromatics-based catalytic cycle and form light olefins.

The FID chromatograms of the reaction effluent for acetaldehyde conversion without DME or MeOH, on Conv MFI and SPP MFI at 673 K and 10 min TOS are shown in Figure 7.13. A wide variety of hydrocarbon species were observed in the reaction effluent on both the catalyst samples. The peak at ~7 min retention time corresponds to the unreacted acetaldehyde present in the reaction effluent. Other significant peaks present were those belonging to ethene, propene, and aromatics, especially benzene, toluene, xylenes, and 1,2,4-triMB. No prominent peaks were present at retention times that correspond to a C_4 – C_7 aliphatic hydrocarbons (8 – 15 min).

The presence of aromatics, especially benzene, in the reaction effluent supports the aldol-condensation pathway of acetaldehyde conversion (Scheme 7.1). Acetaldehyde

undergoes keto-enol tautomerization on Brønsted acid sites in MFI to form vinyl alcohol (Scheme 7.4a),[119,126] which then reacts with chemisorbed acetaldehyde to form chemisorbed 3-hydroxybutanal that can either desorb as 3-hydroxybutanal or undergo dehydration to form crotonaldehyde. Crotonaldehyde can undergo another aldol-condensation with vinyl alcohol to form 3-hydroxyhex-4-enal, which can subsequently dehydrate to form sorbaldehyde (Scheme 7.4b). Finally, the enol form of sorbaldehyde i.e., hexa-1,3,5-trienol, can undergo ring-closure to form cyclohexa-2,4-dienol, which can then dehydrate on a Brønsted acid site to form benzene (Scheme 7.4c). A similar ring-closure of the aldol-condensation product of sorbaldehyde i.e., 2,4,6-octatrienal, followed by dehydration will result in the formation of styrene. The aldol-condensation pathway of acetaldehyde conversion results in the formation of aromatics inside the zeolite pores.

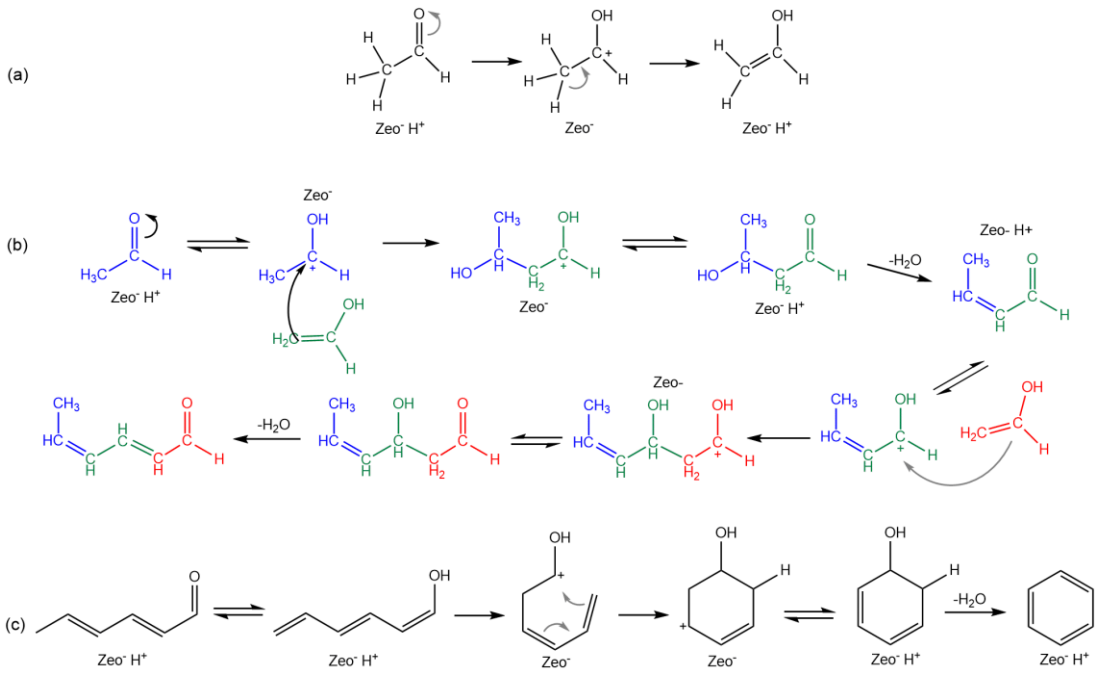

Scheme 7.4: (a) Keto-enol tautomerization of acetaldehyde to form vinyl alcohol, (b) aldol-condensation reactions of acetaldehyde to form higher homologues (e.g., crotonaldehyde, sorbaldehyde), and (c) ring-closure of sorbaldehyde followed by dehydration to form benzene.

It is important to note that the formation of other aromatics like toluene, xylenes, and 1,2,4-triMB, cannot be explained via the aldol-condensation pathway. The aldol-condensation pathway necessitates the removal of carbonyl-oxygen from an aldehyde ($C_nH_{n+2}O$) as H_2O, thereby leaving behind a C_nH_n backbone, which can only form hydrocarbons with a hydrogen-to-carbon ratio equal to 1, like benzene (C_6H_6) or styrene (C_8H_8). The polyMBs observed in the reaction effluent, like toluene (C_7H_8), xylenes (C_8H_{10}), or 1,2,4-triMB (C_9H_{12}), have hydrogen-to-carbon ratios >1 and therefore, their formation must involve a different reaction pathway. Similarly, the presence of olefins like ethene (C_2H_4) and propene (C_3H_6) also advocates for the existence of another acetaldehyde conversion pathway. The alternate reaction pathway for acetaldehyde conversion on Brønsted acid sites must involve either hydrogen-transfer, or removal of the carbonyl-oxygen as CO and not H_2O, to account for hydrogen-to-carbon ratio greater than unity.

We have discussed in Section 7.3.3 that a bimolecular hydrogen transfer pathway exists in the pores of MFI-type zeolites (Scheme 7.2). This pathway involves hydrogen transfer to acetaldehyde or its aldol-condensation products to form the corresponding alcohols, which then dehydrate on Brønsted acid sites to form olefins (including dienes and trienes). The bimolecular hydrogen transfer pathway, however, only redistributes the hydrogen within the hydrocarbons. The presence of hydrocarbon species with hydrogen-to-carbon ratio >1 must therefore be accompanied by the production of hydrocarbon species with hydrogen-to-carbon ratio <1, such as naphthalene ($C_{10}H_8$) or anthracene ($C_{14}H_{10}$) and their methylated homologues. Such hydrocarbon species were however not detected in the reaction effluent, implying that the propagation of a bimolecular hydrogen-transfer pathway alone cannot justify the observed product distribution in the reaction effluent of acetaldehyde conversion on MFI-type zeolites.

Removal of carbonyl-oxygen from an aldehyde ($C_nH_{n+2}O$) as CO forms a $C_{n-1}H_{n+2}$ carbon backbone, which has hydrogen-to-carbon ratio >1. A thermal conductivity detector was used to detect and quantify CO production during acetaldehyde conversion on Conv MFI at 673 K, ~126 kPa total feed pressure, ~2.2 kPa acetaldehyde pressure, and 0.68 mol C (mol Al-s)$^{-1}$ acetaldehyde space-velocity. The observed CO-to-propene molar ratio in the reaction effluent at 10 min and 40 min TOS was 1.33 and 1.28, respectively. The presence of CO in the reaction effluent implies that a reaction pathway that involves the removal of carbonyl-oxygen as CO exists. Decarbonylation of oxygenates like furan,[127] benzofuran,[127] 2,4,6-trimethylbenzaldehyde,[128,129] and 2,4,6-tri-*iso*-propylbenzaldehyde[130] has been reported in the aqueous solutions of strong acids as well as on solid acid catalysts including HZSM-5. Cheng et al.[127] investigated the conversion of furan on HZSM-5 at 873 K and proposed a decarbonylation pathway that resulted in the formation of an allene and CO.

We propose a similar aldehyde-decarbonylation pathway for the conversion of acetaldehyde or its homologues (e.g., crotonaldehyde, sorbaldehyde) on MFI-type zeolites. One possible mechanism is aldehyde interacting with a Brønsted acid site to form an adsorbed cationic complex that subsequently undergoes C-C bond cleavage at the *β*-position to form the corresponding hydrocarbon species i.e., and olefin or a polyene, and an adsorbed HCO^+ complex, which can desorb as CO and regenerate the Brønsted acid site. Olefins or polyenes formed as a result of decarbonylation can subsequently interact with other hydrocarbon-pool species via the olefins- or the aromatics- based catalytic cycles (Scheme 7.3). Propagation of the aldehyde-decarbonylation pathway together with the bimolecular hydrogen-transfer pathway (Scheme 7.2) provides a justification for the observed product distribution in the reaction effluent of acetaldehyde conversion on MFI.

Decarbonylation of crotonaldehyde, which is the aldol-condensation product of acetaldehyde, results in the formation of propene and CO (Scheme 7.3); as a result, CO and propene were detected in approximately equimolar amounts (CO/propene ~1.3) in the reaction effluent of acetaldehyde conversion on Conv MFI-at 673 K. The presence of slightly more CO compared to propene in the reaction effluent can be explained by the fact that (i) the relative reactivity of propene, compared to CO, is high on SPP MFI catalyst at 673 K; propene can undergo oligomerization on Brønsted acid sites and form higher olefins, which can either crack to form light olefins, or undergo cyclization and hydrogen transfer reactions to form aromatics, and/or (ii) CO is also formed as a result of decarbonylation of other aldehydes (like acetaldehyde and sorbaldehyde), instead of crotonaldehyde, which result in the formation of CH_4 or 1,3-pentadiene, respectively, instead of propene.

An experiment was performed without using the CH_4-Ar mixture (Airgas, 10% CH_4, 90% Ar) as the internal standard to detect CH_4 during acetaldehyde conversion on Conv MFI at 673 K. The quantity of CH_4 detected in the reaction effluent was, however, negligible suggesting that decarbonylation of acetaldehyde on Conv MFI at 673 K to form CH_4 and CO is insignificant under the investigated reaction conditions. The decarbonylation product of sorbaldehyde i.e., 1,3-pentadiene, was also not detected in the reaction effluent. Possible explanations for the negligible concentration of 1,3-pentadiene in the reaction effluent are: (i) a higher driving force of sorbaldehyde to undergo ring-closure and form benzene (which was observed in the reaction effluent with 2.3 – 3.9 C% selectivity) instead of undergoing decarbonylation to form 1,3-pentadiene and CO, and/or (ii) subsequent consumption of 1,3-pentadiene via oligomerization, cracking, cyclization, or hydrogen transfer reactions.

Figure 7.12b shows the product distribution of acetaldehyde conversion on Conv MFI and SPP MFI at 673 K, 108 – 109 kPa total feed pressure, and 1.9 kPa acetaldehyde pressure, as a function of acetaldehyde conversion. The selectivity towards C_4 – C_8 aliphatic hydrocarbons and C_9+ hydrocarbons decreased with increasing acetaldehyde conversion. The selectivity towards MBs, on the other hand, increased with increasing acetaldehyde conversion. These trends suggest that higher aliphatics undergo secondary reactions like cyclization and hydrogen transfer to form MBs. In MTH catalysis, the formation of every MB is accompanied by the formation of three alkanes, to maintain the hydrogen balance.[131,132] In the catalytic conversion of acetaldehyde, however, the amount of alkanes detected in the effluent was insufficient to justify the amount of MBs present in the effluent, even after accounting for the fact that some MBs may be formed directly via the aldol-condensation pathway, which does not involve hydrogen-transfer and therefore does not require the formation of alkanes. A possible justification of this anomaly is the presence of additional hydrogen-acceptors in the zeolite pores. Aldehydes can accept hydrogen to form the corresponding alcohols, which can subsequently dehydrate on Brønsted acid sites to form olefins or polyenes. (Scheme 7.2) This bimolecular hydrogen-transfer between the hydrogen-donors and hydrogen-acceptors i.e., aldehydes, provides a possible explanation for the low concentration of alkanes in the effluent.

The bimolecular hydrogen-transfer pathway of acetaldehyde and its aldol-condensation products viz*.,* crotonaldehyde and sorbaldehyde, results in the formation of ethene, buta-1,3-diene, and hexa-1,3,5-triene, respectively. Ethene was detected in significant concentrations in the reaction effluent. Ethene selectivity was 5.9 – 7.5 C% on Conv MFI and 5.3 – 7.6 C% on SPP MFI. Buta-1,3-diene (~0.2 C% on Conv MFI and ~0.4 C% on SPP MFI) was also detected in the reaction effluent. Hexa-1,3,5-triene was,

however, not detected in the reaction effluent. Dienes and trienes, in general, have higher reactivity on MFI and are therefore likely to react further. Ethene, on the other hand, is relatively inert on MFI at these temperatures. The rate of methylation of ethene is almost an order magnitude lower than the rate of methylation of propene and butenes.[95,96] Ethene, therefore, is not likely to be consumed further justifying its presence in significant concentrations in the reaction effluent. It must, however, be noted that ethene can also be formed as a result of olefin-cracking or aromatic-dealkylation, under the investigated reaction conditions.[75,118,133] We show in Chapter 8 that aromatics do not dealkylate in the absence of a methylating agent, and therefore, it is likely that aromatic-dealkylation did not contribute towards ethene production in the case of acetaldehyde conversion on MFI in the absence of DME or MeOH. Olefin-cracking, however, could potentially contribute towards ethene production. The bimolecular hydrogen-transfer pathway involving the sequential conversion of acetaldehyde to alcohols and subsequent dehydration/cracking of alcohols to form ethene is therefore not the only source of ethene in this chemistry.

The catalytic conversion of acetaldehyde on MFI and its incorporation into MTH proceeds via three different reaction pathways: (i) a pathway that involves multiple aldol-condensations of acetaldehyde to form higher homologues, which subsequently undergo ring-closure followed by dehydration to form aromatics, (ii) an aldehyde-decarbonylation pathway that involves the removal of carbonyl-oxygen from aldehydes as CO to form the corresponding unsaturated aliphatics, which can subsequently cyclize and undergo hydrogen-transfer to form aromatics, and (iii) a pathway that involves hydrogen-transfer between an aldehyde and a hydrogen-donor molecule to form the corresponding alcohol which can readily dehydrate on Brønsted acid sites to form an olefin. A schematic of these reaction pathways is presented in Scheme 7.5.

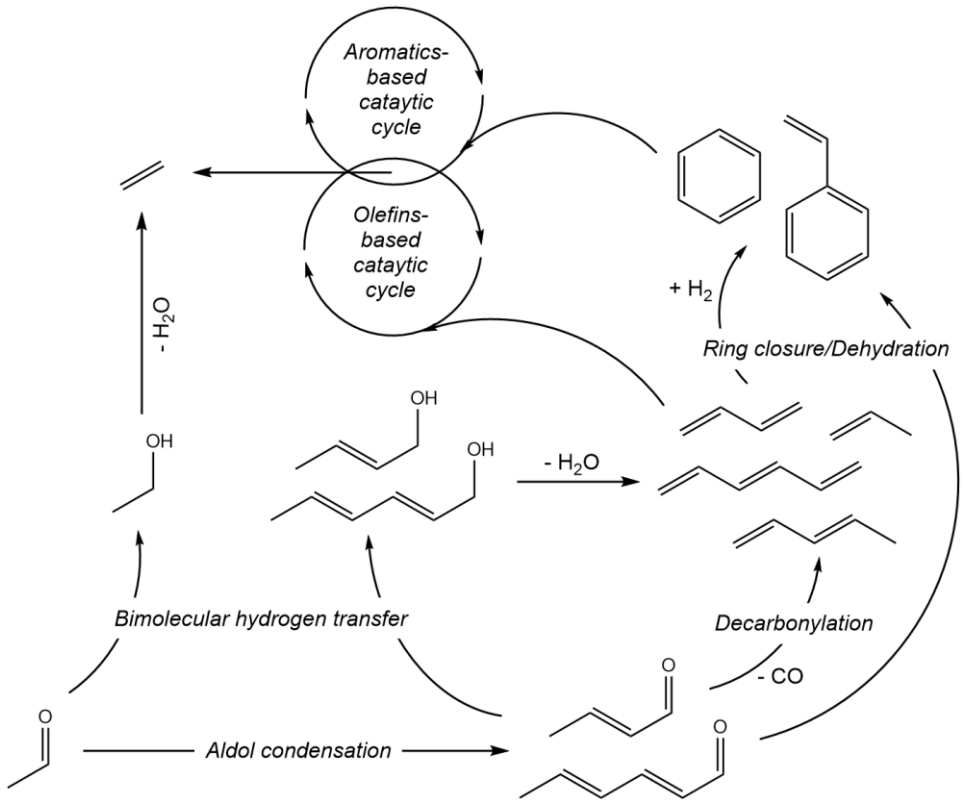

Scheme 7.5: A schematic illustration of the mechanistic pathways of acetaldehyde conversion and its incorporation into the aromatics-based and the olefins- based catalytic cycles in MTH conversion on MFI-type zeolites.

The bimolecular hydrogen transfer pathway results in ethene production from acetaldehyde via a direct ethene synthesis route. The other two reaction pathways i.e., the aldol-condensation pathway and the aldehyde-decarbonylation pathway, enhance the concentration of aromatics inside the zeolite pores. A higher concentration of aromatics enhances the propagation of the aromatics-based catalytic cycle, and therefore, indirectly increases ethene production. Co-feeding small quantities of acetaldehyde (1 – 4 C%) and more generally oxygenates containing carbonyl functionality with DME and methanol therefore represents a simple methodology to enhance ethene and light olefin selectivity in methanol-to-hydrocarbons conversion on zeolites with MFI-type framework.

7.4 Conclusions

Co-feeding acetaldehyde (1 – 4%, on carbon basis) with DME and MeOH at 673 K resulted in a monotonic increase in ethene selectivity from 9.6 C% without co-feed to 15 C% in the presence of ~4 C% acetaldehyde on Conv MFI, and from 1.3 C% to 6.4 C% on SPP MFI. Selectivity towards MBs also increased systematically from 5.3 C% without co-feed to 7.8 C% in the presence of ~4 C% acetaldehyde on Conv MFI, and from 2.7 C% to 5.3 C% on SPP MFI. The selectivity towards propene, C_4 – C_7 olefins, as well as the selectivity towards C_4 – C_7 alkanes, decreased monotonically with increasing acetaldehyde concentration in the feed on both the catalyst samples. Acetaldehyde undergoes aldol-condensation reactions to form higher homologues, which after subsequent ring-closure and dehydration, form aromatics. This increases the concentration of MBs inside the zeolite pores and enhances the propagation of the aromatics-based catalytic cycle and consequentially results in higher ethene selectivity. Ethene/2MBu, as a result, increased monotonically from 1.3 to 2.5 on Conv MFI, and from 0.18 to 1.1 on SPP MFI, in the presence of ~4 C% acetaldehyde.

Catalytic reactions of acetaldehyde without DME or MeOH were also performed on Conv MFI and SPP MFI at 673 K under reaction conditions similar to the ~4 C% acetaldehyde co-feed experiment. Aldol-condensation of acetaldehyde resulted in the formation of benzene (2.3 – 2.9 C% selectivity), which was observed in the reaction effluent. Reaction pathways other than the aldol-condensation pathway that contributed towards acetaldehyde conversion were also identified: (i) an aldehyde-decarbonylation pathway that removes the carbonyl-oxygen from aldehydes as CO; decarbonylation of crotonaldehyde, the aldol-condensation product of acetaldehyde, resulted in the formation of propene and CO, both of which were observed in approximately equimolar amounts

(CO/propene ~1.3) in the reaction effluent, and (ii) a bimolecular hydrogen-transfer pathway in which aldehydes undergo hydrogen-transfer to form the corresponding alcohols, which dehydrate/crack on Brønsted acid sites to form olefins including ethene.

Isotopically labeled acetaldehyde (~4 C%) was catalytically reacted with ^{12}C-labeled DME and MeOH on Conv MFI and SPP MFI at 673 K. The ^{13}C-content in ethene (11 – 12% on Conv MFI and 45 – 52% on SPP MFI) was significantly higher than the ^{13}C-content in olefins (3 – 6% on both Conv MFI and SPP MFI) or MBs (5 – 6% on Conv MFI and 9 – 17% on SPP MFI), suggesting that in the presence of acetaldehyde, at least some ethene is being formed from a reaction pathway different than the olefins- or the aromatics-based catalytic cycles. Specifically, ethene detected in the reaction effluent was enriched with two ^{13}C labels. This is consistent with a bimolecular hydrogen-transfer pathway that involves hydrogen-transfer to $^{13}C_2$-acetaldehyde or its homologues to form ^{13}C-labeled alcohols, which then dehydrate/crack on Brønsted acid sites to form $^{13}C_2$-ethene.

The catalytic conversion of acetaldehyde and its incorporation into the aromatics- or the olefins-based catalytic cycles in MTH proceeds via three different reaction pathways: (i) an aldol-condensation pathway, (ii) an aldehyde-decarbonylation pathway, and (iii) a bimolecular hydrogen-transfer pathway. The bimolecular hydrogen-transfer pathway enhances ethene selectivity via *direct* ethene production from acetaldehyde or its homologues. The other two reaction pathways viz., the aldol-condensation pathway and the aldehyde-decarbonylation pathway, increase the production of aromatics inside the zeolite pores, which enhances the propagation of the aromatics-based catalytic cycle and indirectly results in higher ethene selectivity in the reaction effluent. Co-feeding acetaldehyde with methanol or DME, therefore, represents a simple approach to enhance ethene selectivity in methanol-to-hydrocarbons conversion on MFI-type zeolites.

CHAPTER ***EIGHT***

Effects of Reaction Temperature and Carbon Space-Velocity on MTH Product Distribution

* Reported from R. Khare and A. Bhan, *Journal of Catalysis* **329** (2015) 218-228

8.1 Introduction

The observed product distribution in MTH can be interpreted as a consequence of the relative extents of propagation of the aromatics-based and the olefins-based catalytic cycles. Reaction parameters such as the reaction temperature and carbon space-velocity have an effect on the relative extents of propagation of aromatics-based and the olefins-based catalytic cycles and consequentially on the observed MTH product distribution. Chang and Silvestri[77] investigated the effects of DME/MeOH space-velocity on MTH conversion on ZSM-5 and noted that C_2 – C_5 olefin selectivity decreases while the selectivity towards paraffins, C_6+ olefins, and aromatics, increases with decreasing DME/MeOH space-velocity. Chang et al.[88] reported, in independent studies, that C_2 – C_3 olefin selectivity decreases while selectivity to paraffins and aromatics increases with a decrease in MeOH space-velocity after 100% DME/MeOH conversion was achieved on HZSM-5 at 773 K.

Chang and Silvestri[77] also investigated the effects of reaction temperature (533 – 841 K) on the product distribution of MeOH conversion on HZSM-5 at a fixed MeOH space-velocity. The conversion of DME/MeOH increased with increasing reaction temperature and reached completion between 613 and 648 K.[77] At lower temperatures, C_2 – C_5 olefins

were the predominant products and an increase in reaction temperature was accompanied by an increase in the formation of aromatics suggesting that secondary reactions like hydrogen transfer and cyclization become more predominant at higher reaction temperatures.

The relative propagation of the aromatics-based and the olefins-based catalytic cycles, in MTH conversion on MFI, is affected by carbon space-velocity and reaction temperature. In this work, we report a mechanistic basis for the effects of reaction temperature (548 – 723 K) on MTH product distribution. We show that the propagation of the aromatics-based catalytic cycle is suppressed at higher temperatures because of a decrease in the number of chain carriers of the aromatics-based catalytic cycle. At 723 K, higher olefins preferred to crack or desorb rather than cyclize and undergo hydrogen transfer reactions (which result in the formation of aromatics), thereby decreasing the concentration of aromatics inside the zeolite pores. This suppressed the propagation of the aromatics-based catalytic cycle inside the pores of the zeolite and resulted in lower selectivity towards ethene and MBs.

We also report the effects of carbon space-velocity on MTH product distribution at 723 K on a self-pillared pentasil MFI zeolite. DME space-velocity was varied between 0.3 and 17 mol C (mol Al-s)$^{-1}$. Complete conversion was achieved at space velocities ≤2.5 mol C (mol Al-s)$^{-1}$. Under reaction conditions that result complete DME conversion, the catalyst bed consists of two stages. The first stage of the catalyst bed performs MTH chemistry in the presence of DME/MeOH; the second stage begins after all DME/MeOH is consumed and the aromatic methylation/cracking cycle is shut down in this stage of the catalyst bed. Downstream olefin inter-conversion reactions, however, continue to propagate and produce ethene in the second stage of the catalyst bed.

8.2 Materials and Methods

8.2.1 Catalyst Synthesis and Preparation

Two zeolite samples: a self-pillared pentasil MFI (referred to as SPP MFI) and a 3DOm-i MFI (referred to as 3DOm-i MFI), were synthesized according to the procedures described in Reference [89]. A conventional MFI zeolite sample was acquired from Zeolyst International Inc. (CBV 8014, SiO_2/Al_2O_3 ~80, referred to as Conv MFI).

The zeolite samples were converted to their respective protonated forms by treating in 1.67 $cm^3\ s^{-1}$ dry air (Minneapolis Oxygen, 20 – 21% O_2, <10 ppm H_2O) at 823 K for 4 h. The temperature was increased from ambient to 823 K in 8 h and was held at 823 K for 4 h before reducing to the reaction temperature. The samples were then pressed into pellets, crushed, and sieved between 40- and 80-mesh sieves to obtain aggregate particles with uniform size between 180 and 425 μm. In some cases, quartz sand (Acros Organics) was used for diluting the catalyst bed to prevent temperature rise due to exothermic reactions. Prior to its use, the quartz sand was washed with 1 M nitric acid (Sigma-Aldrich), then rinsed several times with deionized water, dried, and sieved between 40- and 80-mesh sieves.

8.2.2 Structural and Chemical Characterization

A detailed structural and chemical characterization of SPP MFI and 3DOm-i MFI zeolite samples is described in the Supplementary Information section of Reference [89]. Structural and chemical characterization of Conv MFI sample is reported in Supplementary Information section of Reference [73]. The elemental composition was determined by ICP-OES performed by Galbraith Laboratories, Inc. The analytical method used was GLI procedure ME-70. Zhang et al.[89] estimated the diffusion length in SPP MFI

and 3DOm-i MFI samples and Khare et al.[114] determined the diffusion length in the Conv MFI sample.

8.2.3 Catalytic Conversion of DME or Propene

Catalytic reactions of DME were carried out in a 316/316L stainless steel packed-bed reactor (1/4 in OD; 0.035 in wall thickness) equipped with a concentric thermal well (1/16 in OD, 0.014 in wall thickness). Isothermal conditions were maintained in the catalyst bed using a heating coil (ARi Industries Inc., AeroRod® heating assembly) regulated by a Watlow 96 series temperature controller. Temperature of the catalyst bed was measured using a K-type thermocouple (Omega Engineering) inserted into the concentric thermal well. The reactions were run using 7 – 40 mg catalyst to achieve the desired chemical conversions. MeOH was considered as a reactant in the calculations of net carbon conversion. The catalyst bed was diluted with 100 – 150 mg of quartz sand. Prior to every reaction, the catalyst was pretreated in situ in 1.67 cm^3 s^{-1} He (Minneapolis Oxygen, 99.995% purity) at 823 K for 4 h. The temperature was increased from ambient to 823 K in 8 h and was held at 823 K for 4 h before decreasing it to the reaction temperature.

The reactant stream constituted DME (Matheson Tri-Gas, 99.5% purity) and a mixture of CH_4 and Ar (Airgas, 10% CH_4, 90% Ar) that was used as an internal standard for the FID. For the catalytic reactions of propene, the reactant stream constituted propene (Praxair, 50% propene, 50% Ar) and the CH_4/Ar mixture. In some cases, He (Minneapolis Oxygen, 99.995% purity) was used in balance to keep the concentration of the internal standard comparable to that of the reaction effluents. Gas flow rates were maintained using Brooks Instrument 5850S/SLA5850 series mass flow controllers. All reactions were carried out at 548 – 723 K. The temperature variation in the catalyst was less than 1 K during the reaction.

The reactor effluents were analyzed using an online Agilent 7890 series GC – 5975C series MS equipped with a 100% dimethylpolysiloxane Agilent J&W HP-1 column (50 m × 320 μm × 0.52 μm) connected to an FID and a (5%-Phenyl)-methylpolysiloxane Agilent J&W HP-5ms column (25 m × 320 μm × 0.25 μm) connected to an MSD. The product distributions shown in Section 8.3 include C_8^+ hydrocarbons that were not identified separately and are classified as the "Others". The average hydrogen-to-carbon ratio in the hydrocarbon species present in the "Others" fraction was calculated from the hydrogen- and carbon-content of known species in the converted feed and the reaction effluent, and is reported with the data in some cases.

8.3 Results and Discussion

8.3.1 Structural and Chemical Characterization

The diffusion length in SPP MFI and 3DOm-i MFI, as estimated by Zhang et al.,[89] are reported in Table 8.1. The relevant diffusion length in Conv MFI, as estimated by Khare et al.,[114] is also reported in Table 8.1. The silicon-to-aluminum ratio in the zeolite samples, as estimated from ICP-OES elemental analysis, is also reported in Table 8.1.

Table 8.1: Diffusion lengths, and silicon-to-aluminum ratio, in the zeolite samples investigated in this work.

Zeolite samples	Diffusion length /nm	Si/Al
SPP MFI	1[b]	84[a]
3DOm-i MFI	20[b]	72[a]
Conv MFI	250[c]	43[a]

[a] Estimated from ICP-OES elemental analysis, performed by Galbraith Laboratories, Inc.

[b] Estimated by Zhang et al.[89]

[c] Estimated by Khare et al.[114]

8.3.2 Effects of Reaction Temperature on MTH product distribution

DME was reacted on zeolite samples at different reaction temperatures (548 – 723 K) to investigate the effects of reaction temperature on MTH product distribution. Figure 8.1 shows he product distribution of DME conversion at 548 K, 623 K, and 723 K, and iso-conversion conditions (59 – 61% net conversion). Under these reaction conditions, it can be observed that C_2 selectivity (>99% of which is ethene) and MBs selectivity systematically decreases with increasing temperature. With increasing temperature, an increase in selectivity to C_3 and C_4 – C_7 hydrocarbons is also observed. These monotonic trends in selectivity suggest that as the temperature is increased, the rate of propagation of the olefin-based catalytic cycle increases more than the rate of propagation of the aromatic-based catalytic cycle. A concomitant monotonic decrease in the ethene/2MBu, as shown in Figure 8.1,with increasing temperature is also observed.

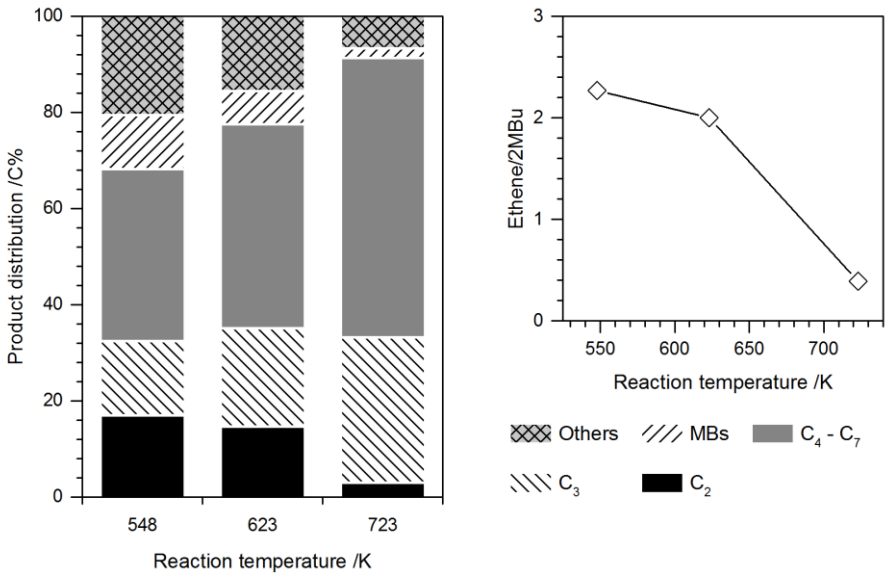

Figure 8.1: The effect of reaction temperature on MTH product distribution and ethene/2MBu yield for the catalytic reaction of 70 kPa DME on Conv MFI at 548 – 723 K and 59 – 61% net conversion. The H/C for the “Others” fraction is: 1.85 at 548 K, 1.88 at 623 K, and 1.77 at 723 K.

At 723 K, the selectivity to ethene and MBs is low compared to that at lower temperatures. To further understand if ethene selectivity is lower at higher temperatures at least in part because of the lower concentration of MBs, toluene was co-reacted with DME at 723 K. At 73% net DME conversion and 74% net toluene conversion, ethene selectivity increased to 15 C% and correspondingly, the ethene/2MBu increased to 3.2, compared to the reaction of DME alone (without toluene) at 723 K and 60% conversion which results in 3.0 C% selectivity to ethene and an ethene/2MBu yield of 0.4. This increase in ethene selectivity suggests that one reason that ethene selectivity is low at high temperatures is due to the low concentration of MBs, and not necessarily because the rate of aromatic dealkylation is slower relative to the rates of olefin methylation and cracking. The selectivity towards MBs is low at 723 K because MBs formation, which requires olefins to undergo both cyclization and dehydrogenation reactions, occurs to a lesser extent at higher temperatures, suggesting that at higher temperatures, olefins prefer other pathways, such as methylation and cracking.

Table 8.2 shows the reaction conditions and product distribution for the reaction of DME on SPP MFI and 3DOm-i MFI at 623 K and 723 K. Reaction conditions and product distribution for DME conversion on Conv MFI at 623 K and 723 K are also reported. We note that ethene and MBs selectivity decrease with increasing reaction temperature. Figure 8.2 shows the fractional change in selectivity as the reaction temperature was increased from 623 K to 723 K. The selectivity toward C_2 and MBs decreased while C_3 and C_4 – C_7 hydrocarbon selectivity increased with an increase in the reaction temperature. These observations again suggest that the aromatics-based catalytic cycle is suppressed at higher temperatures relative to the olefins-based catalytic cycle, which consequentially results in lower selectivity towards ethene and MBs.

Table 8.2: Reaction conditions and product distribution for the catalytic reactions of DME on SPP MFI, 3DOm-i MFI, and Conv MFI, at 623 K and 723 K, 120 kPa total feed pressure, and 20 min TOS. Methanol was considered as a reactant in the calculation of net DME conversion.

	SPP MFI		3DOm-i MFI		Conv MFI	
Reaction temperature /K	623	723	623	723	623	723
Carbon space-velocity /mol C (mol Al-s)$^{-1}$	1.8	9.7	2.2	11	3.2	40
DME pressure /kPa	66	63	64	62	62	73
Net DME conversion /%	59	47	57	57	46	60
Product distribution (in %, on a carbon basis)						
C_2 (Ethene)	1.6 (1.5)	1.1 (1.1)	5.7 (5.7)	2.8 (2.8)	13.2 (13.2)	3.1 (3.1)
C_3 (Propene)	21.0 (20.5)	26.6 (26.2)	21.6 (21.0)	28.7 (28.0)	21.0 (20.0)	30.3 (29.7)
C_4 – C_7	54.4	60.4	50.4	57.7	43.3	58.0
Methylbenzenes	2.1	1.5	5.9	2.8	7.4	2.1
Others[a]	21.0	10.4	16.4	8.0	15.1	6.5
Ethene/2MBu[b]	0.19	0.15	0.70	0.36	1.88	0.41
H/C in "Others"[c]	1.76	1.81	1.78	1.71	1.82	1.76

[a] "Others" fraction includes C_8+ hydrocarbons except polyMBs.

[b] Ratio of the synthesis rates of ethene and 2-methylbutane + 2-methyl-2-butene.

[c] The hydrogen-to-carbon ratio in "Others" fraction was calculated based on the difference in carbon- and hydrogen-content of known hydrocarbon species in the reaction effluent and the converted feed.

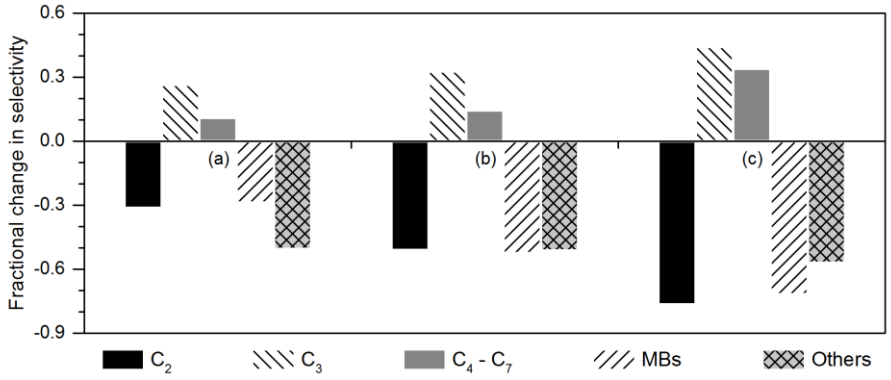

Figure 8.2: Fractional change in selectivity toward C_2, C_3, C_4 – C_7, MBs, and "Others" fraction, as temperature was increased from 623 K to 723 K, for the catalytic conversion of DME on SPP MFI, 3DOm-i MFI, and Conv MFI samples, at 46 – 60% net DME conversion, and 20 min TOS.

8.3.3 Effects of DME Space-Velocity on MTH Product Distribution

Brønsted acid sites in zeolites interact with DME or MeOH to form surface methyls. These surface methyls, together with unsaturated molecules like olefins or aromatics present inside the zeolite pores, act as the co-catalyst for MTH conversion and result in the complex hydrocarbon distribution observed in the effluent. The presence or absence of these methyls can alter the chemistry that occurs inside the zeolite pores. Conversion of DME/MeOH increases as DME space-velocity decreases and eventually reaches 100% when all DME/methanol is consumed. If the space-velocity is further reduced, the catalyst bed can be modeled to comprise two distinct stages: the first stage performs MTH chemistry in the presence of surface methyls; the second stage begins after all DME/MeOH is consumed and, as surface methyls do not exist in this stage, only chemistry that can propagate in their absence occurs in this stage of the catalyst bed. The dual-staged catalytic bed discussed here is analogous to the depiction of time-evolution of a catalyst bed as a “cigar-burn” by Haw et al. As the space-velocity of DME decreases, the fraction of bed acting as the “first-stage” decreases while the fraction of bed acting as the “second-stage” increases. Figure 8.3 shows the fraction of catalyst bed performing MTH chemistry in the presence of DME/MeOH i.e. acting as the “first stage”. It can be observed that the fraction of catalyst bed acting as the “first-stage” decreases as DME space-velocity decreases (or DME space-time increases) and at the lowest space-velocity investigated in this study i.e., 0.31 mol C (mol Al-s)$^{-1}$, only 13% of the catalyst bed is performing MTH chemistry and a majority of the catalyst bed is acting as the “second-stage” and performing a chemistry in the absence of a methylating agent.

DME was reacted on SPP MFI at 723 K, 60 kPa DME pressure, and at DME space-velocity varying between 0.3 and 17 mol C (mol Al-s)$^{-1}$. Figure 8.3 shows the effects of

DME space-velocity on DME conversion. The results consist of three separate experiments. In each experiment, DME space-velocity was decreased sequentially to obtain 7-8 data-points (with replicates in some cases) at a different DME space-velocity. The catalyst was not regenerated between each data-point in an experiment and therefore, the data-points acquired later were affected by catalyst deactivation. The catalyst was regenerated in 1.67 cm^3 s^{-1} dry air (Minneapolis Oxygen, 20 – 21% O_2, <10 ppm H_2O) at 823 K for 4 h between the experiments and the initial data-point in each experiment, as a result, was not affected by catalyst deactivation. DME conversion observed in some cases are therefore slightly different at a similar DME space-time (but in different experiments) due to deactivation of the catalyst bed.

We have segregated the data into two separate sets of data-points to understand the effects of DME space-velocity on product distribution. The first set comprises data where net DME conversion was <100%. These data correspond to DME conversion

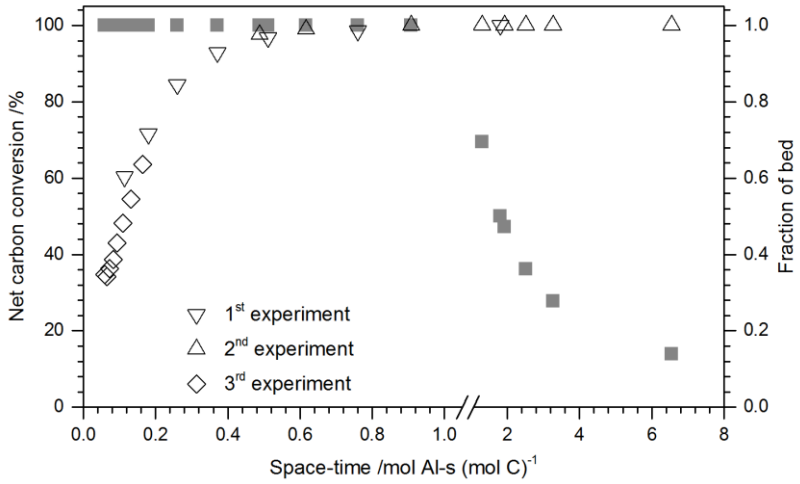

Figure 8.3: Effects of space-velocity (or space-time) on net carbon conversion, for the reaction of DME on SPP MFI at 723 K. DME space-velocity was varied between 0.15 and 17 mol C (mol Al-s)$^{-1}$. MeOH was considered as a reactant in the calculation of net DME conversion. The fraction of catalyst bed acting as the "first-stage" (■) in the presence of DME/MeOH as a function of space-time is also presented.

occurring on a single-staged catalytic bed. The second set of data comprises data where net DME conversion was 100% and no DME or MeOH was observed in the effluent. These data correspond to DME conversion occurring on a two-staged catalytic bed. Data in the second set are reported as product selectivity versus DME space-time and are shown in Figure 8.4b. Data in the first set, however, are presented as product selectivity versus DME conversion instead of DME space-time to account for catalyst deactivation and are shown in Figure 8.4a. Together, the two data-sets represent the effects of DME space-time (or DME space-velocity) on selectivity toward C_2, C_3, C_4 – C_7, MBs, and "Others" fraction, for the reaction of DME on SPP MFI at 723 K and DME space-velocity varying between 0.15 and 17 mol C (mol Al-s)$^{-1}$.

It can be observed from Figure 8.4a that as DME conversion increases (or as DME space-velocity decreases), selectivity toward C_4 – C_7 hydrocarbons and "Others" fraction

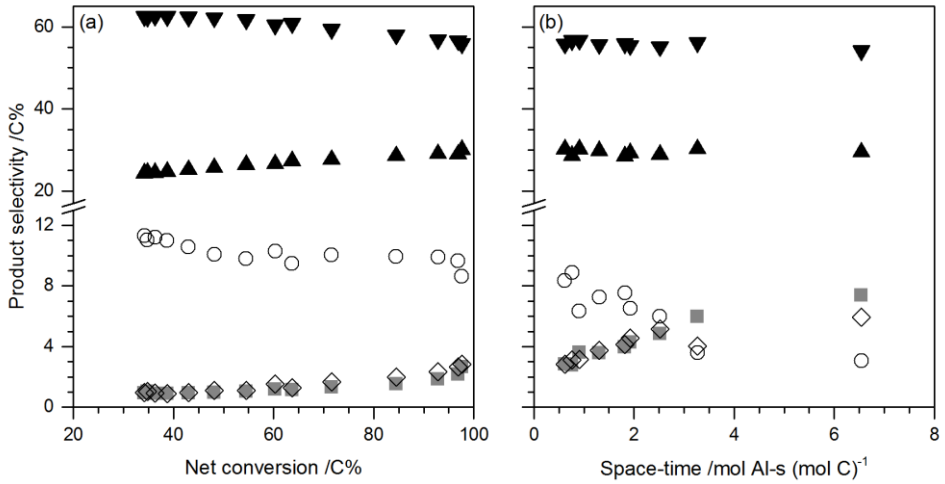

Figure 8.4: Effects of space-velocity (or space-time) on selectivity towards C_2 (■), C_3 (▲), C_4 – C_7 (▼), MBs (◇), and "Others" fraction (○), for the catalytic reaction of DME on SPP MFI at 723 K. DME space-velocity was varied from 0.15 to 17 mol C (mol Al-s)$^{-1}$. (a) Product selectivity versus net DME conversion for data where DME conversion was <100%; MeOH was considered as a reactant in the calculation of net DME conversion. (b) Product selectivity versus DME space-time for data where net DME conversion was 100% and no DME/MeOH was detected in the reaction effluent.

decreases while C_2, C_3, and MBs selectivity increases. These observations suggest that with increasing DME conversion, secondary reactions become more prominent and higher olefins either crack to form lighter olefins or undergo hydrogen transfer and cyclization reactions to form MBs, which in turn can also produce light olefins via aromatic dealkylation reactions. We note that the selectivity towards the "Others" fraction continued to decrease and that towards C_2 and MBs continued to increase with a decrease in DME space-velocity, even after 100% DME conversion was achieved (Figure 8.4b); on the other hand, only a minor change in the selectivity to propene and higher olefins was observed as DME space-velocity was further reduced. It was also noted that even though the overall C_4 – C_7 selectivity seems largely unaffected by the variations in DME space-velocity, the individual selectivity towards C_4 – C_9 aliphatic hydrocarbons changed slightly and are reported in Figure 8.5.

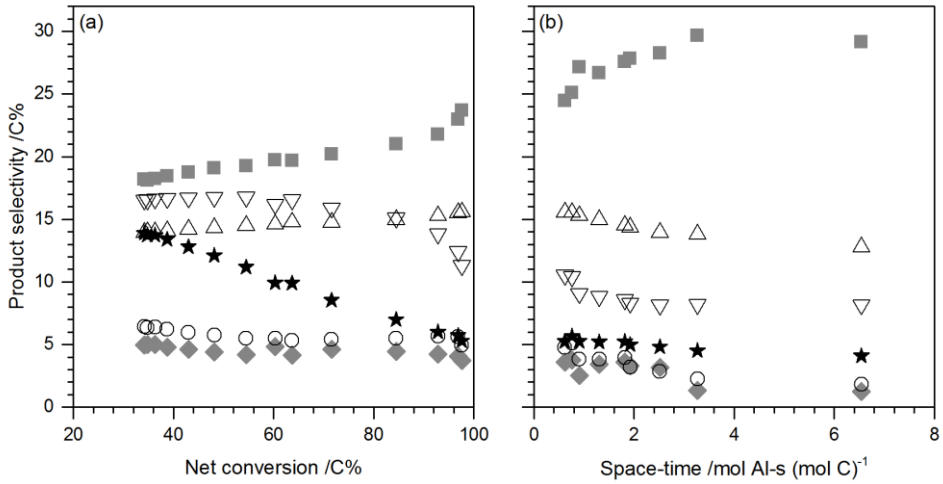

Figure 8.5: Effects of space-velocity (or space-time) on selectivity towards C_4- (■), C_5- (△), C_6- (▽), C_7- (★), C_8- (○), and C_9-aliphatics (◆), for the reaction of DME on SPP MFI at 723 K. (a) Product selectivity versus net DME conversion for data where DME conversion was <100%. MeOH was considered as a reactant in the calculation of net DME conversion. (b) Product selectivity versus DME space-time for data where net DME conversion was 100% and no DME/MeOH was detected in the effluent.

C_4 selectivity increases while the selectivity toward C_5+ aliphatic hydrocarbons (mostly olefins) decreases with an increase in DME space-time. These observations suggest that olefin inter-conversion reactions are occurring in the "second-stage" of the catalyst bed in the absence of surface methyls. Higher olefins crack to form lower olefins and lower olefins undergo oligomerization to form higher olefins. As the selectivity towards C_5+ aliphatic hydrocarbons decreased with increasing space-time, this suggests that the rate of formation of these olefins is lower than their rate of consumption, possibly because higher olefins can cyclize and undergo hydrogen-transfer reactions to form MBs and these reactions act as a carbon sink for these hydrocarbons. There are two possible explanations for the observed increase in ethene selectivity: (i) higher olefins crack to form ethene, and/or (ii) MBs dealkylate in the absence surface methyls (but in the presence of other olefins) to form ethene. Both these reaction events can explain the observed increase in ethene selectivity with decreasing DME space-velocity. Below, we discuss experimental evidence that precludes scenario (ii) above.

8.3.4 Catalytic Conversion of Propene to Hydrocarbons

Propene was reacted on SPP MFI at 723 K and 115 kPa total feed pressure to emulate the second stage of the catalyst bed and investigate olefin inter-conversion reactions in the absence of DME/methanol. Propene space-velocity was varied from 0.4 to 3.0 mol C (mol Al-s)$^{-1}$. Product distribution for this reaction as a function of propene space-velocity is shown in Figure 8.6. Higher olefins were detected in the reaction effluent implying that olefin oligomerization and cracking occurred in the "second-stage" of the catalyst bed in the absence of DME/MeOH. The presence of MBs in the reaction effluent suggests that higher olefins can also undergo cyclization and hydrogen-transfer reactions in the absence of DME/MeOH to form MBs. A significant amount of ethene was also

observed in the reaction effluent. As briefly discussed previously, there are two possible routes for the formation of ethene: (i) cracking of higher olefins, and/or (ii) dealkylation of MBs, in the absence of DME/methanol. A mixture of MBs was therefore co-fed with propene to assess whether aromatic methylation/dealkylation sequences propagate in absence of DME/MeOH.

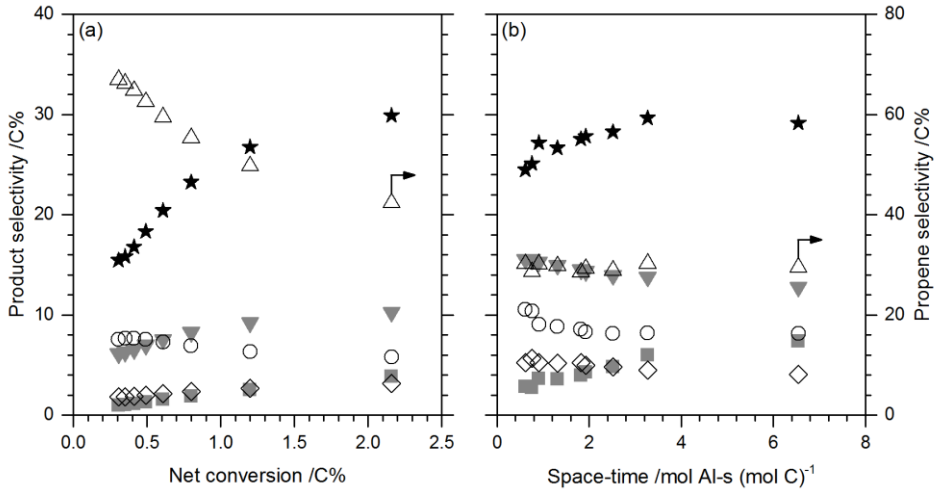

Figure 8.6: Effects of space-velocity (or space-time) on selectivity toward C_2- (■), C_3 (△), C_4- (★), C_5- (▼), C_6- (○), and C_7-aliphatics (◇), for the reaction of propene on SPP MFI at 723 K and 40 kPa propene pressure. The data for product distribution versus space-time for the catalytic reaction of DME on SPP MFI at 723 K and 60 kPa DME pressure are also shown, for comparison.

8.3.5 Catalytic Reaction of Propene with Methylbenzenes

Propene was reacted with a mixture of MBs (38 mol% toluene, 33 mol% *p*-xylene, and 29 mol% 1,2,4-triMB) on SPP MFI at 723 K and ~115 kPa total feed pressure. Table 8.3 shows the feed composition and product distribution for this reaction. Reaction conditions and product distribution for the reaction of propene alone (without MBs co-feed) on SPP MFI at 723 K and similar carbon space-velocity are also reported in Table 8.3, for comparison. Addition of MBs to the feed resulted in a 9-fold increase in the concentration

of MBs in the effluent stream and it is likely that the concentration of MBs inside the pores was also increased. If ethene were to form via aromatic dealkylation reactions in the absence of a methylating agent, a significant increase in the concentration of MBs inside the zeolite pores must have resulted in higher ethene selectivity. It was however observed that co-feeding MBs with propene did not change ethene selectivity or the overall product distribution, when estimated after excluding MBs from the calculations (also reported in Table 8.3). These observations suggest that MBs do not dealkylate in the absence of a methylating agent. Ethene observed in the reaction effluent therefore, is not a significant product of aromatic dealkylation reactions. The aromatics-based catalytic cycle is shut down in the absence of a methylating agent as MBs, even though being formed from higher olefins, cannot undergo dealkylation in the absence of a methylating agent to complete the catalytic cycle.

8.3.6 Catalytic Reactions of Propene with Ethene

Figure 8.4 shows that ethene selectivity increased from 3.1% to 7.4%, after complete DME conversion was achieved, as DME space-time increased from 0.6 to 6.5 mol Al-s (mol C)$^{-1}$. The change in selectivity toward C_4 – C_9 aliphatic hydrocarbons with DME space-time is reported in Figure 8.5. It can be observed that the selectivity towards C_3+ aliphatics (mostly olefins) was not affected to the same extent as ethene selectivity. Ethene selectivity increased by ~130% in comparison with a <23% change in the selectivity toward C_3+ aliphatics. The relatively small change in selectivity towards C_3 – C_7 aliphatic hydrocarbons can be attributed to olefin inter-conversion reactions which render the rate of formation of C_3+ olefins nearly equal to the rate of consumption of these olefins by C-C bond scission. The significantly larger change in ethene selectivity suggests that the rate of formation of ethene from olefin cracking is significantly higher than the rate of

consumption of ethene via oligomerization reactions, under the investigated reaction conditions. A possible reason for the continual increase in ethene selectivity with increasing DME space-time (or decreasing DME space-velocity) is that ethene does not participate in olefin inter-conversion, at least to the same extent as C_3+ olefins, possibly due to its lower reactivity. Hill et al. showed that the ethene methylation is at least an order of magnitude slower than methylation of C_3+ olefins on MFI.

Table 8.3: Reaction conditions, overall product distribution, and MBs-free product distribution, for the reaction of propene with/without MBs on SPP MFI at 723 K, ~120 kPa total feed pressure, and 20 min TOS.

	Propene	**Propene + MBs**
Feed composition (in %, on a carbon basis)		
Propene	100	87
Methylbenzenes[a]	0	13
Product selectivity (in %, on a carbon basis)		
C_2 (Ethene)	3.9 (3.9)	3.3 (3.3)
C_3 (Propene)	41.9 (40.3)	37.8 (36.5)
C_4 – C_7	49.3	40.7
Methylbenzenes	1.6	14.1
Others[b]	3.2	4.1
MBs-free product selectivity (in %, on a carbon basis)[c]		
C_2 (Ethene)	4.0 (4.0)	3.8 (3.8)
C_3 (Propene)	42.6 (41.0)	44.0 (42.5)
C_4 – C_7	50.2	47.4
Others[b]	3.3	4.8

[a] MBs co-feed comprised a mixture of 38 mol% toluene, 33 mol% *p*-xylene, and 29 mol% 1,2,4-triMB.

[b] The "Others" fraction includes C_8+ hydrocarbons, except polyMBs.

[c] MBs were not included in the calculation of product selectivity

Table 8.4: Feed composition and product distribution, for the catalytic reaction of propene with and without 6.9 – 11 C% ethene co-feed on SPP MFI at 723 K, ~115 kPa total feed pressure, ~40 kPa propene pressure, and 20 min TOS.

	Propene	**Propene + Ethene**	
Feed composition (in %, on a carbon basis)			
Propene	100	93	89
Ethene	-	6.9	11
Product distribution (in %, on a carbon basis)			
C_2 (Ethene)	3.3 (3.2)	7.8 (7.8)	10.6 (10.6)
C_3 (Propene)	39.3 (37.7)	37.7 (36.2)	38.6 (37.4)
C_4 – C_7	51.3	49.1	46.0
Methylbenzenes	1.6	1.1	1.0
Others[a]	4.6	4.3	3.7

[a] The "Others" fraction includes C_8+ hydrocarbons except polyMBs.

Propene was reacted on SPP MFI at ~723 K in the presence of ethene to confirm our hypothesis that ethene does not participate in olefin inter-conversion reactions, to the similar extent as C_3+ olefins, due to its lower reactivity. Table 6 shows the reaction conditions and product selectivity for the reaction of propene in the presence of ethene on SPP MFI at 723 K. Product selectivity for the reaction of propene alone on SPP MFI at 723 K and similar propene space-velocity is also reported in Table 6, for comparison. In the case when 6.9% ethene was co-reacted with propene, ethene selectivity observed in the effluent was slightly higher (7.8%) than ethene concentration in the feed suggesting that the net rate of formation of ethene under these reaction conditions was positive. In the case when 11.2% ethene was co-reacted with propene, however, the concentration of ethene in the effluent was slightly lower (10.6%) than that in the feed suggesting that as the concentration of ethene increases inside the zeolite pores, the rate of consumption of

ethene via oligomerization surpasses the rate of ethene production via olefin cracking reactions, and the net rate of ethene formation approaches zero and eventually becomes negative as ethene concentration in the effluent increases.

Early work by Haag et al. acknowledges MTH conversion on MFI as a diffusion disguised process, and our recent report suggests that the selectivity of DME conversion is a strong function of diffusion length in MFI. Investigation of MTH conversion on diffusion-free MFI samples, in this study, therefore provides an intrinsic mechanistic basis of MTH conversion on MFI type zeolites in the absence of any diffusion limitations. The olefins-based hydrocarbon pool is "saturated" inside the pores of MFI at <100% conversion, but its intrinsic contribution towards the formation of ethene is minimal. The aromatics-based catalytic cycle, on the other hand, is a significant contributor to ethene formation; however, it is suppressed in the pores of diffusion-free MFI samples due to the low number of chain carriers of the aromatics-based cycle and the short diffusion length. MFI therefore, is intrinsically a poor ethene synthesis catalyst at 723 K and <100% conversion. Under industrially relevant reaction conditions i.e., high temperature (723 K) and low DME space-velocity (≤2.5 mol C (mol Al-s)$^{-1}$), that result in complete DME conversion, the catalyst bed comprises two catalytic stages: the first stage performs MTH chemistry with concurrent propagation of aromatic/olefin methylation and cracking cycles while the second stage, which begins after 100% DME conversion is achieved, mostly performs olefin inter-conversion.

Two critical mechanistic inferences can be deduced from this systematic investigation: (i) ethene is primarily formed under MTH conditions (<100% conversion) as a consequence of diffusion limitations; and (ii) reaction conditions that result in complete DME conversion and therefore the absence of surface methyl groups, result in aromatic

methylation/dealkylation cycle being absent in the majority of the bed and the downstream chemistry primarily constitutes olefin inter-conversion reactions. Mechanistic consequences as to the predominance of the aromatics- or the olefins-based catalytic cycle and the identity and reactivity of specific hydrocarbon pool components therefore cannot be rigorously inferred under experimental conditions that result in complete DME/methanol conversion.

8.4 Conclusions

SPP MFI (~1 nm diffusion length) exhibited low ethene selectivity (1.1%), for the reaction of DME at 723 K and <100% conversion suggesting that MFI, in the absence of diffusion limitations and at industrially relevant reaction temperatures (>723 K), is a poor ethene synthesis catalyst. Low ethene selectivity under these reaction conditions is attributed to the near absence of the aromatics-based methylation/C-C bond scission catalytic cycle inside the pores of SPP MFI. A 3DOm-i MFI sample (~20 nm diffusion length) and a conventional MFI sample (~250 nm diffusion length), in comparison exhibited higher ethene selectivity (2.8% on 3DOm-i MFI and 3.1% on Conv MFI, respectively) under similar reaction conditions.

Co-feeding propene or 1-hexene with DME on SPP MFI and 3DOm-i MFI at 723 K did not affect the overall product selectivity or ethene/2MBu yield, suggesting that the concentration of olefins is saturated inside the pores of diffusion-free MFI zeolite and co-feeding olefins does not significantly enhance the propagation of the olefins-based catalytic cycle. The selectivity towards ethene was low (1.1% on SPP MFI and 2.8% on 3DOm-i MFI) even under the conditions where the olefins-based hydrocarbon pool is “saturated” implying that the contribution of olefins-based methylation/cracking cycle towards ethene production is minimal at 723 K and <100% conversion. Co-feeding toluene

or p-xylene with DME on SPP MFI and 3DOm-i MFI at 723 K, on the other hand, enhanced the concentration of MBs inside the zeolite pores and a corresponding increase in ethene selectivity was observed suggesting that the low contribution of the aromatics-based catalytic cycle towards ethene production in SPP MFI at 723 K and <100% conversion is because the number of chain carriers of the aromatics-based catalytic cycle, typically MBs, inside the zeolite pores is low.

The presence of a large fraction of external Brønsted acid sites in SPP MFI (~29%) does not affect the overall product selectivity of MTH conversion at 723 K. The methylation of MBs to higher MB homologues, which occurs on the external surface, is suppressed by passivation of the external acid sites by DTBP titration. Aromatic dealkylation reactions, which are precursors to ethene formation, however occur only within the confinement of zeolite micropores and are therefore not affected by the passivation of external Brønsted acid sites.

At higher reaction temperatures (>723 K) and low DME space-velocities (≤2.5 mol C (mol Al-s)$^{-1}$) i.e., conditions more relevant to HZSM-5 based industrial MTH processes, the catalyst bed comprises of two catalytic stages: the first stage performs MTH chemistry in the presence of a methylating agent (DME/MeOH) and the second stage performs chemistry that can take place in the absence of the methylating agent. Aromatics-based catalytic cycle ceased to exist in the second stage of the catalytic bed, as MBs cannot undergo dealkylation reactions in the absence of DME/MeOH and the dominant pathway to ethene formation under these industrially relevant reaction conditions is, therefore, olefin inter-conversion reactions.

Bibliography

(1) Chang, C. D. *Catal. Rev. Sci. Eng.* **1984**, *26* (3–4), 323–345.

(2) Kaeding, W. W.; Butter, S. A. *J. Catal.* **1980**, *61* (1), 155–164.

(3) Wilson, S.; Barger, P. T. *Micro. Meso. Mater.* **1999**, *29* (1–2), 117–126.

(4) Chang, C. D.; Silvestri, A. J.; Smith, R. L. Production of gasoline hydrocarbons. United States Patent 3,928,483, December 23, 1975.

(5) Chang, C. D.; Kuo, J. C. W.; Lang, W. H.; Jacob, S. M.; Wise, J. J.; Silvestri, A. J. *Ind. Eng. Chem. Process Des. Dev.* **1978**, *17* (3), 255–260.

(6) Avidan, A. A. *Stud. Surf. Sci. Catal.* **1988**, *36*, 307–323.

(7) Meisel, S. L.; McCullogh, J. P.; Lechthaler, C. H.; Weisz, P. B. *Chemtech* **1976**, *6* (2), 86–89.

(8) Ono, Y.; Adachi, H.; Senoda, Y. *J. Chem. Soc. Faraday Trans. 1 Phys. Chem. Condens. Phases* **1988**, *84* (4), 1091.

(9) Inoue, Y.; Nakashiro, K.; Ono, Y. *Micro. Mater.* **1995**, *4* (5), 379–383.

(10) Krohn, D. E.; Melconian, M. G. *Stud. Surf. Sci. Catal.* **1988**, *36*, 679–689.

(11) Yurchak, S. *Stud. Surf. Sci. Catal.* **1988**, *36*, 251–272.

(12) Chang, C. D. *Catal. Today* **1992**, *13* (1), 103–111.

(13) Chen, J. Q.; Bozzano, A.; Glover, B.; Fuglerud, T.; Kvisle, S. *Catal. Today* **2005**, *106* (1–4), 103–107.

(14) Koempel, H.; Liebner, W. *Stud. Surf. Sci. Catal.* **2007**, *167*, 261–267.

(15) Kolboe, S. *Stud. Surf. Sci. Catal.* **1988**, *36*, 189–193.

(16) Dahl, I. M.; Kolboe, S. *Catal. Letters* **1993**, *20* (3–4), 329–336.

(17) Dahl, I. M.; Kolboe, S. *J. Catal.* **1994**, *149* (2), 458–464.

(18) Kolboe, S.; Dahl, I. M. *Stud. Surf. Sci. Catal.* **1995**, *94*, 427–434.

(19) Dahl, I. M.; Kolboe, S. *J. Catal.* **1996**, *161* (1), 304–309.

(20) Svelle, S.; Joensen, F.; Nerlov, J.; Olsbye, U.; Lillerud, K.-P.; Kolboe, S.; Bjørgen, M. *J. Am. Chem. Soc.* **2006**, *128* (46), 14770–14771.

(21) Haw, J. F.; Song, W.; Marcus, D. M.; Nicholas, J. B. *Acc. Chem. Res.* **2003**, *36* (5), 317–326.

(22) Song, W.; Haw, J. F.; Nicholas, J. B.; Heneghan, C. S. *J. Am. Chem. Soc.* **2000**, *122* (43), 10726–10727.

(23) Smalley, R. E. *MRS Bull.* **2005**, *30* (6), 412–417.

(24) Whitesides, G. M.; Crabtree, G. W. *Science* **2007**, *315* (5813), 796–798.

(25) Fierro, J. L. G. *Catal. Letters* **1993**, *22* (1–2), 67–91.

(26) Lunsford, J. H. *Catal. Today* **2000**, *63* (2), 165–174.

(27) Olah, G. A. *Catal. Letters* **2004**, *93* (1–2), 1–2.

(28) Olah, G. A. *Angew. Chemie Int. Ed.* **2005**, *44* (18), 2636–2639.

(29) Ragauskas, A. J.; Williams, C. K.; Davison, B. H.; Britovsek, G.; Cairney, J.; Eckert, C. A.; Frederick, W. J.; Hallett, J. P.; Leak, D. J.; Liotta, C. L.; Mielenz, J. R.; Murphy, R. B.; Templer, R.; Tschaplinski, T. *Science* **2006**, *311* (5760), 484–489.

(30) Behrens, M.; Studt, F.; Kasatkin, I.; Kühl, S.; Hävecker, M.; Abild-Pedersen, F.; Zander, S.; Girgsdies, F.; Kurr, P.; Kniep, B.-L.; Tovar, M.; Fischer, R. W.; Nørskov,

J. K.; Schlögl, R. *Science* **2012**, *336* (6083), 893–897.

(31) Hereijgers, B. P. C.; Bleken, F.; Nilsen, M. H.; Svelle, S.; Lillerud, K.-P.; Bjørgen, M.; Weckhuysen, B. M.; Olsbye, U. *J. Catal.* **2009**, *264* (1), 77–87.

(32) Teketel, S.; Svelle, S.; Lillerud, K.-P.; Olsbye, U. *ChemCatChem* **2009**, *1* (1), 78–81.

(33) Degnan, T. F. *J. Catal.* **2003**, *216* (1–2), 32–46.

(34) Schenk, M.; Smit, B.; Vlugt, T. J. H.; Maesen, T. L. M. *Angew. Chemie Int. Ed.* **2001**, *40* (4), 736–739.

(35) Santilli, D. S.; Zones, S. I. *Catal. Letters* **1991**, *7* (5–6), 383–387.

(36) Ilias, S.; Bhan, A. *J. Catal.* **2014**, *311*, 6–16.

(37) Olsbye, U.; Svelle, S.; Bjørgen, M.; Beato, P.; Janssens, T. V. W.; Joensen, F.; Bordiga, S.; Lillerud, K.-P. *Angew. Chemie Int. Ed.* **2012**, *51* (24), 5810–5831.

(38) Stöcker, M. *Micro. Meso. Mater.* **1999**, *29* (1–2), 3–48.

(39) Chang, C. D. *Catal. Rev. Sci. Eng.* **1983**, *25* (1), 1–118.

(40) Database of Zeolite Structures. International Zeolite Association http://www.iza-online.org/ (accessed Aug 12, 2016).

(41) Argauer, R. J.; Landolt, G. R. Crystalline zeolite ZSM-5 and method of preparing the same. 3,702,866, November 14, 1972.

(42) Kokotailo, G. T.; Lawton, S. L.; Olson, D. H.; Meier, W. M. *Nature* **1978**, *272*, 437–438.

(43) Olson, D. H.; Kokotailo, G. T.; Lawton, S. L.; Meier, W. M. *J. Phys. Chem.* **1981**, *85*

(15), 2238–2243.

(44) June, R. L.; Bell, A. T.; Theodorou, D. N. *J. Phys. Chem.* **1990**, *94* (4), 1508–1516.

(45) Zhu, W.; van de Graaf, J. M.; van den Broeke, L. J. P.; Kapteijn, F.; Moulijn, J. A. *Ind. Eng. Chem. Res.* **1998**, *37* (5), 1934–1942.

(46) Lesthaeghe, D.; Van Speybroeck, V.; Marin, G. B.; Waroquier, M. *Angew. Chemie Int. Ed.* **2006**, *45* (11), 1714–1719.

(47) Lesthaeghe, D.; Van Speybroeck, V.; Marin, G. B.; Waroquier, M. *Ind. Eng. Chem. Res.* **2007**, *46* (26), 8832–8838.

(48) Lesthaeghe, D.; Van Speybroeck, V.; Marin, G. B.; Waroquier, M. *Chem. Phys. Lett.* **2006**, *417* (4), 309–315.

(49) Marcus, D. M.; McLachlan, K. A.; Wildman, M. A.; Ehresmann, J. O.; Kletnieks, P. W.; Haw, J. F. *Angew. Chemie Int. Ed.* **2006**, *45* (19), 3133–3136.

(50) Song, W.; Marcus, D. M.; Fu, H.; Ehresmann, J. O.; Haw, J. F. *J. Am. Chem. Soc.* **2002**, *124* (15), 3844–3845.

(51) Langner, B. E. *Appl. Catal.* **1982**, *2* (4–5), 289–302.

(52) Mole, T.; Whiteside, J. A.; Seddon, D. *J. Catal.* **1983**, *82* (2), 261–266.

(53) Mole, T.; Bett, G.; Seddon, D. *J. Catal.* **1983**, *84* (2), 435–445.

(54) Mikkelsen, Ø.; Rønning, P. O.; Kolboe, S. *Micro. Meso. Mater.* **2000**, *40* (1–3), 95–113.

(55) Ono, Y.; Mori, T. *J. Chem. Soc. Faraday Trans. 1 Phys. Chem. Condens. Phases* **1981**, *77* (9), 2209.

(56) Chen, N. Y.; Reagan, W. J. *J. Catal.* **1979**, *59* (1), 123–129.

(57) Dessau, R. M.; LaPierre, R. B. *J. Catal.* **1982**, *78* (1), 136–141.

(58) Dessau, R. M. *J. Catal.* **1986**, *99* (1), 111–116.

(59) Bjørgen, M.; Svelle, S.; Joensen, F.; Nerlov, J.; Kolboe, S.; Bonino, F.; Palumbo, L.; Bordiga, S.; Olsbye, U. *J. Catal.* **2007**, *249* (2), 195–207.

(60) Bjørgen, M.; Joensen, F.; Lillerud, K.-P.; Olsbye, U.; Svelle, S. *Catal. Today* **2009**, *142* (1–2), 90–97.

(61) Ilias, S.; Bhan, A. *ACS Catal.* **2013**, *3* (1), 18–31.

(62) Bjørgen, M.; Olsbye, U.; Peterson, D.; Kolboe, S. *J. Catal.* **2004**, *221* (1), 1–10.

(63) Sassi, A.; Wildman, M. A.; Haw, J. F. *J. Phys. Chem. B* **2002**, *106* (34), 8768–8773.

(64) Lesthaeghe, D.; Horré, A.; Waroquier, M.; Marin, G. B.; Van Speybroeck, V. *Chem. - A Eur. J.* **2009**, *15* (41), 10803–10808.

(65) Seiler, M.; Wang, W.; Buchholz, A.; Hunger, M. *Catal. Letters* **2003**, *88* (3–4), 187–191.

(66) Arstad, B.; Nicholas, J. B.; Haw, J. F. *J. Am. Chem. Soc.* **2004**, *126* (9), 2991–3001.

(67) Sullivan, R. F.; Egan, C. J.; Langlois, G. E.; Sieg, R. P. *J. Am. Chem. Soc.* **1961**, *83* (5), 1156–1160.

(68) Wang, C.-M.; Wang, Y.-D.; Liu, H.-X.; Xie, Z.-K.; Liu, Z.-P. *Micro. Meso. Mater.* **2012**, *158*, 264–271.

(69) Arstad, B.; Kolboe, S.; Swang, O. *J. Phys. Chem. A* **2005**, *109* (39), 8914–8922.

(70) Lesthaeghe, D.; De Sterck, B.; Van Speybroeck, V.; Marin, G. B.; Waroquier, M.

Angew. Chemie Int. Ed. **2007**, *46* (8), 1311–1314.

(71) Wang, C.-M.; Wang, Y.-D.; Xie, Z.-K.; Liu, Z.-P. *J. Phys. Chem. C* **2009**, *113* (11), 4584–4591.

(72) Ilias, S.; Bhan, A. *J. Catal.* **2012**, *290*, 186–192.

(73) Ilias, S.; Khare, R.; Malek, A.; Bhan, A. *J. Catal.* **2013**, *303*, 135–140.

(74) Sun, X.; Mueller, S.; Shi, H.; Haller, G. L.; Sanchez-Sanchez, M.; van Veen, A. C.; Lercher, J. A. *J. Catal.* **2014**, *314*, 21–31.

(75) Sun, X.; Mueller, S.; Liu, Y.; Shi, H.; Haller, G. L.; Sanchez-Sanchez, M.; van Veen, A. C.; Lercher, J. A. *J. Catal.* **2014**, *317*, 185–197.

(76) Chang, Y. C.; Ko, A. N. *Appl. Catal. A Gen.* **2000**, *190* (1–2), 149–155.

(77) Chang, C. D.; Silvestri, A. J. *J. Catal.* **1977**, *47* (2), 249–259.

(78) Hoang, T. Q.; Zhu, X.; Sooknoi, T.; Resasco, D. E.; Mallinson, R. G. *J. Catal.* **2010**, *271* (2), 201–208.

(79) Hutchings, G. J.; Johnston, P.; Lee, D. F.; Warwick, A.; Williams, C. D.; Wilkinson, M. *J. Catal.* **1994**, *147* (1), 177–185.

(80) Sugimoto, M.; Katsuno, H.; Takatsu, K.; Kawata, N. *Zeolites* **1987**, *7* (6), 503–507.

(81) Rownaghi, A. A.; Hedlund, J. *Ind. Eng. Chem. Res.* **2011**, *50* (21), 11872–11878.

(82) Rownaghi, A. A.; Rezaei, F.; Hedlund, J. *Catal. Commun.* **2011**, *14* (1), 37–41.

(83) Choi, M.; Na, K.; Kim, J.; Sakamoto, Y.; Terasaki, O.; Ryoo, R. *Nature* **2009**, *461* (7261), 246–249.

(84) Bleken, B.-T. L.; Wragg, D. S.; Arstad, B.; Gunnæs, A. E.; Mouzon, J.; Helveg, S.;

Lundegaard, L. F.; Beato, P.; Bordiga, S.; Olsbye, U.; Svelle, S.; Lillerud, K.-P. *Top. Catal.* **2013**, *56* (9–10), 558–566.

(85) Kim, W.; Ryoo, R. *Catal. Letters* **2014**, *144* (7), 1164–1169.

(86) Wei, R.; Li, C.; Yang, C.; Shan, H. *J. Nat. Gas Chem.* **2011**, *20* (3), 261–265.

(87) Wan, Z.; Wu, W.; Li, G.; Wang, C.; Yang, H.; Zhang, D. *Appl. Catal. A Gen.* **2016**, *523*, 312–320.

(88) Chang, C. D.; Chu, C. T.-W.; Socha, R. F. *J. Catal.* **1984**, *86* (2), 289–296.

(89) Zhang, X.; Liu, D.; Xu, D.; Asahina, S.; Cychosz, K. A.; Agrawal, K. V.; Al Wahedi, Y.; Bhan, A.; Al Hashimi, S.; Terasaki, O.; Thommes, M.; Tsapatsis, M. *Science* **2012**, *336* (6089), 1684–1687.

(90) Chiang, H.; Bhan, A. *J. Catal.* **2010**, *271* (2), 251–261.

(91) Liu, D.; Bhan, A.; Tsapatsis, M.; Al Hashimi, S. *ACS Catal.* **2011**, *1* (1), 7–17.

(92) Price, G. L.; Iglesia, E. *Ind. Eng. Chem. Res.* **1989**, *28* (6), 839–844.

(93) Moseley, H. N. *BMC Bioinformatics* **2010**, *11* (1), 139–144.

(94) Cheung, P.; Bhan, A.; Sunley, G. J.; Law, D. J.; Iglesia, E. *J. Catal.* **2007**, *245* (1), 110–123.

(95) Hill, I. M.; Al Hashimi, S.; Bhan, A. *J. Catal.* **2012**, *285* (1), 115–123.

(96) Hill, I. M.; Al Hashimi, S.; Bhan, A. *J. Catal.* **2012**, *291*, 155–157.

(97) Hill, I. M.; Ng, Y. S.; Bhan, A. *ACS Catal.* **2012**, *2* (8), 1742–1748.

(98) Svelle, S.; Rønning, P. O.; Kolboe, S. *J. Catal.* **2004**, *224* (1), 115–123.

(99) Svelle, S.; Rønning, P. O.; Olsbye, U.; Kolboe, S. *J. Catal.* **2005**, *234* (2), 385–400.

(100) Zheng, S.; Heydenrych, H. R.; Jentys, A.; Lercher, J. A. *J. Phys. Chem. B* **2002**, *106* (37), 9552–9558.

(101) Emeis, C. A. *J. Catal.* **1993**, *141* (2), 347–354.

(102) Ferreira, A. F. P.; Mittelmeijer-Hazeleger, M. C.; v.d. Bergh, J.; Aguado, S.; Jansen, J. C.; Rothenberg, G.; Rodrigues, A. E.; Kapteijn, F. *Micro. Meso. Mater.* **2013**, *170*, 26–35.

(103) Yu, M.; Wyss, J. C.; Noble, R. D.; Falconer, J. L. *Micro. Meso. Mater.* **2008**, *111* (1), 24–31.

(104) Xu, D.; Swindlehurst, G. R.; Wu, H.; Olson, D. H.; Zhang, X.; Tsapatsis, M. *Adv. Funct. Mater.* **2014**, *24* (2), 201–208.

(105) Crank, J. *The Mathematics of Diffusion*, Second.; Clarendon Press: Oxford, 1975.

(106) Kärger, J.; Ruthven, D. M.; Theodorou, D. N. *Diffusion in Nanoporous Materials*; Wiley-VCH: Weinheim, 2012.

(107) Ferreira, A. F. P.; Mittelmeijer-Hazeleger, M. C.; Bliek, A. *Adsorption* **2007**, *13* (2), 105–114.

(108) Cavalcante, C. L.; Ruthven, D. M. *Ind. Eng. Chem. Res.* **1995**, *34*, 185–191.

(109) Xiao, J.; Wei, J. *Chem. Eng. Sci.* **1992**, *47* (5), 1143–1159.

(110) Svelle, S.; Tuma, C.; Rozanska, X.; Kerber, T.; Sauer, J. *J. Am. Chem. Soc.* **2009**, *131* (2), 816–825.

(111) Abbot, J.; Wojciechowski, B. W. *Can. J. Chem. Eng.* **1985**, *63* (3), 462–469.

(112) Abbot, J.; Wojciechowski, B. W. *Can. J. Chem. Eng.* **1985**, *63* (3), 451–461.

(113) Baertsch, C. D.; Funke, H. H.; Falconer, J. L.; Richard, D. N. *J. Phys. Chem.* **1996**, *100*, 7676–7679.

(114) Khare, R.; Millar, D.; Bhan, A. *J. Catal.* **2015**, *321*, 23–31.

(115) Tsay, C. S.; Chiang, A. S. T. *Micro. Meso. Mater.* **1998**, *26* (1), 89–99.

(116) van Grieken, R.; Sotelo, J. L.; Menéndez, J. M.; Melero, J. A. *Micro. Meso. Mater.* **2000**, *39* (1–2), 135–147.

(117) Tukur, N. M.; Al-Khattaf, S. *Energy & Fuels* **2007**, *21*, 2499–2508.

(118) Khare, R.; Bhan, A. *J. Catal.* **2015**, *329*, 218–228.

(119) Liu, C.; Evans, T. J.; Cheng, L.; Nimlos, M. R.; Mukarakate, C.; Robichaud, D. J.; Assary, R. S.; Curtiss, L. A. *J. Phys. Chem. C* **2015**, *119* (42), 24025–24035.

(120) Lee, C. S. Catalytic conversion of methanol to light olefins. United States Patent 4,374,295, February 15, 1983.

(121) Maass, O.; Boomer, E. H. *J. Am. Chem. Soc.* **1922**, *44* (8), 1709–1728.

(122) Kraikul, N.; Rangsunvigit, P.; Kulprathipanja, S. *Adsorption* **2006**, *12* (5–6), 317–327.

(123) Jae, J.; Tompsett, G. A.; Foster, A. J.; Hammond, K. D.; Auerbach, S. M.; Lobo, R. F.; Huber, G. W. *J. Catal.* **2011**, *279* (2), 257–268.

(124) Ramasamy, K. K.; Gerber, M. A.; Flake, M.; Zhang, H.; Wang, Y. *Green Chem.* **2014**, *16* (2), 748–760.

(125) Gayubo, A. G.; Aguayo, A. T.; Atutxa, A.; Aguado, R.; Olazar, M.; Bilbao, J. *Ind. Eng. Chem. Res.* **2004**, *43* (11), 2619–2626.

(126) Solans-Monfort, X.; Bertran, J.; Branchadell, V.; Sodupe, M. *J. Phys. Chem. B* **2002**, *106* (39), 10220–10226.

(127) Cheng, Y. T.; Huber, G. W. *ACS Catal.* **2011**, *1* (6), 611–628.

(128) Schubert, W. M.; Burkett, H. *J. Am. Chem. Soc.* **1956**, *78* (1), 64–68.

(129) Burkett, H.; Schubert, W. M.; Schultz, F.; Murphy, R. B.; Talbott, R. *J. Am. Chem. Soc.* **1959**, *81* (15), 3923–3929.

(130) Schubert, W. M.; Myhre, P. C. *J. Am. Chem. Soc.* **1958**, *80* (7), 1755–1761.

(131) Bercaw, J. E.; Diaconescu, P. L.; Grubbs, R. H.; Hazari, N.; Kay, R. D.; Labinger, J. A.; Mehrkhodavandi, P.; Morris, G. E.; Sunley, G. J.; Vagner, P. *Inorg. Chem.* **2007**, *46* (26), 11371–11380.

(132) Hazari, N.; Iglesia, E.; Labinger, J. A.; Simonetti, D. A. *Acc. Chem. Res.* **2012**, *45* (4), 653–662.

(133) Chen, C. J.; Rangarajan, S.; Hill, I. M.; Bhan, A. *ACS Catal.* **2014**, *4* (7), 2319–2327.

Appendix A

DME Conversion to Hydrocarbons on [Fe]-ZSM-5

A.1 Catalyst Preparation and Catalytic Conversion of DME

The [Fe]-ZSM-5 (Si/Fe ~40) sample was obtained in its NH_4^+ form University of Delaware. A conventional [Al]-ZSM-5 sample was purchased from Zeolyst International Inc. (CBV 8014, Si/Al ~43) in its NH_4^+ form. The catalysts were converted to their protonated forms by treating in 1.67 cm^3 s^{-1} dry air (Minneapolis Oxygen, 20 – 21% O_2, <10 ppm H_2O) at 773 K for 4 h. The temperature was increased from ambient to 773 K in 12 h and was held at 773 K for 4 h before cooling down to the ambient temperature.

Catalytic reactions of DME were carried out in a 316/316L stainless steel packed-bed reactor (1/4 in OD; 0.035 in wall thickness) equipped with a concentric thermal well (1/16 in OD, 0.014 in wall thickness). A detailed description of the experimental setup can be found in Chapter 3. The reactant stream constituted DME (Matheson Tri-Gas, 99.5% purity) and a mixture of CH_4 and Ar (Airgas, 10% CH_4, 90% Ar) that was used as an internal standard. The reactions were run using 10 – 50 mg catalyst and the catalyst bed was diluted with 100 – 150 mg of quartz sand to prevent temperature rise due to exothermic nature of MTH reactions. Methanol was considered as a reactant in the calculation of net carbon conversion. The reactions were carried out at 623 K and the temperature variation in the bed was less than 1 K during the reaction. The reactor effluents were analyzed using an online Agilent 7890 series GC – 5975C series MS equipped with a 100% dimethylpolysiloxane Agilent J&W HP-1 column (50 m × 320 μm × 0.52 μm) connected to an FID and a (5%-phenyl)-methylpolysiloxane Agilent J&W HP-5ms column (25 m × 320 μm × 0.25 μm) connected to an MSD.

A.2 Results and Discussion

Figure A.1a shows net carbon converted as a function of time-on-stream for the catalytic reactions of DME on [Fe]-ZSM-5 (Si/Fe ~40) and [Al]-ZSM-5 (Si/Al ~43) at ~623 K, ~130 kPa total feed pressure, ~70 kPa DME pressure. The DME space-velocity was 0.54 mol C (mol Fe-s)$^{-1}$ on [Fe]-ZSM-5 and 4.8 mol C (mol Al-s)$^{-1}$ on [Al]-ZSM-5. It can be observed from Figure A.1a that [Fe]-ZSM-5 deactivated significantly faster compared to [Al]-ZSM-5. The net carbon converted decreased from 37% to 16% in 100 min on [Fe]-ZSM-5. In comparison, the carbon conversion decreased only marginally (from 38% to 34% in 60 min) on [Al]-ZSM-5.

Figure A.1b shows the product selectivity as a function of time-on-stream for the catalytic conversion of DME to hydrocarbons on [Fe]-ZSM-5 (Si/Fe ~40) and [Al]-ZSM-5 (Si/Al ~43) at ~623 K, ~130 kPa total feed pressure, and ~70 kPa DME pressure. It can be observed that the product distribution was nearly invariant with time-on-stream on both

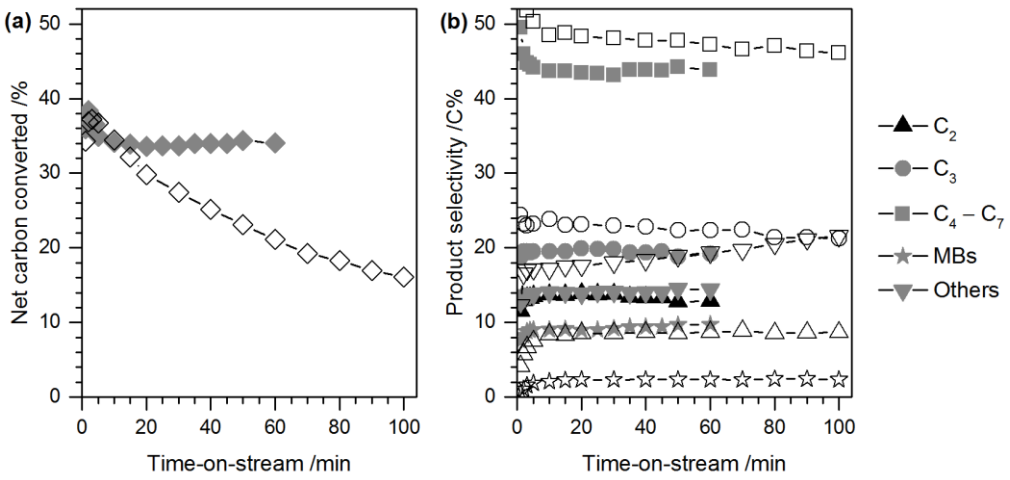

Figure A.1: (a) Net carbon converted versus TOS, and (b) product selectivity versus TOS, for the catalytic reaction of DME on (i) [Fe]-ZSM-5 (open symbols), and (ii) [Al]-ZSM-5 (filled symbols), at 623 K, 130 kPa total feed pressure, 70 kPa DME pressure. The DME space-velocity was 0.54 mol C (mol Fe-s)$^{-1}$ on [Fe]-ZSM-5 and 4.8 mol C (mol Al-s)$^{-1}$ on [Al]-ZSM-5.

the zeolite samples. It must be noted that the even though the [Fe]-ZSM-5 sample deactivated significantly with time-on-stream, the catalyst deactivation did not have any effect on the product selectivity. These results suggest that coke deposition on [Fe]-ZSM-5 only resulted in a decrease in the number of catalytically active Brønsted acid sites and did not have any mechanistic effects on the MTH chemistry.

The reaction conditions and product distribution for the catalytic conversion of DME to hydrocarbons on [Fe]-ZSM-5 and [Al]-ZSM-5 at ~623 K and 10 min time-on-stream are reported in Table A.1 and Figure A.2. It can be observed that MBs selectivity was significantly lower on [Fe]-ZSM-5 (2.1%) than on [Al]-ZSM-5 (9.1%), suggesting that the propagation of the aromatics-based catalytic cycle decreased on [Fe]-ZSM-5 catalyst. A concomitant decrease in ethene selectivity (from 14% on [Al]-ZSM-5 to 8.4% on [Fe]-ZSM-5) and ethene/2MBu yield (from 1.81 on [Al]-ZSM-5 to 1.58 on [Fe]-ZSM-5) was also observed at iso-conversion conditions (~34% net DME conversion). Propene selectivity

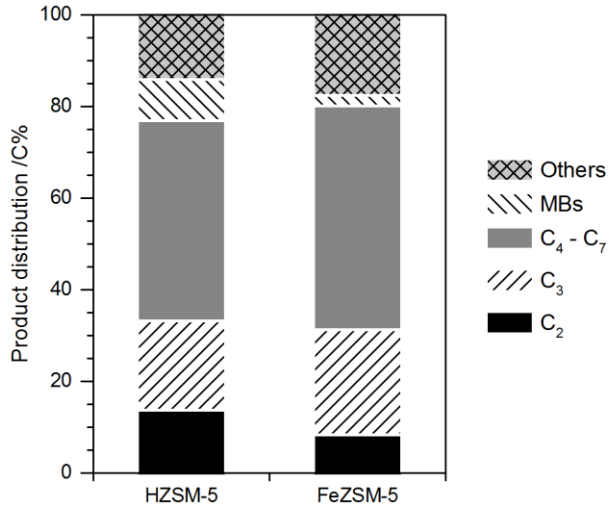

Figure A.2: Product distribution for the catalytic conversion of DME to hydrocarbons on (i) [Fe]-ZSM-5 (Si/Fe ~40), and (ii) [Al]-ZSM-5 (Si/Al ~43), at ~623 K, ~130 kPa total feed pressure, ~70 kPa DME pressure, and 10 min TOS. The DME space-velocity was 0.54 mol C (mol Fe-s)$^{-1}$ on [Fe]-ZSM-5 and 4.8 mol C (mol Al-s)$^{-1}$ on [Al]-ZSM-5.

(from 20% on [Al]-ZSM-5 to 24% on [Fe]-ZSM-5) and $C_4 – C_7$ selectivity (from 44% on [Al]-ZSM-5 to 49% on [Fe]-ZSM-5), on the other hand, increased suggesting increased propagation of the olefins-based catalytic cycle.

Table A.1: Reaction conditions and product distribution of DME conversion to hydrocarbons on (i) [Fe]-ZSM-5 (Si/Fe ~40), and (ii) [Al]-ZSM-5 (Si/Al ~43), at ~623 K and 10 min TOS.

Catalyst sample	**[Al]-ZSM-5**	**[Fe]-ZSM-5**
DME space-velocity /mol C (mol [Al or Fe]-s)$^{-1}$	4.8	0.54
DME partial pressure /kPa	70	70
DME conversion /%	34	34
Product distribution (in %, on a carbon basis)		
C_2	13.7	8.4
C_3	19.5	23.9
$C_4 – C_7$	43.6	48.5
Methylbenzenes	9.1	2.1
Others[a]	14.0	17.2
Ethene/2MBu[b]	1.81	1.58
Hydrogen transfer index (HTI)[c]	0.29	0.08
H/C in “Others”[d]	1.82	1.95

[a] The “Others” fraction includes C_8+ hydrocarbons excluding polyMBs.

[b] Ratio of the synthesis rates of ethene and the sum of 2-methylbutane and 2-methyl-2-butene.

[c] Ratio of the synthesis rates of $C_2 – C_6$ alkanes and total $C_2 – C_6$ aliphatic hydrocarbons.

[d] The hydrogen-to-carbon ratio in “Others” fraction was calculated based on the difference in carbon- and hydrogen-content of known hydrocarbon species in the reaction effluent and the converted feed.

The systematic changes in product distribution and ethene/2MBu yield suggest that the aromatics-based catalytic cycle is suppressed in the pores of [Fe]-ZSM-5, in comparison to [Al]-ZSM-5. A possible explanation for this suppression is the decrease in

the number of chain carriers of the aromatics-based catalytic cycle i.e. MBs. Figure A.3 shows the normalized FID chromatograms of the reactor effluent (at 10 min TOS) of DME conversion on [Fe]-ZSM-5 and [Al]-ZSM-5 at ~623 K, ~130 kPa total feed pressure, and ~70 kPa DME pressure.

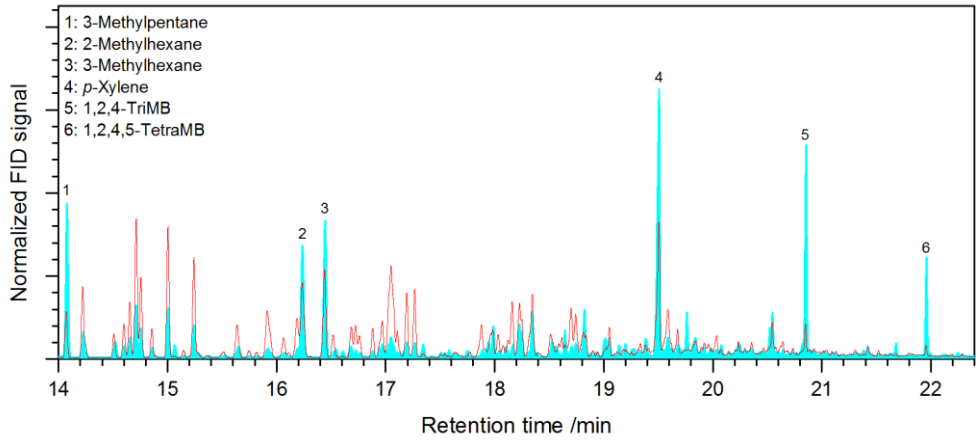

Figure A.3: Normalized (to CH_4/Ar internal standard) FID chromatograms of the reactor effluent (at 10 min TOS) of DME conversion on (i) [Fe]-ZSM-5 (red), and (ii) [Al]-ZSM-5 (cyan), at ~623 K, ~130 kPa total feed pressure, and ~70 kPa DME pressure. The DME space-velocity was 0.54 mol C (mol Fe-s)$^{-1}$ on [Fe]-ZSM-5 and 4.8 mol C (mol Al-s)$^{-1}$ on [Al]-ZSM-5.

It can be observed that the concentration of MBs in the reactor effluent of [Fe]-ZSM-5 was significantly lower than MBs concentration on [Al]-ZSM-5. These observations suggest that formation of MBs was suppressed in the pores of [Fe]-ZSM-5 which resulted in a decrease in the propagation of the aromatics-based catalytic cycle. It must also be noted that hydrogen transfer index, ratio of the synthesis rates of C_2 – C_6 alkanes and total C_2 – C_6 aliphatic hydrocarbons, decreased from 0.29 on [Al]-ZSM-5 to 0.08 on [Fe]-ZSM-5, therefore suggesting that hydrogen transfer was significantly suppressed in the pores of [Fe]-ZSM-5 thereby resulting in lower MBs formation as MBs are formed as a result of hydrogen transfer to C_6+ olefins.

Appendix B

Analysis of Retained Hydrocarbons in MFI Zeolites by HF Dissolution and Extraction with CH_2Cl_2

B.1 Materials and Methods

B.1.1 Catalyst Synthesis and Preparation

The conventional (Conv) ZSM-5 sample was acquired from Zeolyst International Inc. (CBV 8014, Si/Al ~43). The self-pillared pentasil (SPP) MFI sample (Si/Al ~88) and a ZSM-5 sample with 17 μm crystallites (referred to as 17μm-MFI) were synthesized according to procedures described in Chapter 4. Three silylated samples were synthesized by single-cycle silylation (for SiMFI-1x) as well as multi-cycle silylation (twice and thrice for SiMFI-2x and SiMFI-3x, respectively) treatments following the procedures described in Chapter 4. The catalysts were converted to their protonated form by treating in 1.67 $cm^3\ s^{-1}$ dry air (Minneapolis Oxygen, 20 – 21% O_2, <10 ppm H_2O) at 773 K for 4 h. The temperature was increased from ambient to 773 K in 12 h and was held at 773 K for 4 h before cooling down to the ambient temperature.

B.1.2 Catalytic Reactions of DME with/without Oxygenate Co-feeds

Catalytic reactions of DME were carried out in a 316/316L stainless steel packed-bed reactor (1/4 in OD; 0.035 in wall thickness) equipped with a concentric thermal well (1/16 in OD, 0.014 in wall thickness). A detailed description of the experimental setup can be found in Chapter 4. The reactant stream constituted DME (Matheson Tri-Gas, 99.5% purity) and a mixture of CH_4 and Ar (Airgas, 10% CH_4, 90% Ar) that was used as an internal standard. Propene (Praxair, 50% propene, 50% Ar), acetone (Sigma-Aldrich 99.9% purity), propanal (Sigma-Aldrich >99% purity), furan (Sigma-Aldrich >99% purity),

methanol (Fisher Scientific, HPLC grade, 99.9% purity), or acetaldehyde (Acros Organics, 99.5% purity) were co-fed with DME in some cases.

The reactions were run using 10 – 25 mg catalyst and the catalyst bed was diluted with 100 – 150 mg of quartz sand to prevent temperature rise due to exothermic reactions. The flow rates were adjusted to obtain the desired carbon space-velocity. Methanol was considered as a reactant in the calculation of net conversion. The reactions were carried out at 623 K and the temperature variation in the bed was less than 1 K during the reaction. The reactor effluents were analyzed using Agilent 7890 series GC – 5975C series MS equipped with a 100% dimethylpolysiloxane Agilent J&W HP-1 column (50 m × 320 μm × 0.52 μm) connected to an FID and a (5%-phenyl)-methylpolysiloxane Agilent J&W HP-5ms column (25 m × 320 μm × 0.25 μm) connected to an MSD.

B.1.3 Analysis of Retained Hydrocarbons in the Spent Catalyst by HF Dissolution

The spent catalyst was quenched immediately after the reaction by spraying liquid N_2 or cold N_2 gas (at liquid N_2 boiling temperature). During the quenching, reaction temperature decreased from 623 K (reaction temperature) to <373 K in less than 120 s. The catalyst was carefully removed from the catalyst-bed holder and was dissolved in 1 cm^3 15% HF aqueous solution. After 1 h, 2 cm^3 CH_2Cl_2 (Sigma-Aldrich, chemical purity grade) was added, the vial was shaken vigorously, and the resulting solution was kept aside for 15 min to extract all the organics and separate the organic and aqueous phases. Finally, 0.5 cm^3 of the organic phase (which now contained entrained hydrocarbons) was extracted and mixed with 0.25 cm^3 of CH_2Cl_2 solution containing *n*-hexane (13.5 mm^3 *n*-hexane in 100 cm^3 CH_2Cl_2) as an external standard. The resulting mixture was manually injected into the front S/SL inlet of an Agilent 7890 series GC – 5975C series MS and was analyzed for entrained hydrocarbons using the FID.

B.2 Results and Discussion

B.2.1 Catalytic Reaction of DME on ZSM-5 at Varying DME Space-Velocity

Table B.1 and Figure B.1 show the reaction conditions, product distribution, and the catalytic activity of ZSM-5 catalyst for DME conversion at varying DME space-velocity. Table B.1 and Figure B.2 show the composition of retained hydrocarbons in the spent catalyst after 20 – 60 min time-on-stream.

Table B.1: Reaction conditions, product distribution, and MBs content in the spent catalyst, at varying DME space-velocity (2.5 – 9.0 mol C (mol Al-s)$^{-1}$), for the catalytic reaction of DME on ZSM-5 (Si/Al ~43) catalyst at ~623 K, 120 – 130 kPa total feed pressure, 65 – 70 kPa DME pressure, and 20 – 60 min TOS.

DME space-velocity /mol C (mol Al-s)$^{-1}$	**9.0**	**4.8**	**3.2**	**3.0**	**2.9**	**2.8**	**2.5**
Weight of catalyst /mg	5.7	11	16	21	21	21	21
Net DME conversion /%	9	34	46	50	51	59	60
Product distribution (in %, on a carbon basis)							
C_2	6.7	12.9	11.6	13.7	12.0	13.5	10.7
C_3	22.4	19.2	19.8	20.2	17.9	20.1	16.7
C_4 – C_7	47.8	43.8	44.3	43.5	45.9	44.3	46.2
Methylbenzenes	3.0	9.7	8.3	6.2	7.5	6.2	9.8
Others[a]	20.1	14.4	16.0	16.4	16.7	15.9	16.5
MBs content per unit cell in the spent catalyst							
Toluene	n/a	0.01	0.01	0.01	0.01	n/a	0.01
Xylenes	0.29	0.11	0.16	0.05	n/a	0.14	0.16
TriMBs	0.06	0.02	0.10	n/a	n/a	n/a	0.09
TetraMBs	0.29	0.08	0.38	0.09	0.08	0.10	0.31
PentaMB	0.29	0.12	0.39	0.22	0.19	0.25	0.32
HexaMB	0.42	0.22	0.58	0.91	0.56	0.84	0.52
Total	**1.34**	**0.55**	**1.62**	**1.28**	**0.83**	**1.33**	**1.40**

[a] The “Others” fraction includes C_8+ hydrocarbons except polyMBs.

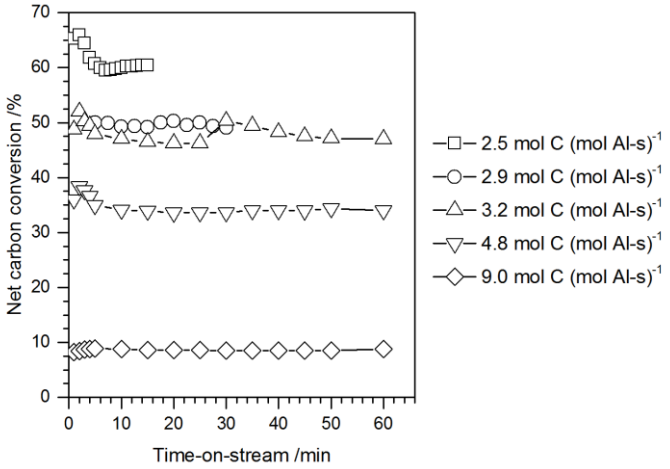

Figure B.1: Net carbon converted versus TOS at varying space-velocity (2.5 – 9.0 mol C (mol Al-s)$^{-1}$), for the catalytic reaction of DME on ZSM-5 (Si/Al ~43) catalyst at 623 K.

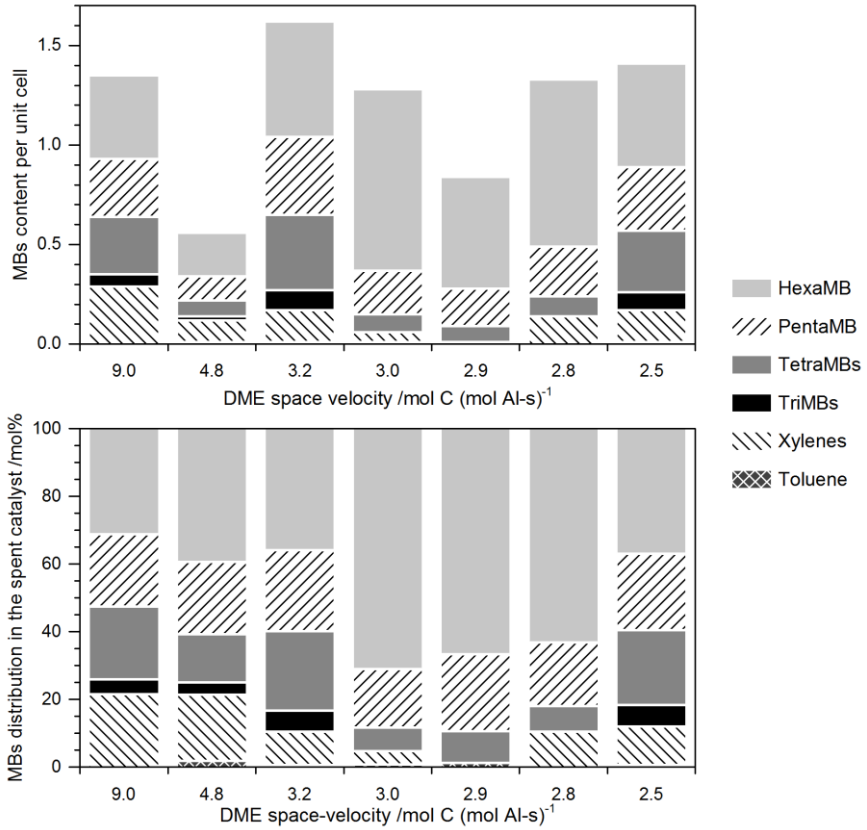

Figure B.2: (a) MBs content, and (b) MBs distribution, in the spent catalyst at varying space-velocity (2.5 – 9.0 mol C (mol Al-s)$^{-1}$), for the reaction of DME on ZSM-5 (Si/Al ~43) at 623 K.

B.2.2 DME Conversion to Hydrocarbons on Various MFI-Type Zeolites

Table B.2 and Figure B.3 show the reaction conditions, product distribution, and the catalytic activity of MFI-type zeolites with varying diffusion characteristics for the catalytic reaction of DME at ~623 K. Table B.2 and Figure B.4 show the composition of retained hydrocarbons in the spent catalyst after 60 min time-on-stream.

Table B.2: Reaction conditions, product distribution, and MBs content in the spent catalyst, for the catalytic reactions of DME on different MFI-type zeolites at ~623 K, 120 – 130 kPa total feed pressure, and 60 – 70 kPa DME pressure, and 20 – 60 min TOS.

Zeolite sample	**Conv MFI**	**SPP MFI[a]**	**17µm-MFI**	**SiMFI-1x**	**SiMFI-2x**	**SiMFI-3x**
Weight of the catalyst /mg	16	22	39	16	15	15
DME space-velocity /mol C (mol Al-s)$^{-1}$	3.2	4.7	0.61	3.4	3.5	3.5
Net carbon converted /%	46	15	46	47	48	25
Product distribution (in %, on a carbon basis)						
C_2	11.6	0.40	20.3	16.8	19.3	22.7
C_3	19.8	33.5	27.9	23.4	26.6	31.9
C_4 – C_7	44.3	46.0	37.9	41.7	40.6	34.8
Methylbenzenes	8.3	0.88	5.5	7.1	6.0	4.3
Others[b]	16.0	19.3	8.4	11.1	7.6	6.2
MBs content per unit cell in the spent catalyst						
Toluene	0.01	n/a	0.11	0.01	0.05	0.07
Xylenes	0.16	0.07	0.26	0.15	0.33	0.36
TriMBs	0.10	0.03	0.07	0.06	0.08	0.14
TetraMBs	0.38	0.04	0.12	0.22	0.42	0.37
PentaMB	0.39	0.02	0.10	0.18	0.44	0.34
HexaMB	0.58	0.02	0.13	0.21	0.44	0.27
Total	**1.62**	**0.19**	**0.80**	**0.82**	**1.76**	**1.54**

[a] The reaction was performed in the presence of ~3.8 kPa propene co-feed.

[b] The “Others” fraction includes C_8+ hydrocarbons except polyMBs.

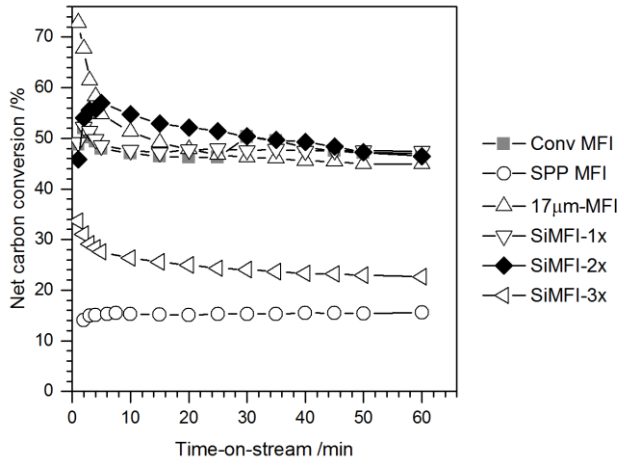

Figure B.3: Net carbon converted versus TOS for the catalytic reactions of DME on MFI-type zeolite with different diffusion characteristics at ~623 K.

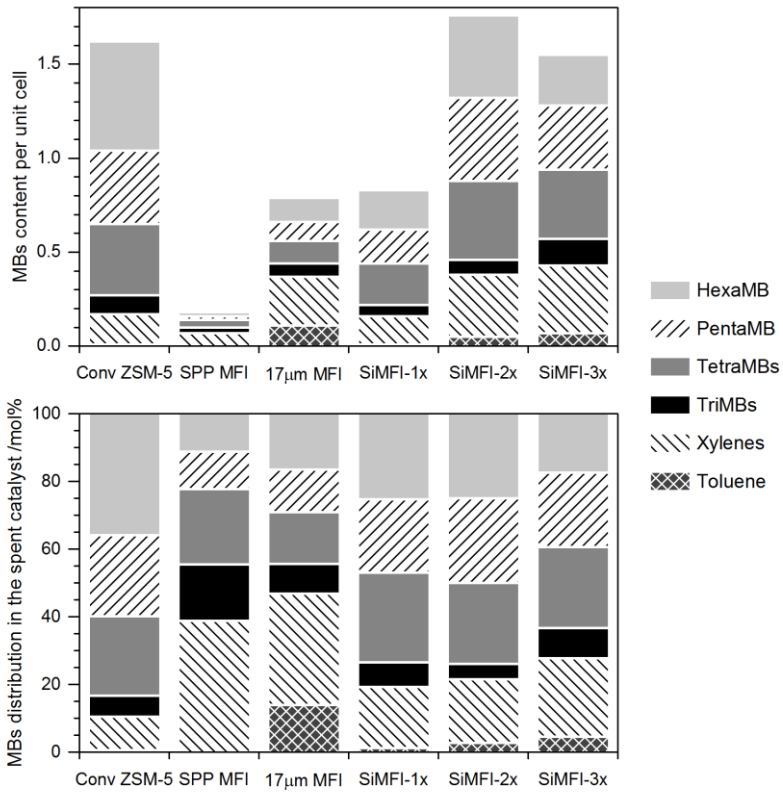

Figure B.4: (a) MBs content per unit cell, and (b) MBs distribution, in the spent catalyst, for the catalytic reactions of DME on MFI-type zeolites with different diffusion characteristics at ~623 K.

B.2.3 DME Conversion to Hydrocarbons in the Presence of Oxygenate Co-Feeds

Table B.3 and Figure B.5 show the reaction conditions, product distribution, and the catalytic activity of ZSM-5 catalyst for the reaction of DME in the presence of oxygenate co-feeds. Table B.3 and Figure B.6 show the composition of retained hydrocarbons in the spent catalyst after 20 – 60 min time-on-stream.

Table B.3: Reaction conditions, product distribution, and MBs contents in the spent catalyst, for the catalytic reaction of DME in the presence of oxygenate co-feeds at ~623 K, 120 – 130 kPa total feed pressure, 55 – 65 kPa DME pressure, 2 – 3 kPa co-feed pressure, and 20 – 60 min TOS.

Co-feed	**None**	**Acetone**	**Propanal**	**Furan**	**Acetaldehyde**	**Methanol**
Weight of the catalyst /mg	21	20	10	20	21	21
Carbon space-velocity /mol C (mol Al-s)$^{-1}$	2.8	2.5	2.8	2.9	2.8	2.8
Net carbon converted /%	59	64	64	10	42	58
Product distribution (in %, on a carbon basis)						
C_2	13.5	8.4	9.3	17.7	16.6	12.9
C_3	20.1	16.3	15.6	19.9	20.6	18.7
C_4 – C_7	44.3	49.6	42.2	36.9	39.4	45.4
Methylbenzenes	6.2	8.3	12.8	11.7	7.7	7.6
Others[a]	15.9	17.4	20.1	13.9	15.6	15.3
MBs content per unit cell in the spent catalyst						
Toluene	n/a	0.01	0.02	0.03	0.04	0.03
Xylenes	0.14	0.15	0.16	0.17	0.06	n/a
TriMBs	n/a	0.08	0.09	0.13	0.06	n/a
TetraMBs	0.10	0.25	0.26	0.41	0.36	0.22
PentaMB	0.25	0.22	0.23	0.25	0.38	0.41
HexaMB	0.84	0.37	0.38	0.24	0.56	0.84
Total	**1.33**	**1.08**	**1.13**	**1.34**	**1.47**	**1.49**

[a] The “Others” fraction includes C_8+ hydrocarbons except polyMBs.

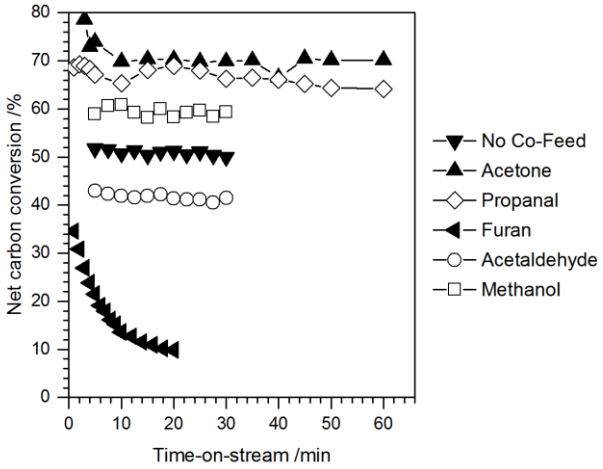

Figure B.5: Net carbon converted versus TOS for the catalytic reactions of DME in the presence of oxygenate co-feeds on ZSM-5 (Si/Al ~43) catalyst at ~623 K.

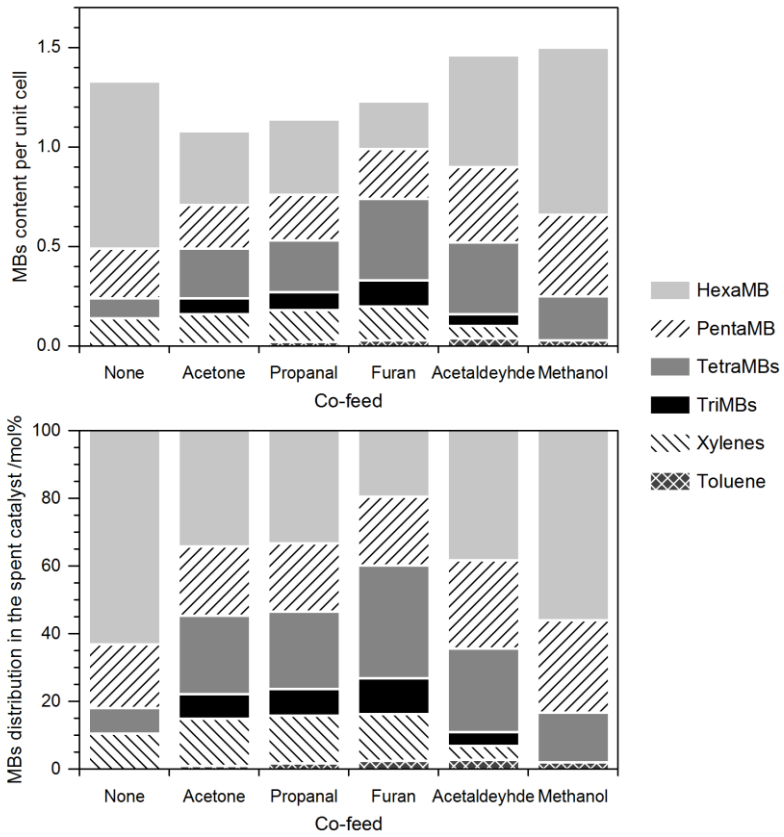

Figure B.6: (a) MBs content per unit cell, and (b) MBs distribution, in the spent catalyst for the reaction of DME in the presence of oxygenate co-feeds on ZSM-5 (Si/Al ~43) at ~623 K.

The results reported in Section B.2 show that the total content as well as the composition of the retained hydrocarbons show no discernable trend with catalyst deactivation, DME space-velocity, diffusion characteristics in the zeolite, or the feed composition. These results suggest that HF dissolution is not a quantitative technique for analyzing the total content of retained hydrocarbons or their concentrations inside the zeolite pores. HF dissolution and subsequent extraction by CH_2Cl_2 can only be used to qualitatively assess the isotopic composition of the retained hydrocarbons and not their relative concentration inside the pores.

Several factors come into play when analyzing the spent catalyst by this technique: (i) quenching of the catalyst bed may not be fast enough and the aromatics present initially may further react or desorb, (ii) the hydrocarbons may also react further in the highly acidic HF solution, (iii) the hydrocarbons may leave the aqueous solution as vapors, and finally (iv) the separation factor of aromatics may be different for their extraction by CH_2Cl_2. The HF dissolution experiments must be complimented with other quantitative techniques such as MAS-NMR spectroscopy and TGA analysis of the spent catalyst. The quenched catalyst bed can be analyzed by MAS-NMR spectroscopy to quantitatively assess the concentration of the functional groups present in the aromatics while the TGA analysis can be used to quantitatively determine the total coke content in the spent catalyst after the reaction. This will eliminate the limitation from factors (ii) – (iv) as mentioned above. The slow or inadequate quenching of the catalyst bed may, however, still affect the assessed aromatic concentration as hydrocarbons may further react or desorb. To suppress this effect, the catalyst must be quenched using liquid N_2 or water (due to its high specific heat capacity) to reduce the temperature of the bed as quickly as possible in flowing DME conditions.

Appendix C

Effects of Co-Feeding Oxygenates on MTH Selectivity

C.1 Catalyst Preparation and Catalytic Reactions of DME with Oxygenates

The conventional ZSM-5 sample was obtained from Zeolyst International Inc. (CBV 8014, 0.5 μm crystallite size, SiO_2/Al_2O_3 ~80). The catalyst was converted to its protonated form by treating in 1.67 $cm^3\ s^{-1}$ dry air (Minneapolis Oxygen, 20 – 21% O_2, <10 ppm H_2O) at 773 K for 4 h. The temperature was increased from ambient to 773 K in 12 h and was held at 773 K for 4 h before cooling down to the ambient temperature.

Catalytic reactions of DME were carried out in a 316/316L stainless steel packed-bed reactor (1/4 in OD; 0.035 in wall thickness) equipped with a concentric thermal well (1/16 in OD, 0.014 in wall thickness). A detailed description of the experimental setup can be found in Chapter 5. The reactant stream constituted DME (Matheson Tri-Gas, 99.5% purity) and a mixture of CH_4 and Ar (Airgas, 10% CH_4, 90% Ar) that was used as an internal standard. Acetone (Sigma-Aldrich 99.9% purity), propanal (Sigma-Aldrich >99% purity), furan (Sigma-Aldrich >99% purity), or acetaldehyde (Acros Organics, 99.5% purity), were co-reacted with DME, in some cases.

The reactions were run using 10 – 25 mg catalyst and the catalyst bed was diluted with ~100 mg of quartz sand to prevent temperature rise due to exothermic nature of MTH reactions. The carbon space velocity was varied between 2.5 and 9.9 mol C $(mol\ Al\text{-}s)^{-1}$ to achieve the desired chemical conversions. Methanol was considered as a reactant in the calculation of net carbon conversion. The reactions were carried out at 623 K and the temperature variation in the bed was less than 1 K during the reaction. The reactor

effluents were analyzed using Agilent 7890 series GC – 5975C series MS equipped with a 100% dimethylpolysiloxane Agilent J&W HP-1 column (50 m × 320 μm × 0.52 μm) connected to an FID and a (5%-phenyl)-methylpolysiloxane Agilent J&W HP-5ms column (25 m × 320 μm × 0.25 μm) connected to an MSD.

C.1.1 Analysis of Retained Hydrocarbons in the Spent Catalyst by HF Dissolution

The spent catalyst was quenched immediately after the reaction using liquid N_2 or cold N_2 gas (at liquid N_2 boiling temperature). During the quenching, temperature of the catalyst bed decreased from 623 K to below 373 K in less than 120 s. The catalyst was carefully removed from the catalyst-holder and was dissolved in 1 cm^3 15% HF aqueous solution. After 1 h, 2 cm^3 CH_2Cl_2 (Sigma-Aldrich, chemical purity grade) was added to the solution, the vial was shaken vigorously, and the solution was kept aside for 15 min to extract organics. Finally, 0.5 cm^3 of the organic phase (which now contained entrained hydrocarbons from the spent catalyst) was extracted and mixed with 0.25 cm^3 of CH_2Cl_2 solution containing *n*-hexane (13.5 mm^3 *n*-hexane in 100 cm^3 CH_2Cl_2) as an external standard. The resulting mixture was manually injected into the front S/SL inlet of the Agilent 7890 series GC – 5975C series MS and was analyzed for retained hydrocarbons using the FID.

C.2 Effects of Co-Feeding Acetone on MTH Conversion and Selectivity

Table C.1 shows the reaction conditions and the product distribution for the reaction of DME (~66 kPa) with acetone (~2.5 kPa) on ZSM-5 (Si/Al ~43) catalyst at ~623 K and ~130 kPa total feed pressure. Reaction conditions and product distribution for the reaction of DME alone (without co-feed) under similar reaction conditions are also reported for comparison. The net acetone converted was <40% (15% at 60 min time-on-stream). It

can be observed that the product distribution was invariant with acetone co-feed. Ethene selectivity (from 11% to 8.4%) and MBs selectivity (from 9.8% to 8.3%) decreased marginally in the presence on acetone co-feed. Ethene/2MBu yield also decreased marginally from 1.31 without co-feed to 1.02 in the presence of acetone co-feed.

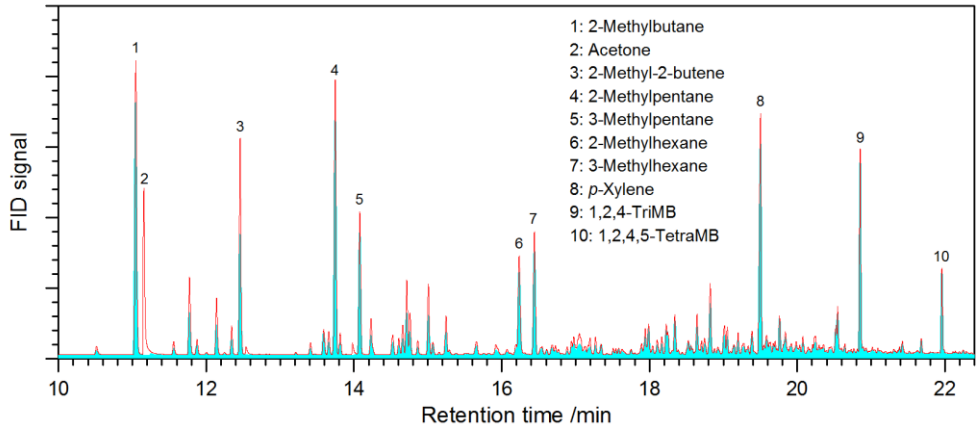

Figure C.1: Normalized (to CH_4/Ar internal standard) FID chromatograms of reactor effluent at 15 – 60 min TOS for the catalytic reactions of (i) DME alone at ~66 kPa (■), and (ii) DME (~61 kPa) with ~2.5 kPa acetone co-feed (□), on ZSM-5 (Si/Al ~43) catalyst at ~623 K, ~130 kPa total feed pressure, and 60 – 64% net conversion.

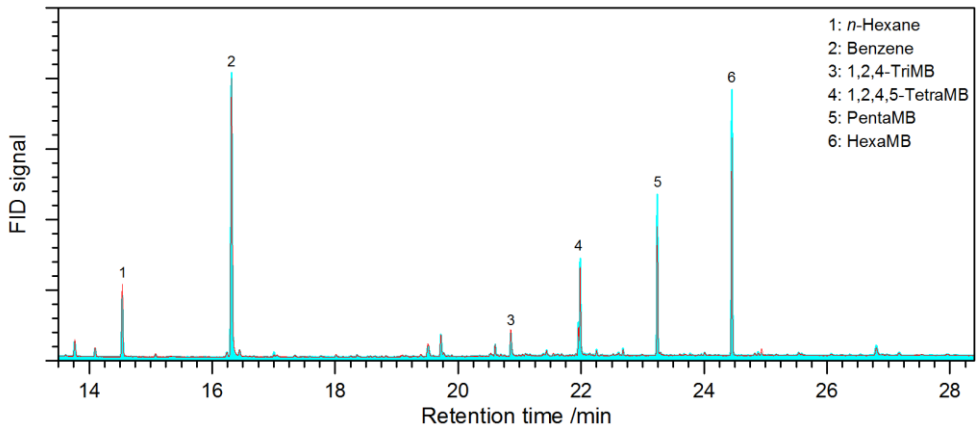

Figure C.2: Normalized (to *n*-hexane external standard) FID chromatograms of entrained hydrocarbons in the spent catalyst at 15 – 60 min TOS for the catalytic reactions of (i) DME alone at 66 kPa (■), and (ii) DME (~61 kPa) with ~2.5 kPa acetone co-feed (□), on ZSM-5 (Si/Al ~43) catalyst at ~623 K, ~130 kPa total feed pressure, and 60 – 64% net conversion.

Table C.1: Reaction conditions and product distribution for the catalytic reactions of DME with acetone or propanal on ZSM-5 (Si/Al ~43) catalyst at ~623 K, ~130 kPa total feed pressure, 60 – 66 kPa DME pressure, 2.1 – 2.5 kPa co-feed pressure, and 60 – 64% net conversion.

Co-feed	**None**	**Acetone**	**Propanal**
Total space-velocity /mol C (mol Al-s)$^{-1}$	2.9	2.5	2.8
Net carbon conversion /%	60	64	64
Co-feed conversion /%	-	<40	87
Product distribution (in %, on a carbon basis)			
C_2	10.7	8.4	9.3
C_3	16.7	16.3	15.6
C_4 – C_7	46.2	49.6	42.2
Methylbenzenes	9.8	8.3	12.8
Others[a]	16.5	17.4	20.1
Ethene/2MBu[b]	1.31	1.02	1.37
Hydrogen transfer index (HTI)[c]	0.33	0.31	0.28

[a] The "Others" fraction includes C_8+ hydrocarbons excluding polyMBs.

[b] Ratio of the synthesis rates of ethene and the sum of 2-methylbutane and 2-methyl-2-butene.

[c] Ratio of the synthesis rates of C_2 – C_6 alkanes and total C_2 – C_6 aliphatic hydrocarbons.

Figure C.1 shows the normalized FID chromatograms of reaction effluent (at 15 – 60 min time-on-stream) for the reaction of DME with/without acetone co-feed at 623 K. It can be observed that the identity of hydrocarbons and their relative concentration in the effluent was not affected by co-feeding acetone. Table C.2 shows the composition of the retained hydrocarbons, specifically MBs, in the spent catalyst after the reaction, and Figure C.2 shows the normalized FID chromatograms of the hydrocarbons extracted using the HF dissolution and CH_2Cl_2 extraction procedure. It can be observed that co-feeding ~2.5 kPa acetone did not have an effect on the identity or the composition of retained hydrocarbons in the spent catalyst. These results suggest that acetone blended, at least

to some extent, in the hydrocarbon pool and did not affect MTH conversion and its product distribution under the investigated reaction conditions. It is also important to note that acetone was relatively unreactive under the investigated reaction conditions as net acetone conversed was <40% (and only 15% at 60 min time-on-stream).

Table C.2: Composition of entrained MBs in the spent catalyst for the catalytic reaction of DME with acetone or propanal on ZSM-5 (Si/Al ~43) at ~623 K, ~130 kPa total feed pressure, 60 – 66 kPa DME pressure, 2.1 – 2.5 kPa co-feed pressure, 60 – 64% net conversion, and 15 – 60 min TOS.

Co-feed	**None**	**Acetone**	**Propanal**
Toluene	0.01	0.01	0.02
Xylenes	0.16	0.15	0.16
TriMBs	0.09	0.08	0.09
TetraMBs	0.31	0.25	0.26
PentaMB	0.32	0.22	0.23
HexaMB	0.52	0.37	0.38
Total	**1.40**	**1.08**	**1.13**

C.3 Effects of Co-Feeding Propanal on MTH Conversion and Selectivity

Table C.1 shows the reaction conditions and the product distribution for the reaction of DME (~66 kPa) with propanal (~2.1 kPa) on ZSM-5 (Si/Al ~43) catalyst at ~623 K and ~130 kPa total feed pressure. Reaction conditions and product distribution for the reaction of DME alone (without co-feed) under similar reaction conditions are also reported for comparison. The net propanal conversion (~87%) was much higher than acetone conversion (<40%) under similar reaction conditions, suggesting that propanal is more reactive than acetone on ZSM-5. It can be observed from Table C.1 that the product distribution of DME conversion was nearly invariant with the presence/absence of

propanal co-feed. Ethene selectivity decreased (from 11% to 9.3%) while MBs selectivity increased (from 9.8% to 13%) in the presence on propanal co-feed. Ethene/2MBu yield was however invariant, changing only slightly from 1.31 without co-feed to 1.37 in the presence of propanal co-feed. Figure C.3 shows the normalized FID chromatograms of reactor effluent (at 15 – 60 min time-on-stream) for the reaction of DME with/without propanal co-feed at ~623 K. It can be observed that, like acetone co-feed experiment, the identity of hydrocarbon species and their relative concentration in the reaction effluent was not affected by co-feeding small quantities (~2.1 kPa) of propanal.

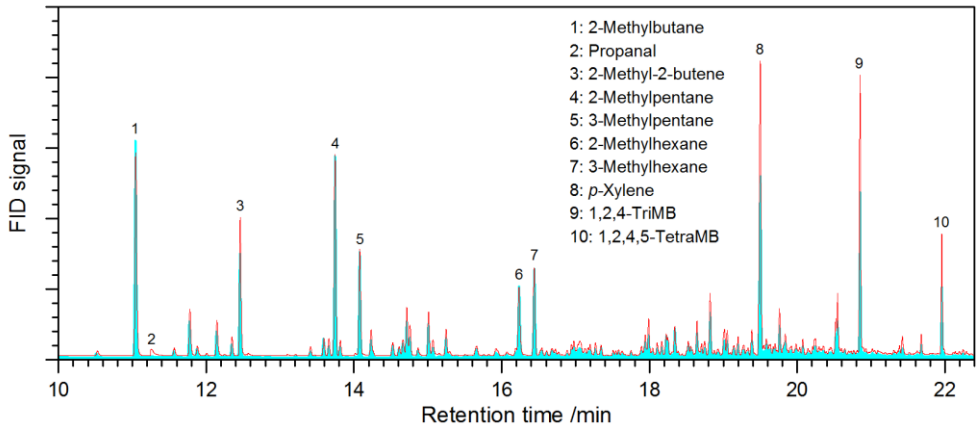

Figure C.3: Normalized (to CH_4/Ar internal standard) FID chromatograms of reactor effluent (at 15 – 60 min TOS) for the catalytic reactions of (i) DME alone at ~66 kPa (■), and (ii) DME (~61 kPa) with ~2.1 kPa propanal co-feed (□), on ZSM-5 (Si/Al ~43) catalyst at ~623 K, ~130 kPa total feed pressure, and 60 – 64% net carbon conversion.

Table C.2 shows the concentration of retained MBs in the spent catalyst after the reaction, and Figure C.4 shows the normalized FID chromatograms of the hydrocarbons extracted using HF dissolution and CH_2Cl_2 extraction procedure, for the reaction of DME at ~623 K. It can be seen that co-feeding propanal did not affect the identity or the concentration of retained MBs in the spent catalyst. These observations suggest that

propanal, similar to the acetone co-feed experiment, blended in the hydrocarbon pool, at least to some extent, and did not affect MTH conversion and its product distribution under the investigated reaction conditions.

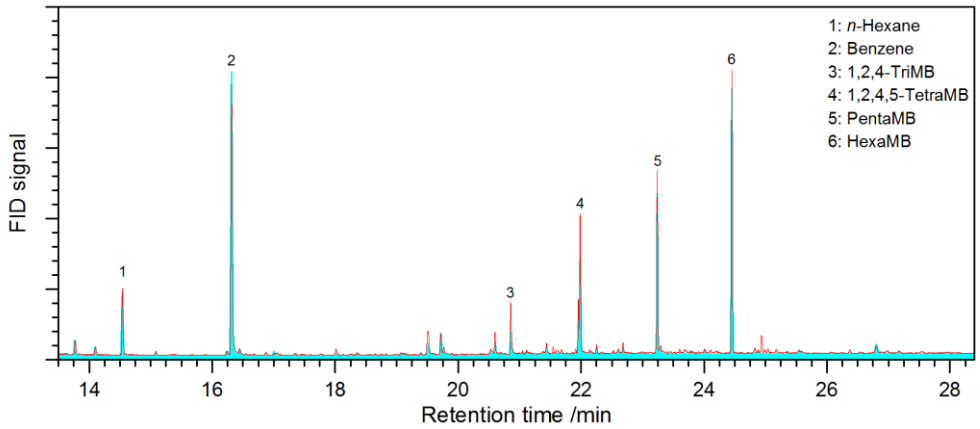

Figure C.4: Normalized (to *n*-hexane external standard) FID chromatograms of retained hydrocarbons in the spent catalyst (after 15 – 60 min TOS) for the catalytic reactions of (i) DME alone at ~66 kPa (■), and (ii) DME (~61 kPa) with ~2.1 kPa propanal co-feed (□), on ZSM-5 (Si/Al ~43) catalyst at~ 623 K, ~130 kPa total feed pressure, and 60 – 64% net conversion.

C.4 Effects of Co-Feeding Furan on MTH Conversion and Selectivity

Table C.3 shows the reaction conditions and the product distribution for the catalytic reaction of DME (~65 kPa) with furan (~2.4 kPa) on ZSM-5 (Si/Al ~43) catalyst at ~623 K and ~130 kPa total feed pressure. Reaction conditions and product distribution for the reaction of DME alone (without co-feed) under similar reaction conditions are also reported for comparison. The net furan conversion was <40% initially but decreased significantly with time-on-stream reaching <1% in 20 min. The product distribution changed significantly in presence of furan in the feed. Ethene selectivity increased significantly (from 6.7% to 18%) and MBs selectivity also increased (from 3.0% to 12%) in

the presence of furan co-feed. Ethene/2MBu yield also increased significantly from 1.23 without co-feed to only 4.38 in the presence of furan co-feed. These results suggest that co-feeding furan increased the propagation of the aromatics-based catalytic cycle, which consequentially resulted higher ethene selectivity, higher MBs selectivity, and a higher ethene/2MBu yield.

Figure C.5 shows the normalized FID chromatograms of reactor effluent (at 20 – 60 min time-on-stream) for the reaction of DME with and without furan co-feed at ~623 K and 9 -10 %. It can be observed that the identity of hydrocarbon species in the reactor effluent was not affected by furan co-feed; however, their relative concentration in the reactor effluent was affected by the presence of furan in the feed. The reactor effluent comprised of a higher concentration of MBs in the case of furan co-feed therefore suggesting that co-feeding furan increased the production of MBs inside the zeolite pores and consequentially increased the propagation of the aromatics-based catalytic cycle as well as ethene/2MBu yield and ethene selectivity.

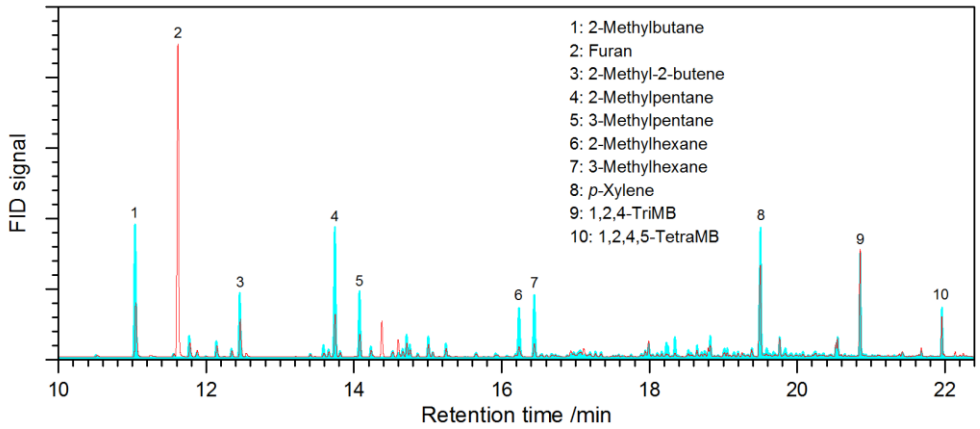

Figure C.5: Normalized (to CH_4/Ar internal standard) FID chromatograms of reactor effluents (at 20 – 60 min TOS) for the catalytic reactions of (i) DME alone at ~65 kPa (■), and (ii) DME (~62 kPa) in the presence of ~2.4 kPa furan co-feed (□), on ZSM-5 (Si/Al ~43) catalyst at ~623 K, ~130 kPa total feed pressure, and 9 – 10% conversion.

Table C.3: Reaction conditions and product distribution for the catalytic reaction of DME with furan on ZSM-5 (Si/Al ~43) catalyst at ~623 K, ~130 kPa total feed pressure, 62 – 65 kPa DME pressure, ~2.4 kPa co-feed pressure, 9 – 10% net carbon conversion, and 20 – 60 min TOS.

Co-feed	**None**	**Furan**
Total space-velocity /mol C (mol Al-s)-1	9.9	2.9
Net carbon conversion /%	8.8	9.8
Co-feed conversion /%	-	<40
Product distribution (in %, on a carbon basis)		
C_2	6.7	17.7
C_3	22.4	19.9
C_4 – C_7	47.8	36.9
Methylbenzenes	3.0	11.7
Others[a]	20.1	13.9
Ethene/2MBu[b]	1.23	4.38
Hydrogen transfer index (HTI)[c]	0.14	0.15

[a] The "Others" fraction includes C_8+ hydrocarbons excluding polyMBs.

[b] Ratio of the synthesis rates of ethene and the sum of 2-methylbutane and 2-methyl-2-butene.

[c] Ratio of the synthesis rates of C_2 – C_6 alkanes and total C_2 – C_6 aliphatic hydrocarbons.

Figure C.6 shows the composition of the retained hydrocarbons, specifically MBs, in the spent catalyst after the reaction, and Figure C.6 shows the normalized FID chromatograms of the retained hydrocarbons (after 20 – 60 min time-on-stream) extracted using HF dissolution and CH_2Cl_2 extraction procedure, for the reaction of DME at ~623 K in the presence of furan co-feed. It can be observed that co-feeding furan did not affect the identity of retained hydrocarbons in the spent catalyst; however, the concentration of MBs was significantly higher in the case of furan co-feed experiment. These results further suggest that co-feeding furan increased MBs production inside the zeolite pores, thereby increasing the propagation of the aromatics-based catalytic cycle, which consequentially

resulted in the observed increase in ethene selectivity, MBs selectivity, and the ethene/2MBu yield. This observation also explains the fast catalyst deactivation as MBs are precursors to coke (polycyclic aromatics) and their enhanced production also increases the production of coke inside the catalyst.

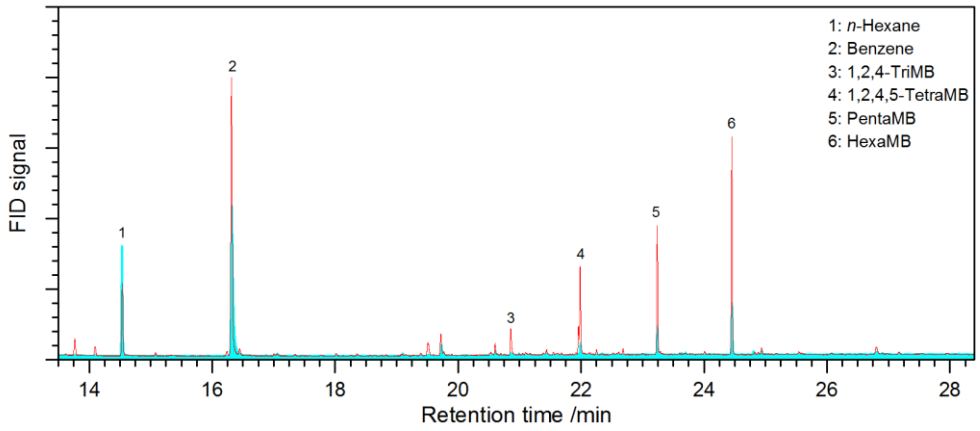

Figure C.6: Normalized (to *n*-hexane external standard) FID chromatograms of retained hydrocarbons in the spent catalyst at 20 – 60 min TOS for the catalytic reactions of (i) DME alone at ~65 kPa (■), and (ii) DME (~62 kPa) with ~2.4 kPa furan co-feed (□), on ZSM-5 (Si/Al ~43) catalyst at ~623 K, ~130 kPa total feed pressure, and 9 – 10% conversion.

C.5 Effects of Co-Feeding Acetaldehyde on MTH Conversion

Table C.4 shows the reaction conditions and the product distribution for the reaction of DME in the presence of acetaldehyde co-feed on ZSM-5 (Si/Al ~43) catalyst at ~623 K. Reaction conditions and product distribution for the reaction of DME alone (without co-feed) under similar reaction conditions are also reported. The product distribution of DME conversion was affected by the presence of acetaldehyde in the feed. Ethene selectivity and MBs selectivity increased in the presence of acetaldehyde co-feed. Ethene/2MBu yield also increased significantly in the presence of acetaldehyde co-feed.

These observations suggest that co-feeding acetaldehyde, like co-feeding furan, increased the production of MBs inside the pores of the zeolite, thereby increasing the propagation of the aromatics-based catalytic cycle.

Table C.4: Reaction conditions and product distribution for the catalytic reactions of DME with acetaldehyde on ZSM-5 (Si/Al ~43) catalyst at ~623 K, ~130 kPa total feed pressure, ~60 kPa DME pressure, ~2 kPa co-feed pressure, and 54 – 55% net conversion.

Co-feed	**None**	**Acetaldehyde**
Total space-velocity /mol C (mol Al-s)-1	2.9	2.9
Net carbon conversion /%	51	42
Co-feed conversion /%	-	<60
Product distribution (in %, on a carbon basis)		
C_2	12.0	16.6
C_3	17.9	20.6
C_4 – C_7	45.9	39.4
Methylbenzenes	7.5	7.7
Others[a]	16.7	15.6
Ethene/2MBu[b]	1.44	2.45
MBs content per unit cell in the spent catalyst		
Toluene	n/a	0.04
Xylenes	0.14	0.06
TriMBs	n/a	0.06
TetraMBs	0.10	0.36
PentaMB	0.25	0.38
HexaMB	0.84	0.56
Total	**1.33**	**1.47**

[a] The “Others” fraction includes C_8+ hydrocarbons excluding polyMBs.

[b] Ratio of the synthesis rates of ethene and the sum of 2-methylbutane and 2-methyl-2-butene.

C.6 Effects of Co-Feeding Oxygenates on Ethene/2MBu Yield

Figure C.7 shows the effects of co-feeding oxygenates with DME on ethene/2MBu yield (a descriptor of the relative extents of propagation of the aromatics-based and the olefins-based catalytic cycles). Figure C.7 describes the change in ethene/2MBu yield in the presence of an oxygenate co-feed in comparison to observed value of ethene/2MBu in the absence of the oxygenate under similar reaction conditions and at iso-conversion conditions. It can be observed that oxygenates like furan and acetaldehyde enhance the propagation of the aromatics-based catalytic cycle and result in higher ethene/2MBu, while oxygenates like propanol (which readily dehydrate to propene on Brønsted acid sites) selectivity propagate the olefins-based catalytic cycle and result in a decrease in ethene/2MBu yield. Acetone and propanal, however, do not enhance the propagation of either catalytic cycle and blend with the hydrocarbon pool that exists in the absence of the oxygenate. Ethene/2MBu did not change in the presence of such oxygenates.

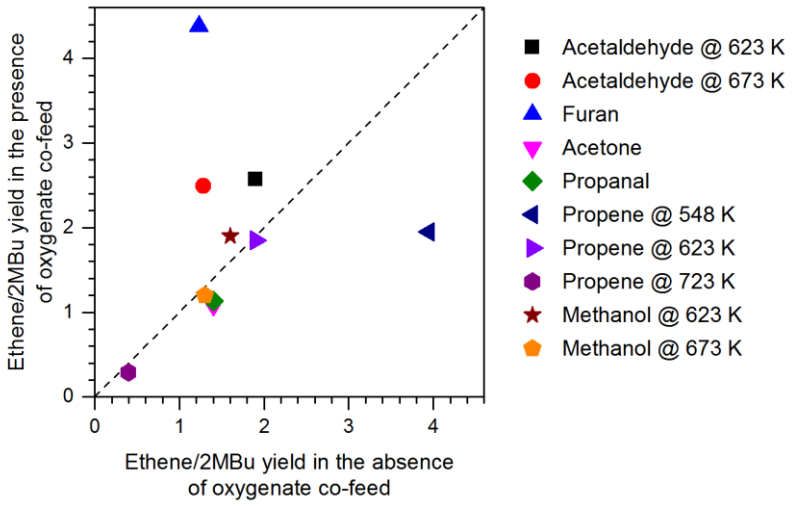

Figure C.7: Ethene/2MBu, for the reaction of DME on ZSM-5 (Si/Al ~43) at 548 – 723 K, 55 – 70 kPa DME pressure, in the presence of 2 – 4 kPa oxygenate co-feed versus ethene/2MBu in the absence of co-feed under similar reaction conditions.

Appendix D

DME Conversion on Phosphorus-Modified ZSM-5 Samples

D.1 Synthesis of Phosphorus-Modified ZSM-5 Samples

A commercially available ZSM-5 zeolite, acquired from Zeolyst International Inc. (CBV 8014, 0.5 μm crystallite size, SiO_2/Al_2O_3 ~80), was used as the parent material for the synthesis of phosphorus-modified ZSM-5 samples. Three different P-modified ZSM-5 samples were synthesized (which are referred to as [X]P-ZSM-5, where X was the P/Al in the final material) with phosphorus-content varying between 0.6 – 1.8 wt%. Prior to P-modification, the parent material was treated in dry air at 823 K for 4 h. P-modification was performed by incipient wetness impregnation method using 10 g of parent material and $NH_4H_2PO_4$ as the phosphorus precursor. The amount of precursor was varied to achieve the desired phosphorus-to-aluminum ratio (0.24 g for [0.5]P-ZSM-5, 0.49 g for [1.0]P-ZSM-5, and 0.70 g for [1.5]P-ZSM-5). The final materials were dried overnight at 393 K and were subsequently treated in dry air at 823 K for 4 h.

D.1.1 Synthesis of Steamed Phosphorus-Modified ZSM-5 Samples

The as-synthesized P-modified ZSM-5 samples (3 g) were treated in steam (50% H_2O, 50% Ar) at 723 K for 240 h to obtain three steamed P-modified ZSM-5 samples with varying phosphorus-content. These samples are referred to as St-[X]P-ZSM-5 where X is the P/Al in the zeolite. Prior to the catalytic reactions, all zeolite samples were pretreated in 1.67 $cm^3\ s^{-1}$ dry air (Minneapolis Oxygen, 20 – 21% O_2, <10 ppm H_2O) at 773 K for 4 h. The temperature was increased from ambient to 773 K in 12 h and was held at 773 K for 4 h before cooling down to the ambient temperature.

D.2 Structural and Chemical Characterization

Elemental composition of the zeolite samples was determined by ICP-OES using a Thermo Fischer iCap 7000 instrument. The samples were digested in HF prior to the elemental analysis and Yttrium was used as an internal standard. The bulk Si/Al and P/Al in the ZSM-5 samples are reported in Table D.1.

XPS measurements were performed on an SSX-100 system (Surface Science Laboratories, Inc.) equipped with a monochromatic Al-Kα X-ray source, a hemispherical sector analyzer, and a resistive anode detector. The base pressure of the system was 5.0 $\times$ 10^{-10} Torr. During the data collection, the pressure was ~1.0 $\times$ 10^{-8} Torr. Each sample was mounted individually on a sample stage using a piece of carbon sticking tape. Care was taken to ensure the surface was covered with a sufficiently thick layer of the sample. The samples were not conductive and a low energy beam (10 eV) was used for charge neutralization. The X-ray spot size was 1 $\times$ 1 mm^2, which corresponds to an X-ray power of 200 W. The survey spectrum was collected using 150 eV pass energy and 1 eV/step. The high resolution spectra were collected using 50 eV pass energy and 0.1 eV/step. The collected XPS spectra of the P-modified ZSM-5 samples (as well as the parent zeolite) are reported in Figure D.1.

The surface atomic percentages in the P-modified ZSM-5 samples were calculated from the survey spectrum using the ESCA Hawk software. For high resolution data, the lowest binding energy C 1s peak was set at 285 eV and used as the reference for the other elements. The surface elemental composition, as estimated by ESCA, are reported in Table D.1. It can be observed that the surface elemental composition was similar to the bulk elemental composition therefore suggesting that the phosphorus species were not confined just to the external surface of the synthesized zeolite materials.

Table D.1: Bulk elemental composition and surface elemental composition of the P-modified ZSM-5 samples (as well as the parent zeolite) investigated in this work.

Zeolite sample	Bulk[a]			Surface[b]	
	Si/Al	P/Al	P/(Si + Al)	Si/Al	P/(Si + Al)
Parent ZSM-5	40	-	-	39	-
As-synthesized P-modified ZSM-5 samples:					
[0.5]P-ZSM-5	40	0.62	0.015	131	0.005
[1.0]P-ZSM-5	43	1.18	0.027	39	0.042
[1.5]P-ZSM-5	42	1.59	0.037	90	0.032
Steamed P-modified ZSM-5 samples:					
St-[0.5]P-ZSM-5	41	0.50	0.012	147	0.012
St-[1.0]P-ZSM-5	43	1.14	0.026	75	0.044
St-[1.5]P-ZSM-5	42	1.59	0.037	56	0.055

[a] Bulk elemental composition was estimated from ICP-OES elemental analysis

[b] Surface elemental composition was estimated from ESCA

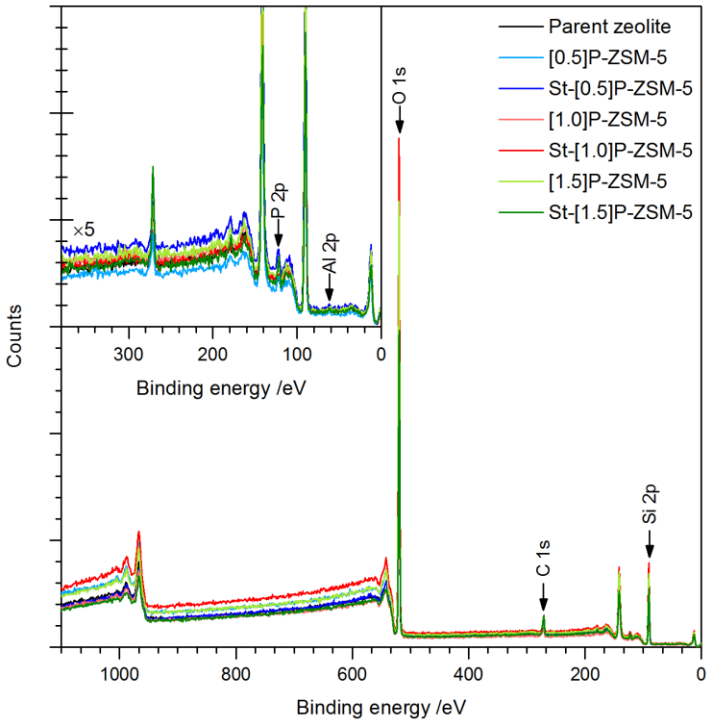

Figure D.1: XPS spectra of P-modified ZSM-5 samples (as well as the parent zeolite) collected using a monochromatic Al-Kα X-ray source, 150 eV pass energy, and 1 eV/step.

XRD patterns were obtained on a Siemens D-500 Diffractometer using Co-Kα radiation (1.79 Å). The scans were collected for 2θ values between 5° and 55° at a scan rate of 0.02°/min. Figure D.2 shows the obtained XRD patterns of the P-modified ZSM-5 samples as well as the parent zeolite. A simulated XRD pattern for MFI-type framework is also shown, for comparison. It can be observed that that the zeolites investigated in this work are crystalline and have an MFI-type framework. These results confirm that P-modification via incipient wetness impregnation did not affect the MFI-type crystal structure of the parent zeolite.

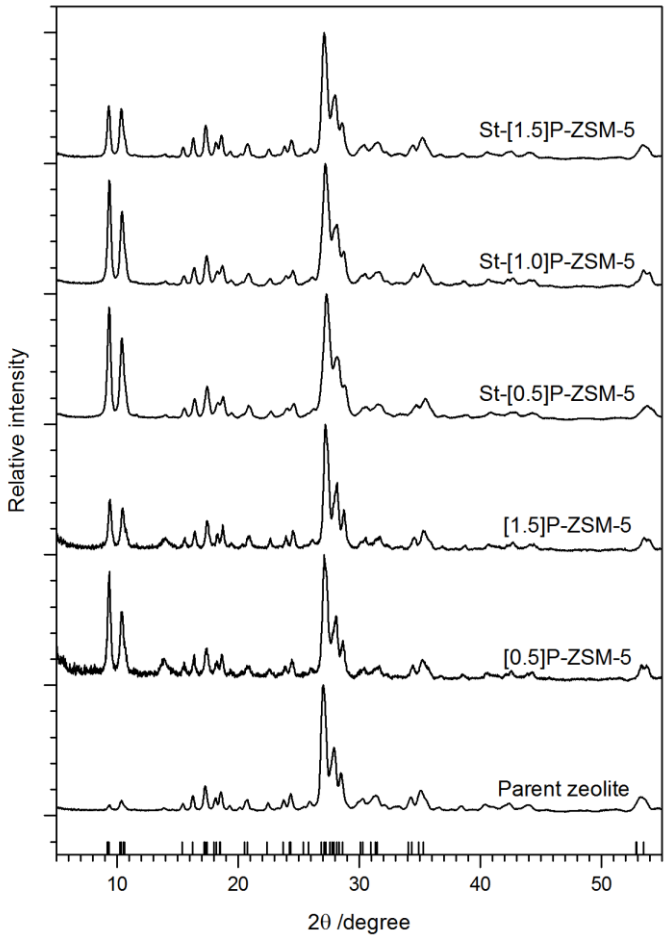

Figure D.2: XRD patterns of the P-modified ZSM-5 samples investigated in this work using the Co-Kα radiation (1.79 Å). The markers represent the simulated XRD pattern of an MFI-type framework. The XRD pattern of the parent zeolite sample is also shown, for comparison.

D.3 Effects of Phosphorus Modification on MTH Product Distribution

Catalytic reactions of DME were carried out in a 316/316L stainless steel packed-bed reactor (1/4 in OD; 0.035 in wall thickness) equipped with a concentric thermal well (1/16 in OD, 0.014 in wall thickness). A detailed description of the experimental setup can be found in Chapter 6. The reactant stream constituted DME (Matheson Tri-Gas, 99.5% purity) and a mixture of CH_4 and Ar (Airgas, 10% CH_4, 90% Ar) that was used as an internal standard. The reactions were run using 21 – 43 mg catalyst and the catalyst bed was diluted with ~100 of quartz sand (Acros Organics) to prevent temperature rise due to exothermic reactions. The carbon space-velocity was varied between 0.20 – 2.7 mol C (mol Al-s)$^{-1}$ to achieve the desired chemical conversions. Methanol was considered as a reactant in the calculation of net carbon conversion. The total feed pressure was maintained at 103 – 114 kPa and all the reactions were carried out at 623 K. The temperature variation in the bed was less than 1 K during the reaction. The reactor effluents were analyzed using an online Agilent 7890A series GC – 5975C series MS equipped with a 100% dimethylpolysiloxane Agilent J&W HP-1 column (50 m × 320 μm × 0.52 μm) connected to an FID and an MSD, and an Agilent J&W GS-GasPro column (60 m × 320 μm) connected to a TCD.

Figure D.3 shows net DME converted as a function of DME space-velocity (or DME space-time) for the catalytic reactions of DME on P-modified ZSM-5 samples at ~623 K, 103 – 114 kPa total feed pressure, and 48 – 63 kPa DME pressure. DME space-velocity was varied between 0.20 – 2.7 mol C (mol Al-s)$^{-1}$. Figure D.4a shows net carbon converted at a constant DME space-velocity (2.9 – 3.0 mol C (mol Al-s)$^{-1}$) and Figure D.4b shows the space-velocity required to achieve iso-conversion of DME (46 – 55% net DME conversion) on all zeolite samples investigated in this work.

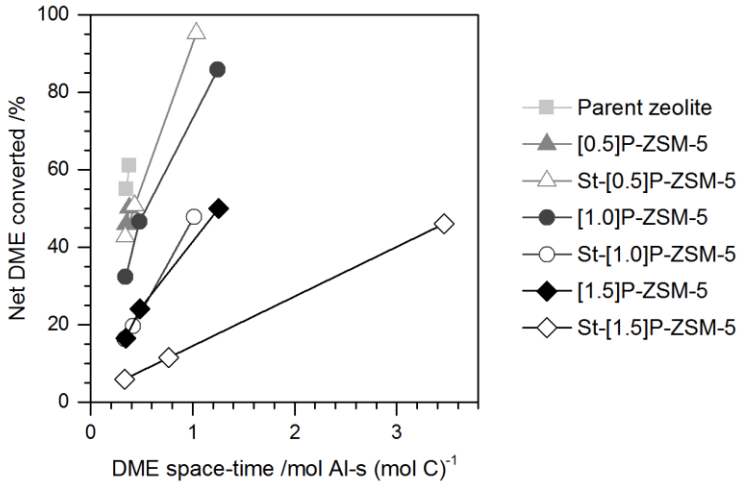

Figure D.3: Net DME converted as a function of DME space-time (inverse of DME space-velocity) for the catalytic reactions of DME on the zeolite samples investigated in this work at ~623 K, 103 – 114 total feed pressure, 48 – 63 kPa DME pressure. DME space velocity was varied between 0.20 – 2.7 mol C (mol Al-s)$^{-1}$.

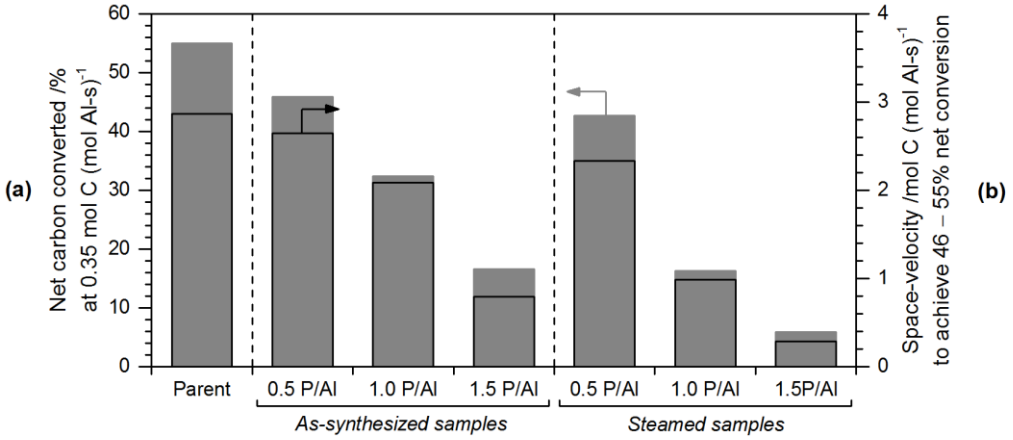

Figure D.4: (a) Net carbon converted (■) on the zeolite samples at a constant DME space-velocity (2.9 – 3.0 mol C (mol Al-s)$^{-1}$). (b) DME space-velocity (□) required to achieve DME iso-conversion (46 – 55% net DME conversion) on zeolite samples investigated in this work.

It can be observed from Figure D.4a that DME converted, at a constant DME space-velocity (2.9 – 3.0 mol C (mol Al-s)$^{-1}$), decreased monotonically with increasing P/Al in the P-modified ZSM-5 samples as well as the steamed P-modified ZSM-5 samples. In addition, the space-velocity required to achieve iso-conversion of DME (46 – 55% net

DME conversion) also decreased monotonically with increasing P/Al in the P-modified ZSM-5 samples. These results suggest the concertation of catalytically active Brønsted acid sites decreased with increasing phosphorus-content in the zeolites. It was also noted that steam treatment (with 50% H_2O, 50% Ar) at 723 K for 240 h resulted in a further reduction in the concentration of Brønsted acid sites.

Figure D.5 shows the product distribution for the catalytic conversion of DME to hydrocarbons on P-modified ZSM-5 samples and the steamed P-modified ZSM-5 samples (compared to the parent zeolite) at ~623 K, 103 – 114 total feed pressure, 48 – 63 kPa DME pressure, and iso-conversion of DME (46 – 55% net DME conversion). It can be observed that the product distribution, for DME conversion to hydrocarbons at 623 K, was invariant despite phosphorus modification (or steam treatment) of the parent zeolite under the investigated reaction conditions.

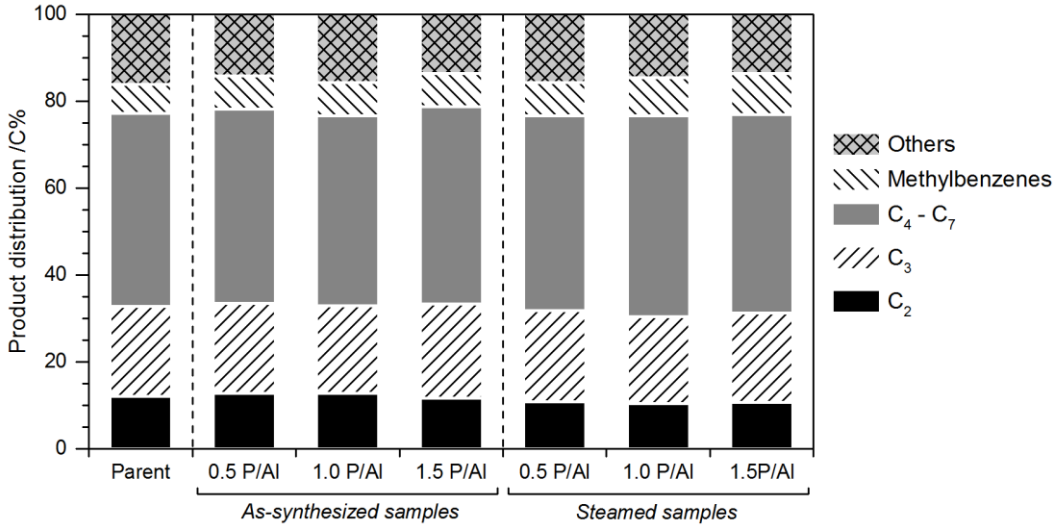

Figure D.5: Product distribution for the catalytic reaction of DME on P-modified ZSM-5 samples at ~623 K, 103 – 114 total feed pressure, 48 – 63 kPa DME pressure, and 46 – 55% net DME conversion. DME space velocity was varied between 0.20 – 2.7 mol C (mol Al-s)$^{-1}$.